

ORGANOMETALLIC AND SINGLE-ELECTRON-TRANSFER
MECHANISMS OF COPPER(II)-CATALYZED AEROBIC C-H OXIDATION

by

Alison M. Suess

A dissertation submitted in partial fulfillment of
the requirements for the degree of

Doctor of Philosophy
(Chemistry)

at the

UNIVERSITY OF WISCONSIN-MADISON

2013

Date of final oral examination: August 21st, 2013

This dissertation is approved by the following members of the Final Oral Committee:

Shannon S. Stahl, Professor, Inorganic Chemistry
Clark R. Landis, Professor, Inorganic Chemistry
John F. Berry, Associate Professor, Inorganic Chemistry
Tehshik P. Yoon, Professor, Organic Chemistry
Jennifer M. Schomaker, Assistant Professor, Organic Chemistry

**Organometallic and Single-Electron-Transfer Mechanisms of Copper(II)-Catalyzed
Aerobic C-H Oxidation**

Alison M. Suess

Under the supervision of Professor Shannon S. Stahl

At the University of Wisconsin-Madison

ABSTRACT: Copper-catalyzed aerobic C-H oxidation strategies are of great synthetic interest and are under active development. Cu^{II} promotes a wide range of oxidative coupling reactions and these reactions can be linked to aerobic catalytic turnover due to the facile oxidation of Cu^{I} to Cu^{II} by O_2 . However, the mechanisms of these reactions are not well understood. Cu^{II} can promote single-electron oxidation of electron-rich substrates, but new reactions have been developed featuring substrates that are electron-deficient or appear unlikely to undergo single-electron-transfer (SET). Evidence for organometallic intermediates has been obtained in some of these reactions. This thesis describes mechanistic studies of Cu^{II} -mediated C-H oxidations that were carried out in order to gain further understanding of factors that promote organometallic or SET mechanisms.

Procedures for Cu^{II} -mediated C-H oxidation of an amidoquinoline substrate were developed and divergent regioselectivity of functionalization was observed depending on reaction conditions. Experimental and computational analysis is consistent with a switch between organometallic and SET-based C-H oxidation pathways upon changing from basic to acidic reaction conditions. The presence of a Brønsted basic ligand on the Cu^{II} center facilitates C-H

activation by an organometallic mechanism, while acidic conditions enhance the Cu^{II} reduction potential, thereby favoring SET. The results of this study show that a macrocyclic chelate is not required to achieve organometallic C–H activation by Cu^{II} .

Kinetic studies of Cu^{II} -catalyzed oxidative halogenation of the electron-rich substrates 1,3-dimethoxybenzene and phenol were performed. Though chlorination and bromination occur under similar reaction conditions, the mechanisms are different. Experiments indicate the chlorination mechanism is consistent with a single-electron-transfer mechanism in which successive equivalents of Cu^{II} -halide oxidize the arene to an aryl-radical-cation and deliver a chlorine atom. This mechanism is different than the commonly proposed mechanism in which a Cu^{II} -phenoxide undergoes intramolecular electron-transfer to generate Cu^{I} and a phenoxy radical. The bromination mechanism is more consistent with electrophilic bromination by Br_2 , which may be generated from disproportionation of CuBr_2 .

Aryl- Pd^{IV} triazamacrocyclic complexes were generated which are analogous to known aryl- Cu^{III} triazamacrocyclic intermediates in Cu-mediated aerobic aryl-C-H bond oxidation. In contrast, oxidation of aryl- Pd^{II} to higher oxidation states does not occur under O_2 alone, and once oxidation to aryl- Pd^{IV} is achieved, reductive elimination does not easily occur. Unusually for Pd, radical intermediates are implicated in the formation of the aryl- Pd^{IV} complexes. The behavior of aryl-Pd in this system serves to underscore the benefits of using Cu catalysts, linked with O_2 oxidant, to functionalize arene C-H bonds.

ACKNOWLEDGEMENTS

This work would not have been possible without the excellence of my colleagues, the faculty and the staff at University of Wisconsin-Madison, as well as the support of my family and friends. I thank my advisor, Professor Shannon S. Stahl, for excellent research mentorship and guidance throughout my doctoral studies.

Funding for this work was provided by Teaching and Research Assistantships from the University of Wisconsin-Madison and by Basic Energy Sciences at the U. S. Department of Energy, Office of Science.

TABLE OF CONTENTS

Abstract	i
Acknowledgements	iii
Table of Contents	iv
List of Tables	xi
List of Figures	xiii
List of Schemes	xvii
Abbreviations and Acronyms	xx
Chapter 1. <i>Introduction to the Methodology and Mechanisms of Copper-Catalyzed Aerobic Aryl C-H Bond Oxidation</i>	
<i>Aerobic Aryl C-H Bond Oxidation</i>	1
1.1. Introduction.	2
1.2. Phenol Oxygenation and Carbon-Carbon Coupling.	3
1.2.1. Phenol Oxygenation to Quinones.	3
1.2.2. Phenol Polymerization.	7
1.2.3. Naphthol and Phenol Coupling.	10
1.3. Oxidative Halogenation of Phenols and Dimethoxybenzenes.	13
1.3.1. Phenols.	13
1.3.2. Dimethoxybenzenes.	15
1.4. Chelate-Directed Oxidations.	18
1.5. Functionalization of Acidic C-H Bonds.	19
1.6. Oxidative Annulations.	21

1.7. Aryl-Copper Complexes Relevant to Organometallic C-H Activation Mechanisms.	24
1.8. Conclusions.	27
1.9. References and Notes.	28

Chapter 2. *Divergence between Organometallic and Single-Electron-Transfer*

<i>Mechanisms in Copper(II)-Mediated Aerobic C-H Oxidation</i>	39
2.1. Introduction.	40
2.2. Cu ^{II} -Mediated C-H Oxidation of <i>N</i> -(8-quinolinyl)benzamide under Different Conditions.	43
2.2.1. Methoxylation and Chlorination of the Benzamide.	43
2.2.2. Chlorination of the Quinoline.	45
2.2.3. Comments on the Divergent Reactivity.	46
2.3. Mechanistic Study of Cu ^{II} -Mediated C-H Oxidation of the Benzamide.	46
2.3.1. Initial Rates of Electronically-Varied Derivatives and Hammett Parameter for Benzamide Methoxylation.	46
2.3.2. Deuteration and Isotope Effect Experiments for Benzamide Methoxylation.	49
2.3.3. Reactivity of <i>N</i> -methyl- <i>N</i> -(8-quinolinyl)benzamide in Benzamide Methoxylation Conditions.	51
2.4. Mechanistic Study of Cu ^{II} -Mediated C-H Oxidation of the Quinoline.	52
2.4.1. Deuteration and Isotope Effect Experiments for Quinoline Chlorination.	52
2.4.2. Reactivity of <i>N</i> -methyl- <i>N</i> -(8-quinolinyl)benzamide in Quinoline Chlorination Conditions.	54
2.5. Preliminary Assessment of the Divergent Mechanisms.	55

2.6. Summary of Computational Analysis of the Divergent Mechanisms.	56
2.6.1. Computational analysis of an organometallic pathway for Cu ^{II} -mediated C–H oxidation.	57
2.6.2. Computational analysis of a single-electron transfer pathway for Cu ^{II} -mediated C–H oxidation.	62
2.7. Reasons for the Mechanistic Divergence Under Different Reaction Conditions.	66
2.8. Conclusions.	67
2.9. Contributions.	68
2.10. Experimental.	68
2.10.1. General Considerations.	68
2.10.2. General Method of Benzamide Methoxylation.	69
2.10.3. General Method of Quinoline Chlorination.	70
2.10.4. Initial Rates and Hammett Plot for Benzoyl Moiety Methoxylation.	71
2.10.5. Deuteration and Isotope Effect Experiments for Benzamide Methoxylation.	72
2.10.6. Deuteration and Isotope Effect Experiments for Quinoline Chlorination.	73
2.10.7. Synthesis and Characterization of Substrates.	74
2.10.8. Characterization of Products.	77
2.10.9. Synthesis and Characterization of Deuterium-Labeled Substrates.	80
2.11. References and Notes.	82

Chapter 3. Copper-Catalyzed Aerobic Oxidative Chlorination of Electron-Rich Arenes	
<i>to Generate Chloroarenes and Quinones</i>	90
3.1. Introduction.	91
3.2. Kinetic Studies.	95
3.2.1. 1,3-Dimethoxybenzene Chlorination.	95
3.2.2. Phenol Chlorination.	101
3.3. Hydrogen/Deuterium Exchange and Kinetic Isotope Effects.	107
3.3.1. 1,3-Dimethoxybenzene Chlorination.	107
3.3.2. Phenol Chlorination.	108
3.4. Spectroscopic Studies of the Catalyst Resting State.	108
3.4.1. UV-Vis Spectroscopy of 1,3-Dimethoxybenzene and Phenol Oxidation.	109
3.4.2. EPR Spectroscopy of 1,3-Dimethoxybenzene and Phenol Oxidation.	110
3.5. Oxidation of 2,6-Dimethylphenol to 2,6-Dimethylquinone.	111
3.6. Proposed Mechanisms.	112
3.7.1. 1,3-Dimethoxybenzene Chlorination.	112
3.7.2. Phenol Chlorination.	114
3.7. Conclusions.	117
3.8. Contributions.	118
3.9. Experimental.	118
3.9.1. General Considerations.	118
3.9.2. GC Analysis of Reaction Timecourses.	119
3.9.3. Characterization.	119
3.10. References and Notes	120

Chapter 4. Copper-Catalyzed Aerobic Oxidative Bromination of Electron-Rich Arenes.	124
4.1. Introduction.	125
4.2. Kinetic Studies.	128
4.2.1. 1,3-Dimethoxybenzene Bromination.	128
4.2.2. Phenol Bromination.	133
4.3. Hydrogen/Deuterium Exchange and Kinetic Isotope Effects.	139
4.3.1. 1,3-Dimethoxybenzene Bromination.	139
4.4. Spectroscopic Studies of the Reaction Solution and Catalyst Resting State.	140
4.4.1. UV-Vis Spectroscopy of 1,3-Dimethoxybenzene and Br ₂ .	141
4.4.2. EPR Spectroscopy of 1,3-Dimethoxybenzene and Phenol Oxidation.	142
4.5. Other Studies Attempting to Address the Possibility of Br ₂ Generation.	144
4.5.1. Reaction Solution Vacuum Transfer and UV-Vis Analysis.	144
4.5.2. Bromination of Cyclooctene in the Reaction and UV-Vis Analysis.	145
4.5.3. Comments on the Previous Experiments.	147
4.6. Proposed Mechanisms.	148
4.6.1. 1,3-Dimethoxybenzene Bromination.	148
4.6.2. Phenol Bromination.	150
4.7. Conclusions.	151
4.8. Contributions.	151
3.9. Experimental.	151
4.9.1. General Considerations.	152
4.9.2. GC Analysis of Reaction Timecourses.	152
4.9.3. Characterization.	152

4.10. References and Notes.	152
-----------------------------	-----

Chapter 5. *Synthesis of Novel Aryl-Pd^{IV} Triazamacrocyclic Complexes and Comparison to Analogous Aryl-Cu^{III} Complexes.* 156

5.1. Introduction.	157
--------------------	-----

5.2. Synthesis of Novel Aryl-Pd ^{IV} Triazamacrocyclic Complexes.	158
--	-----

5.3. Comparison of Aryl-Pd ^{IV} and Aryl-Cu ^{III} Triazamacrocyclic Complexes.	161
--	-----

5.4. Lack of Reductive Elimination from [Aryl-Pd ^{IV} Cl ₂] ₂ BF ₄ .	162
---	-----

5.5. One-Electron Oxidation of [Aryl-Pd ^{II}] ₂ BF ₄ .	163
--	-----

5.5.1. Observation of an EPR-Active Species During [Aryl-Pd ^{IV} (NCS)] ₂ BF ₄ Synthesis.	163
--	-----

5.5.2. One-Electron Oxidation of [Aryl-Pd ^{II}] ₂ BF ₄ by Cyclic Voltammetry.	164
---	-----

5.5.3. Controlled Potential Electrolysis of [Aryl-Pd ^{II}] ₂ BF ₄ and EPR Spectroscopy.	165
---	-----

5.6. Conclusions.	166
-------------------	-----

5.7. Contributions.	167
---------------------	-----

5.8. Experimental.	168
--------------------	-----

5.8.1. General Considerations.	168
--------------------------------	-----

5.8.2. Synthesis of the Triazamacrocyclic Arene.	168
--	-----

5.8.3. Synthesis of the Aryl-Palladium(II) Triazamacrocyclic Complex.	170
---	-----

5.8.4. Synthesis of Aryl-Palladium(IV) Triazamacrocyclic Complexes.	171
---	-----

5.9. References and Notes.	172
----------------------------	-----

Appendix 1. <i>NMR Spectra for Chapter 2.</i>	174
--	-----

Appendix 2. Other Transformations of <i>N</i>-(8-Quinoliny)benzamide and Similar Substrates.	195
A2.1. Directed Benzamide Methoxylation of 3-Substituted and 3,5-Disubstituted <i>N</i> -(8-Quinoliny)benzamide Derivatives.	196
A2.2. Isolation and Analysis of Crystalline Copper(II)-Amidate Complexes from <i>N</i> -(8-Quinoliny)benzamide, Including Observation of Oxidase Reactivity.	198
A2.3. <i>N</i> -(8-Quinoliny)benzamide C-C Homocoupling in the Presence of Cu(ClO ₄) ₂ .	202
A2.4. <i>N</i> -(8-Quinoliny)benzamide Bromination, Methoxylation and Dimerization in Methanol.	203
A2.5. Reactivity of Other Directing-Group-Containing Substrates.	205
A2.6. Contributions.	207
A2.7. References and Notes.	207
Appendix 3. NMR Spectra and Crystal Structure Data for Appendix 2.	210
Appendix 4. NMR Spectra and Crystal Structure Data for Chapter 5.	240

LIST OF TABLES

Table 1.1.	Electron-Rich Phenols are More Easily Oxidized to <i>Para</i> -Quinones.	4
Table 1.2.	Cu ^{II} -Mediated Oxidative Halogenation of Anisole and 2-Methoxynaphthalene.	17
Table 2.1.	Directed C–H Methoxylation and Chlorination of the Benzamide.	44
Table 2.2.	C–H Chlorination of the Quinoline.	45
Table 2.3.	Initial Rates of Product Yield for Benzamide Methoxylation of Substrates 2a-d,f.	47
Table 2.4.	Hammett Parameter, Initial Rate, and Relevant Calculated Data.	48
Table 2.5.	Reactivity of <i>N</i> -methyl substrate 6a in Benzoyl Moiety Methoxylation Conditions.	51
Table 2.6.	Reactivity of <i>N</i> -methyl substrate 6a in Quinolinyll Moiety Chlorination Conditions.	55
Table 2.7.	Calculated Stability of Possible Cu- 2a Complexes under the Benzamide C–H Methoxylation Conditions.	57
Table 2.8.	Redox Couples Calculated for Oxidation of Aryl-Cu ^{II} to Aryl-Cu ^{III} in the Benzamide C–H Methoxylation Reaction.	60
Table 2.9.	Redox Couples Calculated for the Oxidation of Cu ^{II} to Aryl-Radical- Cation-Ligated Cu ^{II} Complex during Quinoline C–H Chlorination.	64
Table 2.10.	Computed Redox Potentials of Species Available in Acidic and Basic Reaction Conditions.	67
Table 5.1.	Comparison of Aryl-Pd ^{IV} and Aryl-Cu ^{III} Triazamacrocyclic Complexes.	162

Table A2.1.	Lack of selectivity in directed methoxylation of electron-rich and electron-poor benzamide groups of 3-substituted <i>N</i> -(8-quinolinyl)-benzamides.	197
Table A2.2.	Lack of selectivity in directed methoxylation of electron-rich and electron-poor benzamide groups of <i>N</i> -(8-quinolinyl)-3-substituted-benzamides.	198
Table A2.3.	Reaction utilizing a pyridine-containing directing group resulted in debenylation rather than the desired directed methoxylation.	205
Table A2.4.	Reaction utilizing a pyridine-containing directing group with a protected benzylic position did not result in the desired directed methoxylation.	206

LIST OF FIGURES

Figure 1.1.	Structural Variety of Phenol Homocoupling Products.	13
Figure 1.2.	Aryl-C-H Bond pK_a Values.	20
Figure 1.3.	Aryl-Cu ^{II} and Aryl-Cu ^{III} Complexes of <i>N</i> -Confused Porphyrins.	25
Figure 2.1.	Initial rates of methoxylation of substrates 2a-d .	48
Figure 2.2.	Hammett plot from initial rates of 2a-d methoxylation.	49
Figure 2.3.	Independent Initial Rate Comparison k_H/k_D for Benzoyl Moiety Methoxylation.	50
Figure 2.4.	(A) Product appearance and (B) starting material consumption in the independent initial rate comparison k_H/k_D for benzamide methoxylation.	54
Figure 2.5.	The lowest excited-state doublet derives from excitation of a beta electron from the nominally doubly occupied HOMO-1 (GS-A) and HOMO (GS-B), contributing with equal weight, into the singly occupied SOMO (ES).	63
Figure 3.1.	Representative timecourse for 1,3-dimethoxybenzene chlorination.	96
Figure 3.2.	Kinetic data from 1,3-dimethoxybenzene chlorination assessing the kinetic dependence on (A) [CuCl ₂], (B) [LiCl], and (C) [1,3-dimethoxybenzene].	98
Figure 3.3.	(A) 1 st order and (B) 2 nd order fits of rate dependence on [CuCl ₂] do not model the data well.	99
Figure 3.4.	Reaction time course dependence plots for (A) [CuCl ₂], (B) [LiCl], and (C) [1,3-dimethoxybenzene].	100
Figure 3.5.	Reaction time course plots under 1 atm O ₂ or air are initially identical,	

	but after 30 min the reaction with air shows deactivation.	101
Figure 3.6.	Representative time course for phenol chlorination.	102
Figure 3.7.	Reaction profiles with the typical 20 mol % CuCl_2 or alternatively a mix of 20 mol % CuCl_2 and 20 mol % LiOAc , which shows no induction period.	103
Figure 3.8.	Kinetic data from phenol chlorination assessing the kinetic dependence on (A) $[\text{CuCl}_2]$, (B) $[\text{LiCl}]$, and (C) $[\text{phenol}]$.	104
Figure 3.9.	(A) 1 st order and (B) 2 nd order fits of rate dependence on $[\text{CuCl}_2]$ do not model the data well.	105
Figure 3.10.	Reaction time course dependence plots for (A) $[\text{CuCl}_2]$, (B) $[\text{LiCl}]$, and (C) $[\text{phenol}]$.	106
Figure 3.11.	Reaction time courses under 1 atm O_2 or air have similar slopes but the air trace may show deactivation after 20 min.	107
Figure 3.12.	UV-visible spectra of the reaction solutions and a CuCl_2 solution in AcOH .	109
Figure 3.13.	UV-visible spectra of 1:20 $\text{CuCl}_2/\text{LiCl}$ and $\text{Cu}(\text{OAc})_2$ solutions in AcOH .	110
Figure 3.14.	EPR spectra of $\text{CuCl}_2/\text{LiCl}$ in AcOH , the phenol reaction solution, and the 1,3-dimethoxybenzene reaction solution, 145 K.	111
Figure 3.15.	Oxidation of 2,6-dimethylphenol produces two intermediates, 4-chloro- and 4-acetoxy-2,6-dimethylphenol, before 2,6-dimethylquinone is formed.	112
Figure 4.1.	A representative timecourse for 1,3-dimethoxybenzene bromination.	129
Figure 4.2.	Kinetic data from 1,3-dimethoxybenzene bromination assessing the kinetic dependence on (A) $[\text{CuBr}_2]$, (B) $[\text{LiBr}]$, and (C) $[\text{1,3-dimethoxybenzene}]$.	130
Figure 4.3.	(A) 1 st order and (B) 2 nd order fits of rate dependence on $[\text{CuCl}_2]$ do not model the data well.	131

Figure 4.4.	Reaction time course dependence plots for (A) [CuBr ₂], (B) [LiBr], and (C) [1,3-dimethoxybenzene].	132
Figure 4.5.	Reaction time course plots under 1 atm O ₂ or air exhibit similar profiles.	133
Figure 4.6.	A representative timecourse for phenol bromination with (A) 10 mol % CuBr ₂ and (B) 20 mol % CuBr ₂ .	134
Figure 4.7.	Kinetic data from phenol bromination assessing the kinetic dependence on (A) [CuBr ₂], (B) [LiBr], and (C) [phenol].	136
Figure 4.8.	A mixed 2 nd /1 st order dependence on CuBr ₂ concentration (2 nd order at low [Cu] and 1 st order at high [Cu]) models the data well, but has more variable coefficients than a 2 nd order fit.	137
Figure 4.9.	Reaction time course dependence plots for (A) [CuBr ₂], (B) [LiBr], and (C) [phenol].	138
Figure 4.10.	Reaction time course plots under 1 atm O ₂ or air exhibit similar profiles.	139
Figure 4.11.	UV-visible spectra of the reaction solutions, a CuBr ₂ solution, and Br ₂ in AcOH.	141
Figure 4.12.	UV-visible spectra of 1:20 CuBr ₂ /LiBr, Cu(OAc) ₂ , and 1:20 Cu(OAc) ₂ /LiBr solutions in AcOH.	142
Figure 4.12.	The 5 mM CuBr ₂ /100 mM LiBr solution in AcOH shows thermochromic behavior.	143
Figure 4.14.	X-Band EPR spectra of CuBr ₂ /LiBr in AcOH, the phenol reaction solution, and the 1,3-dimethoxybenzene reaction solution, 145 K.	144
Figure 4.15.	UV-visible spectrum of the reaction solution condensate, compared to the Br ₂ spectra in AcOH.	145

- Figure 4.16. (A) The distinctive peaks of the bromination reaction UV-visible spectrum rapidly decay after 40 equiv cyclooctene addition. (B) Decay of each peak is plotted as % intensity of absorbance. 147
- Figure 5.1. Structure of [aryl-Pd^{II}]BF₄ complex 2 determined by X-ray crystallography. 158
- Figure 5.2. Structure of [aryl-Pd^{IV}Cl₂]BF₄ complex 3 determined by X-ray crystallography. 159
- Figure 5.3. Structure of [aryl-Pd^{IV}(NCS)]BF₄ complex 4 determined by X-ray crystallography. (A) Front and (B) side views. 160
- Figure 5.4. Structure of [aryl-Pd^{IV}Br₂]BF₄ complex 5 determined by X-ray crystallography. 161
- Figure 5.5. Isotropic EPR spectrum ($g_{\text{iso}} = 2.006$) derived from crude mixture of 3, 4, 2 in CH₃CN, 77 K. 164
- Figure 5.6. Cyclic voltammetry indicates that [aryl-Pd^{II}]BF₄ complex 2 undergoes one-electron oxidation. 165
- Figure 5.7. EPR spectrum obtained after controlled potential electrolysis of 2, CH₃CN, 77 K. 166
- Figure A2.1. Crystallographically-analyzed literature copper(II) amidate complexes. 199
- Figure A2.2. Cu₂(OAc)₄(py)₂ chemical structure drawing. 199
- Figure A2.3. Copper(II)-phenoxide complex crystalized after methanol reflux. 200
- Figure A2.4. Bis-ligated copper(II) bis-amidate complex crystalized after acetone reflux. 201
- Figure A2.5. Time course of *N*-(8-quinolinyl)benzamide bromination, methoxylation, and dimerization in methanol. 204

LIST OF SCHEMES

Scheme 1.1.	Possible Mechanisms for Phenol Oxidation to <i>Para</i> -Quinones.	6
Scheme 1.2.	Oxidation of Phenol to Quinones and Diphenoquinones via a Binuclear Complex.	6
Scheme 1.3.	<i>Ortho</i> -Oxygenation of Phenol by a Bis- μ -Oxodicopper(III)-Phenolate Complex.	7
Scheme 1.4.	(A) Ionic and (B) Radical Mechanisms for 2,6-Dimethylphenol Polymerization.	9
Scheme 1.5.	Naphthol Coupling via (A) Radical-Radical or (B) Radical-Anion Mechanisms.	11
Scheme 1.6.	Alternative Naphthol Coupling Mechanism with Intermolecular Oxidation.	11
Scheme 1.7.	Binuclear Naphthol Coupling Mechanism Proposed for a Gas-Phase Reaction.	12
Scheme 1.8.	Phenol Halogenation Mechanism Proposed by Gusevskaya and Coworkers.	14
Scheme 1.9.	Proposed Mechanism for CuCl ₂ -Mediated Ketone/Enol Chlorination.	15
Scheme 1.10.	Proposed Mechanism for Dimethoxybenzene Chlorination.	16
Scheme 1.11.	Proposed Mechanism for Arene Bromination Based on CuBr ₂ Disproportionation to Generate Br ₂ .	17
Scheme 1.12.	Proposed Mechanism for 2-Methoxynaphthalene Chlorination.	17
Scheme 1.13.	Single-Electron-Transfer Mechanism Proposed for 2-Phenylpyridine Chlorination.	19

Scheme 1.14. Anilide Cyclization Kinetic Isotope Intramolecular Competition Experiment.	23
Scheme 1.15. Anilide Cyclization Radical Probe Experiment.	24
Scheme 1.16. Proposed Mechanism for Radical Cyclization of Anilide to Oxindole.	24
Scheme 1.17. Mechanism of “Cross-Dehydrogenative Coupling” Amine α -Functionalization.	24
Scheme 1.18. Proposed Catalytic Cycle for Cu-Catalyzed Aerobic Oxidative Methoxylation of the Triazamacrocyclic Arene.	27
Scheme 2.1. Proposed Single-Electron Transfer (SET) Mechanism for Oxidative Chlorination of 2-Phenylpyridine.	40
Scheme 2.2. Divergent Reactivity in Cu ^{II} -Mediated C–H Oxidation of 2a .	46
Scheme 2.3. Cu ^{II} -Mediated Methoxylation from Methanol to Yield Substituted Anisoles.	47
Scheme 2.4. Deuteration and Isotope Effect Experiments for the Benzamide C–H Methoxylation Reaction.	50
Scheme 2.5. Deuteration and Isotope Effect Experiments for the Quinolinyll C–H Chlorination Reaction.	53
Scheme 2.6. Calculated Mechanism for the Cu ^{II} -Mediated Benzamide C–H Methoxylation Reaction.	59
Scheme 2.7. Cu ^{II} vs. Cu ^{III} C–H Activation Mechanisms.	61
Scheme 2.8. Calculated Mechanism for the Cu ^{II} -Mediated Quinoline C–H Chlorination Reaction.	65
Scheme 3.1. Phenol Chlorination Mechanism Proposed by Gusevskaya and Coworkers.	91

Scheme 3.2.	<i>Ortho</i> -Oxygenation of Phenol by a Bis- μ -Oxodicopper(III)-Phenolate Complex.	93
Scheme 3.3.	Ionic Mechanism for 2,6-Dimethylphenol Polymerization.	93
Scheme 3.4.	Alternative Naphthol Coupling Mechanism with Intermolecular Oxidation.	93
Scheme 3.5.	Proposed Mechanism for Dimethoxybenzene Chlorination.	94
Scheme 3.6.	Proposed Mechanism for Cu ^{II} -Amidate Arene Chlorination.	95
Scheme 3.7.	Proposed Mechanism for Cu-Catalyzed Aerobic Oxidative Chlorination of 1,3-Dimethoxybenzene.	114
Scheme 3.8.	Proposed Mechanism for Cu-Catalyzed Aerobic Oxidative Chlorination of Phenol.	116
Scheme 3.9.	Phenoxy Radical Mechanism for Phenol Oxidation (Not Proposed).	117
Scheme 4.1.	Proposed Mechanism for Arene Bromination Based on CuBr ₂ Disproportionation to Generate Br ₂ .	126
Scheme 4.2.	Phenol Oxidative Bromination Mechanism Proposed by Gusevskaya and coworkers.	127
Scheme 4.3.	Proposed Mechanism for Cu-Catalyzed Aerobic Oxidative Chlorination of 1,3-Dimethoxybenzene.	149
Scheme 4.4.	Proposed Mechanism for Cu-Catalyzed Aerobic Oxidative Chlorination of Phenol.	151

ABBREVIATIONS AND ACRONYMS

% RSM	percent recovered starting material
atm	atmosphere
cat	catalyst/catalytic
CPE	controlled potential electrolysis
EPR	electron paramagnetic resonance
equiv	equivalents
GC	gas chromatograph/chromatography
KIE	kinetic isotope effect
NBS	<i>N</i> -bromosuccinimide
NCS	<i>N</i> -chlorosuccinimide
PPE	polyphenylene ether
PPO	polyphenylene oxide (see “PPE” for correct usage)
SET	single-electron-transfer

Chapter 1:

Introduction to the Methodology and Mechanisms of Copper-Catalyzed Aerobic Aryl C-H Bond Oxidation

*Portions of this chapter were adapted from: Wendlandt, A. E.; Sues, A. M.; Stahl, S. S. "Copper-Catalyzed Aerobic Oxidative C-H Functionalizations: Trends and Mechanistic Insights." *Angew. Chem. Int. Ed.* **2011**, *50*, 11062-11087.*

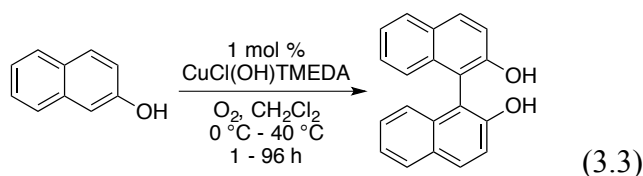
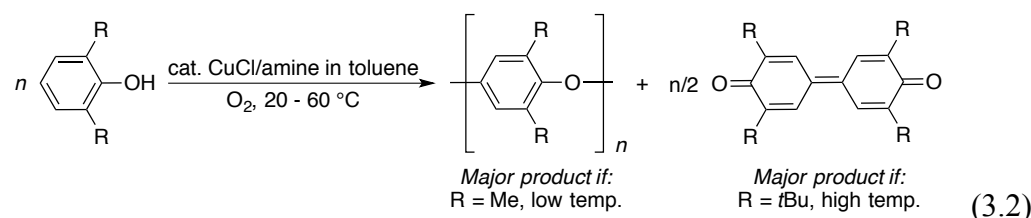
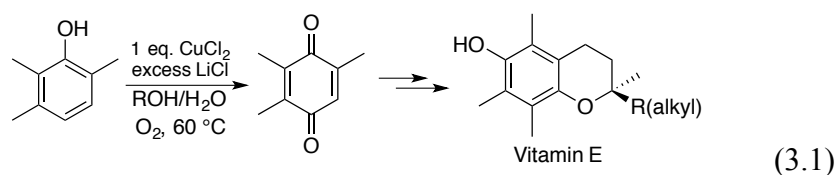
1.1. Introduction.

Copper-catalyzed aerobic C-H oxidation strategies are of great synthetic interest and are under active development.^{1,2,3} Cu^{II} promotes a wide range of oxidative coupling reactions and these reactions can be linked to aerobic catalytic turnover due to the facile oxidation of Cu^I to Cu^{II} by O₂.⁴ However, the mechanisms of these reactions are not well-understood. Cu^{II} can promote single-electron oxidation of electron-rich substrates, but new reactions have been developed featuring substrates that are electron-deficient or appear unlikely to undergo single-electron-transfer (SET). Evidence for organometallic intermediates has been obtained in some of these reactions. This thesis describes mechanistic studies of Cu^{II}-mediated C-H oxidations that were carried out in order to gain further understanding of factors that promote organometallic or SET mechanisms.

This chapter provides an introduction to the methodology and mechanisms of Cu^{II}-mediated aerobic aryl-C-H oxidation. This chapter first presents C-H oxidations for which single-electron-transfer mechanisms are proposed. An extended discussion of phenol oxygenation, carbon-carbon coupling, and halogenation is presented, as this topic is relevant to later chapters of this thesis but has not been previously extensively reviewed by the author. Next, C-H oxidations that resemble organometallic reactions but have ambiguous mechanisms are highlighted. Representative examples of chelate-directed oxidations, functionalization of acidic C-H bonds, and oxidative annulations are presented. Finally, the reactivity of aryl-copper complexes relevant to the proposed organometallic C-H activation mechanisms is surveyed.

1.2. Phenol Oxygenation and Carbon-Carbon Coupling.

Phenols are particularly useful substrates in Cu-catalyzed aerobic oxidation procedures. In an industrial setting 2,3,6-trimethylphenol is oxidized to a *para*-quinone vitamin E precursor (eq 3.1).⁵ Phenols are polymerized to form polyphenylene ether (PPE; also known as polyphenylene oxide or PPO), a commodity thermoplastic (eq 3.2).⁶ Naphthol coupling has also been well-studied and is the preferred route to make BINOL ligands (eq 3.3).⁷ In this section, these reactions and their proposed mechanisms are detailed.



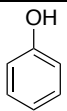
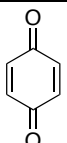
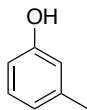
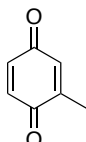
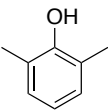
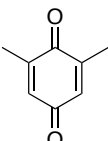
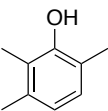
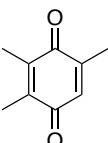
1.2.1. Phenol Oxygenation to Quinones.

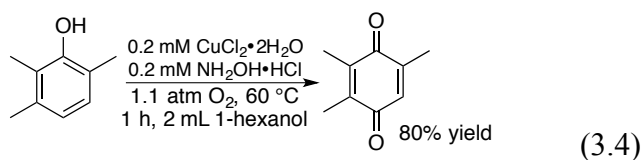
Phenols oxidation to produce *para*-quinones is an industrially important aerobic process and is used to synthesize 2,3,5-trimethylbenzoquinone, a vitamin E precursor (3.1). Early patent literature reports the use of stoichiometric CuCl₂, CuCl, CuBr₂, CuBr, and CuSO₄/NaBr in DMF or acetone under O₂ to effect the oxidation.⁸ Further development reported a *n*-hexanol/H₂O solvent mixture used with stoichiometric copper halide salts such as

Li[CuCl₃]•2H₂O or Cs₂[CuBr₄] and noted that an induction period could be eliminated with the use of Cu(OH)₂ or CuCl.⁹ Current production of 2,3,5-trimethylbenzoquinone uses stoichiometric CuCl₂•2H₂O, 4 eq LiCl, and a biphasic alcohol/H₂O solvent that allows re-use of the aqueous catalyst mixture.¹⁰

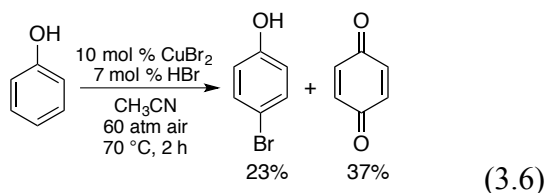
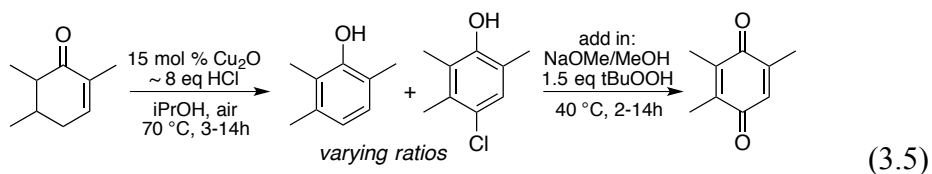
Electron-rich phenols are more easily oxidized to *para*-quinones. A comparison of the literature indicates that phenol can only be converted to benzoquinone under forcing conditions,¹¹ but 2,3,6-trimethylphenol can be converted to the quinone at relatively low O₂ concentration and temperature (Table 1.1).^{8,12} Another report examined the conversion of various phenol derivatives under low [O₂] and temperature conditions; in addition to 2,3,6-dimethylphenol, 2,6-dimethylphenol could be oxidized to the quinone, but the 2-methyl, 3-methyl, 2,3-dimethyl, 2,4-dimethyl, and 3,5-dimethyl phenol derivatives did not afford the quinone (eq 3.4).¹³

Table 1.1. Electron-Rich Phenols are More Easily Oxidized to *Para*-Quinones.

Entry	Substrate	Product	[CuCl ₂]	[O ₂]	Temperature	Solvent	Time	Yield
1			0.42 equiv	34 atm	100 °C	DMF	30 min	58 % ¹²
2			1.2 equiv	30 atm	60 °C	acetone/H ₂ O	3 h	75 % ⁸
3			1.2 equiv	30 atm	60 °C	acetone/H ₂ O	2.5 h	85 % ⁸
4			1.2 equiv	1 atm	60 °C	acetone/H ₂ O	3 h	96 % ⁸



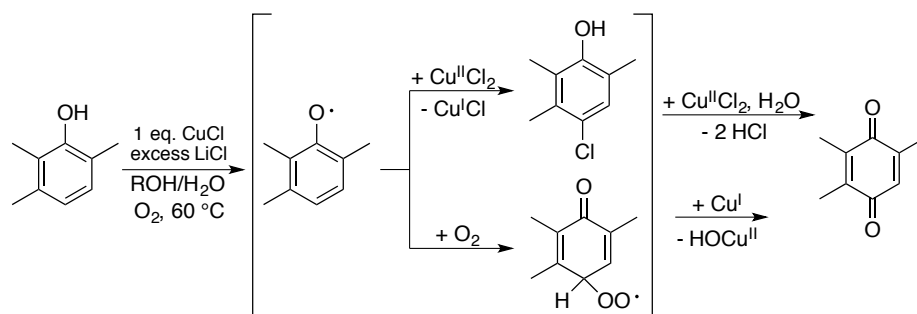
The industrial conditions use significant quantities of chloride salts (eq 3.1), and *para*-chlorophenols have been observed as intermediates in the oxidation. In a system using hydroxylamine-hydrochloride or lithium chloride additives (eq 3.4), the *para*-chlorophenol was observed to reach a maximum yield then decrease over the course of the reaction, indicating it could be an intermediate.¹³ In the timecourse it is produced simultaneously with the quinone, indicating that quinone may also be produced independently without prior chlorination. The *para*-chlorophenol was also observed as an intermediate in a similar enone oxidation (eq 3.5).¹⁴ The phenol and *para*-chlorophenol were present in varying ratios, depending on HCl concentration, but showed full conversion to the benzoquinone. *Para*-bromophenol was observed in an oxidation of phenol to benzoquinone, with increasing HBr concentration favoring the bromophenol product (eq 3.6).¹⁵



The mechanism for these oxidations, if discussed, is typically proposed to be coordination of phenol to Cu^{II} as a Cu^{II}-phenoxide, with an intramolecular oxidation yielding the phenoxyl radical and Cu^I (this intramolecular oxidation is a common feature of phenol oxidation

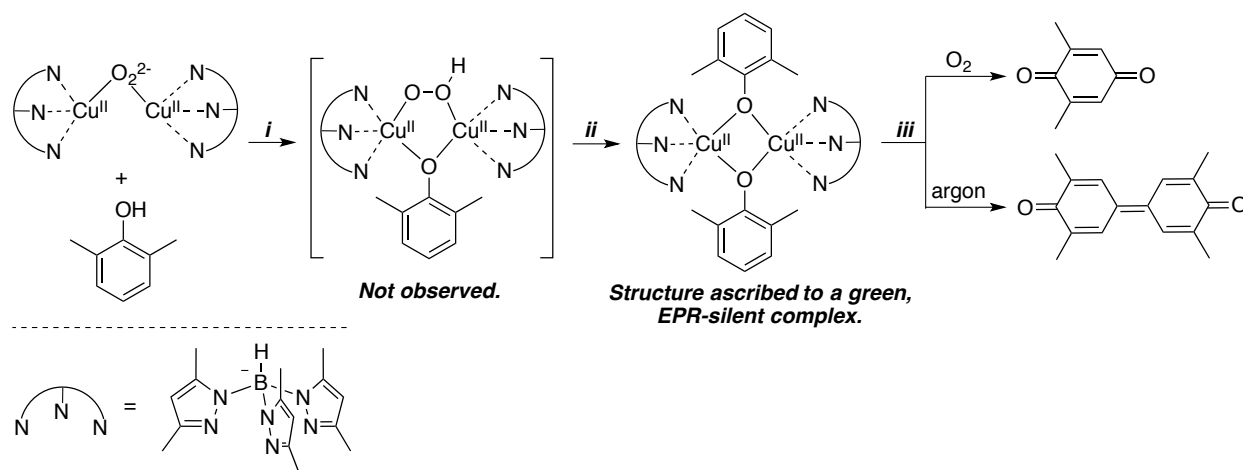
mechanistic proposals; see for example Scheme 1.4B and Scheme 1.5 below).^{12,13,14} The phenoxy radical can then react with a chloride radical or oxygen to ultimately yield chlorophenols and quinones (Scheme 1.1).

Scheme 1.1. Possible Mechanisms for Phenol Oxidation to *Para*-Quinones.



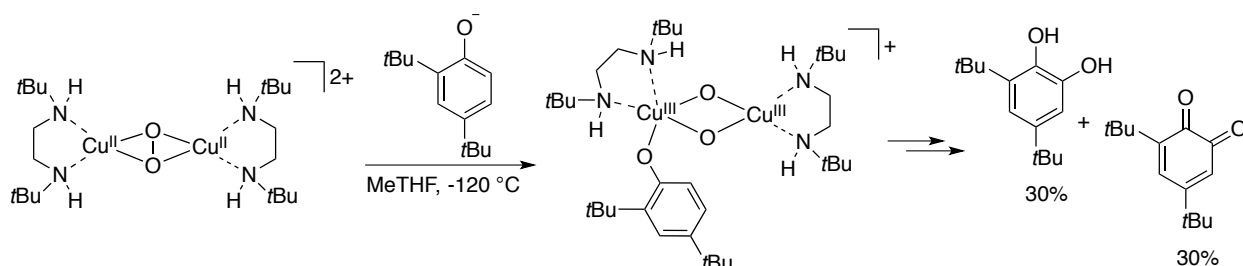
Phenol oxidation to benzoquinone has also been studied using a μ -peroxo binuclear copper complex.¹⁶ Upon phenol addition, a putative bis-phenolate complex forms (*i-ii*) and decomposes (*iii*) to either benzoquinone or diphenoquinone under O_2 or argon, respectively (Scheme 1.2). The authors proposed decomposition of the binuclear Cu^{II}_2 complex would give Cu^I and phenoxy radicals, resulting in the observed reactivity. The reaction showed an induction period attributed to slow deprotonation/coordination of phenol to Cu.

Scheme 1.2. Oxidation of Phenol to Quinones and Diphenoquinones via a Binuclear Complex.



Phenols may also be oxidized to *ortho*-quinones, though there are fewer synthetic methods available when compared to *para*-quinone synthesis.² Research has focused on mechanistic studies to mimic tyrosinase. Stack and coworkers reported that phenolate addition at low temperature to a bis- μ -peroxodicopper(II) complex forms a spectroscopically-identified bis- μ -oxodicopper(III)-phenolate complex in which the O–O bond is fully cleaved (Scheme 1.3).¹⁷ Decomposition of the complex yields catechol and *ortho*-quinone. An electrophilic aromatic substitution mechanism for oxidation of the phenolate was justified by a large negative Hammett parameter (-2.2), inverse kinetic isotope effect (0.83, independent rates of 6-H- or 6-D-substrate), and DFT computations. More recently, a similar bis- μ -peroxodicopper(II) complex with a tridentate neutral nitrogen-donor ligand displayed catalytic activity to yield the *ortho*-quinone with similar Hammett parameter.¹⁸ A base was necessary for phenol oxidation to occur.

Scheme 1.3. *Ortho*-Oxygenation of Phenol by a Bis- μ -Oxodicopper(III)-Phenolate Complex.



1.2.2. Phenol Polymerization.

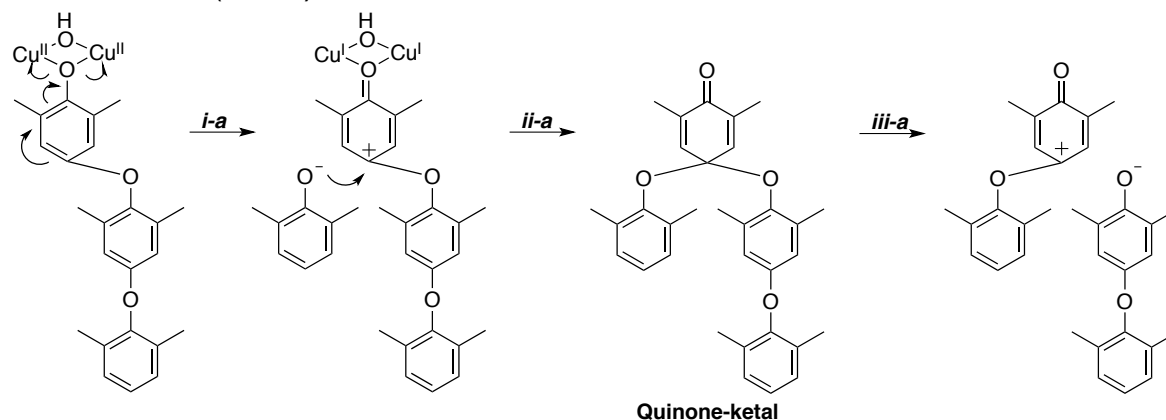
Polymerization of 2,6-dimethylphenol to yield polyphenylene ether (PPE) was first reported using catalytic CuCl under O₂ with excess pyridine and an organic solvent such as nitrobenzene (eqn 3.2).¹⁹ Modern industrial production uses an amine-ligated Cu^{II} catalyst with basic hydroxide ligands in toluene.⁶ With small R groups, such as methyl, or at low

temperatures, PPE is the major reaction product. With large R groups, such as *t*-butyl, or higher temperatures, diphenoquinone is the major product.

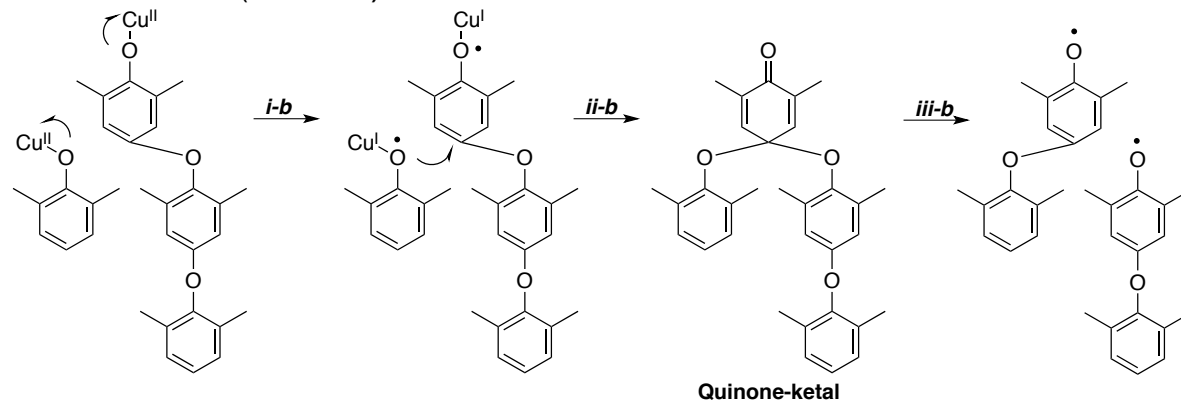
The polymerization mechanism is still under debate, with either ionic or radical mechanism proposed.^{20,21} In the ionic mechanism (Scheme 1.4A), coordination of 2 Cu^{II} centers to phenoxide facilitates a 2-electron oxidation of the arene to yield an aryl-cation (***i-a***). A second phenoxide attacks the cation, resulting in the quinone-ketal intermediate (***ii-a***). “Redistribution” (***iii-a***) of the quinone-ketal remakes an aryl-cation and phenoxide, and polymerization proceeds similarly. In the radical mechanism (Scheme 1.4B), a Cu^{II} coordinates independently to each phenoxide, and oxidation of each to a Cu^I-phenoxyl radical occurs (***i-b***). The quinone-ketal intermediate is formed (***ii-b***) and “redistribution” (***iii-b***) allows polymerization to proceed.

Scheme 1.4. (A) Ionic and (B) Radical Mechanisms for 2,6-Dimethylphenol Polymerization.

A. Ionic Mechanism (Favored)

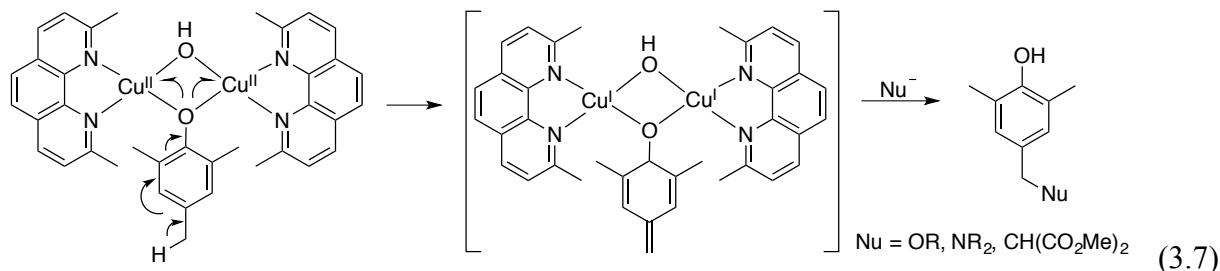


B. Radical Mechanism (Not Favored)



Both proposals involve stepwise rather than chain polymerization as analysis of the polymerization reaction mixture indicated that short oligomers were present throughout the reaction (indicative of stepwise polymerization), rather than just long chains and monomers (indicative of chain polymerization).²² Support for the ionic mechanism includes observation of a 1.7-2.0 [Cu] rate dependence,²³ computational studies supporting the ionic pathway, and crystallization of the proposed neocuproine-ligated Cu^{II}_2 -phenoxide-bridged dimer using 5-fluorophenol.²⁰ Support for the proposed ionic mechanism also includes use of the mechanism to design a Cu-mediated coupling of the *para*-methylphenol sp^3 carbon and nucleophiles (eq 3.7).²⁴

The mechanism presumably proceeds via similar electron-transfer within the Cu^{II}_2 -phenoxide-bridged dimer to give a *para*-alkene that may be attacked by nucleophiles.



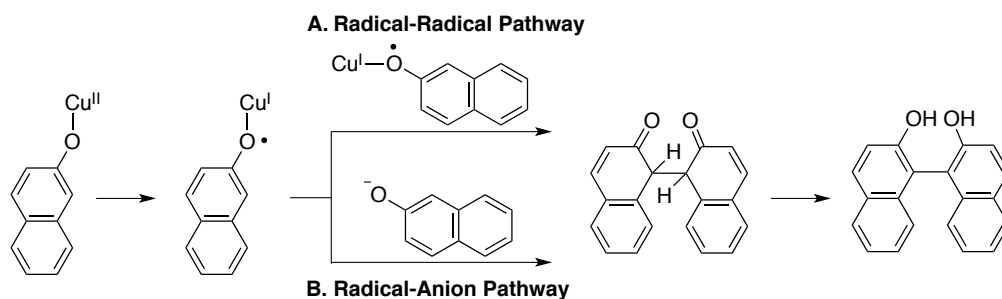
1.2.3. Naphthol and Phenol Coupling.

Naphthol coupling is quite regioselective, can be made enantioselective, and is the preferred route to make BINOL ligands (eq 3.3).⁷ Oxidative dimerization of naphthols was first introduced using silver oxide or potassium ferricyanide as a one-electron oxidant.²⁵ There are two common mechanistic proposals for naphthol coupling; either a radical-radical coupling ($\text{A}\cdot + \text{B}\cdot$; Scheme 1.5A) or a radical-anion coupling ($\text{A}\cdot + \text{B}^-$; Scheme 1.5B).²⁶ Discrimination between these two mechanisms is generally based on analysis of cross-coupled products of electron-rich and electron-poor naphthols. The radical-radical coupling should give homocoupled and cross-coupled products in a ratio based on the reactivity of the naphthols toward one-electron oxidation.²⁷ The radical-anion coupling should be selective for cross-coupling, in which an electron-rich (more easily oxidized) naphthol is oxidized to the radical and then attacked by a naphthoxide formed from the more electron-poor (and more stable anion) naphthol. Product analysis has been used to justify each mechanism for a variety of transition-metal catalysts and mediators. Some examples include proposal of the radical-anion mechanism for copper,²⁸ and the radical-radical mechanism for copper,²⁹ vanadium,³⁰ and heterogeneous ruthenium.³¹ These mechanisms typically show (if drawn at all) an intramolecular oxidation to give the naphthoxyl

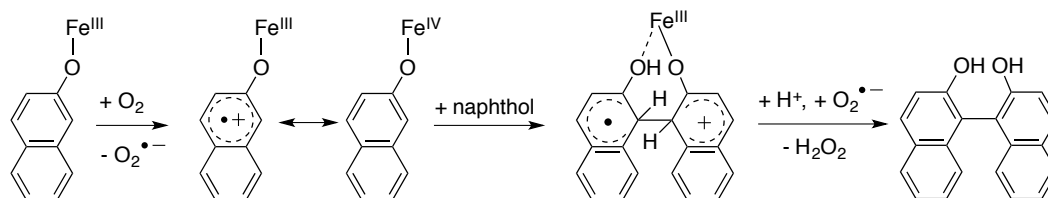
radical (with concurrent reduction of the ligated Cu^{II} to Cu^{I} ; for example Scheme 1.5).

However an intermolecular oxidation by O_2 to give an iron-ligated aryl-radical-cation is proposed in one example (Scheme 1.6).³²

Scheme 1.5. Naphthol Coupling via (A) Radical-Radical or (B) Radical-Anion Mechanisms.



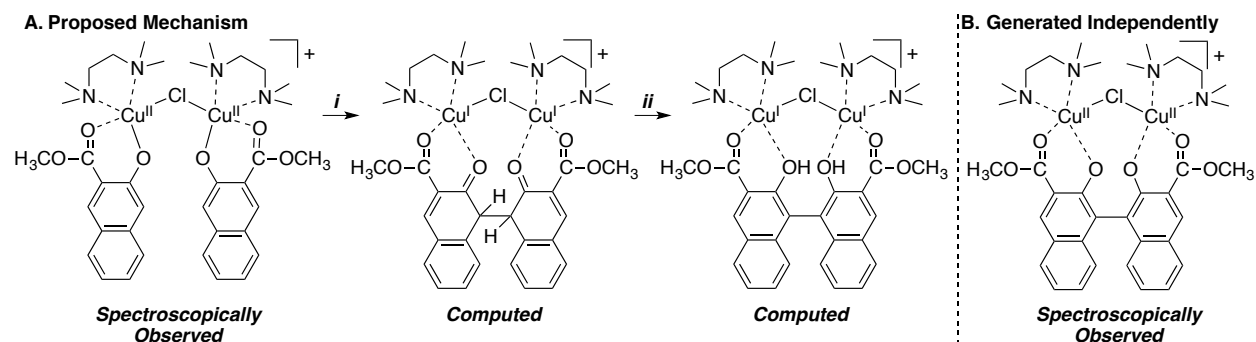
Scheme 1.6. Alternative Naphthol Coupling Mechanism with Intermolecular Oxidation.



Catalysts containing 2 metal ions are often used for naphthol coupling reactions,⁷ suggesting the coupling may take place at a binuclear species. A gas-phase study observed a Cu^{II}_2 -binuclear cluster containing 2 uncoupled naphthol units (Scheme 1.7A).³³ Computations led to the proposed mechanism of (i) C-C coupling in which each Cu^{II} is reduced to Cu^{I} and (ii) a keto-enol tautomerization that yields the BINOL product and is the driving force for the reaction. The actual mechanism of step *i* is unclear (whether radical-radical or radical-anion as previously discussed), though it seems to involve intramolecular electron-transfer from the naphthoxide units to Cu. Direct evidence for this mechanism is not provided as the cluster containing 2 uncoupled naphthol units produced free BINOL with no Cu ligation observed under the reaction

conditions. However, independent generation of a Cu^{II} -binuclear BINOL-ligated cluster (not Cu^{I}) was observed starting from the BINOL (Scheme 1.7B).

Scheme 1.7. Binuclear Naphthol Coupling Mechanism Proposed for a Gas-Phase Reaction.



Phenol coupling is not as regioselective as naphthol coupling and a variety of structurally different products are possible, depending on substitution patterns (Figure 1.1; substrates not limited to *t*-butyl substitution).⁷ The poor regioselectivity is proposed to result from a phenoxy radical intermediate, which has a variety of resonance structures that can account for the varied *para*-, *ortho*-, and O-atom-coupling locations. Mechanistic studies were described above (Scheme 1.2); decomposition of a putative Cu^{II} -diphenoxide complex under argon was proposed to give phenoxy radicals that coupled to give diphenoquinones. The reaction showed an induction period in substrate formation that was base-dependent and ascribed to slow deprotonation/coordination of phenol to Cu.^{16,34} A study of CuCl_2 -mediated oxidation of phenol to diphenoquinone also observed that base was necessary for the reaction to occur.³⁴

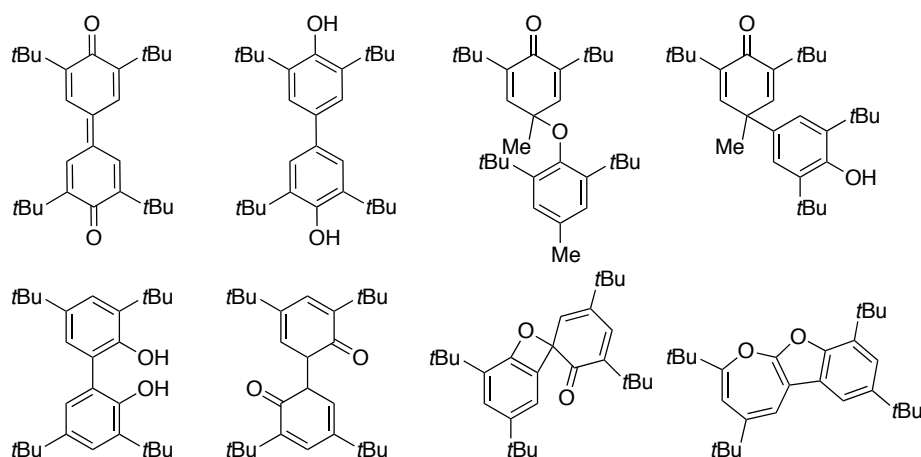


Figure 1.1. Structural Variety of Phenol Homocoupling Products.

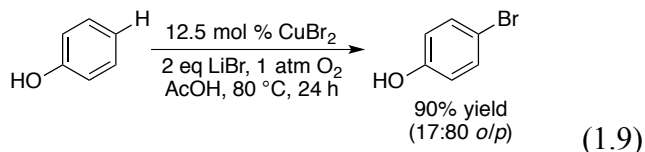
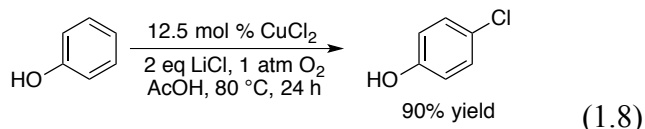
1.3. Oxidative Halogenation of Phenols and Dimethoxybenzenes.

Phenols may be selectively halogenated without over-oxidation to the quinone. Intriguingly, 1,3-dimethoxybenzene may also be halogenated under very similar reaction conditions, despite the substrate's lack of an acidic chelating group. In this section, these reactions are surveyed and their proposed mechanisms are contrasted.

1.3.1. Phenols.

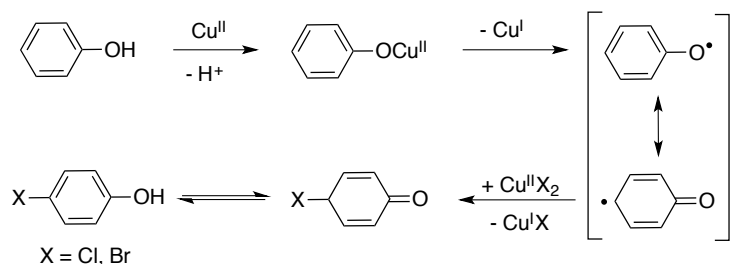
Gusevskaya and coworkers report selective oxidation of phenol (and derivatives) to 4-chlorophenol (eqn 1.8).³⁵ The reaction conditions are similar to those used for industrial oxidation of 2,3,6-trimethylphenol to the *para*-quinone (see previous section), however Gusevskaya and coworkers do not report any overoxidation to the quinone. The selectivity for chlorophenol rather than quinone may result from the less electron-rich nature of phenol compared to the trimethyl-substituted vitamin E precursor. The oxidative *para*-bromination could be carried out under similar reaction conditions using CuBr_2 and LiBr instead of chloride

salts, though it displays lower *para:ortho* selectivity (eq 1.9).³⁶ Anilines may be halogenated under similar conditions.³⁷



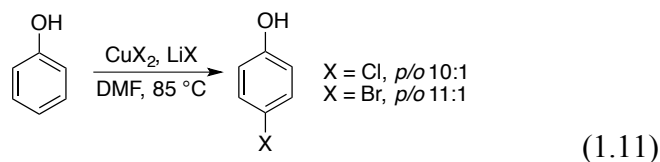
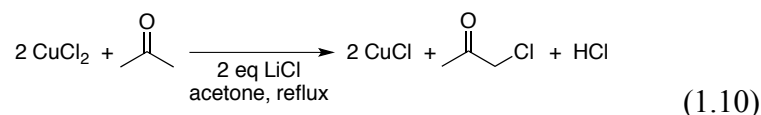
Gusevskaya and coworkers propose a reaction mechanism in which a Cu^{II} -phenoxide forms and subsequently intramolecular electron transfer occurs to generate a phenoxyl radical and Cu^{I} (Scheme 1.8). The phenoxyl radical then abstracts a halide atom from CuX_2 ($\text{X} = \text{Cl}, \text{Br}$) and the haloarene product is generated after tautomerization. Cu^{I} is aerobically reoxidized to the Cu^{II} catalyst. This mechanism is essentially similar to that proposed for phenol and naphthol C-C coupling (see previous section) in that it has the same key steps of Cu^{II} -phenoxide formation followed by an intramolecular electron transfer to generate a phenoxyl radical.

Scheme 1.8. Phenol Halogenation Mechanism Proposed by Gusevskaya and Coworkers.

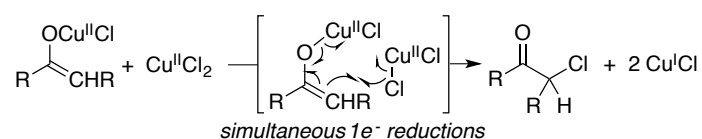


There is some mechanistic precedent for such a proposal. Kochi and coworkers studied CuCl_2 -mediated ketone chlorination rates by reaction aliquot removal and titration of the resultant $\text{Cu}^{\text{I}}\text{Cl}$ (eq 1.10).³⁸ The reaction was determined to be $\frac{1}{2}$ order in Cu concentration and 1st order in halide concentration.³⁹ Kosower and coworkers observed phenol chlorination and

bromination under similar reaction conditions (eq 1.11).⁴⁰ They discussed their observation in context of Kochi's mechanistic study and proposed that a Cu^{II}-phenolate or Cu^{II}-enolate forms under the reaction conditions, and oxidative halogenation occurs by simultaneous electron transfers (Scheme 1.9). One electron from the substrate reduces the ligated Cu^{II}, and a second electron from the substrate combines with a chloride atom, reducing an equivalent of CuCl₂ during the chloride atom transfer. They note that Kochi's ½ order Cu concentration dependence could be caused by dimeric resting state and a rate-determining step (such as oxidation) depending on monomeric Cu.



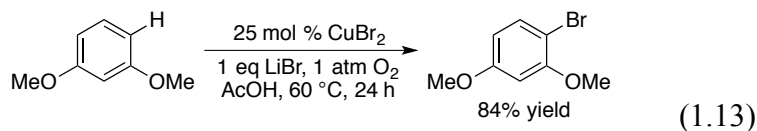
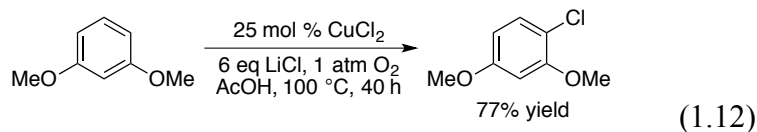
Scheme 1.9. Proposed Mechanism for CuCl₂-Mediated Ketone or Phenol Chlorination.



1.3.2. Dimethoxybenzene.

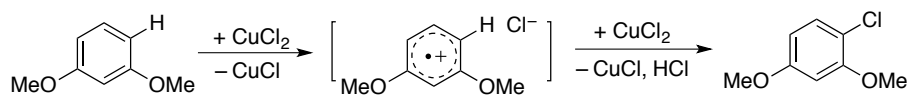
Stahl and coworkers reported Cu-catalyzed aerobic chlorination and bromination of electron-rich methoxy-substituted arenes with halide salts in acetic acid (eqn 1.12 and 1.13).⁴¹ Bromination is more facile than chlorination, proceeding well at lower temperatures (60 vs. 100 °C for the chlorination). The conversion of dimethoxybenzene demonstrates that an acidic

coordinating group (as is present in phenol) is not necessary for arene oxidation. However, dimethoxybenzene chlorination is not as facile as phenol chlorination, requiring higher temperatures and longer reaction times.

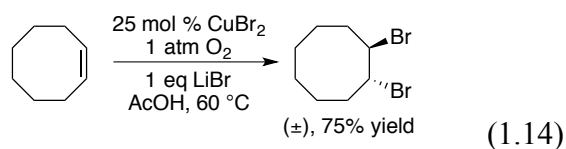


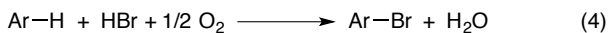
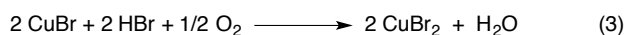
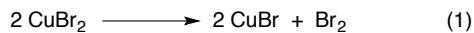
Stahl and coworkers proposed a chlorination mechanism in which Cu^{II} oxidizes the electron-rich arene to the aryl-radical-cation (Scheme 1.10). Chlorine atom transfer occurs from a second equivalent of CuCl_2 and the Wheland-type intermediate (not shown) is deprotonated to give the final product. Cu^{I} is aerobically reoxidized to the Cu^{II} catalyst.

Scheme 1.10. Proposed Mechanism for Dimethoxybenzene Chlorination.



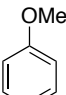
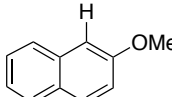
A different mechanism was proposed for dimethoxybenzene bromination. *Cis*-cyclooctene was dibrominated under the same reaction conditions (eq 1.14). This observation was used to support a proposed mechanism in which CuBr_2 disproportionation generates Br_2 and CuBr , and Br_2 brominates the arene (Scheme 1.11). This electrophilic bromination is quite different from the proposed mechanism for chlorination, in which a copper chloride is the active chlorinating reagent.

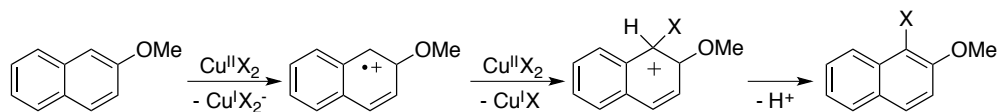


Scheme 1.11. Proposed Mechanism for Arene Bromination Based on CuBr_2 Disproportionation to Generate Br_2 .

There is some precedent for similar methoxyarene halogenation. Bansal and coworkers reported Cu^{II} -mediated chlorination and bromination of anisole and 2-methoxynaphthalene (Table 1.2).⁴² They proposed a mechanism in which the electron-rich arene is oxidized to a radical cation by one equivalent of Cu^{II} , with a second equivalent of Cu^{II} delivering the halide atom (Scheme 1.12). Their proposal was based on previous work that studied electrochemical oxidation of anisole and determined that when anisole is oxidized by 1 electron, it undergoes C-C dimerization at the *para* position.⁴³ Trimethoxybenzene may also be coupled with arylboronic acids⁴⁴ or disulfides and diselenides⁴⁵ under Cu-catalyzed aerobic conditions.

Table 1.2. Cu^{II} -Mediated Oxidative Halogenation of Anisole and 2-Methoxynaphthalene.

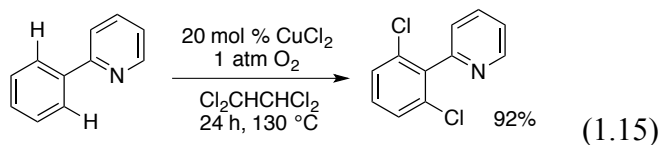
Substrate	Cu	Solv. (reflux)	t (h)	<i>o</i> -X	<i>p</i> -X
	CuCl_2	PhCl	216	4	75
	CuBr_2	PhCl	23	10	90
	CuCl_2	PhCl	5	>98	-
	CuBr_2	PhCl	3	>98	-

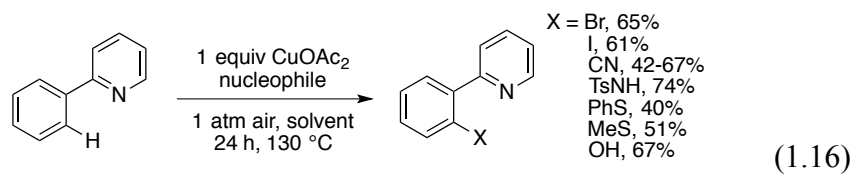
Scheme 1.12. Proposed Mechanism for 2-Methoxynaphthalene Chlorination.

1.4. Chelate-Directed Oxidations.

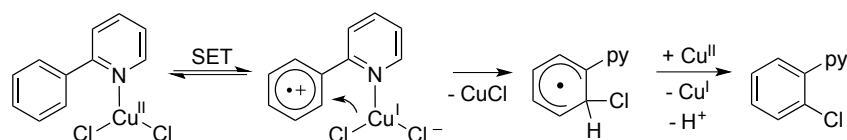
Chelating directing groups enable aryl-C-H oxidations with a variety of nucleophiles. Directing groups can facilitate intermolecular coupling or intramolecular annulation. These reactions resemble Pd-catalyzed chelate-directed C-H functionalization reactions,⁴⁶ but by using Cu can be linked to aerobic catalytic turnover. The mechanisms of these reactions, whether single-electron-transfer or organometallic, are ambiguous. Leading examples of this type of reactivity, as well as any mechanistic data, are surveyed in this section.

Yu and coworkers reported the first aerobic Cu-catalyzed oxidation of 2-phenylpyridine.⁴⁷ Catalytic chlorination was possible at forcing conditions, with HCl generated from the solvent (eq 1.15). Reactivity with diverse other nucleophiles was also possible, but required stoichiometric copper (eq 1.16).⁴⁸ Some mechanistic detail was provided based on experiments with chlorination and bromination; electron-donating groups aided reactivity and with an *ortho*-mono-deuterated substrate, there was no intramolecular kinetic isotope effect (KIE = 1). The lack of KIE indicates that the rate-determining step of the reaction does not involve C-H activation. From these data a single-electron-transfer mechanism was proposed (Scheme 1.13). In the proposed mechanism, Cu^{II} coordinates to the pyridine nitrogen and an intramolecular electron-transfer occurs to give the aryl-radical-cation and Cu^I. Chloride transfer from Cu^I generates a radical intermediate that is subsequently deprotonated to yield the final product. It is uncertain if this mechanism holds true for the non-halide nucleophiles.

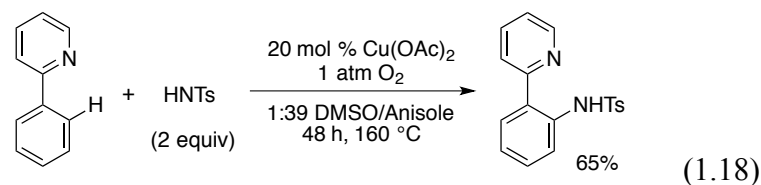
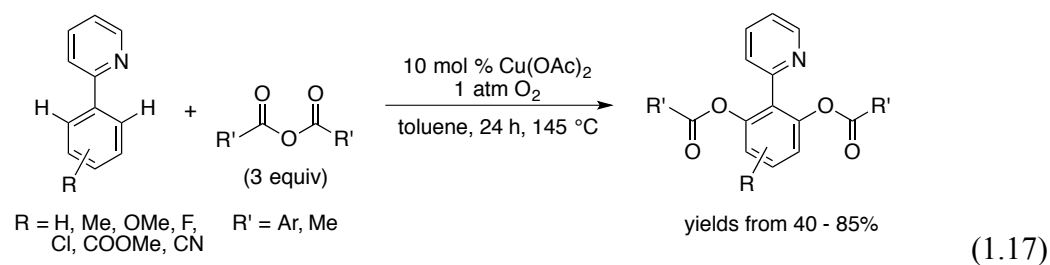




Scheme 1.13. Single-Electron-Transfer Mechanism Proposed for 2-Phenylpyridine Chlorination.



Later reports achieved catalytic C-O and C-N bond formation under high-temperature conditions. Chang and coworkers reported catalytic difunctionalization of 2-arylpyridines using alkyl and aryl anhydrides (eq 1.17).⁴⁹ Nicholas and coworkers achieved catalytic amidation of 2-phenylpyridine through judicious solvent choice and high temperatures (eq 1.18).⁵⁰ Mechanistic studies are not available for these reactions.



1.5. Functionalization of Acidic C-H Bonds.

Arenes with relatively acidic C-H bonds are good substrates for Cu-catalyzed functionalization at the acidic site (Figure 1.2).⁵¹ Reactions include homocoupling, C-C coupling

between acidic C-H bonds, and cross-coupling with nucleophiles. Leading examples of these reactions are presented in this section.

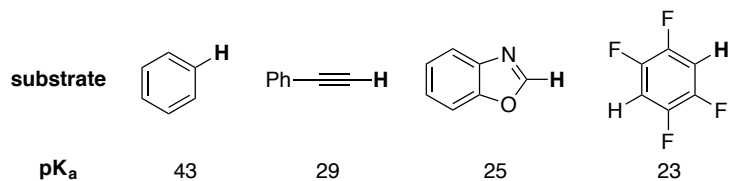
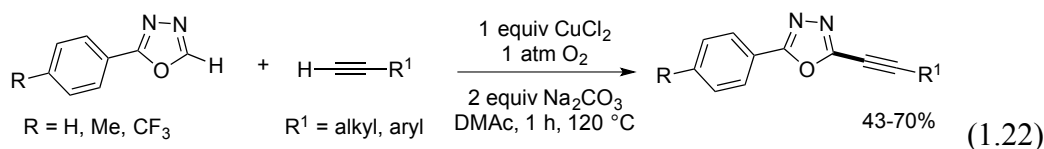
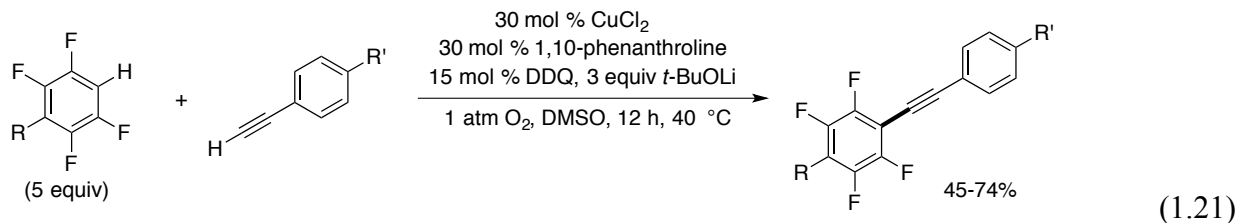
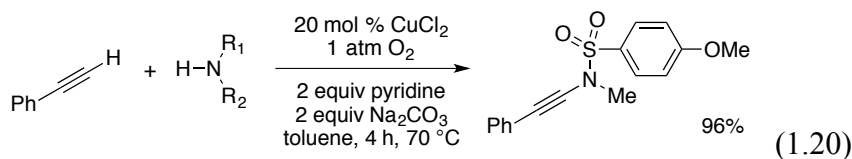
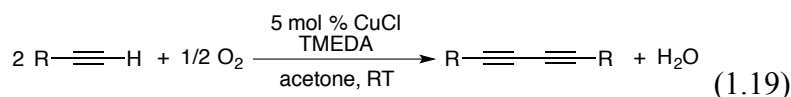
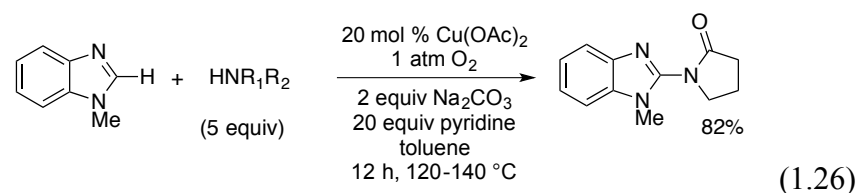
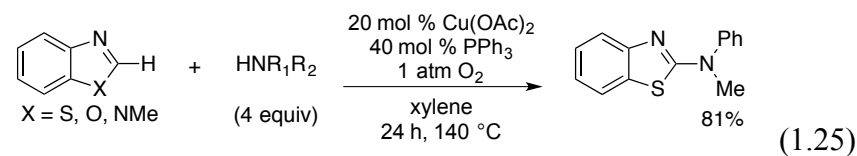
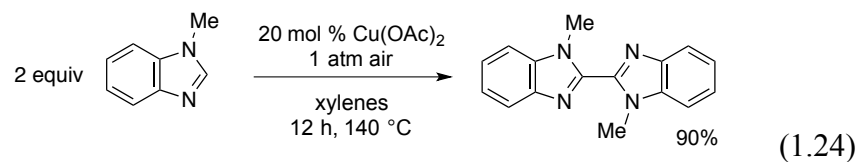
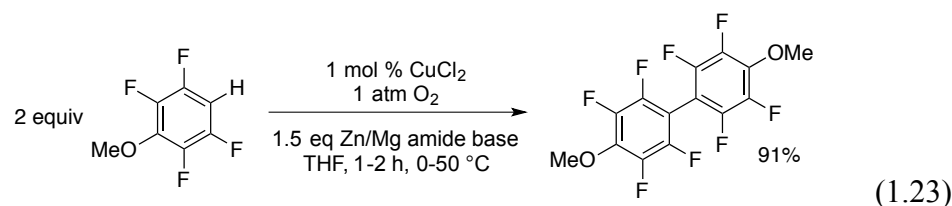


Figure 1.2. Aryl-C-H Bond pK_a Values.

The Glaser-Hay coupling of terminal alkynes is a prominent and historic example of Cu-catalyzed reactivity of acidic C-H bonds (eq 1.19).⁵² Stahl and coworkers synthesized ynamides by coupling alkynes with amide nucleophiles (eq 1.20).⁵³ Su and coworkers demonstrated cross-coupling of alkynes and fluoroarenes (eq 1.21).⁵⁴ Miura and coworkers coupled alkynes with heteroarenes (1.22).⁵⁵



Daugulis and coworkers reported Cu-catalyzed homocoupling of electron-deficient fluoroarenes and heteroarenes, which required Zn/Mg amide bases (eq 1.23).⁵⁶ Bao and coworkers extended the methodology of coupling of heteroarenes such as benzimidazoles, benzoxazoles, and thiazoles, with no base needed (eq 1.24).⁵⁷ Mori and coworkers developed heterocycle cross-coupling with aryl and alkyl amines (eq 1.25).⁵⁸ Shortly after, Schreiber and coworkers developed a similar cross coupling, with pyridine instead of PPh₃ (eq 1.26).⁵⁹

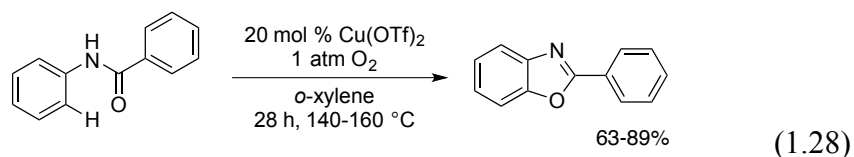
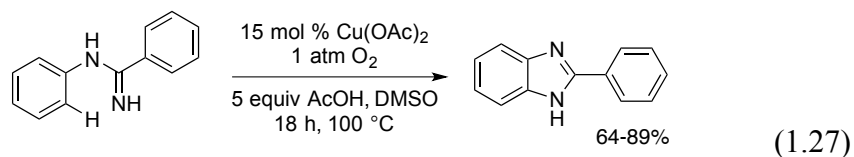


1.6. Oxidative Annulations.

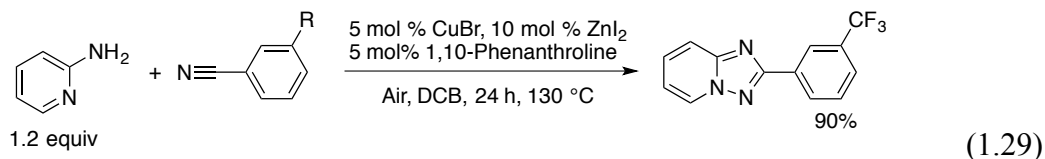
Various 5- and 6-membered heteroarenes have been synthesized by Cu-catalyzed aerobic oxidative annulation. Typically an arene C-H bond couples with a pendant heteroatom functionality. Presumably the heteroatom coordinates to Cu, serving a directing group to position

Cu near the aryl-C-H bond, and subsequent coupling can occur. A few leading examples are presented in this section.

Buchwald and coworkers developed cyclization of amidines to yield benzimidazoles (eq 1.27).⁶⁰ Nagasawa and coworkers reported a similar cyclization of benzanilides to yield benzoxazoles (eq 1.28).⁶¹ The mechanisms of these reactions are uncertain. Both groups noted that the reactions proceed more rapidly with electron-rich substrates. Nagasawa and coworkers reported the lack of a deuterium isotope effect in an intramolecular competition study with a mono-*ortho*-deuterated substrate (KIE =1).

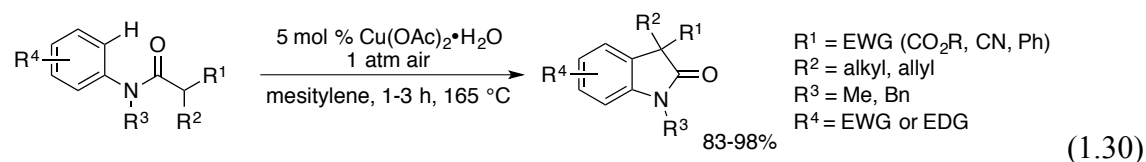


Aryl nitriles also serve as good substrates for cycloadditions.⁶² These reactions are somewhat reminiscent of Cu-catalyzed alkyne-azide cycloaddition “click” reactions,⁶³ but are much less facile.

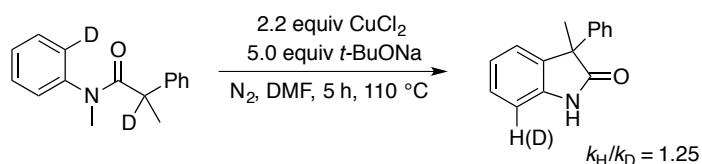


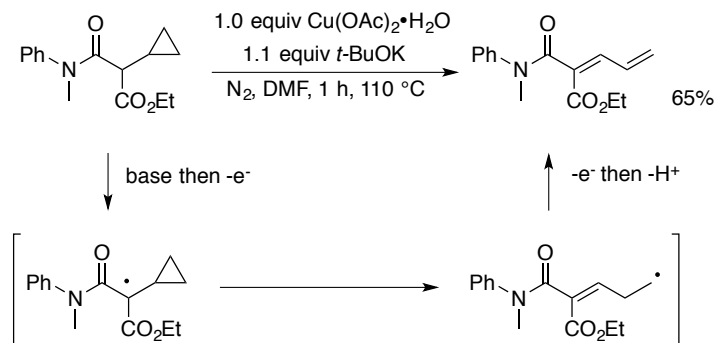
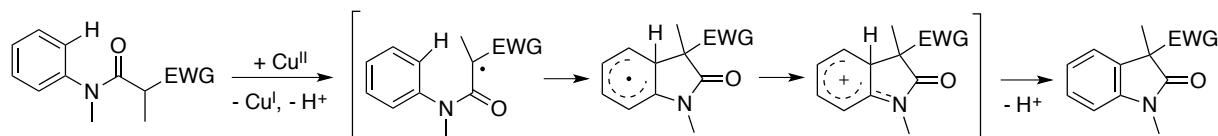
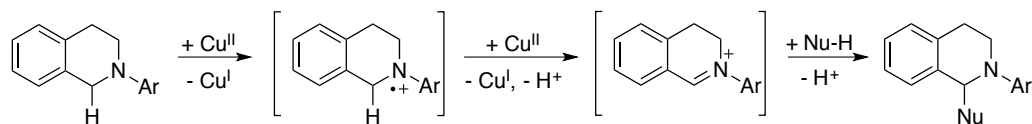
Taylor and coworkers developed Cu-catalyzed cyclization of amide-enolates. Anilides were converted to oxindoles at high temperatures under air (eq 1.30).⁶⁴ Kündig and coworkers determined that the reaction has a secondary isotope effect of 1.25, which indicates that C-H bond cleavage is not involved in the rate-determining step of the reaction (Scheme 1.14).⁶⁵

Taylor and coworkers subjected an anilide substrate containing a cyclopropyl radical probe to the reaction conditions (Scheme 1.15).⁶⁶ No oxindole products were detected; instead a dienyl aniline from radical fragmentation of the cyclopropyl substituent was produced. Based on these experiments, it is likely that Cu^{II} oxidizes the anilide to generate a radical amide-enolate intermediate (Scheme 1.16). Subsequent cyclization and deprotonation yield the oxindole product. This mechanism is reminiscent of the mechanism of amine α -functionalization, or “cross-dehydrogenative coupling” (Scheme 1.17).⁶⁷ In that reaction, 2 equivalents of Cu^{II} successively oxidize the electron-rich amine to an amine radical-cation, then an iminium. A nucleophile then attacks the iminium and after deprotonation yields the α -functionalized product.



Scheme 1.14. Anilide Cyclization Kinetic Isotope Intramolecular Competition Experiment.



Scheme 1.15. Anilide Cyclization Radical Probe Experiment.**Scheme 1.16.** Proposed Mechanism for Radical Cyclization of Anilide to Oxindole.**Scheme 1.17.** Mechanism of “Cross-Dehydrogenative Coupling” Amine α -Functionalization.**1.7. Aryl-Copper Complexes Relevant to Organometallic C-H Activation Mechanisms.**

Macrocyclic aryl ligands appear to be beneficial in stabilizing high Cu oxidation states. Confused porphyrin ligands have been used to generate aryl- Cu^{II} and aryl- Cu^{III} complexes. Simpler macrocyclic ligands have also been used, and studies by Stahl and Ribas in particular have provided valuable insight into organometallic mechanisms of Cu-mediated C-H functionalization. Leading examples of these complexes and relevant mechanistic studies are surveyed in this section.

Latos-Grażyński and co-workers prepared **1** by mixing the ligand with $\text{Cu}(\text{OAc})_2$ in THF under an inert atmosphere, and also prepared an *N*-methyl version not shown (Figure 1.3).⁶⁸ **1** was characterized with UV-visible and NMR spectroscopy. Furuta and Otsuka prepared **2** and **3** by mixing the ligands with $\text{Cu}(\text{OAc})_2$ in CHCl_3 at room temperature or reflux, respectively.^{69,70} **2** and **3** were characterized with X-ray crystallography. Furuta, Otsuka, and coworkers determined that the aryl- Cu^{II} complex **4** could be oxidized to the aryl- Cu^{III} complex **5** with DDQ, and reversibly reduced with *p*-toluenesulfonylhydrazide (eq 1.31).⁷¹ These results confirm that Cu^{II} salts can metalate aryl-C-H bonds to form aryl- Cu^{II} complexes that can be subsequently oxidized to aryl- Cu^{III} complexes.

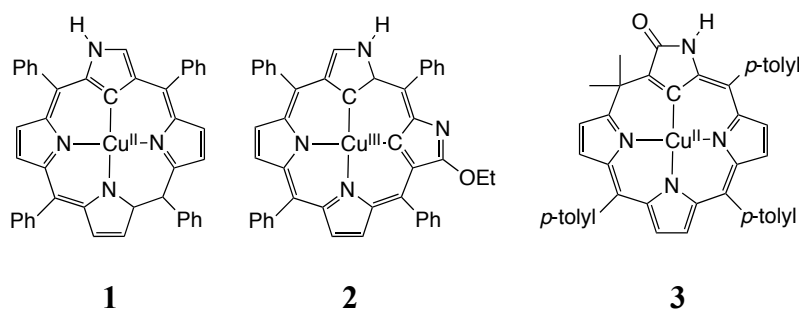
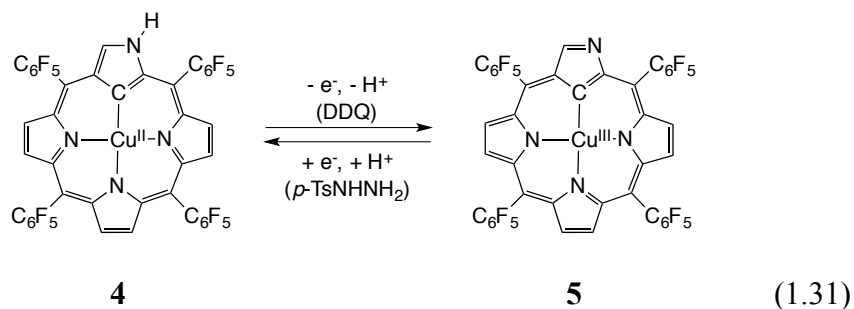
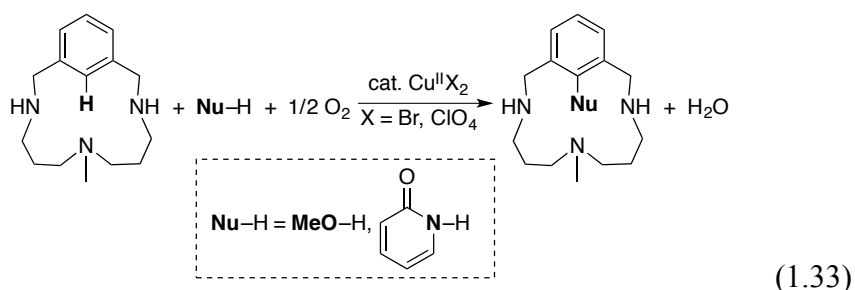
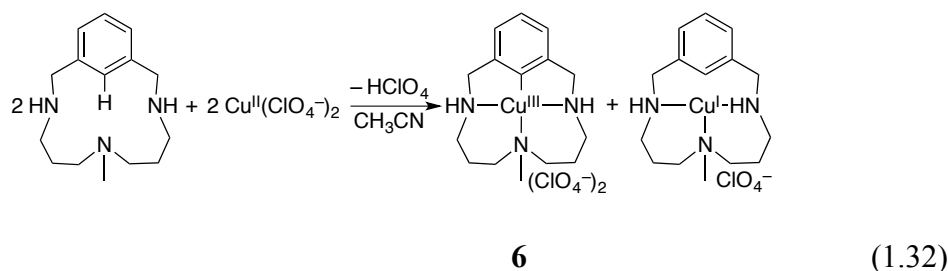


Figure 1.3. Aryl- Cu^{II} and Aryl- Cu^{III} Complexes of *N*-Confused Porphyrins.



Ribas, Llobet, Stack and coworkers reported that a triazamacrocyclic aryl- Cu^{III} complex **6** could be generated from mixing the ligand and $\text{Cu}(\text{ClO}_4)_2$ (eq 1.32).⁷² The Cu^{II} salt disproportionates into 0.5 eq aryl- Cu^{III} and 0.5 eq Cu^{I} . A mechanistic study provided evidence

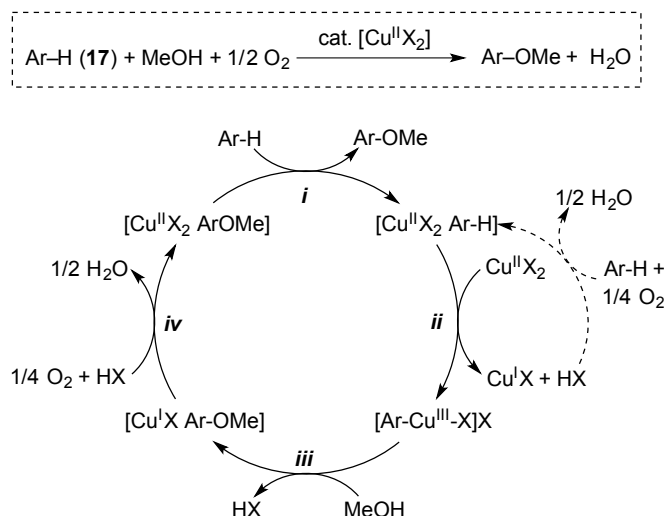
that formation of **6** occurs directly from the ligand through concerted proton-coupled electron-transfer (PCET).⁷³ Huffman and Stahl reported C-N reductive elimination from **6**.⁷⁴ Stahl, Ribas, and coworkers demonstrated the relevance of this reactivity to catalytic C-H oxidation by showing that CuBr₂ and Cu(ClO₄)₂ catalyze aerobic oxidation of the arene C-H bond in to C=O and C-N bonds in the presence of methanol and pyridone, respectively (eq 1.33).⁷⁵ The aryl-Cu^{III} species was directly observed and established as a kinetically competent intermediate. This work provided the first direct evidence for an organometallic pathway in Cu-catalyzed aerobic C-H oxidation. Reactivity was further extended to other oxygen⁷⁶ and halogen⁷⁷ nucleophiles. Wang and coworkers reported similar reactivity with a related macrocyclic aryl-Cu^{III} complex.⁷⁸



These observations provide the clearest mechanistic insights to date into a Cu-catalyzed aerobic C-H oxidation reaction. The proposed mechanism (Scheme 1.18) is initiated by complexation of the macrocyclic arene to Cu^{II} (*i*), followed by C-H activation through Cu^{II} disproportionation to give the aryl-Cu^{III} intermediate (*ii*). Subsequent reaction of the aryl-Cu^{III} with methanol results in formation of the methoxylated arene and Cu^I (*iii*). Rapid reoxidation of

Cu^{I} to Cu^{II} by O_2 (**iv**) completes the catalytic cycle; the same aerobic reoxidation of Cu^{I} occurs in the stoichiometric synthesis of the aryl- Cu^{III} complex (dashed arrows).

Scheme 1.18. Proposed Catalytic Cycle for Cu-Catalyzed Aerobic Oxidative Methoxylation of the Triazamacrocyclic Arene.



1.8. Conclusions.

A variety of coupling reactions can be carried out using Cu^{II} -mediated aerobic oxidation procedures. The reactions are of interest on industrial and laboratory scale, however little is known about the mechanisms of these reactions. Oxidations of electron-rich arenes such as phenols likely proceed through SET mechanisms. Oxidations of less electron-rich substrates may proceed through either SET or organometallic mechanisms. Studies of macrocyclic organometallic aryl- Cu^{II} and aryl- Cu^{III} complexes have provided insight into organometallic mechanisms of Cu^{II} -mediated C-H activation. Further research is necessary to understand the divergent SET and organometallic mechanisms and the conditions that select for each mechanism.

1.9. References and Notes.

1. Wendlandt, A. E.; Suess, A. M.; Stahl, S. S. "Copper-Catalyzed Aerobic Oxidative C-H Functionalizations: Trends and Mechanistic Insights." *Angew. Chem. Int. Ed.* **2011**, *50*, 11062-11087.
2. Allen, S. E.; Walvoord, R. R.; Padilla-Salinas, R.; Kozlowski, M. C. "Aerobic Copper-Catalyzed Organic Reactions." *Chem. Rev.* **2013**, DOI: 10.1021/cr300527g.
3. (a) Shi, Z.; Zhang, C.; Tang, C.; Jiao, N. "Recent advances in transition-metal catalyzed reactions using molecular oxygen as the oxidant." *Chem. Soc. Rev.* **2012**, *41*, 3381-3430. (b) Punniyamurthy, T.; Rout, L. "Recent advances in copper-catalyzed oxidation of organic compounds." *Coord. Chem. Rev.* **2008**, *252*, 134-154. (c) Gamez, P.; Aubel, P. G.; Driessen, W. L.; Reedijk, J. "Homogeneous bio-inspired copper-catalyzed oxidation reactions." *Chem. Soc. Rev.* **2001**, *30*, 376-385. (d) Liu, C.; Zhang, H.; Shi, W.; Lei, A. "Bond Formations between Two Nucleophiles: Transition Metal Catalyzed Oxidative Cross-Coupling Reactions." *Chem. Rev.* **2011**, *111*, 1780-1824.
4. Zuberbüler, A. D. "Interaction of Cu^I Complexes with Dioxygen." In *Metal Ions in Biological Systems, Vol. 5*; Marcel Dekker, **1976**, 325-368.
5. Baldenius, K.-U.; von dem Bussche-Hünnefeld, L.; Hilgemann, E.; Hoppe, P.; Stürmer, R. "Vitamins, 4. Vitamin E (Tocopherols, Tocotrienols)." In *Ullmann's Encyclopedia of Industrial Chemistry*; Wiley-VCH Verlag GmbH & Co. KGaA: 2000.
6. Bussink, J.; van de Grampel, H. T. "Poly(Phenylene) Oxides." In *Ullmann's Encyclopedia of Industrial Chemistry*; Wiley-VCH Verlag GmbH & Co. KGaA: 2000.
7. For a recent comprehensive review that includes naphthol and phenol coupling, see ref 2.

8. Brenner, W. (Hoffmann-La Roche Inc.), "Process for Oxidizing Phenols to Quinones." US 3796732, **1974**.
9. (a) Isshiki, T.; Yui, T.; Abe, M.; Jono, M. (Mitsubishi Gas Chemical Company, Inc.), "Process for the Preparation of 2,3,5-Trimethylbenzoquinone." EP 167153, **1985**. (b) Isshiki, T.; Yui, T.; Abe, M.; Jono, M.; Uno, H. (Mitsubishi Gas Chemical Company, Inc.), "Process for the Production of 2,3,5-Trimethylbenzoquinone." US 4828762, **1989**.
10. (a) Bockstiegel, B.; Hoercher, U.; Laas, H.; Jessel, B.; Grafen, P. (BASF Aktiengesellschaft) "Verfahren zur Herstellung von 2,3,5-Trimethyl-p-benzochinon." EP 475272, **1991**. (b) Hirose, N.; Hamamura, K.; Inai, Y.; Ema, K.; Banba, T.; Kijima, S. (Eisai Co., Ltd.), "Process for Preparing 2,4,5-Trimethylbenzoquinone." US 5104996, **1992**.
11. Benzoquinone is commercially produced by (a) diisopropylbenzene oxidation using O₂ and acid (which also produces acetone), (b) phenol oxidation using H₂O₂, or (c) historically by aniline oxidation using MnO₂/H₂SO₄. See the following leading examples, respectively: (a) Franz, G.; Sheldon, R. A. "Oxidation." In *Ullmann's Encyclopedia of Industrial Chemistry*; Wiley-VCH Verlag GmbH & Co. KGaA: 2000. (b) Hudnall, P. M. "Hydroquinone." In *Ullmann's Encyclopedia of Industrial Chemistry*; Wiley-VCH Verlag GmbH & Co. KGaA: 2000. (c) Shearon, W. H.; Davy, L. G.; von Bramer, H. "Hydroquinone Manufacture." *Ind. Eng. Chem.* **1952**, *44*, 1730-1735.
12. Beltrame, P.; Beltrame, P. L.; Carniti, P. "Kinetics and Byproducts of the Liquid-Phase Oxidation of Phenol to *p*-Benzoquinone Catalyzed by CuCl₂." *Ind. Eng. Chem. Prod. Res. Dev.* **1979**, *18*, 208-211.

13. (a) Shimizu, M.; Watanabe, Y.; Orita, H.; Hayakawa, T.; Takehira, K. "Synthesis of Alkyl Substituted *p*-Benzoquinones from the Corresponding Phenols Using Molecular Oxygen Catalyzed by Copper(II) Chloride-Amine Hydrochloride Systems." *Bull. Chem. Soc. Jpn.* **1992**, *65*, 1522-1526. (b) Takehira, K.; Orita, H.; Shimizu, M.; Hayakawa, T. (The State of Japan), "Method for the Preparation of 2,3,5-Trimethylbenzoquinone." EP 369823, **1989**.
14. Thoemel, F.; Hoffmann, W. (BASF Aktiengesellschaft), "Preparation of 2,3,5-Trimethyl-*p*-Benzoquinone." US 4491545, **1991**.
15. Mills, R. C.; Chuck, T. L. (General Electric Co.), "Method of Preparing Mixtures of Bromophenols and Benzoquinones." US 6693221, **2004**.
16. Kitajima, N.; Koda, T.; Iwata, Y.; Morooka, Y. "Reaction aspects of a μ -peroxo binuclear copper(II) complex." *J. Am. Chem. Soc.* **1990**, *112*, 8833-8839.
17. Mirica, L. M.; Vance, M.; Rudd, D. J.; Hedman, B.; Hodgson, K. O.; Solomon, E. I.; Stack, T. D. P. "Tyrosinase Reactivity in a Model Complex: An Alternative Hydroxylation Mechanism." *Science* **2005**, *308*, 1890-1892.
18. Hoffmann, A.; Citek, C.; Binder, S.; Goos, A.; Rübhausen, M.; Troeppner, O.; Ivanović-Burmazović, I.; Wasinger, E. C.; Stack, T. D. P.; Herres-Pawlis, S. "Catalytic Phenol Hydroxylation with Dioxygen: Extension of the Tyrosinase Mechanism beyond the Protein Matrix." *Angew. Chem. Int. Ed.* **2013**, *52*, 5398-5401.
19. (a) Hay, A. S.; Blanchard, H. S.; Endres, G. F.; Eustance, J. W. "Polymerization by Oxidative Coupling." *J. Am. Chem. Soc.* **1959**, *81*, 6335-6336. (b) Hay, A. S. "Polymerization by oxidative coupling: Discovery and commercialization of PPO® and Noryl® resins." *J. Polym. Sci., Part A: Polym. Chem.* **1998**, *36*, 505-517.

20. For a review of the mechanistic debate with emphasis on experimental data corroborating the ionic pathway, see: Gamez, P.; Gupta, S.; Reedijk, J. "Copper-catalyzed oxidative coupling of 2,6-dimethylphenol: A radicalar or an ionic polymerization?" *C. R. Chimie* **2007**, *10*, 295-304.
21. The review by Kozlowski et al. (ref 2) and Ullmann's Encyclopedia (ref 6) also cover the mechanistic debate, noting that the ionic mechanism is favored over the radical mechanism.
22. Endres, G. F.; Kwiatek, J. "Polymerization by oxidative coupling. III. Mechanistic type in the copper-amine catalyzed polymerization of 2,6-dimethylphenol." *Journal of Polymer Science* **1962**, *58*, 593-609.
23. Chung, Y. M.; Ahn, W. S.; Lim, P. K. "Organic/aqueous interfacial synthesis of poly(2,6-dimethyl-1,4-phenylene oxide) using surface-active copper complex catalysts." *Appl. Catal. A Gen.* **2000**, *192*, 165-174.
24. Boldron, C.; Gamez, P.; Tooke, D. M.; Spek, A. L.; Reedijk, J. "Copper-Mediated Selective Oxidation of a C-H Bond." *Angew. Chem. Int. Ed.* **2005**, *44*, 3585-3587.
25. Pummerer, R.; Frankfurter, F. "Über ein neues organisches Radikal. I. Mitteilung über die Oxydation der Phenole." *Chem. Ber.* **1914**, *47*, 1472-1493.
26. A third proposal is often mentioned in the following references, but generally not supported by the authors: A naphthoxide may be oxidized by 2 electrons to the arene cation, then attacked by a second naphthoxide to give the coupled product. This mechanism is similar to the "ionic" mechanism proposed for phenol polymerization.
27. "Reactivity" of the naphthol starting material is generally correlated to cyclic voltammetry measurement of the oxidation potential of the naphthol; see the following references.

28. The radical-anion coupling mechanism was proposed based on high cross-coupling selectivity between electron-rich and electron-poor substrates as well as ab initio calculations: Smrcina, M.; Vyskocil, S.; Maca, B.; Polasek, M.; Claxton, T. A.; Abbott, A. P.; Kocovsky, P. "Selective Cross-Coupling of 2-Naphthol and 2-Naphthylamine Derivatives. A Facile Synthesis of 2,2',3-Trisubstituted and 2,2',3,3'-Tetrasubstituted 1,1'-Binaphthyls." *J. Org. Chem.* **1994**, *59*, 2156-2163.
29. The radical-radical coupling mechanism was proposed based on statistical mixtures (based on reactivity) of cross-coupled products and some sideproducts ascribed to radical reactions, such as quinones and aryl-iodides: Li, X.; Hewgley, J. B.; Mulrooney, C. A.; Yang, J.; Kozlowski, M. C. "Enantioselective Oxidative Biaryl Coupling Reactions Catalyzed by 1,5-Diazadecalin Metal Complexes: Efficient Formation of Chiral Functionalized BINOL Derivatives." *J. Org. Chem.* **2003**, *68*, 5500-5511.
30. The radical-radical coupling mechanism was proposed based on statistical mixtures (based on reactivity) of cross-coupled products: Guo, Q.-X.; Wu, Z.-J.; Luo, Z.-B.; Liu, Q.-Z.; Ye, J.-L.; Luo, S.-W.; Cun, L.-F.; Gong, L.-Z. "Highly Enantioselective Oxidative Couplings of 2-Naphthols Catalyzed by Chiral Bimetallic Oxovanadium Complexes with Either Oxygen or Air as Oxidant." *J. Am. Chem. Soc.* **2007**, *129*, 13927-13938.
31. The radical-radical coupling mechanism was proposed based on statistical mixtures (based on reactivity) of cross-coupled products: Matsushita, M.; Kamata, K.; Yamaguchi, K.; Mizuno, N. "Heterogeneously Catalyzed Aerobic Oxidative Biaryl Coupling of 2-Naphthols and Substituted Phenols in Water." *J. Am. Chem. Soc.* **2005**, *127*, 6632-6640.

32. Egami, H.; Matsumoto, K.; Oguma, T.; Kunisu, T.; Katsuki, T. "Enantioenriched Synthesis of C1-Symmetric BINOLs: Iron-Catalyzed Cross-Coupling of 2-Naphthols and Some Mechanistic Insight." *J. Am. Chem. Soc.* **2010**, *132*, 13633-13635.
33. Roithová, J.; Milko, P. "Naphthol Coupling Monitored by Infrared Spectroscopy in the Gas Phase." *J. Am. Chem. Soc.* **2009**, *132*, 281-288.
34. Ochiai, E. "Mechanism of oxidative coupling reaction catalysed by cuprous chloride-amine complex." *Tetrahedron* **1964**, *20*, 1831-1841.
35. (a) Menini, L.; Gusevskaya, E. V. "Novel highly selective catalytic oxychlorination of phenols." *Chem. Commun.* **2006**, 209-211. (b) Menini, L.; Gusevskaya, E. V. "Aerobic oxychlorination of phenols catalyzed by copper(II) chloride." *Appl. Catal. A: Gen.* **2006**, *309*, 122-128.
36. Menini, L.; Parreira, L. A.; Gusevskaya, E. V. "A practical highly selective oxybromination of phenols with dioxygen." *Tetrahedron Lett.* **2007**, *48*, 6401-6404.
37. Menini, L.; da Cruz Santos, J. C.; Gusevskaya, E. V. "Copper-Catalyzed Oxybromination and Oxychlorination of Primary Aromatic Amines Using LiBr or LiCl and Molecular Oxygen." *Adv. Synth. Catal.* **2008**, *350*, 2052-2058.
38. Kochi, J. K. "The Reduction of Cupric Chloride by Carbonyl Compounds." *J. Am. Chem. Soc.* **1955**, *77*, 5274-5278.
39. In this study, Kochi proposes a mechanism where one molecule of CuCl_2 is reduced by 2 electrons to Cu^0 , yielding the chlorinated product and HCl. The 2-electron reduction of Cu is no longer generally accepted, so the mechanism proposed by Kosower and coworkers is preferentially discussed.

40. (a) Kosower, E. M.; Cole, W. J.; Wu, G. S.; Cardy, D. E.; Meisters, G. "Halogenation with Copper(II). I. Saturated Ketones and Phenol." *J. Org. Chem.* **1963**, *28*, 630-633. (b) Kosower, E. M.; Wu, G. S. "Halogenation with Copper(II). II. Unsaturated Ketones." *J. Org. Chem.* **1963**, *28*, 633-638.
41. Yang, L.; Lu, Z.; Stahl, S. S. "Regioselective copper-catalyzed chlorination and bromination of arenes with O₂ as the oxidant." *Chem. Commun.* **2009**, 6460-6462.
42. Bansal, S. R.; Nonhebel, D. C.; Mancilla, J. M. "Reactions of copper(II) halides with aromatic compounds-IX: Reactions of 1- and 2-alkoxynaphthalenes." *Tetrahedron* **1973**, *29*, 993-999.
43. Bechgaard, K.; Hammerich, O.; Moe, N. S.; Ronlán, A.; Svanholm, U.; Parker, V. D. "Anodic coupling of simple aryl ethers. Electrochemical synthesis of methoxybiphenyl cation radicals." *Tetrahedron Lett.* **1972**, *13*, 2271-2274.
44. Ban, I.; Sudo, T.; Taniguchi, T.; Itami, K. "Copper-Mediated C-H Bond Arylation of Arenes with Arylboronic Acids." *Org. Lett.* **2008**, *10*, 3607-3609.
45. Zhang, S.; Qian, P.; Zhang, M.; Hu, M.; Cheng, J. "Copper-Catalyzed Thiolation of the Di- or Trimethoxybenzene Arene C-H Bond with Disulfides." *J. Org. Chem.* **2010**, *75*, 6732-6735.
46. Lyons, T. W.; Sanford, M. S. "Palladium-Catalyzed Ligand-Directed C-H Functionalization Reactions." *Chem. Rev.* **2010**, *110*, 1147-1169.
47. Chen, X.; Hao, X.-S.; Goodhue, C. E.; Yu, J.-Q. "Cu(II)-Catalyzed Functionalizations of Aryl C-H Bonds Using O₂ as an Oxidant." *J. Am. Chem. Soc.* **2006**, *128*, 6790-6791.

48. A concurrent report described stoichiometric Cu-mediated amination of 2-phenylpyridine and noted that product inhibition occurred: Uemura, T.; Imoto, S.; Chatani, N. "Amination of the Ortho C-H Bonds by the Cu(OAc)₂-mediated Reaction of 2-Phenylpyridines with Anilines." *Chem. Lett.* **2006**, *35*, 842-843.
49. Wang, W.; Luo, F.; Zhang, S.; Cheng, J. "Copper(II)-Catalyzed Ortho-Acyloxylation of the 2-Arylpyridines sp² C-H Bonds with Anhydrides, Using O₂ as Terminal Oxidant." *J. Org. Chem.* **2010**, *75*, 2415-2418.
50. John, A.; Nicholas, K. M. "Copper-Catalyzed Amidation of 2-Phenylpyridine with Oxygen as the Terminal Oxidant." *J. Org. Chem.* **2011**, *76*, 4158-4162.
51. For a compilation of pK_a values, see: Shen, K.; Fu, Y.; Li, J.-N.; Liu, L.; Guo, Q.-X. "What are the pK_a values of C-H bonds in aromatic heterocyclic compounds in DMSO?" *Tetrahedron* **2007**, *63*, 1568-1576.
52. For landmark reports and a review, see: (a) Glaser, C. "Beiträge zur Kenntniss des Acetylnylbenzols." *Chem. Ber.* **1869**, *2*, 422-424. (b) (c) Hay, A. S. "Oxidative Coupling of Acetylenes. III." *J. Org. Chem.* **1962**, *27*, 3320-3321. (d) Siemsen, P.; Livingston, R. C.; Diederich, F. "Acetylenic Coupling: A Powerful Tool in Molecular Construction." *Angew. Chem. Int. Ed.* **2000**, *39*, 2632-2657.
53. Hamada, T.; Ye, X.; Stahl, S. S. "Copper-Catalyzed Aerobic Oxidative Amidation of Terminal Alkynes: Efficient Synthesis of Ynamides." *J. Am. Chem. Soc.* **2008**, *130*, 833-835.
54. Wei, Y.; Zhao, H.; Kan, J.; Su, W.; Hong, M. "Copper-Catalyzed Direct Alkynylation of Electron-Deficient Polyfluoroarenes with Terminal Alkynes Using O₂ as an Oxidant." *J. Am. Chem. Soc.* **2010**, *132*, 2522-2523.

55. Kitahara, M.; Hirano, K.; Tsurugi, H.; Satoh, T.; Miura, M. "Copper-Mediated Direct Cross-Coupling of 1,3,4-Oxadiazoles and Oxazoles with Terminal Alkynes." *Chem. Eur. J.* **2010**, *16*, 1772-1775.
56. Do, H.-Q.; Daugulis, O. "An Aromatic Glaser-Hay Reaction." *J. Am. Chem. Soc.* **2009**, *131*, 17052-17053.
57. Li, Y.; Jin, J.; Qian, W.; Bao, W. "An efficient and convenient Cu(OAc)₂/air mediated oxidative coupling of azoles via C-H activation." *Org. Biomol. Chem.* **2010**, *8*, 326-330.
58. Monguchi, D.; Fujiwara, T.; Furukawa, H.; Mori, A. "Direct Amination of Azoles via Catalytic C-H, N-H Coupling." *Org. Lett.* **2009**, *11*, 1607-1610.
59. Wang, Q.; Schreiber, S. L. "Copper-Mediated Amidation of Heterocyclic and Aromatic C-H Bonds." *Org. Lett.* **2009**, *11*, 5178-5180.
60. Brasche, G.; Buchwald, S. L. "C-H Functionalization/C-N Bond Formation: Copper-Catalyzed Synthesis of Benzimidazoles from Amidines." *Angew. Chem. Int. Ed.* **2008**, *47*, 1932-1934.
61. Ueda, S.; Nagasawa, H. "Synthesis of 2-Arylbenzoxazoles by Copper-Catalyzed Intramolecular Oxidative C-O Coupling of Benzanilides." *Angew. Chem. Int. Ed.* **2008**, *47*, 6411-6413.
62. Ueda, S.; Nagasawa, H. "Facile Synthesis of 1,2,4-Triazoles via a Copper-Catalyzed Tandem Addition-Oxidative Cyclization." *J. Am. Chem. Soc.* **2009**, *131*, 15080-15081.
63. For a recent mechanistic study, see: Worrell, B. T.; Malik, J. A.; Fokin, V. V. "Direct Evidence of a Dinuclear Copper Intermediate in Cu(I)-Catalyzed Azide-Alkyne Cycloadditions." *Science* **2013**, *340*, 457-460.

64. Klein, J. E. M. N.; Perry, A.; Pugh, D. S.; Taylor, R. J. K. "First C-H Activation Route to Oxindoles using Copper Catalysis." *Org. Lett.* **2010**, *12*, 3446-3449.
65. Jia, Y.-X.; Kündig, E. P. "Oxindole Synthesis by Direct Coupling of C_{sp2}-H and C_{sp3}-H Centers." *Angew. Chem. Int. Ed.* **2009**, *48*, 1636-1639.
66. Perry, A.; Taylor, R. J. K. "Oxindole synthesis by direct C-H, Ar-H coupling." *Chem. Commun.* **2009**, 3249-3251.
67. Zhang, C.; Tang, C.; Jiao, N. "Recent advances in copper-catalyzed dehydrogenative functionalization via a single electron transfer (SET) process." *Chem. Soc. Rev.* **2012**, *41*, 3464-3484.
68. Chmielewski, P. J.; Latos-Grażyński, L.; Schmidt, I. "Copper(II) Complexes of Inverted Porphyrin and Its Methylated Derivatives." *Inorg. Chem.* **2000**, *39*, 5475-5482.
69. Furuta, H.; Maeda, H.; Osuka, A. "Doubly N-Confused Porphyrin: A New Complexing Agent Capable of Stabilizing Higher Oxidation States." *J. Am. Chem. Soc.* **2000**, *122*, 803-807.
70. Furuta, H.; Ishizuka, T.; Osuka, A.; Uwatoko, Y.; Ishikawa, Y. "Metal Complexes of an N-Confused Calix[4]pyrin Derivative—The First X-ray Structure of an Organometallic Compound of Divalent Copper." *Angew. Chem. Int. Ed.* **2001**, *40*, 2323-2325.
71. Maeda, H.; Ishikawa, Y.; Matsuda, T.; Osuka, A.; Furuta, H. "Control of Cu(II) and Cu(III) States in N-Confused Porphyrin by Protonation/Deprotonation at the Peripheral Nitrogen." *J. Am. Chem. Soc.* **2003**, *125*, 11822-11823.
72. (a) Ribas, X.; Jackson, D. A.; Donnadiou, B.; Mahía, J.; Parella, T.; Xifra, R.; Hedman, B.; Hodgson, K. O.; Llobet, A.; Stack, T. D. P. "Aryl C-H Activation by Cu^{II} To Form an

- Organometallic Aryl-Cu^{III} Species: A Novel Twist on Copper Disproportionation." *Angew. Chem. Int. Ed.* **2002**, *41*, 2991-2994.
73. Ribas, X.; Calle, C.; Poater, A.; Casitas, A.; Gómez, L.; Xifra, R.; Parella, T.; Benet-Buchholz, J.; Schweiger, A.; Mitrikas, G.; Solà, M.; Llobet, A.; Stack, T. D. P. "Facile CH Bond Cleavage via a Proton-Coupled Electron Transfer Involving a C-H...Cu^{II} Interaction." *J. Am. Chem. Soc.* **2010**, *132*, 12299-12306.
74. Huffman, L. M.; Stahl, S. S. "Carbon-Nitrogen Bond Formation Involving Well-Defined Aryl-Copper(III) Complexes." *J. Am. Chem. Soc.* **2008**, *130*, 9196-9197.
75. King, A. E.; Huffman, L. M.; Casitas, A.; Costas, M.; Ribas, X.; Stahl, S. S. "Copper-Catalyzed Aerobic Oxidative Functionalization of an Arene C-H Bond: Evidence for an Aryl-Copper(III) Intermediate." *J. Am. Chem. Soc.* **2010**, *132*, 12068-12073.
76. Huffman, L. M.; Casitas, A.; Font, M.; Canta, M.; Costas, M.; Ribas, X.; Stahl, S. S. "Observation and Mechanistic Study of Facile C-O Bond Formation between a Well-Defined Aryl-Copper(III) Complex and Oxygen Nucleophiles." *Chem. Eur. J.* **2011**, *17*, 10643-10650.
77. Casitas, A.; King, A. E.; Parella, T.; Costas, M.; Stahl, S. S.; Ribas, X. "Direct observation of Cu^I/Cu^{III} redox steps relevant to Ullmann-type coupling reactions." *Chem. Sci.* **2010**, 326-330.
78. Yao, B.; Wang, D.-X.; Huang, Z.-T.; Wang, M.-X. "Room-temperature aerobic formation of a stable aryl-Cu(III) complex and its reactions with nucleophiles: highly efficient and diverse arene C-H functionalizations of azacalix[1]arene[3]pyridine." *Chem. Commun.* **2009**, 2899-2901.

Chapter 2:

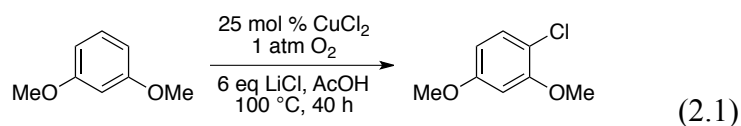
Divergence between Organometallic and Single-Electron-Transfer Mechanisms in Copper(II)-Mediated Aerobic C–H Oxidation

Computational studies in this chapter were performed by Dr. Mehmed Zahid Ertem, a graduate student in Prof. Christopher J. Cramer's group at University of Minnesota.

This work was published as: Suess, A. M.; Ertem, M. Z.; Cramer, C. J.; Stahl, S. S. "Divergence between Organometallic and Single-Electron-Transfer Mechanisms in Copper(II)-Mediated Aerobic C-H Oxidation." *J. Am. Chem. Soc.* **2013**, *135*, 9797-9804.

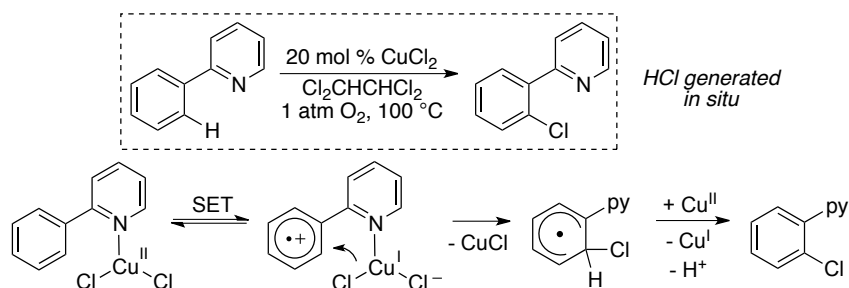
2.1. Introduction.

Copper(II) catalyzes a wide variety of aerobic C–H oxidation reactions (see Chapter 1).¹ Many of these transformations involve electron-rich substrates that undergo initial one-electron oxidation by Cu^{II}. Examples include oxidative dimerization of naphthol,² oxychlorination of phenols and other electron-rich arenes (eqn 2.1, discussed further in Chapters 3 and 4),^{3,4} and cross-dehydrogenative coupling reactions of aromatic and benzylic amines.⁵

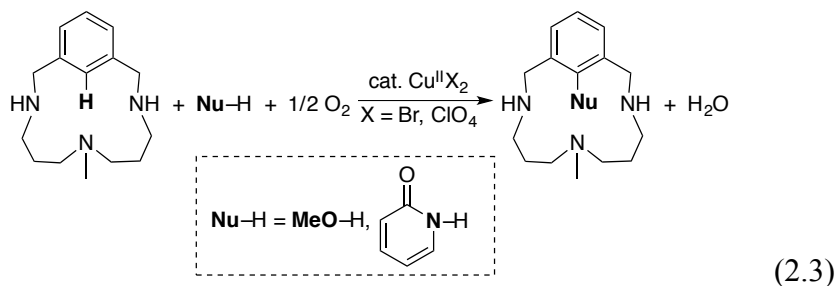
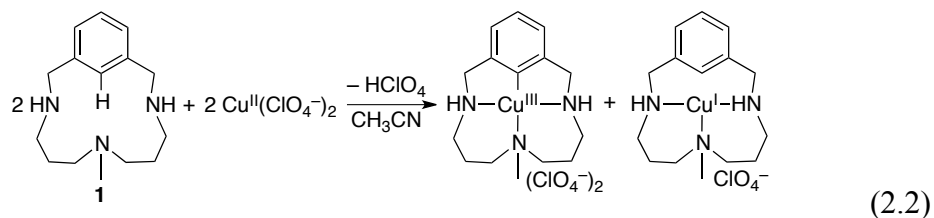


Yu and coworkers proposed a similar single-electron-transfer (SET) mechanism for chelate-directed, aerobic oxidative functionalization of 2-phenylpyridines in which the solvent decomposes to yield HCl, the chloride source (Scheme 2.1).⁶ Their proposed mechanism is initiated by transfer of an electron from the arene, reducing copper. Support for this mechanism was obtained from the lack of a kinetic isotope effect (KIE).⁷ Electron-donating groups on the arene increase the rate of reaction, additionally supporting the SET mechanism. A first-order dependence of reaction rate on substrate and copper was also observed.

Scheme 2.1. Proposed Single-Electron Transfer (SET) Mechanism for Oxidative Chlorination of 2-Phenylpyridine.

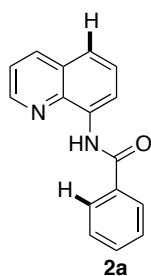


Numerous other Cu-catalyzed aerobic C–H oxidation reactions, including chelated-directed and non-directed examples, have been reported for which the mechanism of C–H activation is not well established (see Chapter 1). Many of these reactions appear similar to those catalyzed by Pd and other noble metals, and we considered whether some of these aerobic oxidation reactions could involve organometallic intermediates. Stoichiometric C–H activation by Cu^{II} had been identified for macrocyclic substrates,⁸ including the triazamacrocyclic arene **1**, reported by Ribas et al.^{9,10} Several of these studies revealed an unusual Cu^{II} disproportionation pathway that yields aryl-Cu^{III} and Cu^I products (eqn 2.2). Stahl et al. recently demonstrated the relevance of this reactivity to catalytic C–H oxidation by showing that Cu^{II} salts, CuBr₂ and Cu(ClO₄)₂, catalyze aerobic oxidation of the arene C–H bond in **1** to C–O and C–N bonds in the presence of methanol and pyridone, respectively (eqn 2.3).¹¹ An aryl-Cu^{III} species, which undergoes facile C–O or C–N reductive elimination to afford the functionalized product,¹² was directly observed and established as a kinetically competent intermediate. This work provided the first direct evidence for an organometallic pathway in Cu-catalyzed aerobic C–H oxidation.



The proof-of-principle studies have an important caveat: the triazamacrocyclic substrate may be predisposed to an organometallic mechanism due to its macrocyclic chelating nature. We expect the organometallic mechanism to be favored for this substrate due to its ability to stabilize copper in close proximity to the C-H bond for which functionalization is desired. Functionalization of the other aryl-C-H bonds in the substrate has not been observed.

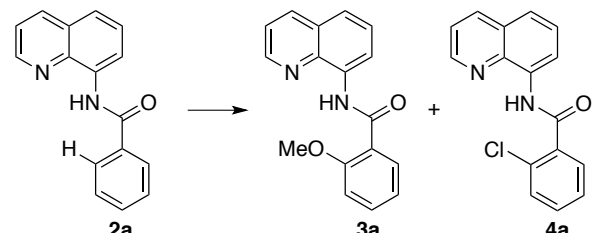
In order to explore the potential role of organometallic intermediates with a less biased substrate, we investigated the reactivity of substrate **2a**, which features an amidoquinoline directing group first used by Daugulis and coworkers in Pd-catalyzed C-H functionalization reactions.^{13,14} In this chapter it is shown that substrate **2a** exhibits divergent reactivity in Cu^{II}-mediated C-H functionalization, depending on the reaction conditions. Directed C-H oxidation occurs under basic conditions while non-directed oxidation of the quinoline ring occurs under acidic conditions. Experimental and computational mechanistic studies provide fundamental insights into the organometallic and single-electron-transfer pathways that give rise to these distinct outcomes.¹⁵ These results have important implications for the ongoing development of Cu^{II}-catalyzed aerobic oxidation reactions.



2.2. Cu^{II}-Mediated C–H Oxidation of *N*-(8-quinolinyl)benzamide under Different Conditions.

2.2.1. Methoxylation and Chlorination of the Benzamide.

Investigation of the reactivity of **2a** was initiated by evaluating Cu^{II}-catalyzed C–H oxidation conditions similar to those reported previously. No reaction was observed under the conditions used for oxidative methoxylation of the triazamacrocyclic arene **1** (see previous eqn 3 and Table 2.1, entry 1). Addition of a stoichiometric base (Cs₂CO₃) to the reaction resulted in small quantities of product **3a**, arising from methoxylation of the *ortho* position of the benzamide (entry 2). The yield of **3a** could be increased up to 56% by employing 2 equiv of Cu(OAc)₂ as the Cu^{II} source. No difunctionalization of the arene was observed under these conditions, and the presence of O₂ enabled a somewhat higher yield relative to anaerobic reaction conditions (entries 3 and 4). Use of CuCl₂ resulted in a mixture of methoxylation and chlorination products **3a** and **4a** (entries 5 and 6). Control experiments suggest that the **3a** formed under these conditions arises from direct C–H methoxylation, not C–H chlorination followed by methoxide substitution of chloride in **4a**. Subjection of **4a** to the oxidative methoxylation conditions in entry 3 resulted in near-complete recovery of **4a** with no formation of **3a**.

Table 2.1. Directed C–H Methoxylation and Chlorination of the Benzamide.


Entry	[Cu]	Base (1 equiv)	Atm. (1 atm)	% 3a	% 4a
1 ^a	10 mol % Cu(ClO ₄) ₂ •6H ₂ O	none	O ₂	0.0	n/a
2 ^a	10 mol % Cu(ClO ₄) ₂ •6H ₂ O	Cs ₂ CO ₃	O ₂	18	n/a
3^b	2 equiv Cu(OAc)₂	Cs₂CO₃	O₂	56	n/a
4 ^b	2 equiv Cu(OAc) ₂	Cs ₂ CO ₃	N ₂	46	n/a
5 ^c	1 equiv CuCl ₂	Na ₂ CO ₃	O ₂	31	10.8
6 ^c	2 equiv CuCl ₂	Na ₂ CO ₃	O ₂	2.0	41.2

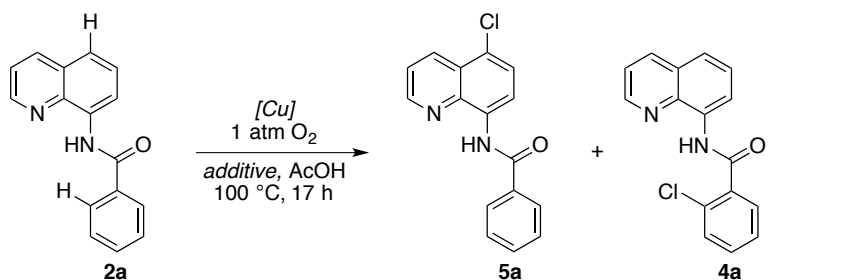
Yields determined by ¹H NMR spectroscopy. Conditions: 50 mM **2a**, 5 mM [Cu], 0 or 50 mM base, 1 mL MeOH, 60 °C, 17 h. ^b50 mM **2a**, 100 mM [Cu], 50 mM base, 1 mL 5.2:1 MeOH/pyridine, 50 °C, 24 h. ^c50 mM **2a**, 50 or 100 mM [Cu], 50 mM base, 1 mL MeOH, 50 °C, 17 h.

These product yields are not sufficiently high to be synthetically useful, but they provide clear evidence for directed C–H oxidation, mediated by Cu^{II}. Control experiments show that the product inhibits the reaction. For example, when a 1:1 mixture of **2a**:**3a** was combined under the conditions of entry 3 (Table 2.1), the quantity of **3a** increased only 8.6 % after 5 h, whereas use of **2a** alone affords a 25% yield of **3a** over the same time period. Analogous product inhibition has been reported for Cu-catalyzed amination of 2-phenylpyridine.¹⁶

2.2.2. Chlorination of the Quinoline.

The reactivity of **2a** was also evaluated under conditions similar to those used for the oxidative chlorination of electron rich arenes (eqn 1). In the presence of 1 atm O₂ and 2 equiv LiCl in AcOH at 100 °C, catalytic CuCl or CuCl₂ promoted chlorination of **2a**. In contrast to the methoxylation results described above, the product **5a** arose from chlorination of the quinoline, not the benzamide (Table 2.2). Higher yields were obtained with CuCl rather than CuCl₂ (entries 1 and 2), and no conversion was observed under these conditions in the absence of Cu (entries 3 and 4). The reactivity with CuCl₂ was nearly identical to that of CuCl when an equal amount of LiOAc (20 mol %) was included in the reaction mixture (entries 2 and 5). This effect is attributed to the role of a Brønsted base to promote substrate binding to the Cu center: the use of a Cu^I catalyst precursor generates an equivalent of base in situ upon reaction with O₂ to afford H₂O₂ or H₂O.¹⁷

Table 2.2. C–H Chlorination of the Quinoline.



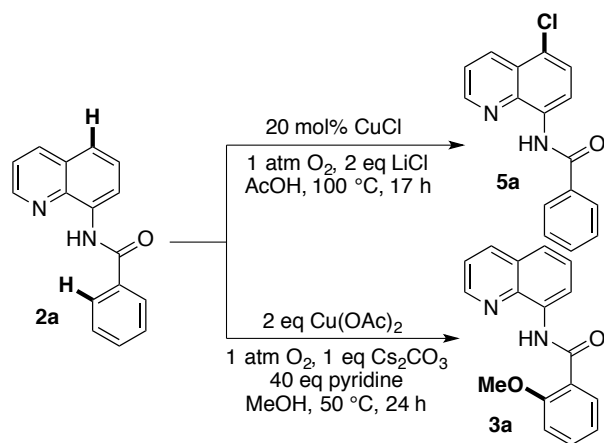
Entry	[Cu]	Additive	% 5a	% 4a
1	20 mol % CuCl ₂	2 equiv LiCl	34	0.0
2	20 mol % CuCl	2 equiv LiCl	81	2.1
3	none	none	0.0	0.0
4	none	2 equiv LiCl	0.0	0.0
5	20 mol % CuCl₂, 20 mol % LiOAc	2 equiv LiCl	88	0.0

Yields determined by ¹H NMR spectroscopy. Conditions: 50 mM **2a**, 10 mM [Cu], 100 mM LiCl in 1 mL AcOH, 1 atm O₂, 100 °C, 17 h.

2.2.3. Comments on the Divergent Reactivity.

These observations, summarized in Scheme 2.2, highlight an unusual condition-dependent selectivity for Cu^{II}-mediated C–H oxidation that has not been previously observed. The reaction conditions that give rise to benzamide or quinoline functionalization have been linked to proposals of either organometallic or single-electron-transfer mechanisms, respectively. Mechanistic understanding of the divergent pathways operating for this single substrate will be valuable for understanding the broader field of Cu^{II}-mediated C–H oxidations.

Scheme 2.2. Divergent Reactivity in Cu^{II}-Mediated C–H Oxidation of **2a**.

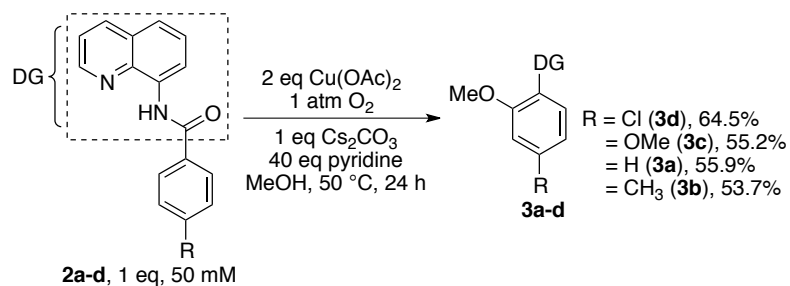


2.3. Mechanistic Study of Cu^{II}-Mediated C–H Oxidation of the Benzamide.

2.3.1. Initial Rates of Electronically-Variied Derivatives and Hammett Parameter for Benzamide Methoxylation.

In order to gain further insight into the methoxylation reaction, substrates with electronically varied substituents on the benzamide ring were prepared and subjected to the methoxylation reaction conditions (**2a-d**, Scheme 2.3).

Scheme 2.3. Cu^{II}-Mediated Methoxylation from Methanol to Yield Substituted Anisoles.



Initial rates were measured for the Cu(OAc)₂-promoted methoxylation of these substrates (Table 2.3 and Figure 2.1). Faster initial rates were observed with substrates bearing electron-withdrawing groups.

Table 2.3. Initial Rates of Product Yield for Benzamide Methoxylation of Substrates **2a-d,f**.

Substrate	Initial Rate (mM/min)
2a (H)	0.0564 ± 0.0013
2b (Me)	0.0536 ± 0.0028
2c (OMe)	0.06636 ± 0.0021
2d (Cl)	0.0899 ± 0.0084
2f (d ₅)	0.00988 ± 0.00016

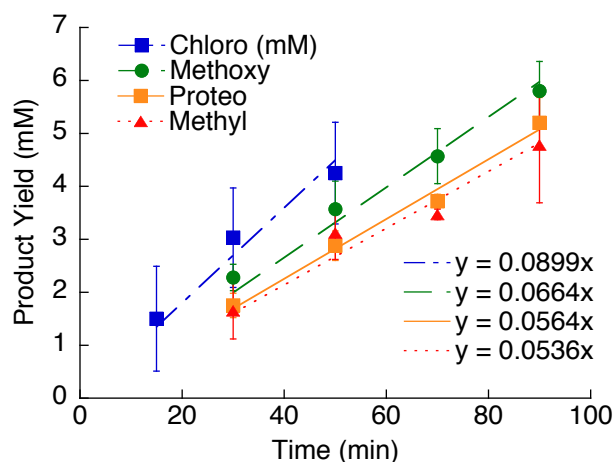


Figure 2.1. Initial rates of methoxylation of substrates **2a-d**. The averages are plotted and each half-error bar represents one standard deviation.

A Hammett plot using σ_{meta} parameters reveals a small, but distinct, positive slope reflecting the rate-accelerating effect of electron-withdrawing groups ($\rho = 0.6 \pm 0.1$; Table 2.4 and Figure 2.2).

Table 2.4. Hammett Parameter, Initial Rate, and Relevant Calculated Data.

Substrate	Hammett σ_{meta} parameter ¹⁸	Initial Rate (mM/min)	k_X/k_H	$\log(k_X/k_H)$
2b (Me)	-0.06	0.0536 ± 0.0028	0.950 ± 0.054	-0.022 ± 0.025
2a (H)	0	0.0564 ± 0.0013	1.000 ± 0.033	0.000 ± 0.014
2c (OMe)	0.1	0.06636 ± 0.0021	1.177 ± 0.046	0.071 ± 0.017
2d (Cl)	0.37	0.0899 ± 0.0084	1.59 ± 0.15	0.201 ± 0.041

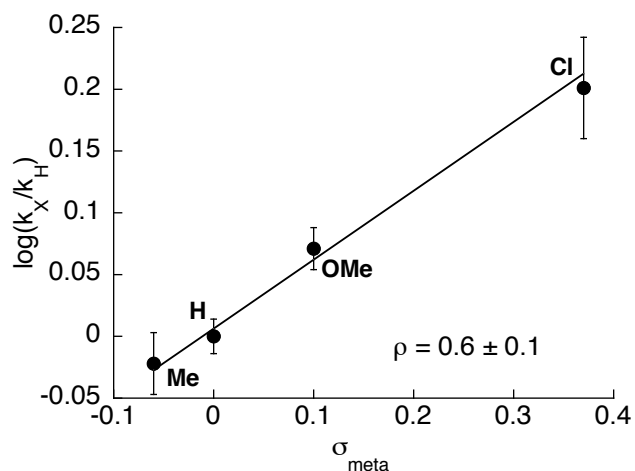


Figure 2.2. Hammett plot from initial rates of **2a-d** methoxylation. Each half-error bar represents one standard deviation.

2.3.2. Deuteration and Isotope Effect Experiments for Benzamide Methoxylation.

When the reaction is performed in CH_3OD , no deuterium is incorporated into the recovered starting material or the product (Scheme 2.4A), suggesting that C–H activation is irreversible. Kinetic isotope effects were obtained by an intramolecular competition experiment (Scheme 2.4B) and by comparison of the independent rates of the *H*- and *D*-labeled substrates (Scheme 2.4C and Figure 2.3). Reaction of the monodeuterated substrate **2e** led to an 84:16 ratio of product isotopologues, favoring reaction of the C–H bond ($\text{KIE} = 5.25 \pm 0.06$). A similar KIE was obtained from the comparison of the initial rates of **2a** and the aryl-*d*₅ substrate **2f** ($\text{KIE} = 5.7 \pm 0.8$; Scheme 4c).

Scheme 2.4. Deuteration and Isotope Effect Experiments for the Benzamide C–H

Methoxylation Reaction.

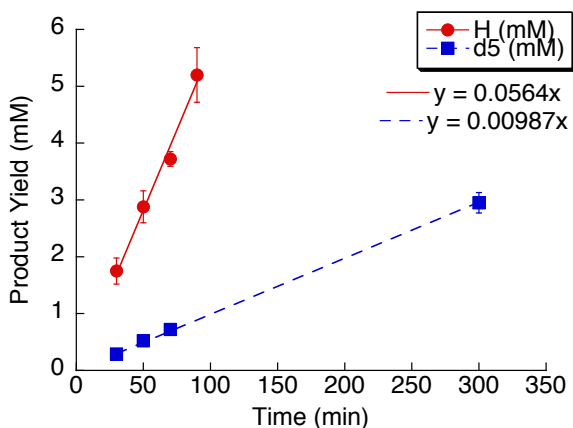
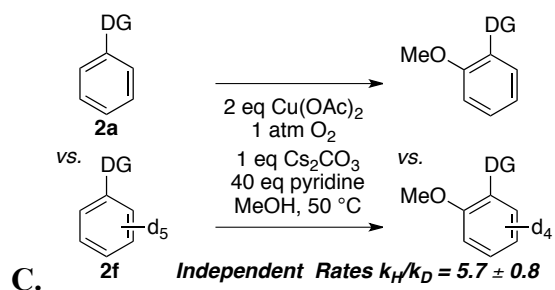
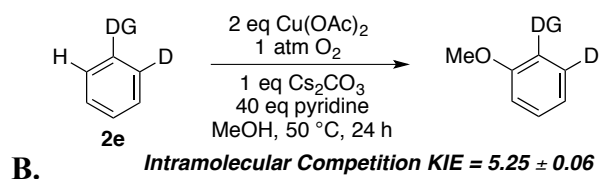
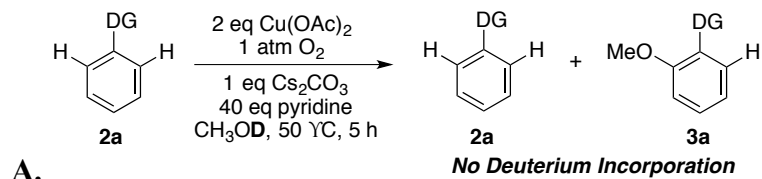


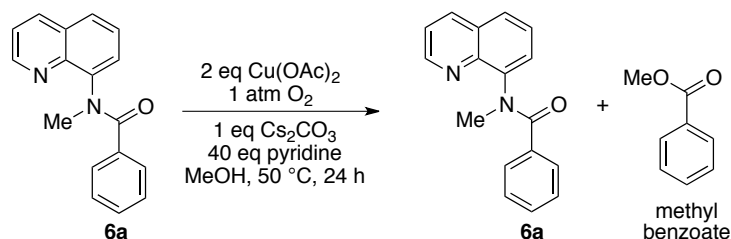
Figure 2.3. Independent Initial Rate Comparison k_H/k_D for Benzoyl Moiety Methoxylation.

2.3.3. Reactivity of *N*-methyl-*N*-(8-quinolinyl)benzamide in Benzamide Methoxylation

Conditions.

N-methylated substrate **6a** was subjected to the typical benzoyl moiety methoxylation reaction conditions (2 repetitions). After 24 hours, >60% of the starting material was recovered (Table 2.5). Significant quantities of methyl benzoate and 8-aminoquinoline were observed, along with trace unidentified species. No peaks were observed in the Me/OMe region of the ¹H NMR spectrum other than from **6a** and methyl benzoate. Methyl benzoate is a liquid so may not be fully quantized; some may have been removed by vacuum during the typical copper removal and reaction work-up procedure.

Table 2.5. Reactivity of *N*-methyl substrate **6a** in Benzoyl Moiety Methoxylation Conditions.



Entry	% 6a recovered	% methyl benzoate ^a
1	63.7	19.5
2	63.3	19.1

^aMethyl benzoate is a liquid so many not be fully quantized; some may have been removed by vacuum during the typical copper removal and reaction work-up procedure. Quinoline fragment was not recovered.

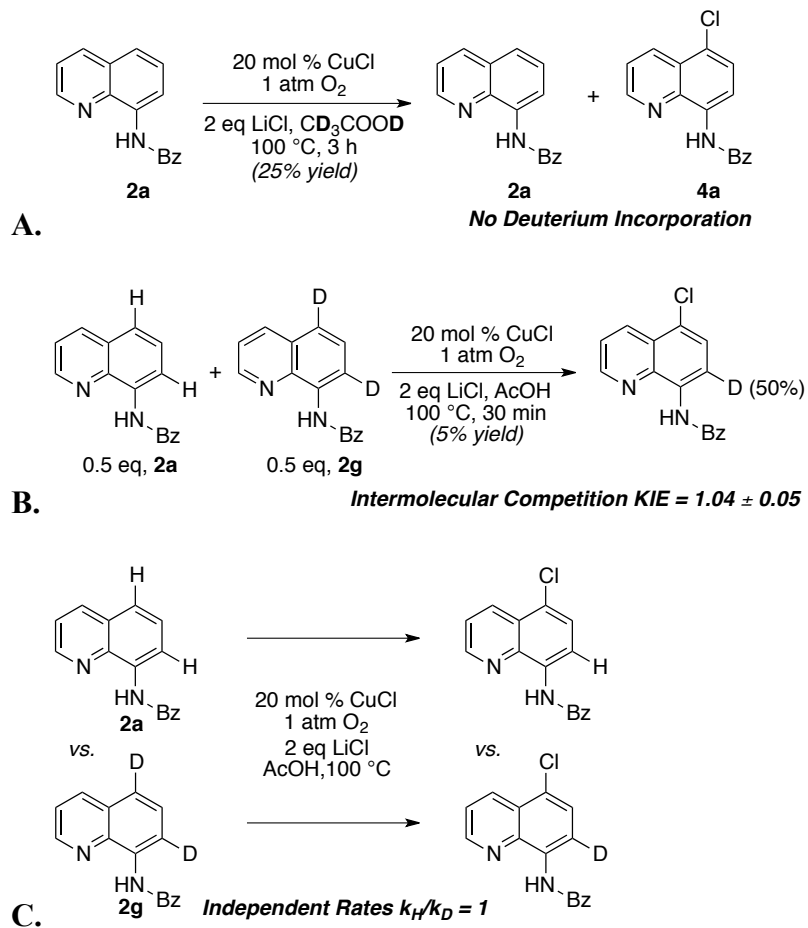
2.4. Mechanistic Study of Cu^{II}-Mediated C–H Oxidation of the Quinoline.

2.4.1. Deuteration and Isotope Effect Experiments for Quinoline Chlorination.

When the quinoline chlorination reaction was performed in CD₃CO₂D, no deuterium incorporation was observed in the recovered starting material or the product (Scheme 2.5A). This result indicates that cleavage of the C–H bond is irreversible. Kinetic isotope effects were obtained by an intermolecular competition experiment and by comparing the independent rates of the *H*- and *D*-labeled substrates. A 1:1 mixture of **2a** and the dideuterated substrate **2g** was submitted to the reaction conditions for 30 min, resulting in approx 5% product yield (Scheme 2.5B). Analysis of the H/D ratio at the 7-position of the quinoline revealed a nearly equal mixture of isotopes, corresponding to a KIE of 1.04 ± 0.05 . Independent reactions of **2a** and **2g** exhibit nearly identical time courses, corresponding to a KIE ~ 1 (Scheme 2.5C and Figure 2.4).

Scheme 2.5. Deuteration and Isotope Effect Experiments for the Quinolinylnyl C–H Chlorination

Reaction.



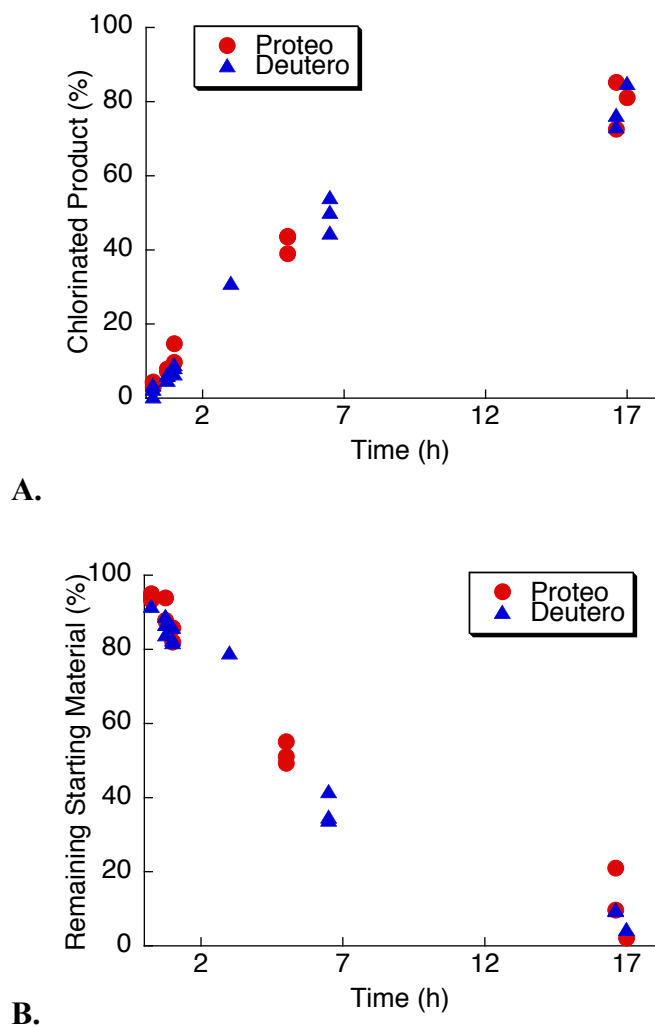
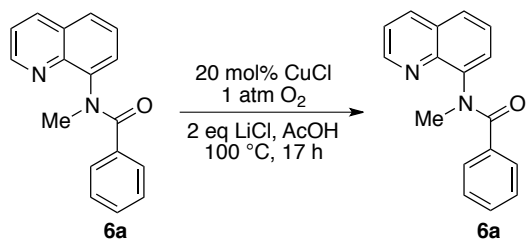


Figure 2.4. (A) Product appearance and (B) starting material consumption in the independent initial rate comparison k_H/k_D for benzamide methoxylation.

2.4.2. Reactivity of *N*-methyl-*N*-(8-quinolinyl)benzamide in Quinoline Chlorination Conditions.

N-methylated substrate **6a** was subjected to the typical quinolinyl moiety chlorination reaction conditions (2 repetitions). After 17 hours >80% of the starting material was recovered, with only trace unidentified byproduct appearing in one experiment (Table 2.6).

Table 2.6. Reactivity of *N*-methyl substrate **6a** in Quinolinyl Moiety Chlorination Conditions.

Entry	% RSM	% byproduct
1	83.3	none
2	75.3	none

Coordination of **2a** to Cu^{II} as an amidate prior to chlorination, even under these acidic conditions, is supported by the lack of reaction of the *N*-methyl substrate **6a**. This substrate is fully recovered after 17 h under the standard reaction conditions. This observation aligns with our interpretation of the beneficial effect of a Brønsted base on the chlorination reaction (Table 2.2, entry 5).

2.5. Preliminary Assessment of the Divergent Mechanisms.

The results outlined above show that Cu^{II} -mediated C–H oxidation of **2a** affords different products and exhibits significantly different mechanistic features under different reaction conditions. On the basis of literature precedents (see Introduction), we attribute these results to the operation of organometallic and SET C–H functionalization pathways for the benzamide methoxylation and quinoline chlorination, respectively.

The positive Hammett slope observed for chelate-directed methoxylation of the benzamide ring (Figure 2.2) is inconsistent with an SET mechanism, which strongly favors

electron-rich substrates.¹⁹ Organometallic C–H activation reactions also typically favor electron-rich substrates, albeit to a lesser extent than SET reactions.²⁰ Several studies of Pd^{II}-mediated C–H activation, however, show that some of these reactions can proceed more rapidly with electron-deficient substrates.²¹ For example, Fagnou and Gorelsky demonstrated C–H arylation reactions of pyridine *N*-oxides that proceed via rate-limiting C–H activation ($k_H/k_D = 3.3$) and exhibit a positive Hammett slope ($\rho = 1.53$).^{21f} These results have been interpreted within the framework of a "concerted metalation-deprotonation" (CMD) mechanism in which C–H activation involves simultaneous electrophilic activation of the arene and deprotonation of the C–H bond. A positive Hammett slope can be observed for reactions in which C–H deprotonation contributes strongly to the transition state, and this pathway is consistent with the large kinetic isotope effect that we observe in the Cu^{II}-mediated C–H methoxylation reaction (KIE \sim 5-6).

The non-chelate-directed chlorination of the quinoline ring of **2a** is consistent with SET reactivity. No kinetic isotope effect is observed for this reaction (KIE \sim 1), and the regioselectivity is consistent with the electronic directing effect of benzamide nitrogen. Deprotonation of the amide group (i.e., upon coordination to the Cu center) would enhance this electronic effect. Similar electronic effects have been observed in SET-based chlorination of other electron-rich arenes.

These considerations provided the basis for the use of density functional theory (DFT) calculations to gain further insights into both of the proposed mechanisms.

2.6. Summary of Computational Analysis of the Divergent Mechanisms.

Computational studies in this chapter were performed by Dr. Mehmed Zahid Ertem, a graduate student in Prof. Christopher J. Cramer's group at University of Minnesota. As these

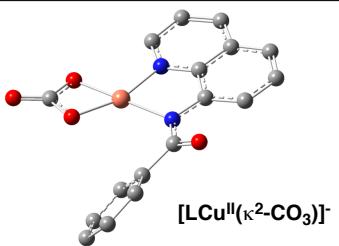
studies are essential for full support of the proposed mechanisms, a summary is included in this chapter. For details of the computational work, please see the publication and its supporting information.¹⁵

2.6.1. Computational analysis of an organometallic pathway for Cu^{II}-mediated C–H oxidation.

DFT methods were used to assess the energetic viability of an organometallic C–H functionalization pathway originating from the Cu^{II}-**2a** complex. The calculations were performed at the M06-L level of density functional theory²², incorporating solvation effects via the appropriate SMD continuum solvation model.²³ A number of Cu^{II} complexes bearing the 8-amidoquinoline ligand were optimized to evaluate the relative energies of possible ground state structures (Table 2.7). The square-planar carbonate complex [LCu^{II}(κ²-CO₃)]⁻ (**I**) (L = deprotonated **2a**) was the most stable structure identified. Species in which the carbonate was replaced with an acetate ligand, methoxide ligands, or five-coordinate structures with a coordinated pyridine ligand were less stable.

Table 2.7. Calculated Stability of Possible Cu-**2a** Complexes under the Benzamide C–H Methoxylation Conditions.

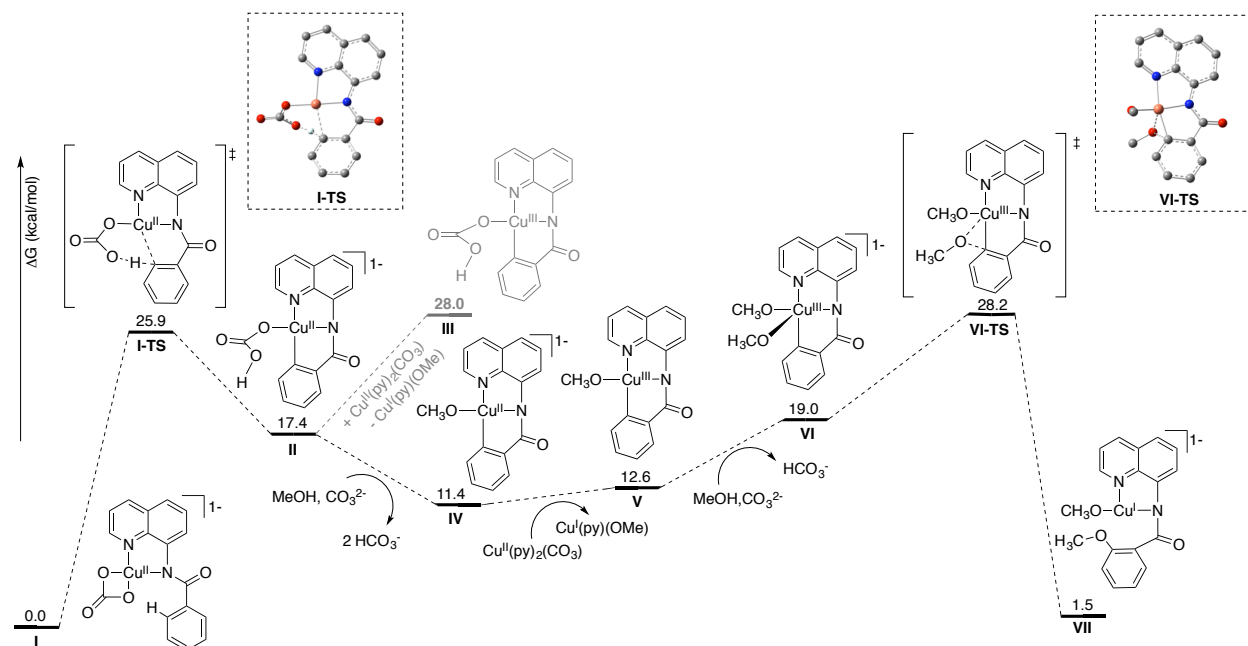
Species	Relative ΔG (kcal/mol)
[LCu ^{II} (κ ² -CO ₃)] ⁻	0.0
[LCu ^{II} (OMe) ₂] ⁻	6.2
[LCu ^{II} (κ ² -CO ₃)py] ⁻	6.9
[LCu ^{II} (κ ² -OAc)]	16.6
[LCu ^{II} (κ ² -OAc)py]	18.0



Starting from the [LCu^{II}(κ²-CO₃)]⁻ complex **I**, a C–H activation pathway was identified that proceeds via transition state **I-TS** (Scheme 2.6). In this mechanism, formation of the aryl-

Cu^{II} complex **II** involves deprotonation of the arene C–H bond by the carbonate ligand with concomitant Cu–C bond formation, analogous to the CMD pathways that have been elaborated for Pd^{II}-mediated C–H activation.²¹ The activation free energy (ΔG^\ddagger) for this step is 25.9 kcal/mol, which compares very favorably to the experimental ΔG^\ddagger of approx 26 kcal/mol calculated from the reaction half-life (9-24 h) at 50 °C.²⁴ The computed KIE for this step ($k_H/k_D = 4.9$) is also very similar to the experimental value ($k_H/k_D = 5.7$). The [LCu^{II}(OMe)₂]⁻ complex is 6.2 kcal/mol less stable than the carbonate complex (Table 3), but this species mediates C–H activation with a barrier of only 20.4 kcal/mol.¹⁵ This comparatively low barrier is consistent with a beneficial effect of the basic methoxide ligand in the CMD C–H activation step. The net activation free energy of 26.6 kcal/mol, which accounts for the ground-state destabilization of this complex, is only slightly higher than the pathway involving the carbonate complex **I**. An analogous pathway involving the acetate complex LCu^{II}(k²-OAc) is significantly higher in energy (net $\Delta G^\ddagger = 45.5$ kcal/mol), largely because the acetate complex starts 16.6 kcal/mol higher in energy than the carbonate complex (Table 2.7).

Scheme 2.6. Calculated Mechanism for the Cu^{II}-Mediated Benzamide C–H Methoxylation Reaction.



The energetics of one-electron oxidation of the aryl-Cu^{II} complex **II** to an aryl-Cu^{III} complex were evaluated by considering possible Cu^{II}/Cu^I redox couples. A number of plausible Cu^{II} and Cu^I species that could be present in the reaction solution were examined (Table 2.8). Assuming ligand exchange in solution is facile, the most stable Cu^{II} and Cu^I species, Cu^{II}(py)₂(CO₃) and Cu^I(py)(OMe), provide the relevant equilibrium redox couple for oxidation of aryl-Cu^{II} to aryl-Cu^{III}.

Table 2.8. Redox Couples Calculated for Oxidation of Aryl-Cu^{II} to Aryl-Cu^{III} in the Benzamide C–H Methoxylation Reaction.

[Cu^{II}]		[Cu^I]	
(Cu ^{II} , CO ₃ ²⁻ , 2 MeOH 2 OAc ⁻ , 2 py)	Relative ΔG (kcal/mol)	(Cu ^I , CO ₃ ²⁻ , 2 MeOH 2 OAc ⁻ , 2 py)	Relative ΔG (kcal/mol)
Cu ^{II} (py) ₂ (CO ₃)	0.0	Cu ^I (py)(OMe)	0.0
Cu ^{II} (py) ₂ (OMe) ₂	4.2	Cu ^I (py)(OAc)	7.4
Cu ^{II} (py)(CO ₃)	4.3	Cu ^I (py)(HCO ₃)	10.2
Cu ^{II} (OMe) ₂ (MeOH) ₂	8.5	Cu ^I (py) ₂ (OAc)	11.6
Cu ^{II} (MeOH) ₂ (CO ₃)	8.7	Cu ^I (py)(OAc) ₂ ⁻	13.3
Cu ^{II} (OMe)(HCO ₃)(py) ₂	14.5	Cu ^I (MeOH)(OAc)	16.7
Cu ^{II} (OMe)(HCO ₃)(MeOH) ₂	15.1	Cu ^I (MeOH) ₂ (CO ₃) ⁻	21.1
Cu ^{II} (py) ₂ (OAc) ₂	16.4	Cu ^I (MeOH) ₂ (OAc)	25.5
Cu ^{II} (MeOH) ₂ (OAc) ₂	16.7		
Cu ^{II} (py)(MeOH)(OAc) ₂	18.0		

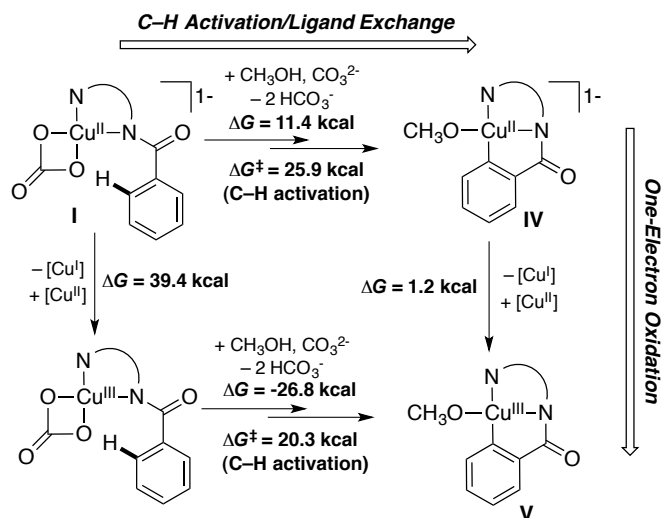
Oxidation of aryl-Cu^{II} complex **II**, which has a bicarbonate ligand, is energetically disfavored (**III**, $\Delta G = 28.0$ kcal/mol relative to **I**; Scheme 2.6). Exchange of the bicarbonate ligand with methoxide to form **IV**, however, is favorable, and subsequent oxidation of **IV** to afford aryl-Cu^{III} species **V** is uphill by only 1.2 kcal/mol. These observations can be rationalized by the ability of the methoxide ligand to stabilize Cu^{III} relative to a bicarbonate ligand.

Reductive elimination from the 4-coordinate Cu^{III}(aryl)(OMe) complex **V** was found to be prohibitive ($\Delta G^\ddagger = 44.2$ kcal/mol).¹⁵ The 5-coordinate dimethoxide complex **VI** is energetically accessible, however, and reductive elimination from this species is more favorable (Scheme 2.6, $\Delta G^\ddagger = 28.2$ kcal/mol relative to **I**). This observation suggests that the reactive methoxide nucleophile enters the coordination sphere following oxidation of Cu^{II} to Cu^{III}. This sequence may vary with other substrates, for example, with those lacking the conformational constraints of the chelating ligand. The reductive elimination transition state **VI-TS** is similar in energy to the C-H activation transition state **I-TS**. The calculated pathway is consistent with the

experimental observation of rate-limiting C-H activation given the expected accuracy of the computational model. Uncertainties in the computed energies derive in part from the relative pKa values of methanol and carbonate, and they may be amplified by the multiple deprotonations of MeOH by carbonate that are performed along the reaction path.

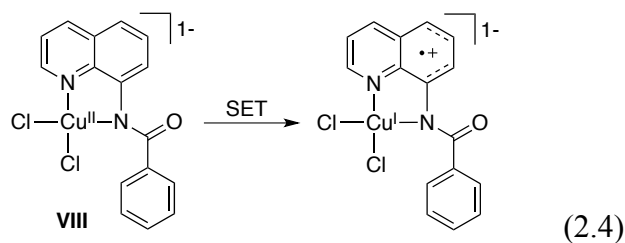
C-H activation by Cu^{III} was also considered (Scheme 2.7, lower pathway)²⁵ and found to have an activation barrier 5.6 kcal/mol lower in energy than the corresponding Cu^{II}-mediated step ($\Delta G^\ddagger_{\text{Cu(III)}} = 20.3$ kcal/mol). Nevertheless, this pathway is strongly disfavored by the highly unfavorable energy for oxidation of the Cu^{II} center to Cu^{III} ($\Delta G = 39.4$ kcal/mol) prior to C-H activation. A concerted proton-coupled electron-transfer process cannot be excluded on the basis of our results, but the computational data presented here are consistent with a stepwise Cu^{II}-mediated C-H activation step followed by one-electron oxidation: **I** \rightarrow **IV** \rightarrow **V** (Schemes 2.6 and 2.7).

Scheme 2.7. Cu^{II} vs. Cu^{III} C-H Activation Mechanisms.



2.6.2. Computational analysis of a single-electron transfer pathway for Cu^{II}-mediated C–H oxidation.

Chlorination of the quinoline ring takes place under conditions similar to those for reactions that have been proposed to proceed by an SET mechanism. Our initial studies probed the possibility of an intramolecular SET step in complex **VIII** (eqn 2.4), similar to that illustrated in Scheme 2.1. The product corresponds to an electronic excited state of the ground-state species, and the energy of this state was evaluated by performing TD-DFT calculations. The lowest-energy internal SET product arises from transfer of a beta-spin electron from a mixture of two doubly occupied orbitals, one associated with the chloride lone pairs (GS-A) and the other with quinoline p electrons (GS-B), to the singly occupied orbital localized on Cu (i.e., $d_{x^2-y^2}$) (Figure 2.5). The excitation energy for this transition is 31.4 kcal/mol. Because chlorination of the aromatic ring would add a further energy barrier, however, we considered whether an intermolecular SET process might exist that provides access to a lower energy pathway.



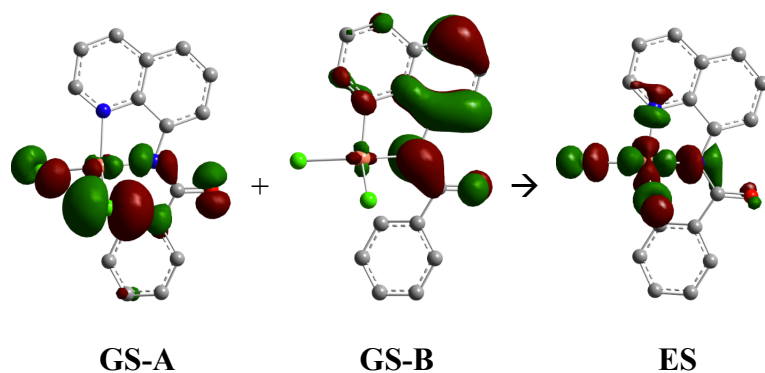


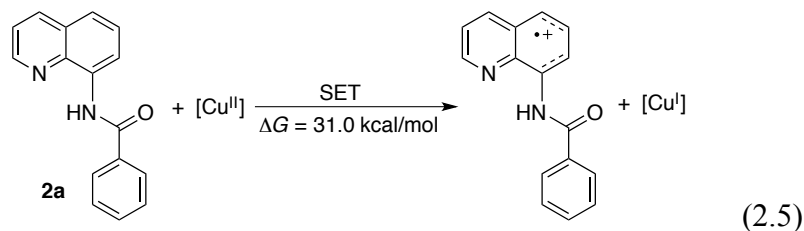
Figure 2.5. The lowest excited-state doublet derives from excitation of a beta electron from the nominally doubly occupied HOMO-1 (GS-A) and HOMO (GS-B), contributing with equal weight, into the singly occupied SOMO (ES). The resulting excited state is 31.4 kcal/mol above the ground state, corresponding to a photon energy of 909.4 nm.

Various $\text{Cu}^{\text{II}}/\text{Cu}^{\text{I}}$ redox couples were considered for the intermolecular SET reaction (Table 2.9). $\text{Cu}^{\text{II}}\text{Cl}_2(\text{AcOH})_2$ and $\text{Cu}^{\text{I}}\text{Cl}_2^-$ were the lowest-energy Cu^{II} and Cu^{I} species identified and were used to calculate the energy of the SET step. One-electron oxidation of **VIII** to the Cu^{II} complex **IX**, bearing a radical-cation amidoquinoline ligand, is thermodynamically uphill by 8.6 kcal/mol. This step is analogous to the Cu^{II} disproportionation step that affords the aryl- Cu^{III} species in the organometallic mechanism (i.e., **IV** \rightarrow **V** in Scheme 2.6); however, in the present case, ligand oxidation is favored over oxidation of the Cu center based on analysis of the computed spin and charge densities.

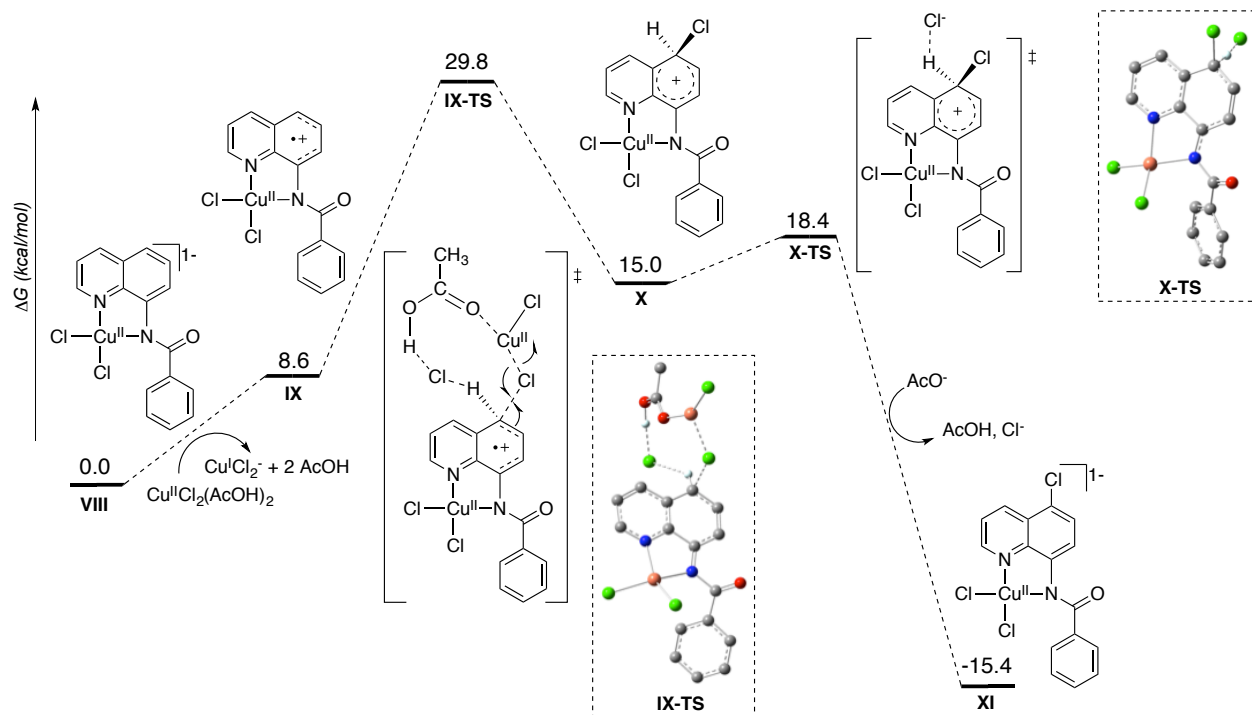
Table 2.9. Redox Couples Calculated for the Oxidation of Cu^{II} to Aryl-Radical-Cation-Ligated Cu^I Complex during Quinoline C–H Chlorination.

[Cu ^{II}] (Cu ^{II} , 4 Cl ⁻ , 2 AcOH)	Relative ΔG (kcal/mol)	[Cu ^I] (Cu ^I , 4 Cl ⁻ , 2 AcOH)	Relative ΔG (kcal/mol)
Cu ^{II} (Cl) ₂ (AcOH) ₂	0.0	Cu ^I Cl ₂ ⁻	0.0
Cu ^{II} Cl ₃ (AcOH) ⁻	1.6	Cu ^I Cl ₂ (AcOH) ⁻	2.0
Cu ^{II} Cl ₄ ²⁻	4.0	Cu ^I Cl(AcOH)	10.4
Cu ^{II} Cl ₂ (AcOH)	5.9	Cu ^I Cl(AcOH) ₂	11.9
Cu ^{II} Cl ₂	18.6	Cu ^I Cl	20.3

This 8.6 kcal/mol thermodynamic barrier for the SET step is much lower than the excitation energy for the intramolecular SET described above, and it is also much lower than one-electron oxidation of the non-coordinated neutral substrate **2a** ($\Delta G = 31.0$ kcal/mol; eq 2.5). The latter observation shows that coordination of the substrate to Cu^{II} as an amidate ligand greatly facilitates intermolecular SET.



Scheme 2.8. Calculated Mechanism for the Cu^{II}-Mediated Quinoline C–H Chlorination Reaction.



Various pathways were considered for chlorination of the radical-cation complex **IX**. The lowest barrier was obtained from a process involving chlorine-atom transfer from CuCl₂, with explicit modeling of an equivalent of chloride and acetic acid (Scheme 2.8). This step proceeds via transition state **IX-TS** and exhibits an activation energy of $\Delta G^\ddagger = 29.8$ kcal/mol. Deprotonation of the resulting Wheland-type intermediate **X** affords the quinoline chlorination product **XI**. The overall barrier for this computed pathway exhibits good agreement with the estimated experimental barrier of approx 30 kcal/mol derived from the reaction half-life at 100 °C (8.5-17 h; energy estimated based on a pseudo first-order reaction²⁴). The computed KIE for this step, $k_H/k_D = 0.91$ is also similar to the value determined experimentally ($k_H/k_D = 1$).

The similarity between the experimental and computed barriers is almost certainly fortuitous, considering the nature of our redox-couple calculation. For example, it is possible that more stable Cu^{II} species may be present in solution than those found in Table 2.9, thereby increasing the thermodynamic barrier for the SET step. A considerably more sophisticated treatment of aggregates and specific solvation effects would be required to assess this point further, but we consider it unlikely that such results would increase the energies of the species in Scheme 2.8 by more than 3 or 4 kcal/mol, which is within the limits of the expected uncertainty for these calculations.

2.7. Reasons for the Mechanistic Divergence Under Different Reaction Conditions.

The experimental and computational results described above provide several insights that can account for the change in mechanism and product selectivity under different reaction conditions. Carbonate is an important additive in the benzamide C–H methoxylation reaction (Table 2.1), and the computational results draw attention to at least two important roles for carbonate. First, a basic ligand is essential for activation of the arene C–H bond by an organometallic CMD mechanism. Acetate could also perform such a role, but carbonate (or methoxide¹⁵) appears to be much more effective, probably owing to its higher basicity. Second, the carbonate dianion is a good ligand that stabilizes Cu^{II} and Cu^{III} species relative to complexes with acetate or bicarbonate ligands (Table 2.7 and Scheme 2.6). This effect is particularly important to access the aryl- Cu^{III} intermediate that can undergo facile C–O bond formation.

The carbonate ligand properties that favor organometallic C–H oxidation disfavor SET C–H oxidation. Specifically, coordination of carbonate to Cu^{II} will lower the $\text{Cu}^{\text{II}}/\text{Cu}^{\text{I}}$ reduction potential and disfavor SET from the aromatic substrate. The acidic reaction conditions associated

with chlorination of the quinoline ring lack strong donor ligands, and Cu^{II} will be present in the form of more-oxidizing halide species. Redox couples were computed for various Cu species to provide further insight into this issue.²⁶ As shown in Table 2.10, the Cu^{II}/Cu^I reduction potentials computed for the major species present under acidic and basic reaction conditions (the top redox couple in each category) can differ by more than 1 V. While these redox potentials have considerable uncertainty, the qualitative trend is clear: acidic conditions are much more amenable to SET-based oxidation of electron-rich substrates.

Table 2.10. Computed Redox Potentials of Species Available in Acidic and Basic Reaction Conditions.

Redox couples	ΔG (kcal/mol)	E (V) vs. NHE
<i>Acidic conditions:</i>		
Cu ^{II} Cl ₂ (AcOH) ₂ + e ⁻ → Cu ^I Cl ₂ ⁻ + 2AcOH	-102.8	0.18
VIII + e ⁻ → IX	-111.4	0.55
<i>Basic conditions:</i>		
Cu ^{II} (py) ₂ CO ₃ + CH ₃ OH + e ⁻ → Cu ^I (py)(OCH ₃) + py + HCO ₃ ⁻	-80.2	-0.80
III + e ⁻ → II	-90.7	-0.34
V + e ⁻ → IV	-81.4	-0.75

2.8. Conclusions.

In summary, an unusual switch in mechanism and product identity has been identified in Cu^{II}-mediated C–H oxidation of the amidoquinoline substrate **2a**. The experimental and computational results are consistent with a switch between organometallic and SET-based C–H oxidation pathways upon changing from basic to acidic reaction conditions. The presence of a Brønsted basic ligand on the Cu^{II} center facilitates C–H activation by an organometallic mechanism, while acidic conditions enhance the Cu^{II} reduction potential, thereby favoring SET. The results of this study show that a macrocyclic chelate (such as **1**; eq 2.2) is not required to achieve organometallic C–H activation by Cu^{II}. The experimental and computational results

highlight the proton-transfer component associated with Cu^{II}-mediated C–H activation. On the basis of this insight, it seems reasonable to speculate that Cu^{II}-catalyzed oxidations of substrates containing acidic C–H bonds follow pathways analogous to the organometallic pathway shown in Scheme 2.6. Many precedents for C–H oxidations of this type, including reactions with alkynes and various aromatic heterocycles, are accomplished with substrates that lack directing groups altogether. Collectively, these insights provide a valuable foundation for continued efforts to expand the scope of Cu-catalyzed aerobic C–H oxidation reactions.

2.9. Contributions.

Dr. Mehmed Zahid Ertem, a graduate student in Prof. Christopher J. Cramer's group at University of Minnesota, performed the computational studies summarized in this chapter. Anh T. Nguyen, an undergraduate student at University of Wisconsin-Madison, was mentored by Alison M. Suess and provided experimental assistance in substrate synthesis and reaction screening while these reactions were initially being developed.

2.10. Experimental.

2.10.1. General Considerations.

¹H, ¹³C, and ²H NMR spectra were recorded on Bruker Avance 300 MHz or 400 MHz or Varian 500 MHz spectrometers. Chemical shifts (δ) are given in parts per million and referenced to the residual solvent signal²⁷ or TMS; all coupling constants are reported in Hz. Quantitative ¹H NMR spectra were obtained with a 25 s relaxation delay. High resolution mass spectra were obtained by the mass spectrometry facility at the University of Wisconsin. Melting points were taken on a Mel-Temp II melting point apparatus. Column chromatography was performed on an

Isco Combiflash instrument or by hand using SiliaFlash® P60 (Silicycle, particle size 40-63 μm , 230-400 mesh) silica gel. All commercial reagents were obtained from Sigma-Aldrich or Acros Organics and used as received unless otherwise noted. The standard deviation of initial rates was calculated using the AnalystSoft Inc. StatPlus:Mac LE plug-in for Microsoft Excel for Mac 2011. NMR spectra were plotted with wxMacNUTS v1.0.2 (Acorn NMR, Inc. 2007) and MestReNova v7.1.2 (MestreLab Research S. L. 2012). Data were plotted with KaleidaGraph v4.01 (Synergy Software 2005).

2.10.2. General Method of Benzamide Methoxylation.

General procedure for benzoyl moiety methoxylation. Reactions were run in 13x100 mm thick-wall culture tubes in a custom 48-well parallel pressure reactor mounted on a Glas-Col vortexer. The headspace was purged with O_2 . Separate stock solutions of substrate plus carbonate base in MeOH/pyridine and copper salt in MeOH/pyridine were added to the culture tubes by syringe to initiate the reaction. Alternatively, solid reagents were added to the culture tubes prior to O_2 purging and the solvent mixture was added to initiate the reaction.

For a N_2 atmosphere (Table 2.1, entry 4), the reaction was carried out in a 10-mL pear-shaped Schlenk flask. Solid reagents were added to the flask, which was evacuated and filled with N_2 (3x). Solvents from Aldrich Sure-Seal N_2 -atmosphere bottles were added by syringe to initiate the reaction.

The typical reaction conditions used for 24-hour yields, initial rates, and KIE experiments were 50 mM substrate, 100 mM $\text{Cu}(\text{OAc})_2$, and 50 mM Cs_2CO_3 in 1 mL 5.18:1 methanol/pyridine solvent per 13x100 mm culture tube.

Copper removal and reaction analysis. At the end of the reaction time, the reaction mixture was diluted with CH_2Cl_2 and evaporated to dryness. The crude reaction material was re-

dissolved in CH₂Cl₂ (1 mL) and aqueous NH₄OH solution (30%, 1 mL). As the layers mixed, Cu dissolved in the aqueous layer, which turned blue. The layers were separated and the aqueous layer was further extracted with CH₂Cl₂ (5x 1 mL). The organic layers were combined, dried with MgSO₄, filtered through Celite, and roto-evaporated. Product yield was evaluated by ¹H NMR spectroscopy and integrated relative to an internal standard (1,4-bis(trimethylsilyl)benzene) added after work-up.

Formation of *N*-methyl-*N*-(8-quinolinyl)carbamate (compound **S1).** Under some conditions for benzoyl moiety methoxylation, *N*-methyl-*N*-(8-quinolinyl)carbamate **S1** was detected; identity was confirmed by independent synthesis. Up to 25% yield of **S1** could be generated with 50 mM **2a**, 50 mM Cu(OTf)₂, 50 mM K₂CO₃ in 0.08 mL pyridine/0.92 mL MeOH at 50 °C for 17 hours. Under those conditions, approximately 25% yield of **3a** was generated, with approximately 50% mass balance.

2.10.3. General Method of Quinoline Chlorination.

General procedure for quinolinyl moiety chlorination. Reactions were run in 13x100 mm thick-wall culture tubes in a custom 48-well parallel pressure reactor mounted on a Glas-Col vortexer. The headspace was purged with O₂. Separate stock solutions of substrate in AcOH and copper salt plus LiCl in AcOH were added to the culture tubes by syringe to initiate the reaction. Alternatively, solid reagents were added to the culture tubes prior to O₂ purging and the solvent mixture was added to initiate the reaction.

The typical reaction conditions used to obtain yields and KIE experiments were 50 mM substrate, 10 mM CuCl, and 100 mM LiCl in 1 mL AcOH solvent per 13x100 mm culture tube.

Copper removal and reaction analysis. At the end of the reaction time, the reaction mixture was diluted with CH₂Cl₂ and evaporated to dryness. The crude reaction material was re-

dissolved in CH_2Cl_2 or CDCl_3 (1 mL). Three drops of aqueous NH_4OH solution (30%) was added and the solution was mixed until color change of the organic layer from green/blue or yellow to colorless was complete. The solution was dried with MgSO_4 and filtered. Alternatively, the reaction mixture was diluted with 10 mL water and 10 mL CH_2Cl_2 . The organic layer was washed with saturated Na_2CO_3 (15 mL) and brine solution (15 mL). The organic layer was dried over MgSO_4 and roto-evaporated. Product yield was evaluated by ^1H NMR spectroscopy and integrated relative to an internal standard (1,4-bis(trimethylsilyl)benzene) added after work-up.

2.10.4. Initial Rates and Hammett Plot for Benzoyl Moiety Methoxylation.

Reactions were run in triplicate under the typical conditions (see section II) and were stopped at the desired time and analyzed by ^1H NMR spectroscopy. To determine the initial rates, each individual data point for a certain substrate was plotted in Microsoft Excel. The data was plotted in terms of product yield (mM) vs. time (min) to give rates in terms of mM/min. Under the typical conditions, initial substrate concentration is 50 mM, therefore a product yield of 10 % is equivalent to 5 mM.

Using the AnalystSoft Inc. StatPlus:Mac LE plug-in for Excel, a standard linear regression with y-intercept set to zero was performed on the plotted data. The StatPlus:Mac LE plug-in outputs various statistics, including the slope of the data (the initial rate) and the standard error (the standard deviation of the initial rate).

The standard deviations of the initial rates were propagated appropriately for the quantities k_X/k_H and $\log(k_X/k_H)$.²⁸ A Hammett plot was generated by plotting $\log(k_X/k_H)$ vs. the Hammett σ_{meta} value (Figure 1). A weighted linear regression (which accounts for the different

standard errors associated with each initial rate)²⁹ of the data gives the equation $y = (0.558 \pm 0.099)x + (0.006 \pm 0.011)$, therefore the Hammett parameter ρ is 0.6 ± 0.1 .

2.10.5. Deuteration and Isotope Effect Experiments for Benzamide Methoxylation.

See Appendix 1 for the relevant NMR spectra.

Irreversible C-H Activation. To probe the reversibility of C-H activation, CH₃OD was substituted for CH₃OH in the typical reaction conditions (section II). After 5 h of reaction time, the reaction solutions in four culture tubes were combined. The starting material **2a** and product **3a** were separated by column chromatography (silica gel, 5 % EtOAc in hexanes). The starting material and product were analyzed by ¹H NMR spectroscopy; deuterium incorporation was not observed (Figures S2 and S3). Therefore, C-H activation is irreversible.

Intramolecular Competition KIE. To determine the intramolecular competition KIE, substrate **2e** was submitted to the typical reaction conditions (section II). After 6 h or 24 h of reaction time, the reaction solutions in 3 culture tubes were combined. The starting material and product were separated by column chromatography (silica gel, 5 % EtOAc in hexanes). By ¹H NMR analysis of the product we observed that approximately 84% of the C-H bond was consumed and 16% of the C-D bond was consumed (Figure S4). The ²H{¹H} NMR spectrum was also obtained (Figure S5). Identical results were obtained for the 6 h and 24 h experiments. An intramolecular KIE of 5.25 ± 0.06 was determined for the methoxylation reaction (error is based on integration of the ¹H NMR spectrum).

Independent Initial Rate Comparison k_H/k_D . The initial reaction rates of the proteo substrate **2a** and the aryl-*d*₅ substrate **2f** were determined to be 0.0564 ± 0.0013 mM/min and 0.00988 ± 0.00016 mM/min, respectively (Table S5, Figure S6). Therefore the KIE (k_H/k_D) was

determined to be 5.7 ± 0.8 for the methoxylation reaction. This result indicates that C-H activation is the rate-determining step of this reaction.

The standard deviation of the KIE value was calculated by propagation of error.⁸ Strict propagation of error gives a standard deviation of 0.16, for a KIE value of 5.7 ± 0.2 . However, this calculated standard deviation is probably too small. The standard deviation of the initial rate of the *d*₅-substrate **2f** is very small because the measured values of product yield are small (Figure S6). We estimate that the actual experimental error should be approximately equal to the experiment error in measurement of the initial rate of the proteo substrate **2a**. Substitution of $\sigma(k_H)$ for $\sigma(k_D)$ gives a standard deviation of 0.79 and thus a KIE value of 5.7 ± 0.8 .

2.10.6. Deuteration and Isotope Effect Experiments for Quinoline Chlorination.

See Appendix 1 for the relevant NMR spectra.

No Deuterium Incorporation. CD₃COOD was substituted for CH₃COOH in the typical reaction conditions (section III). After 3 h of reaction time, the reaction solutions in 2 culture tubes were analyzed independently after copper removal. By ¹H NMR spectroscopy, deuterium incorporation was not observed.

Intermolecular Competition KIE. To determine the intermolecular competition KIE, an equal mixture of substrates **2a** and **2g** were submitted to the typical reaction conditions (section III). After 30 min of reaction time, the reaction solutions in 4 culture tubes were combined. The starting material and product were separated by column chromatography (silica gel, 5 % EtOAc in hexanes). ¹H NMR analysis of the isolated product demonstrated an approximately 1:1 ratio of H/D at the 7-position of the quinoline. An intermolecular competition KIE of 1.04 ± 0.05 was determined for the chlorination reaction. Unless there is an initial irreversible binding of the

substrate to the catalyst, this result indicates the turnover-limiting step does not involve C-H activation.

Independent Rates KIE. Reaction of **2a** or **2g** were run independently in duplicate or triplicate under the typical reaction conditions (section III). At certain timepoints the reactions were stopped and molar quantities of product and recovered starting material were analyzed by ^1H NMR spectroscopy. Within error, the rates of product appearance and starting material consumption overlay well, indicating that $k_{\text{H}}/k_{\text{D}} \sim 1$ (Figure). The overall rates do not fit well to an exponential model, and due to the speed of the reaction, the initial rate with the range examined does not fit well to a linear model. Therefore error for the value of $k_{\text{H}}/k_{\text{D}}$ was not calculated.

2.10.7. Synthesis and Characterization of Substrates.

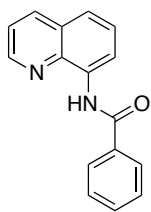
See Appendix 1 for the NMR spectra of novel compounds.

Amide synthesis from the commercially available acid chloride. The aminoquinoline (2.0 mmol) and triethylamine (2.2 mmol) were dissolved in dry CH_2Cl_2 (5 mL) and stirred at room temperature for 10 min, then stirred for a further 10 min while the reaction solution was cooled in an ice bath. The acid chloride (2.0 mmol) was added dropwise (if solid, it was dissolved in a minimum of dry CH_2Cl_2). The reaction solution was allowed to stir overnight while the ice bath melted.

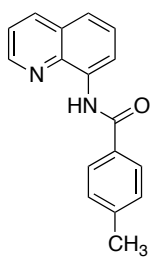
The reaction mixture was dissolved in EtOAc (20 mL) and water (10 mL). The layers were separated and the organic layer was washed further with 1 M NaOH aqueous solution (3x 15 mL). The organic layer was dried with MgSO_4 , filtered, and roto-evaporated. The product was purified by silica gel column with hexane/EtOAc eluent (gradient). If color persisted, the dissolved product was treated with activated carbon overnight, then filtered. The product was

further purified by recrystallization (2 to 3x from hexane/EtOAc). All substrates **2** are colorless solids.

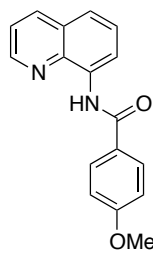
Synthesis of the acid chloride from the commercially-available carboxylic acid. If the acid chloride was not commercially available, it was synthesized. The benzoic acid derivative (2.0 mmol) was added to a dried flask with dry CH₂Cl₂ (5 mL). Oxalyl chloride (2.4 mmol) was added to the reaction solution along with 2 drops of dimethylformamide. The reaction solution was heated at reflux (3 to 5 h). Solvent was removed from the acid chloride by distillation or by using a vacuum manifold with cooled solvent traps (later quenching any excess oxalyl chloride in the collected fluids). The acid chloride was used immediately for amide synthesis.



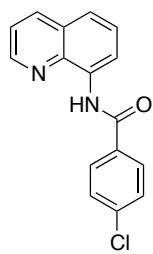
2a (N-(8-quinolinyl)benzamide). Colorless solid; spectral properties are consistent with literature values.³⁰ ¹H NMR (300 MHz, CDCl₃) δ 10.76 (br s, 1H), 8.95 (dd, $J = 7.3, 1.7$ Hz, 1H), 8.86 (dd, $J = 4.2, 1.7$ Hz, 1H), 8.20 (dd, $J = 8.3, 1.7$ Hz, 1H), 8.15-8.04 (m, 2H), 7.66-7.45 (m, 5H).



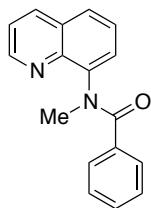
2b (4-methyl-N-(8-quinolinyl)benzamide). Colorless solid; spectral properties are consistent with literature values.² ¹H NMR (300 MHz, CDCl₃) δ 10.72 (br s, 1H), 8.94 (dd, $J = 7.5, 1.6$ Hz, 1H), 8.85 (dd, $J = 4.2, 1.7$ Hz, 1H), 8.18 (dd, $J = 8.3, 1.7$ Hz, 1H), 8.01-7.97 (m, 2H), 7.65-7.42 (m, 3H), 7.35 (d, $J = 8.0$ Hz, 2H), 2.45 (s, 3H).



2c (4-methoxy-*N*-(8-quinolinyl)benzamide). Prepared according to the general amide synthesis procedure. Colorless solid, mp = 118 °C. ^1H NMR (300 MHz, CDCl_3) δ 10.68 (br s, 1H), 8.93 (dd, J = 7.5, 1.5 Hz, 1H), 8.85 (dd, J = 4.2, 1.7 Hz, 1H), 8.18 (dd, J = 8.3, 1.7 Hz, 1H), 8.06-8.04 (m, 2H), 7.62-7.45 (m, 3H), 7.07-7.02 (m, 2H), 3.90 (s, 3H). ^{13}C NMR (75 MHz, CDCl_3) δ 164.83, 162.46, 148.14, 138.66, 136.26, 134.70, 129.09, 127.91, 127.36, 127.33, 121.58, 121.35, 116.23, 113.93, 55.39. HRMS (ESI) m/z calcd for $\text{C}_{17}\text{H}_{14}\text{N}_2\text{O}_2$ $[\text{M}+\text{H}]^+$: 279.1129, found 279.1131 (< 1 ppm).



2d (4-chloro-*N*-(8-quinolinyl)benzamide). Prepared according to the general amide synthesis procedure. Colorless solid, mp = 116-117 °C. ^1H NMR (300 MHz, CDCl_3) δ 10.59 (br s, 1H), 8.84 (dd, J = 7.4, 1.5 Hz, 1H), 8.74 (dd, J = 4.2, 1.6 Hz, 1H), 8.05 (dd, J = 8.3, 1.6 Hz, 1H), 7.95-7.90 (m, 2H), 7.52-7.34 (m, 5H). ^{13}C NMR (75 MHz, CDCl_3) δ 163.98, 148.21, 138.53, 137.97, 136.25, 134.20, 133.33, 128.90, 128.58, 127.83, 127.27, 121.79, 121.64, 116.45. HRMS (ESI) m/z calcd for $\text{C}_{16}\text{H}_{11}\text{ClN}_2\text{O}$ $[\text{M}+\text{H}]^+$: 283.0633, found 283.0643 (3.5 ppm).

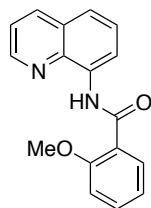


6a (*N*-methyl-*N*-(8-quinolinyl)benzamide). The tertiary amide was synthesized

by methylation of **2a** according to a literature method for a similar compound.³¹ Colorless solid, mp = 137-138 °C. ¹H NMR (300 MHz, CDCl₃) δ 8.98 (dd, *J* = 4.2, 1.7 Hz, 1H), 8.10 (dd, *J* = 8.3, 1.7 Hz, 1H), 7.65 (dd, *J* = 7.8, 1.8 Hz, 1H), 7.42-7.28 (m, 5H), 7.08-6.94 (m, 3H), 3.60 (s, 3H). ¹³C NMR (75 MHz, CDCl₃) δ 172.15, 150.63, 143.95, 142.50, 136.78, 136.27, 129.33, 129.28, 129.21, 127.98, 127.67, 127.41, 126.26, 121.76, 38.52. HRMS (ESI) *m/z* calcd for C₁₇H₁₄N₂O [M+H]⁺: 263.1179, found 263.1169 (3.8 ppm).

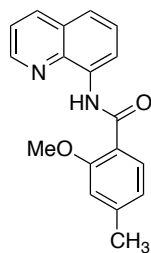
2.10.8. Characterization of Products.

See Appendix 1 for the NMR spectra of novel compounds.



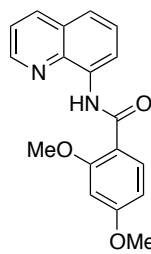
3a (2-methoxy-*N*-(8-quinolinyl)benzamide). Colorless solid, spectral properties are

consistent with literature values.² ¹H NMR (300 MHz, CDCl₃) δ 12.34 (br s, 1H), 9.04 (dd, *J* = 7.5, 1.5 Hz, 1H), 8.88 (dd, *J* = 4.2, 1.7 Hz, 1H), 8.36 (dd, *J* = 7.8, 1.9 Hz, 1H), 8.17 (dd, *J* = 8.3, 1.7 Hz, 1H), 7.61-7.44 (m, 4H), 7.15 (t, *J* = 7.5 Hz, 1H), 7.08 (d, *J* = 8.3 Hz, 1H), 4.21 (s, 3H).

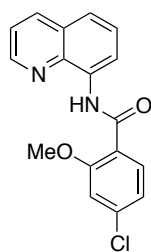


3b (2-methoxy-4-methyl-*N*-(8-quinolinyl)benzamide). Colorless solid, mp = 134-135 °C. ¹H NMR (300 MHz, CDCl₃) δ 12.26 (br s, 1H), 9.01 (dd, *J* = 7.7, 1.1 Hz, 1H), 8.68 (dd,

$J = 4.1, 1.6$ Hz, 1H), 8.21 (d, $J = 8.0$ Hz, 1H), 7.97 (dd, $J = 8.3, 1.7$ Hz, 1H), 7.51-7.46 (m, 1H), 7.38-7.35 (m, 1H), 7.26 (dd, $J = 8.2, 4.2$ Hz, 1H), 6.84 (d, $J = 8.0$ Hz, 1H), 6.69 (s, 1H), 4.01 (s, 3H), 2.30 (s, 3H). ^{13}C NMR (75 MHz, CDCl_3) δ 163.50, 157.50, 148.00, 143.91, 138.99, 135.86, 135.78, 132.02, 127.87, 127.25, 121.85, 121.22, 121.15, 119.32, 116.88, 112.06, 55.76, 21.62. HRMS (ESI) m/z calcd for $\text{C}_{18}\text{H}_{16}\text{N}_2\text{O}_2$ $[\text{M}+\text{H}]^+$: 293.1207, found 293.1208 (<1 ppm).



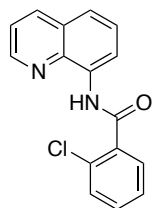
3c (2,4-dimethoxy-*N*-(8-quinolinyl)benzamide). Colorless solid, mp = 137 °C. ^1H NMR (300 MHz, CDCl_3) δ 12.23 (br s, 1H), 9.02 (dd, $J = 7.7, 1.4$ Hz, 1H), 8.81 (dd, $J = 4.2, 1.7$ Hz, 1H), 8.31 (d, $J = 8.7$ Hz, 1H), 8.11 (dd, $J = 8.3, 1.7$ Hz, 1H), 7.57 – 7.37 (m, 3H), 6.63 (dd, $J = 8.8, 2.3$ Hz, 1H), 6.53 (d, $J = 2.3$ Hz, 1H), 4.13 (s, 3H), 3.85 (s, 3H); ^{13}C NMR (75 MHz, CDCl_3) δ 163.81, 163.56, 159.19, 148.22, 139.30, 136.24, 136.06, 134.06, 128.16, 127.64, 121.43, 121.22, 117.17, 115.44, 105.61, 98.64, 56.15, 55.61; HRMS (ESI) m/z calcd for $\text{C}_{18}\text{H}_{16}\text{N}_2\text{O}_3$ $[\text{M}+\text{H}]^+$: 309.1234, found 309.1232 (<1 ppm).



3d (4-chloro-2-methoxy-*N*-(8-quinolinyl)benzamide). Colorless solid, mp = 174-176 °C. ^1H NMR (300 MHz, CDCl_3) δ 12.16 (br s, 1H), 8.96 (dd, $J = 7.6, 1.4$ Hz, 1H), 8.75 (dd, $J = 4.2, 1.7$ Hz, 1H), 8.24 (d, $J = 8.5$ Hz, 1H), 8.07 (dd, $J = 8.3, 1.7$ Hz, 1H), 7.55-7.34 (m, 3H), 7.05 (dd, $J = 8.5, 1.9$ Hz, 1H), 6.94 (d, $J = 1.9$ Hz, 1H), 4.09 (s, 3H). ^{13}C NMR (75 MHz, CDCl_3) δ 162.53, 158.02, 148.26, 139.14, 138.77, 136.19, 135.56, 133.47, 128.06, 127.50, 121.67,

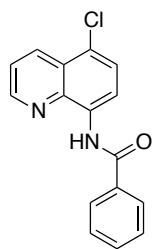
121.53, 121.49, 120.91, 117.30, 112.20, 56.43. HRMS (ESI) m/z calcd for $C_{17}H_{13}ClN_2O_2$

$[M+H]^+$: 313.0739, found 313.0740 (<1 ppm).



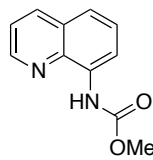
4a (2-chloro-*N*-(8-quinolinyl)benzamide). Colorless solid, spectral properties are

consistent with literature values.² 1H NMR (300 MHz, $CDCl_3$) δ 10.49 (br s, 1H), 8.97 (dd, J = 7.1, 2.0 Hz, 1H), 8.80 (dd, J = 4.2, 1.7 Hz, 1H), 8.19 (dd, J = 8.3, 1.7 Hz, 1H), 7.85-7.79 (m, 1H), 7.64-7.38 (m, 8H).



5a (*N*-(5-chloro-8-quinolinyl)benzamide). Colorless solid, mp = 139-140 °C. 1H

NMR (300 MHz, $CDCl_3$) δ 10.67 (br s, 1H), 9.10-8.73 (m, 2H), 8.57 (dd, J = 8.5, 1.6 Hz, 1H), 8.08-8.05 (m, 2H), 7.65-7.51 (m, 5H). ^{13}C NMR (75 MHz, $CDCl_3$) δ 165.50, 148.87, 139.42, 135.00, 133.99, 133.57, 132.12, 128.97, 127.43, 127.40, 126.12, 124.60, 122.53, 116.58. HRMS (ESI) m/z calcd for $C_{16}H_{11}ClN_2O$ $[M+H]^+$: 283.0633, found 283.0643 (3.5 ppm). 1D nOe experiments verify the position of the chloro substituent.



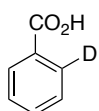
S1 (*N*-methyl-*N*-(8-quinolinyl)carbamate). Colorless solid, mp = 42-43 °C.

Identity was confirmed by independent synthesis from 8-aminoquinoline and methyl chloroformate according to the general amide synthesis procedure. Melting points of 45 °C or 61.5-62.5 °C are reported in previous literature.³² 1H NMR (300 MHz, $CDCl_3$) δ 9.21 (br s, 1H),

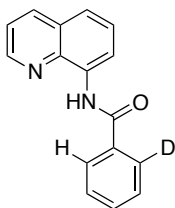
8.78 (dd, $J = 4.2, 1.7$ Hz, 1H), 8.42 (d, $J = 7.5$ Hz, 1H), 8.14 (dd, $J = 8.3, 1.7$ Hz, 1H), 7.56-7.41 (m, 3H), 3.85 (s, 3H). ^{13}C NMR (75 MHz, CDCl_3) δ 154.05, 148.08, 138.15, 136.13, 134.71, 127.97, 127.22, 121.55, 120.56, 114.50, 52.29. HRMS (ESI) m/z calcd for $\text{C}_{11}\text{H}_{10}\text{N}_2\text{O}_2$ $[\text{M}+\text{H}]^+$: 203.0816, found 203.0813 (1.5 ppm).

2.10.9. Synthesis and Characterization of Deuterium-Labeled Substrates.

See Appendix 1 for the NMR spectra of novel compounds.

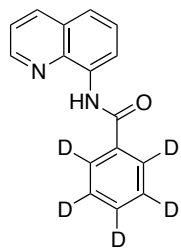


S2 (2-deuteriobenzoic acid). The acid was synthesized by lithiation/ D_2O quench of 2-bromotoluene and subsequent KMnO_4 oxidation according to literature methods; spectral properties are consistent with literature values although the previously the compound was not fully characterized.³³ Colorless solid, mp = 122-123 °C. Quantitative deuterium incorporation. ^1H NMR (300 MHz, CDCl_3) δ 12.10 (br s, 1H), 8.18-8.08 (m, 1H), 7.63 (ddd, $J = 7.7, 7.2, 1.4$ Hz, 1H), 7.55-7.43 (m, 2H). ^{13}C NMR (75 MHz, CDCl_3) δ 172.83, 133.93, 130.32, 130.06 (1:1:1 t, $J = 25$ Hz, 1C), 129.39, 128.58, 128.46. HRMS (ESI) m/z calcd for $\text{C}_7\text{H}_5\text{DO}_2$ $[\text{M}]^+$: 123.0426, found 123.0431 (4.0 ppm).



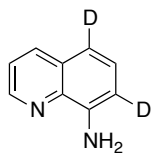
2e (2-deuterio-*N*-(8-quinolinyl)benzamide). Amide **2e** was synthesized from compound **S2** and 8-aminoquinoline according to the general amide synthesis procedure. Colorless solid, mp = 89 °C. ^1H NMR (300 MHz, CDCl_3) δ 10.75 (br s, 1H), 8.95 (dd, $J = 7.3, 1.6$ Hz, 1H), 8.86 (dd, $J = 4.2, 1.7$ Hz, 1H), 8.20 (dd, $J = 8.3, 1.7$ Hz, 1H), 8.13-8.05 (m, 1H), 7.64-7.45 (m, 6H). ^{13}C NMR (75 MHz, CDCl_3) δ 165.31, 148.24, 138.70, 136.30, 135.03,

134.54, 131.82, 128.77, 128.67, 127.93, 127.30, 127.24 (1:1:1 t, $J = 24.5$ Hz), 126.65, 121.67, 121.65, 116.46. HRMS (ESI) m/z calcd for $C_{16}H_{11}DN_2O$ $[M+H]^+$: 250.1086, found 250.1089 (1.2 ppm).



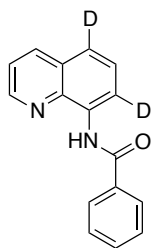
2f (2,3,4,5,6-pentadeuterio-*N*-(8-quinolinyl)benzamide). Amide **2f** was

synthesized from benzoic- d_5 acid and 8-aminoquinoline according to the general amide synthesis procedure. Colorless solid, mp = 89-90 °C. 1H NMR (300 MHz, $CDCl_3$) δ 10.73 (br s, 1H), 8.94 (dd, $J = 7.4, 1.5$ Hz, 1H), 8.83 (dd, $J = 4.2, 1.7$ Hz, 1H), 8.15 (dd, $J = 8.3, 1.6$ Hz, 1H), 7.60-7.42 (m, 3H). ^{13}C NMR (75 MHz, $CDCl_3$) δ 165.31, 148.24, 138.69, 136.30, 134.95, 134.55, 131.31 (1:1:1 t, $J = 23.9$ Hz), 128.26 (1:1:1 t, $J = 24.3$ Hz), 127.93, 127.37, 126.85 (1:1:1 t, $J = 24.4$ Hz), 121.67, 121.65, 116.46. HRMS (ESI) m/z calcd for $C_{16}H_7D_5N_2O$ $[M+H]^+$: 254.1337, found 254.1340 (1.2 ppm).



S3 (5,7-dideuterio-8-aminoquinoline). The deuterated aminoquinoline was

synthesized from 8-aminoquinoline and DCl/D_2O in a microwave according to a literature method; spectral properties are consistent with literature values.³⁴ 1H NMR (300 MHz, $CDCl_3$) δ 8.75 (dd, $J = 4.2, 1.7$ Hz, 1H), 8.10-7.99 (m, 1H), 7.39-7.26 (m, 2H), 4.98 (br s, 2H); 98% deuterium incorporation.



2g (*N*-(5,7-dideuterio-8-quinolinyl)benzamide). The amide was synthesized

from benzoyl chloride and aminoquinoline **S3** according to the general amide synthesis procedure. Colorless solid, mp = 88-89 °C. ^1H NMR (500 MHz, CDCl_3) δ 10.73 (br s, 1H), 8.82-8.81 (m, 1H), 8.14-8.08 (m, 3H), 7.59-7.52 (m, 4H), 7.43 (dd, $J = 8.2, 4.2$ Hz, 1H). ^{13}C NMR (126 MHz, CDCl_3) δ 165.41, 148.30, 148.24, 138.75, 136.33, 136.23, 135.17, 134.51, 131.87, 128.83, 127.92, 127.32, 127.22, 121.70, 121.42 (1:1:1 t, $J = 24.7$ Hz), 116.25 (1:1:1 t, $J = 25.5$ Hz). HRMS (ESI) m/z calcd for $\text{C}_{16}\text{H}_{10}\text{D}_2\text{N}_2\text{O}$ $[\text{M}+\text{H}]^+$: 251.1148, found 251.1141 (2.8 ppm).

2.11. References and Notes.

1. (a) Wendlandt, A. E.; Suess, A. M.; Stahl, S. S. "Copper-Catalyzed Aerobic Oxidative C-H Functionalizations: Trends and Mechanistic Insights." *Angew. Chem. Int. Ed.* **2011**, *50*, 11062-11087. (b) Shi, Z.; Zhang, C.; Tang, C.; Jiao, N. "Recent advances in transition-metal catalyzed reactions using molecular oxygen as the oxidant." *Chem. Soc. Rev.* **2012**, *41*, 3381-3430. (c) Punniyamurthy, T.; Rout, L. "Recent advances in copper-catalyzed oxidation of organic compounds." *Coord. Chem. Rev.* **2008**, *252*, 134-154. (d) Gamez, P.; Aubel, P. G.; Driessen, W. L.; Reedijk, J. "Homogeneous bio-inspired copper-catalyzed oxidation reactions." *Chem. Soc. Rev.* **2001**, *30*, 376-385. (e) Liu, C.; Zhang, H.; Shi, W.; Lei, A. "Bond Formations between Two Nucleophiles: Transition Metal Catalyzed Oxidative Cross-Coupling Reactions." *Chem. Rev.* **2011**, *111*, 1780-1824.

2. (a) Brunel, J. M. "BINOL: A Versatile Chiral Reagent." *Chem. Rev.* **2005**, *105*, 857-898. (b) Sainsbury, M. "Modern methods of aryl-aryl bond formation." *Tetrahedron* **1980**, *36*, 3327-3359. (c) Ashenhurst, J. A. "Intermolecular oxidative cross-coupling of arenes." *Chem. Soc. Rev.* **2010**, *39*, 540-548. (d) Kočovský, P.; Vyskočil, Š.; Smrčina, M. "Non-Symmetrically Substituted 1,1'-Binaphthyls in Enantioselective Catalysis." *Chem. Rev.* **2003**, *103*, 3213-3246. (e) Rosini, C.; Franzini, L.; Raffaelli, A.; Salvadori, P. "Synthesis and Applications of Binaphthyl C₂-Symmetry Derivatives as Chiral Auxiliaries in Enantioselective Reactions." *Synthesis* **1992**, *1992*, 503-517. (f) Wang, H. *Chirality* **2010**, *22*, 827-837.
3. (a) Menini, L.; Gusevskaya, E. V. "Novel highly selective catalytic oxychlorination of phenols." *Chem. Commun.* **2006**, 209-211. (b) Menini, L.; Gusevskaya, E. V. "Aerobic oxychlorination of phenols catalyzed by copper(II) chloride." *Applied Catalysis A: General* **2006**, *309*, 122-128. (c) Menini, L.; Parreira, L. A.; Gusevskaya, E. V. "A practical highly selective oxybromination of phenols with dioxygen." *Tetrahedron Lett.* **2007**, *48*, 6401-6404. (c) Menini, L.; da Cruz Santos, J. C.; Gusevskaya, E. V. "Copper-Catalyzed Oxybromination and Oxychlorination of Primary Aromatic Amines Using LiBr or LiCl and Molecular Oxygen." *Adv. Synth. Catal.* **2008**, *350*, 2052-2058.
4. Yang, L.; Lu, Z.; Stahl, S. S. "Regioselective copper-catalyzed chlorination and bromination of arenes with O₂ as the oxidant." *Chem. Commun.* **2009**, *45*, 6460-6462.
5. For leading references, see: (a) Zhang, C.; Tang, C.; Jiao, N. "Recent advances in copper-catalyzed dehydrogenative functionalization via a single electron transfer (SET) process." *Chem. Soc. Rev.* **2012**, *41*, 3464-3484. (b) Boess, E.; Schmitz, C.; Klussmann, M. "A Comparative Mechanistic Study of Cu-Catalyzed Oxidative Coupling Reactions with N-

- Phenyltetrahydroisoquinoline." *J. Am. Chem. Soc.* **2012**, *134*, 5317-5325. (c) Li, C.-J. "Cross-Dehydrogenative Coupling (CDC): Exploring C-C Bond Formations beyond Functional Group Transformations." *Acc. Chem. Res.* **2009**, *42*, 335-344. (d) Li, C.-J.; Li, Z. "Green chemistry: The development of cross-dehydrogenative coupling (CDC) for chemical synthesis." *Pure Appl. Chem.* **2006**, *78*, 935-945. (e) Li, Z.; Bohle, D. S.; Li, C.-J. "Cu-catalyzed cross-dehydrogenative coupling: A versatile strategy for C-C bond formations via the oxidative activation of sp^3 C-H bonds." *P. Natl. Acad. Sci.* **2006**, *103*, 8928-8933.
6. Chen, X.; Hao, X.-S.; Goodhue, C. E.; Yu, J.-Q. "Cu(II)-Catalyzed Functionalizations of Aryl C-H Bonds Using O_2 as an Oxidant." *J. Am. Chem. Soc.* **2006**, *128*, 6790-6791.
 7. The mechanism was further supported by analogy to Co^{III} -promoted arene C-H oxidation: Kochi, J. K.; Tang, R. T.; Bernath, T. "Mechanisms of aromatic substitution. Role of cation-radicals in the oxidative substitution of arenes by cobalt(III)." *J. Am. Chem. Soc.* **1973**, *95*, 7114-7123.
 8. For leading references, see: (a) Furuta, H.; Maeda, H.; Osuka, A. "Doubly N-Confused Porphyrin: A New Complexing Agent Capable of Stabilizing Higher Oxidation States." *J. Am. Chem. Soc.* **2000**, *122*, 803-807. (b) Chmielewski, P. J.; Latos-Grażyński, L.; Schmidt, I. "Copper(II) Complexes of Inverted Porphyrin and Its Methylated Derivatives." *Inorg. Chem.* **2000**, *39*, 5475-5482. (c) Furuta, H.; Ishizuka, T.; Osuka, A.; Uwatoko, Y.; Ishikawa, Y. "Metal Complexes of an N-Confused Calix[4]pyrin Derivative—The First X-ray Structure of an Organometallic Compound of Divalent Copper." *Angew. Chem. Int. Ed.* **2001**, *40*, 2323-2325. (d) Maeda, H.; Ishikawa, Y.; Matsuda, T.; Osuka, A.; Furuta, H. "Control of Cu(II) and Cu(III) States in N-Confused Porphyrin by Protonation/Deprotonation at the

- Peripheral Nitrogen." *J. Am. Chem. Soc.* **2003**, *125*, 11822-11823. (e) Pawlicki, M.; Kańska, I.; Latos-Grażyński, L. "Copper(II) and Copper(III) Complexes of Pyrrole-Appended Oxacarbaporphyrin." *Inorg. Chem.* **2007**, *46*, 6575-6584.
9. (a) Ribas, X.; Jackson, D. A.; Donnadieu, B.; Mahía, J.; Parella, T.; Xifra, R.; Hedman, B.; Hodgson, K. O.; Llobet, A.; Stack, T. D. P. "Aryl C-H Activation by Cu^{II} To Form an Organometallic Aryl-Cu^{III} Species: A Novel Twist on Copper Disproportionation." *Angew. Chem. Int. Ed.* **2002**, *41*, 2991-2994. (b) Xifra, R.; Ribas, X.; Llobet, A.; Poater, A.; Duran, M.; Solà, M.; Stack, T. D. P.; Benet-Buchholz, J.; Donnadieu, B.; Mahía, J.; Parella, T. "Fine-Tuning the Electronic Properties of Highly Stable Organometallic Cu^{III} Complexes Containing Monoanionic Macrocyclic Ligands." *Chem. Eur. J.* **2005**, *11*, 5146-5156. (c) Ribas, X.; Calle, C.; Poater, A.; Casitas, A.; Gómez, L.; Xifra, R.; Parella, T.; Benet-Buchholz, J.; Schweiger, A.; Mitrikas, G.; Solà, M.; Llobet, A.; Stack, T. D. P. "Facile C-H Bond Cleavage via a Proton-Coupled Electron Transfer Involving a C-H...Cu^{II} Interaction." *J. Am. Chem. Soc.* **2010**, *132*, 12299-12306.
10. For a related macrocyclic arene, see: Yao, B.; Wang, D.-X.; Huang, Z.-T.; Wang, M.-X. "Room-temperature aerobic formation of a stable aryl-Cu(III) complex and its reactions with nucleophiles: highly efficient and diverse arene C-H functionalizations of azacalix[1]arene[3]pyridine." *Chem. Commun.* **2009**, *45*, 2899-2901.
11. King, A. E.; Huffman, L. M.; Casitas, A.; Costas, M.; Ribas, X.; Stahl, S. S. "Copper-Catalyzed Aerobic Oxidative Functionalization of an Arene C-H Bond: Evidence for an Aryl-Copper(III) Intermediate." *J. Am. Chem. Soc.* **2010**, *132*, 12068-12073.

12. For fundamental studies of the C–O/C–N reductive elimination reactions, see: (a) Huffman, L. M.; Stahl, S. S. "Carbon–Nitrogen Bond Formation Involving Well-Defined Aryl–Copper(III) Complexes." *J. Am. Chem. Soc.* **2008**, *130*, 9196-9197. (b) Huffman, L. M.; Casitas, A.; Font, M.; Canta, M.; Costas, M.; Ribas, X.; Stahl, S. S. "Observation and Mechanistic Study of Facile C–O Bond Formation between a Well-Defined Aryl–Copper(III) Complex and Oxygen Nucleophiles." *Chem. Eur. J.* **2011**, *17*, 10643-10650.
13. For leading references, see: (a) Zaitsev, V. G.; Shabashov, D.; Daugulis, O. "Highly Regioselective Arylation of sp^3 C–H Bonds Catalyzed by Palladium Acetate." *J. Am. Chem. Soc.* **2005**, *127*, 13154-13155. (b) Daugulis, O.; Do, H.-Q.; Shabashov, D. "Palladium- and Copper-Catalyzed Arylation of Carbon-Hydrogen Bonds." *Acc. Chem. Res.* **2009**, *42*, 1074-1086.
14. The first application of this ligand to Cu-mediated C–H functionalization (non-aerobic) was reported recently: Tran, L. D.; Popov, I.; Daugulis, O. "Copper-Promoted Sulfenylation of sp^2 C–H Bonds." *J. Am. Chem. Soc.* **2012**, *134*, 18237-18240.
15. Material in this chapter was published as: Suess, A. M.; Ertem, M. Z.; Cramer, C. J.; Stahl, S. S. "Divergence between Organometallic and Single-Electron-Transfer Mechanisms in Copper(II)-Mediated Aerobic C–H Oxidation." *J. Am. Chem. Soc.* **2013**, *135*, 9797-9804.
16. Uemura, T.; Imoto, S.; Chatani, N. "Amination of the Ortho C–H Bonds by the $Cu(OAc)_2$ -mediated Reaction of 2-Phenylpyridines with Anilines." *Chem. Lett.* **2006**, *35*, 842-843.
17. For a similar beneficial catalytic effect arising from in situ generation of a base upon aerobic oxidation of Cu^I in alcohol oxidation reaction, see: Hoover, J. M.; Ryland, B. L.; Stahl, S. S.

- "Mechanism of Copper(I)/TEMPO-Catalyzed Aerobic Alcohol Oxidation." *J. Am. Chem. Soc.* **2013**, *135*, 2357-2367.
18. See, for example: Anslyn, E. V.; Dougherty, D. A. In *Modern Physical Organic Chemistry*; University Science Books: Sausalito, 2006, p 445-453.
19. For example, in Cu-catalyzed oxidative chlorination (ref 4), benzene, toluene and anisole do not react, while dimethoxybenzene, which is significantly more electron-rich, does react. As another example, the reaction of PhOAc is 1000-fold faster than PhO₂CCF₃ in Co^{III}-mediated oxidative trifluoroacetoxylation (ref 7), which is proposed to proceed via SET.
20. For a comparison of the electronic effects of "electrophilic" C–H activation by Pd^{II} and other more-classical electrophiles, see: Stock, L. M.; Tse, K.-t.; Vorvick, L. J.; Walstrum, S. A. "Palladium(II) acetate catalyzed aromatic substitution reaction." *J. Org. Chem.* **1981**, *46*, 1757-1759.
21. See, for example: (a) Ryabov, A. D.; Sakodinskaya, I. K.; Yatsimirsky, A. K. "Kinetics and mechanism of ortho-palladation of ring-substituted NN-dimethylbenzylamines." *J. Chem. Soc., Dalton Trans.* **1985**, *14*, 2629-2638. (b) Karig, G.; Moon, M.-T.; Thasana, N.; Gallagher, T. "C-H Activation and Palladium Migration within Biaryls under Heck Reaction Conditions." *Org. Lett.* **2002**, *4*, 3115-3118. (c) Davies, D. L.; Donald, S. M. A.; Macgregor, S. A. "Computational Study of the Mechanism of Cyclometalation by Palladium Acetate." *J. Am. Chem. Soc.* **2005**, *127*, 13754-13755. (d) García-Cuadrado, D.; Braga, A. A. C.; Maseras, F.; Echavarren, A. M. "Proton Abstraction Mechanism for the Palladium-Catalyzed Intramolecular Arylation." *J. Am. Chem. Soc.* **2006**, *128*, 1066-1067. (e) Gorelsky, S. I.; Lapointe, D.; Fagnou, K. "Analysis of the Concerted Metalation-Deprotonation Mechanism

- in Palladium-Catalyzed Direct Arylation Across a Broad Range of Aromatic Substrates." *J. Am. Chem. Soc.* **2008**, *130*, 10848-10849. (f) Balcells, D.; Clot, E.; Eisenstein, O. "C-H Bond Activation in Transition Metal Species from a Computational Perspective." *Chem. Rev.* **2010**, *110*, 749-823. (g) Sun, H.-Y.; Gorelsky, S. I.; Stuart, D. R.; Campeau, L.-C.; Fagnou, K. "Mechanistic Analysis of Azine N-Oxide Direct Arylation: Evidence for a Critical Role of Acetate in the Pd(OAc)₂ Precatalyst." *J. Org. Chem.* **2010**, *75*, 8180-8189. (h) Gorelsky, S. I.; Lapointe, D.; Fagnou, K. "Analysis of the Palladium-Catalyzed (Aromatic)C-H Bond Metalation-Deprotonation Mechanism Spanning the Entire Spectrum of Arenes." *J. Org. Chem.* **2011**, *77*, 658-668. (i) Ackermann, L. "Carboxylate-Assisted Transition-Metal-Catalyzed C-H Bond Functionalizations: Mechanism and Scope." *Chem. Rev.* **2011**, *111*, 1315-1345.
22. Zhao, Y.; Truhlar, D. G. *J. Chem. Phys.* **2006**, *125*, 194101.
23. Marenich, A. V.; Cramer, C. J.; Truhlar, D. G. *J. Phys. Chem. B* **2009**, *113*, 6378-6396.
24. The activation energy ΔG^\ddagger was estimated using the equation $\Delta G^\ddagger = -RT \ln(k^*h/k_B T)$, where the gas constant $R = 8.315 \text{ J mol}^{-1} \text{ K}^{-1}$, T is the reaction temperature, $k = \ln(2)/t_{1/2}$ where $t_{1/2}$ is the reaction half-life, Planck's constant $h = 6.626 \times 10^{-34} \text{ J s}$, and the Boltzmann constant $k_B = 1.381 \times 10^{-23} \text{ J K}^{-1}$.
25. C-H activation by Cu^{III} has been proposed in the presence of hypervalent iodine reagents: (a) Phipps, R. J.; Grimster, N. P.; Gaunt, M. J. *J. Am. Chem. Soc.* **2008**, *130*, 8172-8174. (b) Phipps, R. J.; Gaunt, M. J. *Science* **2009**, *323*, 1593-1597. (c) Cho, S. H.; Yoon, J.; Chang, S. *J. Am. Chem. Soc.* **2011**, *133*, 5996-6005. (d) Chen, B.; Hou, X.-L.; Li, Y.-X.; Wu, Y.-D. *J. Am. Chem. Soc.* **2011**, *133*, 7668-7671.

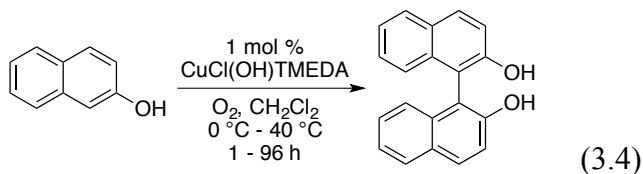
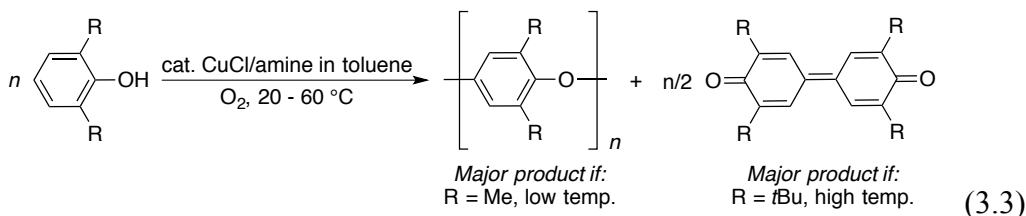
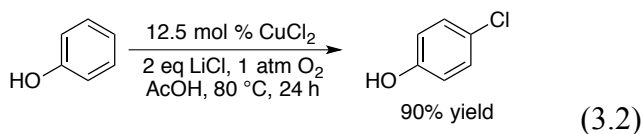
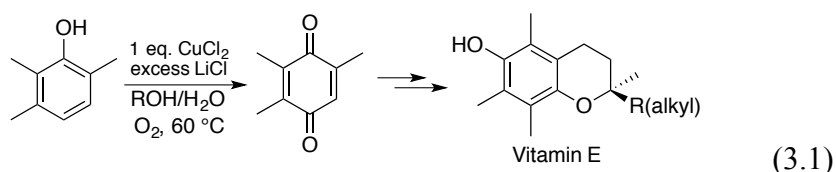
26. E (V vs. NHE) was calculated from DG with the equation $\Delta G = -n \cdot F \cdot E_{\text{abs}}$, in which n = number of electrons exchanged in the balanced redox equation, Faraday's constant F = 96.48 kJ/(mol*V), and E_{abs} = energy of the absolute electrode potential. E (vs NHE) is offset from E_{abs} by 4.28 V. See ref. 15 supporting information for further details.
27. Fulmer, G. R.; Miller, A. J. M.; Sherden, N. H.; Gottlieb, H. E.; Nudelman, A.; Stoltz, B. M.; Bercaw, J. E.; Goldberg, K. I. *Organometallics* **2010**, *29*, 2176-2179.
28. See, for example: Harris, D. C. In *Quantitative Chemical Analysis*; 6th ed.; W. H. Freeman and Company: New York, 2003, p 45-60.
29. See, for example: Kirkup, L. In *Data Analysis with Excel: An Introduction for Physical Scientists*; Cambridge University Press: Cambridge, 2002, p 264-267, 411.
30. Gou, F.-R.; Wang, X.-C.; Huo, P.-F.; Bi, H.-P.; Guan, Z.-H.; Liang, Y.-M. *Org. Lett.* **2009**, *11*, 5726-5729.
31. Yapi, A.-D.; Desbois, N.; Chezal, J.-M.; Chavignon, O.; Teulade, J.-C.; Valentin, A.; Blache, Y. *Eur. J. Med. Chem.* **2010**, *45*, 2854-2859.
32. Respectively, (a) Dikshoorn, R. P. *Recl. Trav. Chim. Pays-Bas* **1929**, *48*, 517-544. (b) Damschroeder, R. E.; Shriner, R. L. *J. Am. Chem. Soc.* **1936**, *58*, 1610-1612.
33. (a) Chiong, H. A.; Pham, Q.-N.; Daugulis, O. *J. Am. Chem. Soc.* **2007**, *129*, 9879-9884. (b) Shacklady-McAtee, D. M.; Dasgupta, S.; Watson, M. P. *Org. Lett.* **2011**, *13*, 3490-3493.
34. Martins, A.; Lautens, M. *Org. Lett.* **2008**, *10*, 4351-4353.

Chapter 3:

Copper-Catalyzed Aerobic Oxidative Chlorination of Electron-Rich Arenes to Generate Chloroarenes and Quinones

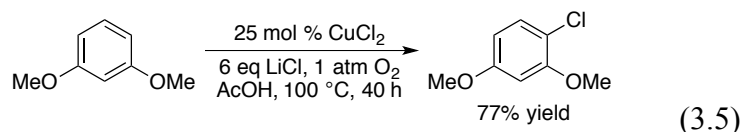
3.1. Introduction.

Cu-catalyzed aerobic oxidation procedures are commonly used to oxidize electron-rich substrates and phenols, in particular, prove to be useful substrates. In an industrial setting, phenols are oxidized to *para*-quinones, including a trimethyl-substituted vitamin E precursor (eq 3.1).¹ Gusevskaya and coworkers report selective oxidation of phenol to 4-chlorophenol with no overoxidation to the quinone (eq 3.2).² Phenols may be polymerized to form polyphenylene ether (PPE; also known as polyphenylene oxide or PPO), a commodity thermoplastic (eq 3.2).³ Naphthol coupling has also been well studied and is the preferred route to make BINOL ligands (eq 3.3).⁴



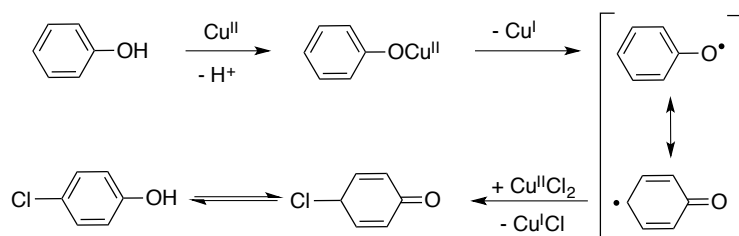
Stahl and coworkers reported Cu-catalyzed aerobic chlorination of electron-rich methoxy-substituted arenes (eq 3.5).⁵ The reaction is performed under similar conditions to those used by Gusevskaya and coworkers for phenol chlorination; however, the proposed mechanisms

for the reactions are different. This chapter focuses on comparative mechanistic studies of the phenol and dimethoxybenzene chlorination reactions, and a short background on the proposed mechanisms is presented in this introduction (see Chapter 1 for more detail).



For the phenol chlorination, Gusevskaya and coworkers propose a reaction mechanism in which a Cu^{II} -phenoxide forms and an intramolecular electron transfer occurs to generate a phenoxyl radical and Cu^{I} (Scheme 3.1).² The phenoxyl radical then abstracts a chlorine atom from CuCl_2 and the chloroarene product is generated after tautomerization. Cu^{I} is aerobically reoxidized to the Cu^{II} catalyst.

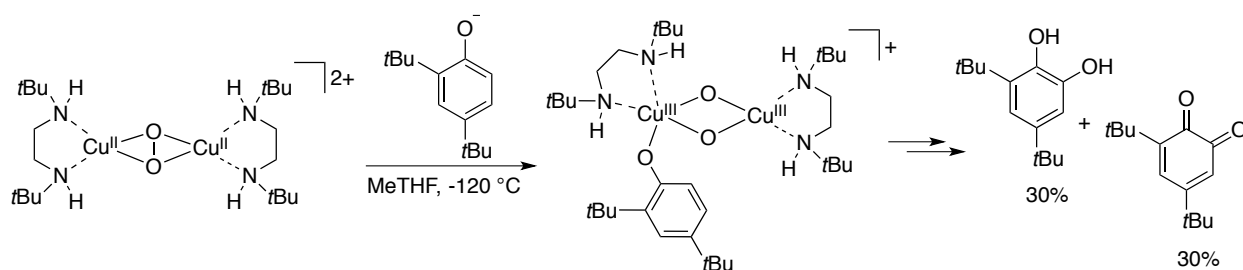
Scheme 3.1. Phenol Chlorination Mechanism Proposed by Gusevskaya and Coworkers.



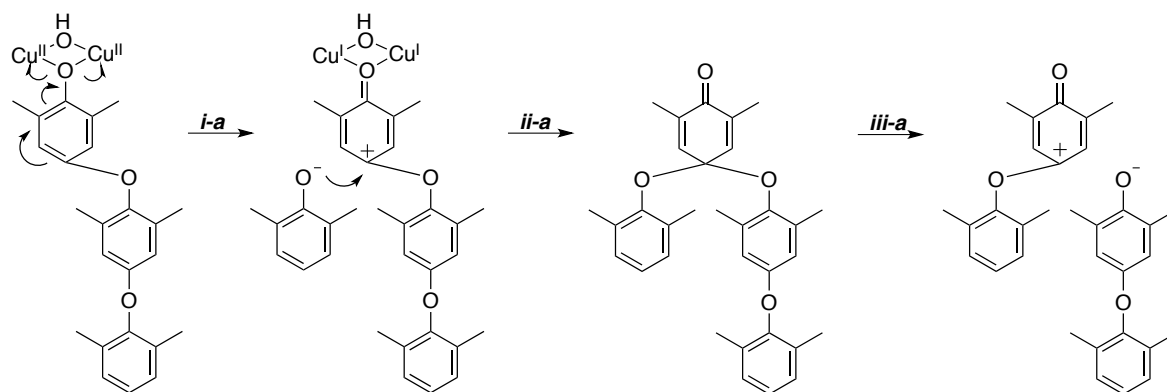
The key step of this mechanism is the Cu^{II} -phenoxide intramolecular electron transfer to generate a phenoxyl radical and Cu^{I} . This step is proposed for virtually all Cu-mediated aerobic phenol oxidations (see Chapter 1), with a few exceptions listed here. Though Cu^{II} -phenoxide intramolecular electron transfer is generally proposed for *para*-quinone formation,⁶ *ortho*-quinone formation has been proposed to occur by electrophilic oxygenation of a phenolate by a bis- μ -oxodicopper(III) complex (Scheme 3.2.)⁷ Phenol polymerization is still under debate, but an ionic mechanism in which coordination of 2 Cu^{II} centers to phenoxide facilitates a 2-electron

oxidation of the arene to yield an aryl-cation (Scheme 3.3) is proposed as an alternative to the more traditional mechanism involving phenoxyl radicals.⁸ The Cu^{II}-phenoxide intramolecular electron transfer is typically proposed to occur for at least one coupling partner in each phenol or naphthol coupling,⁹ though one report of Fe-catalyzed coupling proposes an intermolecular oxidation by O₂ to give an iron-ligated aryl-radical-cation (Scheme 3.4).¹⁰

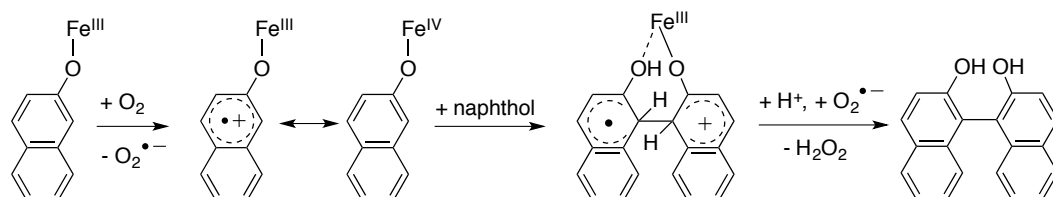
Scheme 3.2. *Ortho*-Oxygenation of Phenol by a Bis- μ -Oxodicopper(III)-Phenolate Complex.



Scheme 3.3. Ionic Mechanism for 2,6-Dimethylphenol Polymerization.

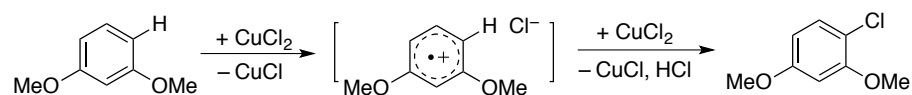


Scheme 3.4. Alternative Naphthol Coupling Mechanism with Intermolecular Oxidation.

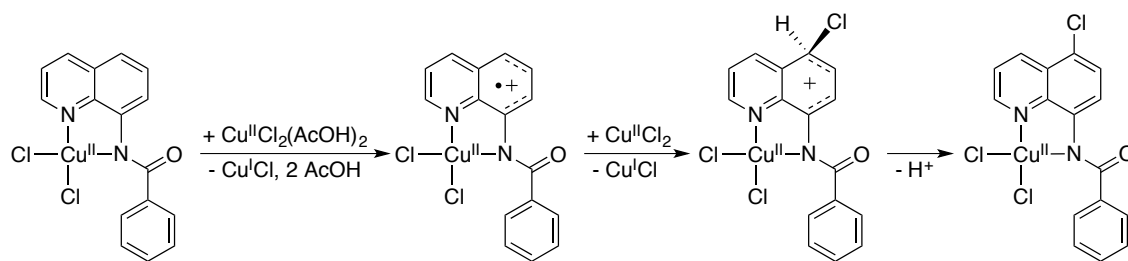


Dimethoxybenzene is chlorinated under similar conditions as phenol, however the oxidation occurs without an acidic coordinating group. Stahl and coworkers proposed a reaction mechanism in which Cu^{II} oxidizes the electron-rich arene to the aryl-radical-cation (Scheme 3.5).⁵ Chlorine atom transfer occurs from a second equivalent of CuCl_2 and the Wheland-type intermediate (not shown) is deprotonated to give the final product. Cu^{I} is aerobically reoxidized to the Cu^{II} catalyst. A similar mechanism was proposed for Cu^{II} -mediated oxidative chlorination of anisole and 2-methoxynaphthalene.¹¹

Scheme 3.5. Proposed Mechanism for Dimethoxybenzene Chlorination.



We later studied Cu^{II} -catalyzed chlorination of an amidoquinoline under the same $\text{CuCl}_2/\text{LiCl}/\text{AcOH}$ reaction conditions used for dimethoxybenzene and phenol chlorination (see Chapter 2 for this study).¹² Experimental and computational studies led to a proposed mechanism in which a Cu^{II} salt oxidizes a Cu^{II} -amidate complex to a Cu^{II} -aryl-radical-cation complex (Scheme 3.6). A second equivalent of CuCl_2 delivers the chlorine atom, and deprotonation of the Wheland-type intermediate gives the final product. Key factors that support this pathway are that (1) the Cu^{II} -amidate complex has a lower oxidation potential than the non-ligated neutral substrate, and (2) the intermolecular electron transfer is more favorable than an intramolecular electron transfer from the arene to the ligated Cu^{II} . This pathway is similar to that proposed for the dimethoxybenzene chlorination (Scheme 3.5) and is also a reasonable alternative to the pathway proposed for phenol chlorination (Scheme 3.1). However, consideration of an inter- vs. intramolecular electron transfer has not been addressed in reference to phenol oxidation.

Scheme 3.6. Proposed Mechanism for Cu^{II}-Amidate Arene Chlorination.

In this chapter, mechanistic studies of Cu-catalyzed aerobic oxidative chlorination of 1,3-dimethoxybenzene and phenol are described. Additionally, it demonstrated that an electron-rich phenol derivative, 2,6-dimethylphenol, is oxidized to the *para*-quinone under identical reaction conditions, with evidence for *para*-chloro and *para*-acetoxy phenol intermediates. The mechanistic data for 1,3-dimethoxybenzene and phenol are compared and a similar reaction mechanism is proposed for each substrate. The proposed mechanisms involve the key aryl-radical-cation intermediate similar to that proposed in Scheme 3.5 and 3.6, which differs from the phenol oxidation mechanism proposed in Scheme 3.1.

3.2. Kinetic Studies.

3.2.1. 1,3-Dimethoxybenzene Chlorination.

The oxidative chlorination of 1,3-dimethoxybenzene catalyzed by CuCl₂ (25 mol %) was reported to proceed to 77% yield in 40 h at 100 °C with 1 equiv 1,3-dimethoxybenzene (300 mM), 6 equiv LiCl, and 1 atm O₂ in AcOH (eq 3.5).⁵ To simplify kinetic studies, only 2 equiv LiCl (600 mM) was used (eq 3.6). A representative timecourse for 1,3-dimethoxybenzene chlorination shows a short initial non-linear “burst” region (0-10 min), a region of linear reaction rate (>10 min), and the beginnings of a decrease in reaction rate (300 min) implying a substrate

concentration dependence (Figure 3.1). The steady state reaction rate of the linear region was analyzed in the following kinetic studies.

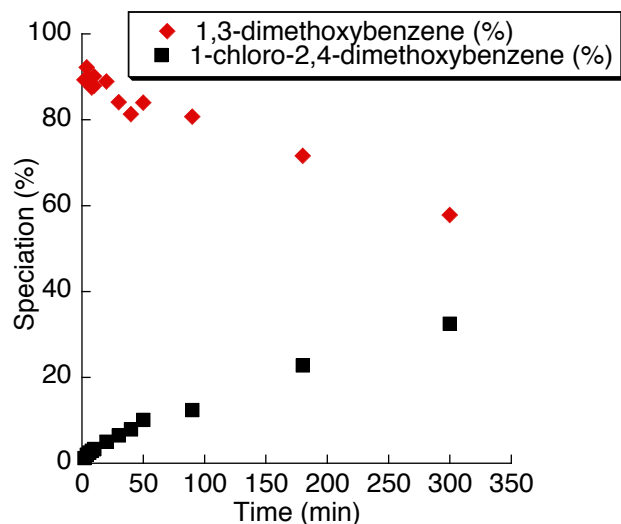
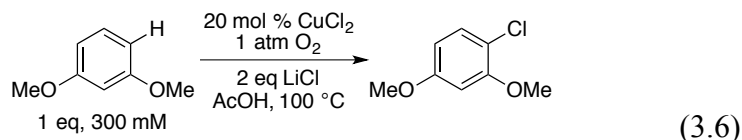


Figure 3.1. Representative timecourse for 1,3-dimethoxybenzene chlorination. Conditions: CuCl_2 (20 mol %, 60 mM), 1,3-dimethoxybenzene (1 equiv, 300 mM), LiCl (600 mM), 100 °C in AcOH.

Initial kinetic studies examined the contribution of the reaction components (copper, substrate, LiCl, and O_2) to the steady state reaction rate. In these studies the reaction rate represents the concentration of chloroarene product over time as determined by GC analysis of reaction aliquots. The reaction rate dependence on CuCl_2 concentration shows curvature, and the best fit corresponds to a mixed dependence: 2nd order at low [Cu] and 1st order at high [Cu] (Figure 3.2A). Other 1st and 2nd order fits do not provide the best modeling (Figure 3.3).

The reaction rate increases as LiCl concentration increases up to 0.5 equiv LiCl (~3 equiv relative to Cu), beyond which additional LiCl inhibits the reaction (Figure 3.2B). The reaction rate shows a saturation dependence on 1,3-dimethoxybenzene concentration (Figure 3.2C). Reaction time course plots for these studies are also shown (Figure 3.4).

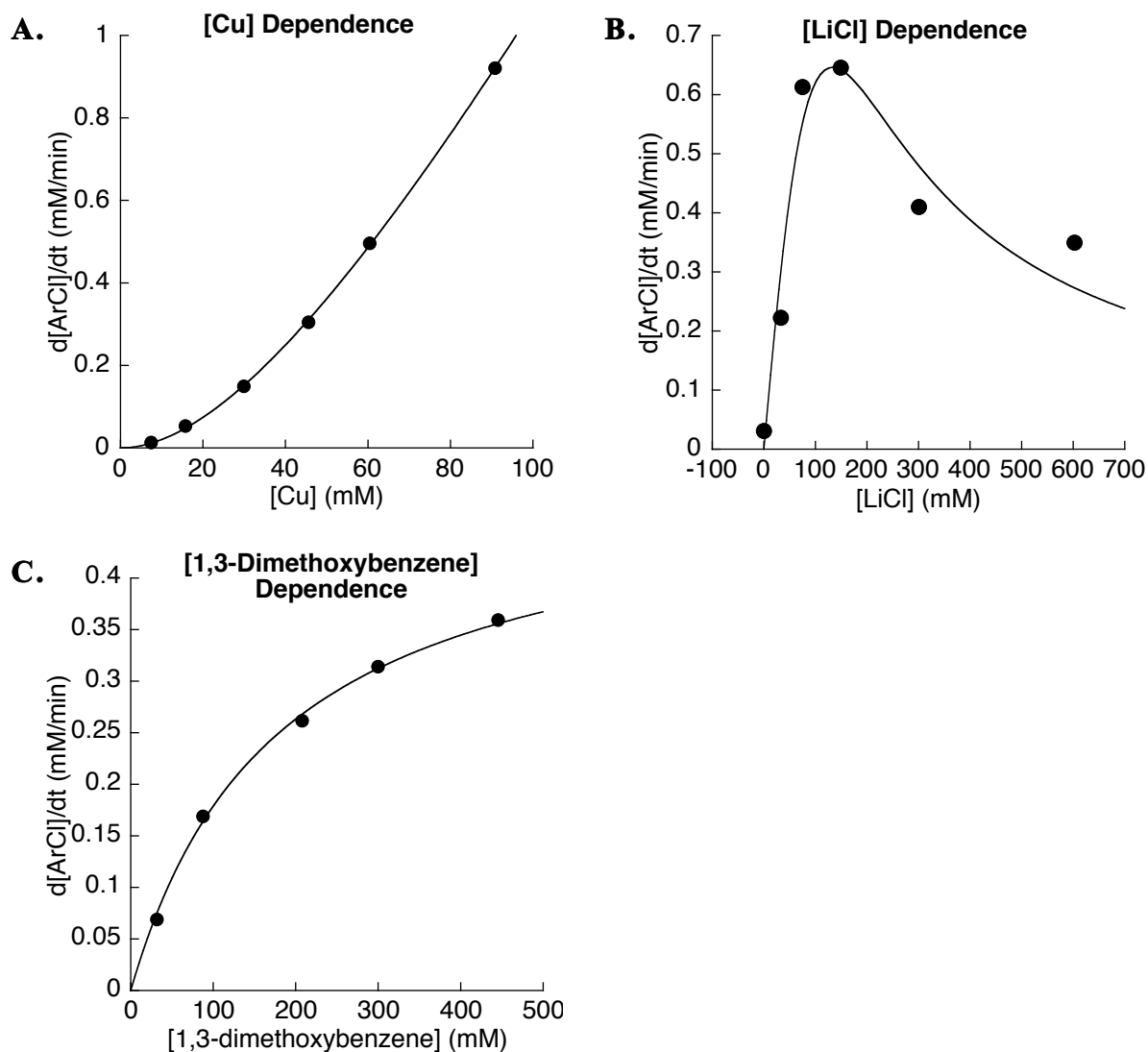


Figure 3.2. Kinetic data from 1,3-dimethoxybenzene chlorination assessing the kinetic dependence on (A) $[\text{CuCl}_2]$, (B) $[\text{LiCl}]$, and (C) $[\text{1,3-dimethoxybenzene}]$. Standard reaction conditions: CuCl_2 (15 mol %, 45 mM), 1,3-dimethoxybenzene (1 equiv, 300 mM), LiCl (600 mM), 100 °C in AcOH. The curves are derived from a nonlinear least-squares fits to (A) $d[\text{ArCl}]/dt = c_1[\text{Cu}]^2/(c_2 + c_3[\text{Cu}])$, (B) $d[\text{ArCl}]/dt = c_1[\text{LiCl}]/(c_2 + c_3[\text{LiCl}]^2)$, and (C) $d[\text{ArCl}]/dt = c_1[\text{arene}]/(c_2 + c_3[\text{arene}])$.

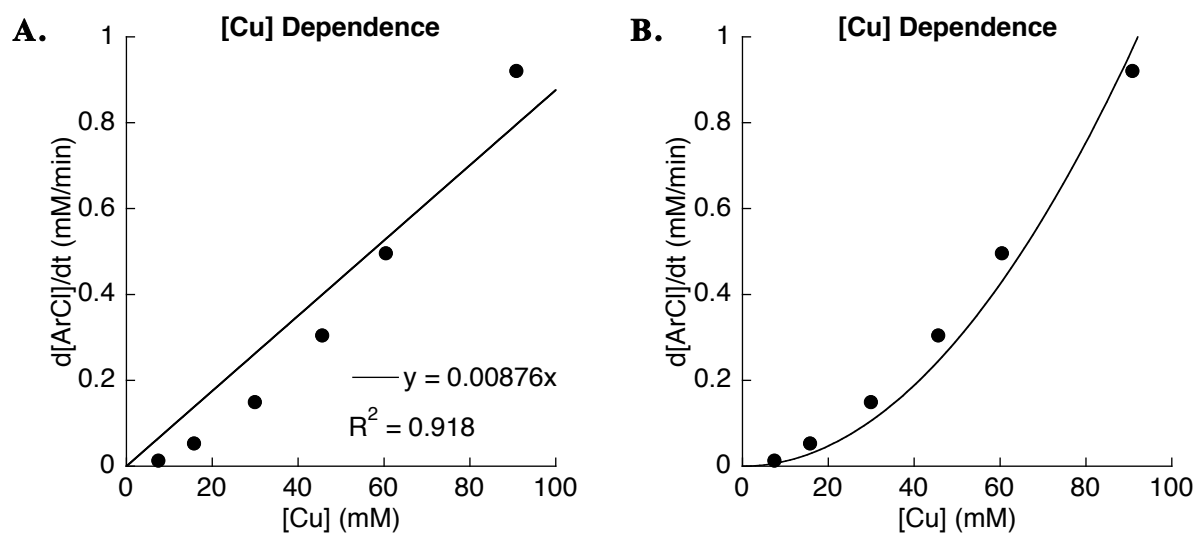


Figure 3.3. (A) 1st order and (B) 2nd order fits of rate dependence on $[\text{CuCl}_2]$ do not model the data well. The curve in (B) is derived from a nonlinear least-squares fit to $\text{rate} = c_1[\text{Cu}]^2$.

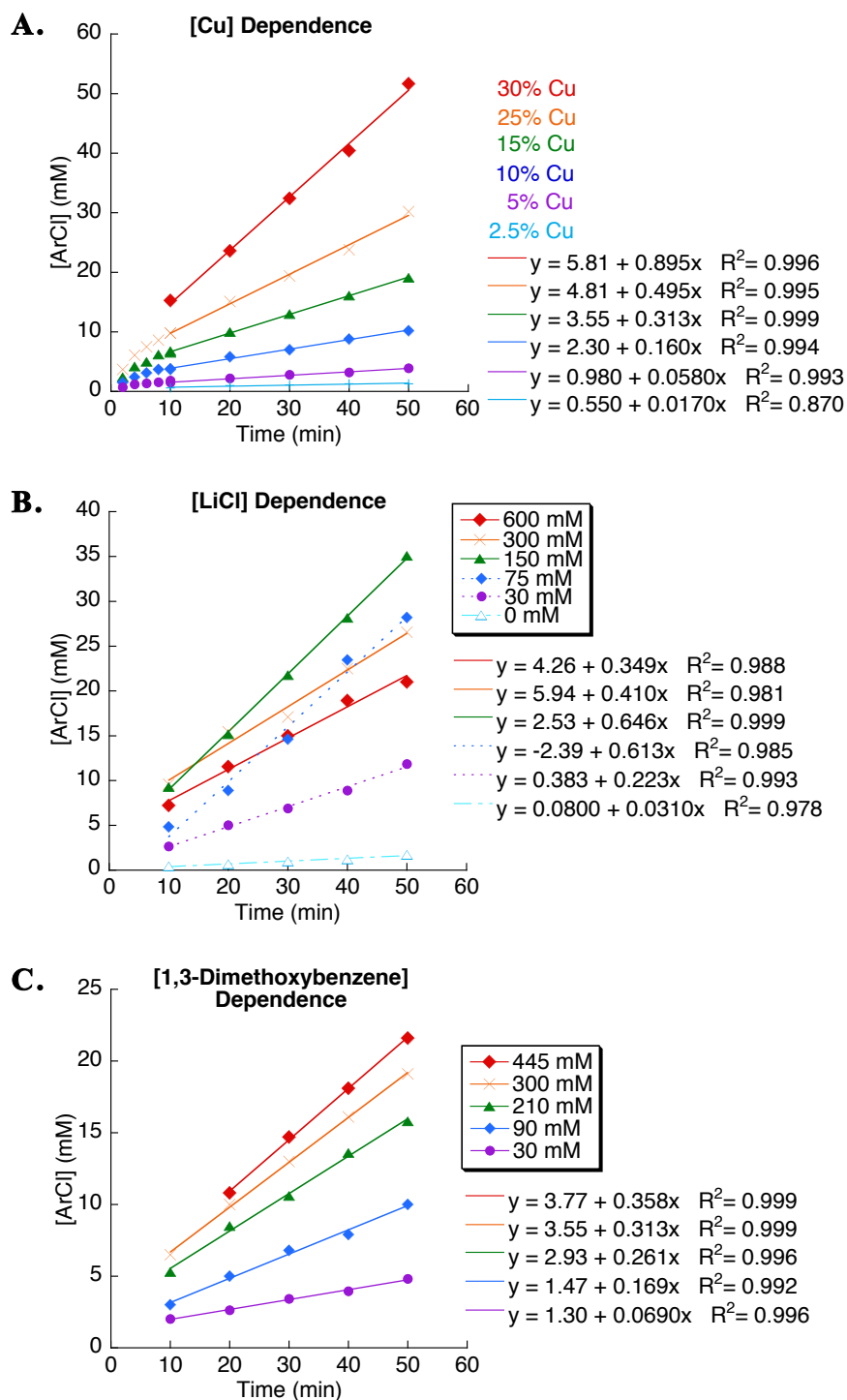


Figure 3.4. Reaction time course dependence plots for (A) $[\text{CuCl}_2]$, (B) $[\text{LiCl}]$, and (C) [1,3-dimethoxybenzene]. Standard reaction conditions: CuCl_2 (10 mol %, 30 mM), 1,3-dimethoxybenzene (1 equiv, 300 mM), LiCl (600 mM), 100 °C in AcOH.

The effect of O₂ partial pressure was studied by comparing the reaction time courses.

Under 1 atm O₂ or air, the time course plots for the reactions are initially identical, but after 30 min the reaction with shows deactivation (Figure 3.5). Based these data, it appears that the O₂ concentration dependence is zero order.

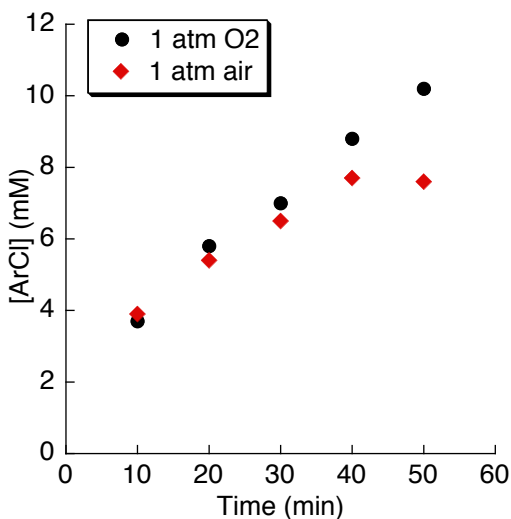


Figure 3.5. Reaction time course plots under 1 atm O₂ or air are initially identical, but after 30 min the reaction with air shows deactivation. Conditions: CuCl₂ (10 mol %, 30 mM), 1,3-dimethoxybenzene (1 equiv, 300 mM), LiCl (600 mM), 100 °C in AcOH.

3.2.2. Phenol Chlorination.

The oxidative chlorination of phenol catalyzed by CuCl₂ (12.5 mol %) was reported to proceed to 93% yield in 24 h at 80°C with 1 equiv phenol (40 mM), 2 equiv LiCl, and 1 atm O₂ in AcOH (eq 3.2).² Kinetic studies of phenol chlorination (eq 3.7) were carried out on the same scale and concentration (300 mM) as the dimethoxybenzene kinetic studies. A representative time course for phenol chlorination shows an initial induction period followed by a region of linear steady state reaction rate (Figure 3.6). Further time course points show a decrease in

reaction rate implying a reaction rate concentration dependence (not shown). The reaction rate of the steady state region was used in the following kinetic studies.

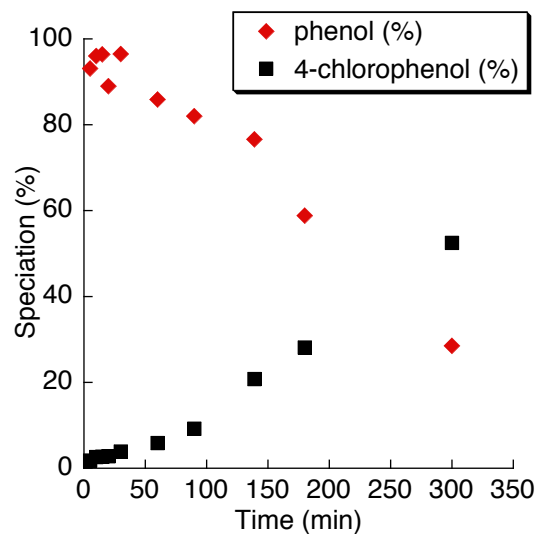
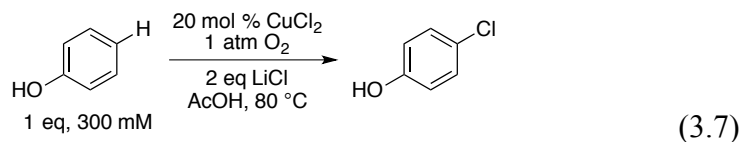


Figure 3.6. Representative time course for phenol chlorination. Conditions: CuCl_2 (20 mol %, 60 mM), phenol (1 equiv, 300 mM), LiCl (600 mM), 80 °C in AcOH .

The induction period may result from slow formation of a Cu-phenoxide, a widely proposed reaction intermediate for phenol and naphthol oxidation (see the chapter introduction). The initial phenol deprotonation/Cu-ligand exchange could be unfavorable in the absence of base (the reaction is performed in AcOH). However after some catalyst turnover, Cu-reoxidation and the linked reduction of O_2 to H_2O_2 or H_2O effectively generate a base, allowing the phenol deprotonation to be more favorable. Use of Cu^{I} or alternatively, Cu^{II} plus a base has been demonstrated to increase reactivity in substrates that require deprotonation such as in oxidative chlorination of amide derivatives or oxidation of alcohols.^{12,13} In the current phenol oxidation

reaction, when a combination of 20 mol % CuCl_2 and 20 mol % LiOAc was used, the induction period was eliminated (Figure 3.7). The steady state reaction rate for each condition is similar within error, indicating that the different catalysts affect only the length of the induction period and not the reaction rate.

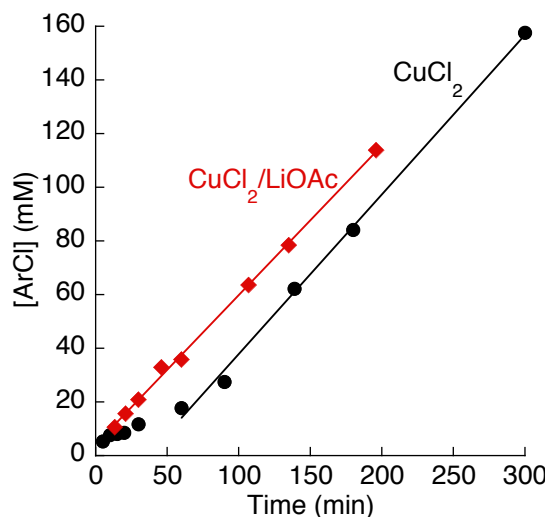


Figure 3.7. Reaction profiles with the typical 20 mol % CuCl_2 or alternatively a mix of 20 mol % CuCl_2 and 20 mol % LiOAc , which shows no induction period. Fits of the linear regions show similar rates. Conditions: phenol (1 equiv, 300 mM), LiCl (600 mM), 80 °C in AcOH .

Initial kinetic studies examined the contribution of the reaction components (copper, substrate, LiCl , and O_2) to the steady state reaction rate. In these studies the reaction rate represents the concentration of chloroarene product over time as determined by GC analysis of reaction aliquots. The reaction rate dependence on CuCl_2 concentration shows curvature, and the best fit corresponds to a mixed dependence: 2nd order at low $[\text{Cu}]$ and 1st order at high $[\text{Cu}]$ (Figure 3.8A). Other 1st and 2nd order fits do not provide the best modeling (Figure 3.9). The reaction rate shows a saturation dependence on LiCl concentration (Figure 3.8B). The reaction

rate shows a 1st order dependence on phenol concentration (Figure 3.8C). Reaction time courses for these studies are also shown (Figure 3.10).

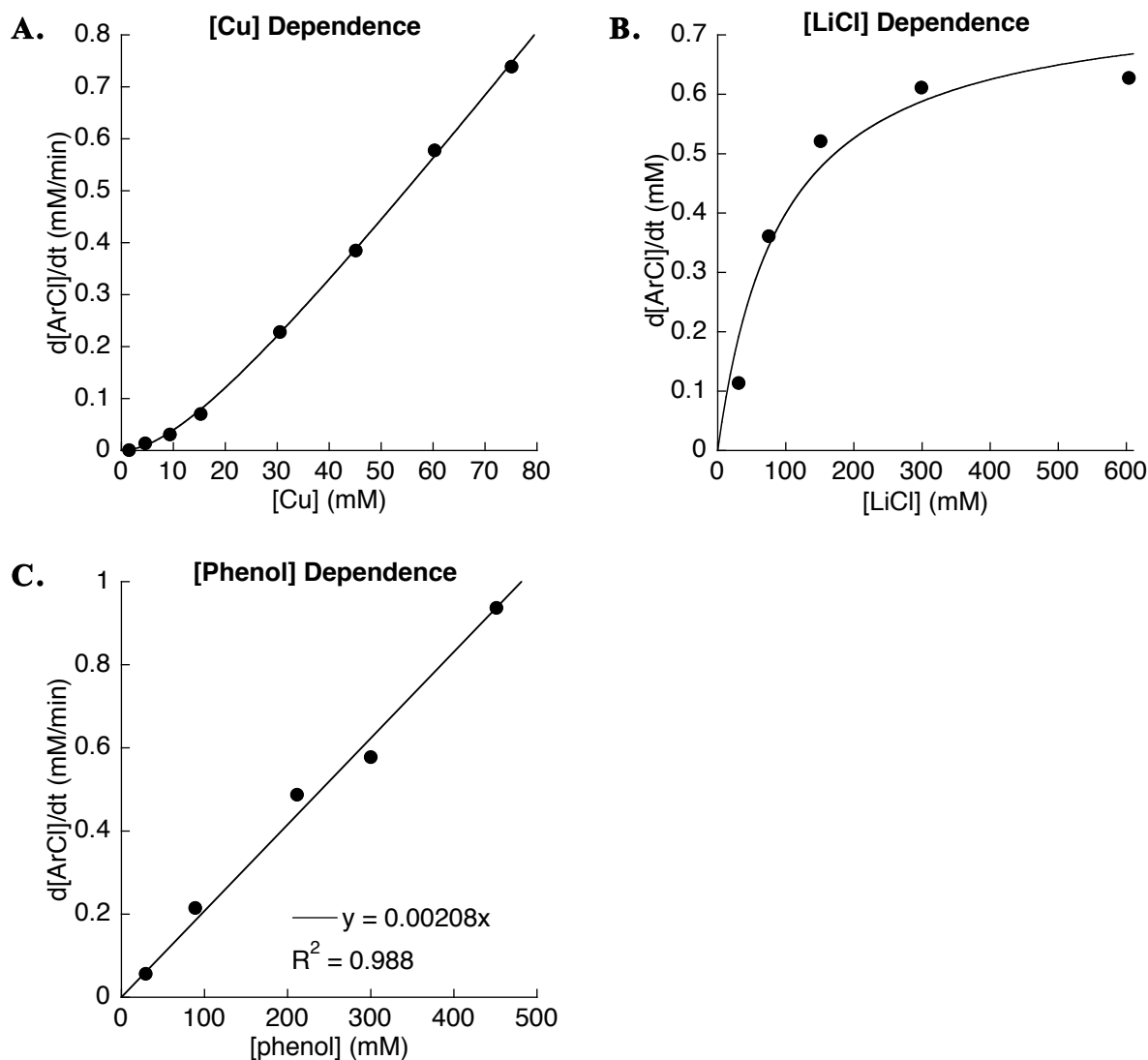


Figure 3.8. Kinetic data from phenol chlorination assessing the kinetic dependence on (A) $[\text{CuCl}_2]$, (B) $[\text{LiCl}]$, and (C) $[\text{phenol}]$. Standard reaction conditions: CuCl_2 (20 mol %, 60 mM), phenol (1 equiv, 300 mM), LiCl (600 mM), 80 °C in AcOH. The curves are derived from nonlinear least-squares fits to (A) $d[\text{ArCl}]/dt = c_1[\text{Cu}]^2/(c_2 + c_3[\text{Cu}])$ and (B) $d[\text{ArCl}]/dt = c_1[\text{Cu}]/(c_2 + c_3[\text{Cu}]^2)$.

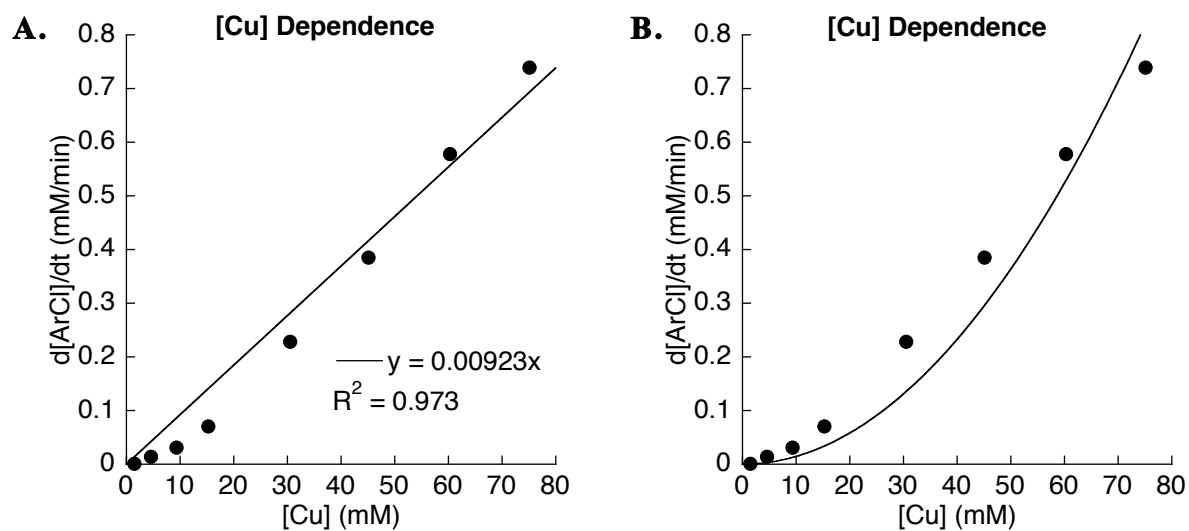


Figure 3.9. (A) 1st order and (B) 2nd order fits of rate dependence on $[\text{CuCl}_2]$ do not model the data well. The curve in (B) is derived from a nonlinear least-squares fit to $\text{rate} = c_1[\text{Cu}]^2$.

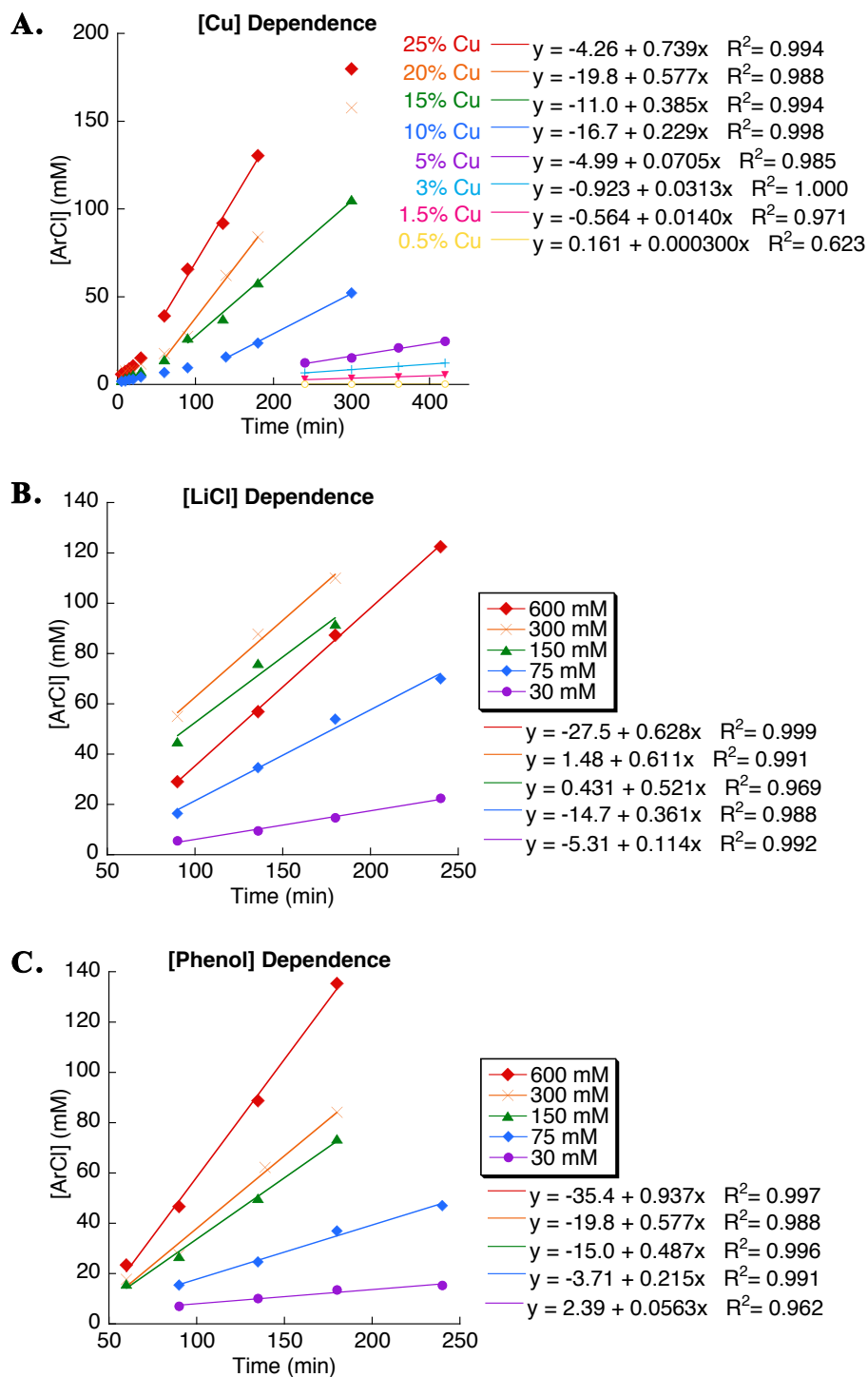


Figure 3.10. Reaction time course dependence plots for (A) $[\text{CuCl}_2]$, (B) $[\text{LiCl}]$, and (C) $[\text{phenol}]$. Standard reaction conditions: CuCl_2 (10 mol %, 30 mM), phenol (1 equiv, 300 mM), LiCl (600 mM), 80°C in AcOH .

The effect of O₂ partial pressure was studied by comparing the reaction time courses.

Reaction time courses under 1 atm O₂ or air have similar slopes (Figure 3.11). The traces do not overlay, indicating they may have induction periods of different length (as seen in Figure 3.7). The air trace may show deactivation after 20 min. Based these data, it appears that the O₂ concentration dependence is zero order.

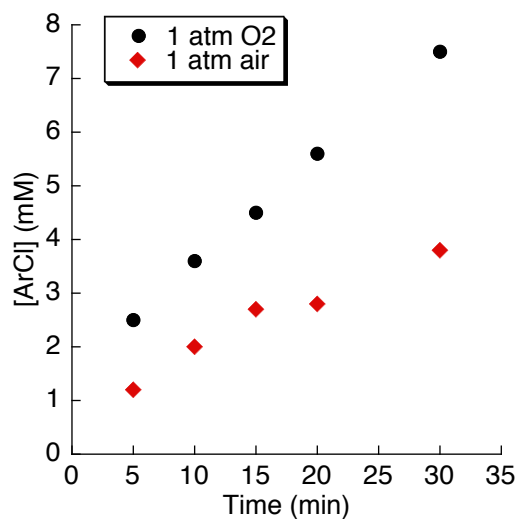


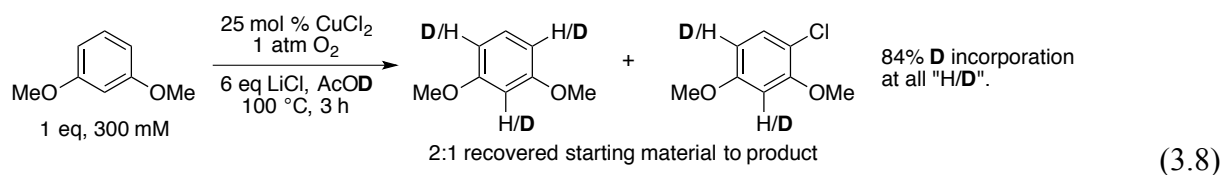
Figure 3.11. Reaction time courses under 1 atm O₂ or air have similar slopes but the air trace may show deactivation after 20 min. The O₂ concentration dependence may be zero order. Conditions: CuCl₂ (15 mol %, 30 mM), phenol (1 equiv, 300 mM), LiCl (600 mM), 80 °C in AcOH.

3.3. Hydrogen/Deuterium Exchange.

3.3.1. 1,3-Dimethoxybenzene Chlorination.

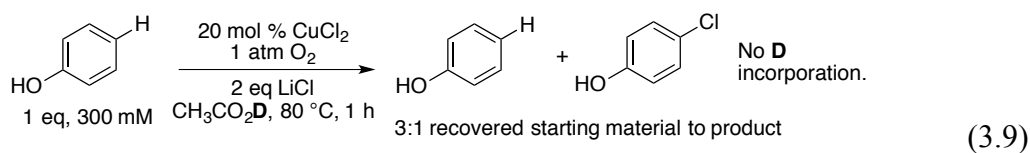
1,3-Dimethoxybenzene was submitted to the typical oxidation conditions except that AcOH was replaced with AcOD (eq 3.8). After 3 h, the reaction was analyzed and there was a 2:1 ratio of recovered starting material to product. At the positions labeled “H/D” (eq 3.8), in

sum there was 84% deuterium incorporation (these peaks overlap in the NMR spectrum and so the sum of deuterium incorporation was evaluated). The non-labeled position *meta* to both methoxy substituents showed no deuterium incorporation, presumably because it is deactivated by the *meta* electron-withdrawing inductive effect of the methoxy substituents. 1,3-Dimethoxybenzene was also submitted to similar reaction conditions without Cu (only LiCl and AcOD were present) and when recovered it showed a similar level of deuterium incorporation, indicating that Cu is not necessary for H/D exchange.



3.3.2. Phenol Chlorination.

Phenol was submitted to the typical oxidation conditions except that AcOH was replaced with AcOD (eq 3.9). After 1 h, the reaction was analyzed and there was a 3:1 ratio of recovered starting material to product. No deuterium incorporation occurred in either the product or the recovered starting material.



3.4. Spectroscopic Studies of the Catalyst Resting State.

During timecourse kinetic studies, both the 1,3-dimethoxybenzene and phenol reaction solutions appeared to be the same yellow color. The reaction solutions appeared to be the same color as a solution of similar concentration of CuCl₂ and LiCl solution in AcOH. This observation may suggest that both reactions may have a similar copper resting state even though

phenol has the ability to form Cu-phenoxides and dimethoxybenzene does not have a similar coordinating ability. As elaborated in the following sections, UV-visible and EPR spectroscopy indicate that the catalyst resting state is the CuCl_4^{2-} cuprate.

3.4.1. UV-Visible Spectroscopy of 1,3-Dimethoxybenzene and Phenol Oxidation.

UV-visible spectroscopy was used to compare the 1,3-dimethoxybenzene and phenol catalytic oxidation reaction solutions to a similar 1:20 $\text{CuCl}_2/\text{LiCl}$ solution in AcOH. The reaction solutions were removed from the reaction vessel under turnover and diluted to 4 mM with AcOH.¹⁴ The spectra overlay, indicating that there is no little to no variation in the catalyst resting state for the different substrates (Figure 3.12). The spectra agree with reported UV-visible spectra for CuCl_4^{2-} .¹⁵

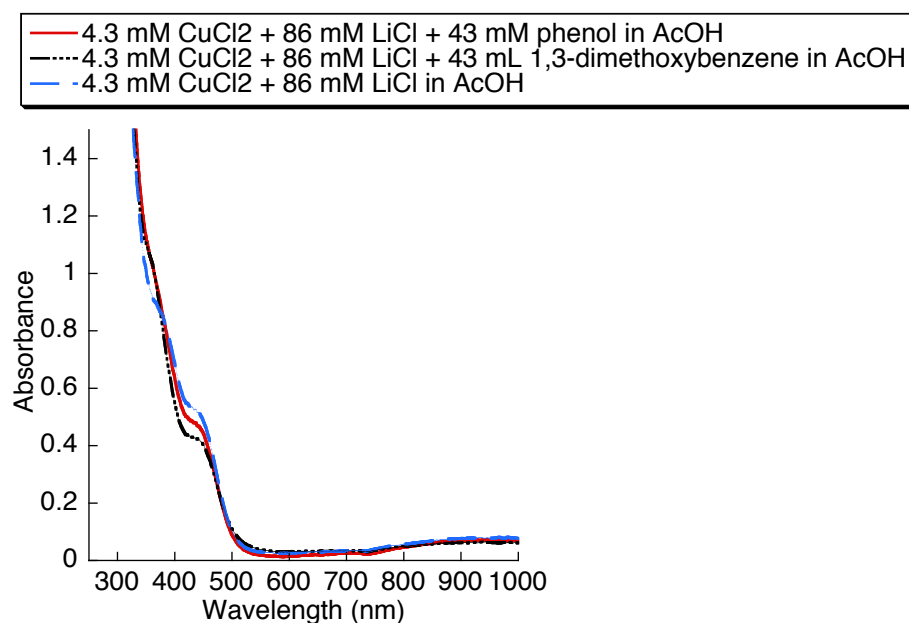


Figure 3.12. UV-visible spectra of the reaction solutions and a CuCl_2 solution in AcOH.

Spectra of 1:20 $\text{CuCl}_2/\text{LiCl}$ and $\text{Cu}(\text{OAc})_2$ AcOH were compared (Figure 3.13). Their UV-visible spectra are quite different, and $\text{Cu}(\text{OAc})_2$ does not appear to be present under the reaction conditions.

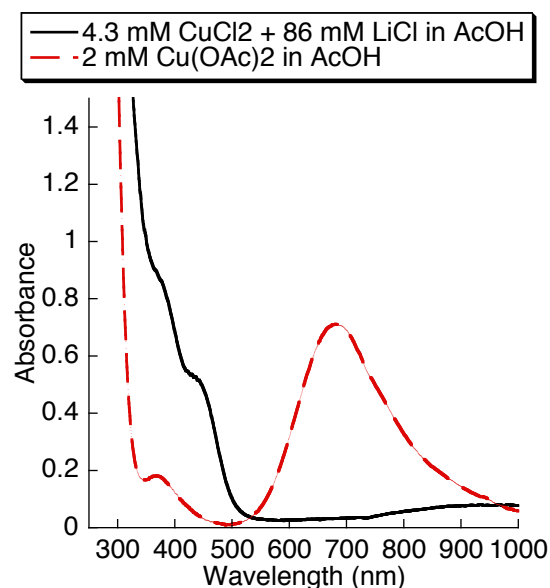


Figure 3.13. UV-visible spectra of 1:20 $\text{CuCl}_2/\text{LiCl}$ and $\text{Cu}(\text{OAc})_2$ solutions in AcOH.

3.4.2. EPR Spectroscopy of 1,3-Dimethoxybenzene and Phenol Oxidation.

EPR spectroscopy was also used to compare the 1,3-dimethoxybenzene and phenol oxidation reaction solutions with the $\text{CuCl}_2/\text{LiCl}$ solution in AcOH. The reaction solutions (adjusted to 5 mM Cu) were removed from the reaction vessels under turnover and flash frozen. A $\text{CuCl}_2/\text{LiCl}$ solution was independently prepared and flash frozen. Spectra of the 1,3-dimethoxybenzene and phenol reaction solutions obtained at 145 K overlay perfectly, indicating that there is no variation in the catalyst resting state for the different substrates (Figure 3.14). The spectra of the $\text{CuCl}_2/\text{LiCl}$ solution in AcOH overlays the reaction solution spectra well,

indicating that the reaction resting state major species is similar to that found in the $\text{CuCl}_2/\text{LiCl}$ solution. These spectra agree with reported g -values for the CuCl_4^{2-} cuprate.¹⁶

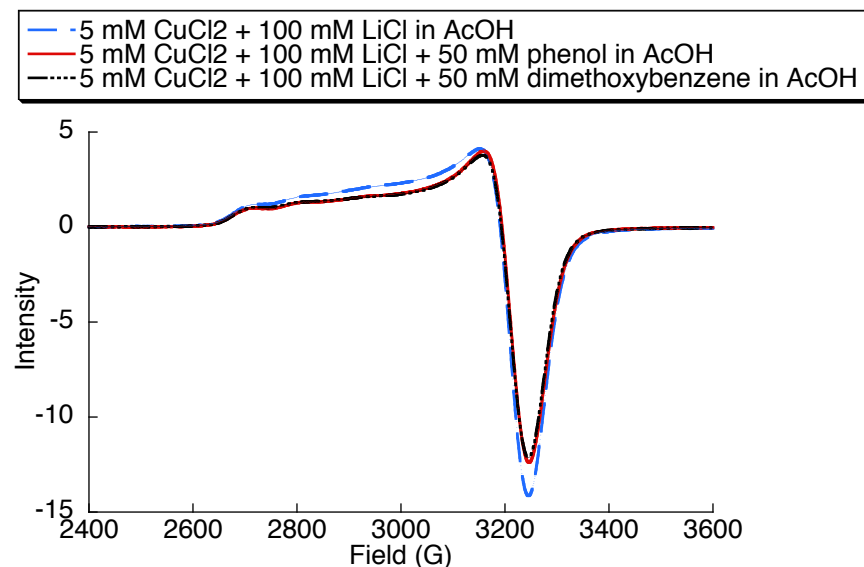


Figure 3.14. EPR spectra of $\text{CuCl}_2/\text{LiCl}$ in AcOH, the phenol reaction solution, and the 1,3-dimethoxybenzene reaction solution, 145 K. Each spectra fits $g_x = g_y = 2.08$, $g_z = 2.32$. Conditions: 5 mM CuCl_2 , 100 mM LiCl, and 0 or 50 mM substrate in AcOH.

3.5. Oxidation of 2,6-Dimethylphenol to 2,6-Dimethylquinone.

The $\text{CuCl}_2/\text{LiCl}/\text{AcOH}$ oxidation conditions and other similar conditions are used to generate *para*-quinones from phenols on industrial scale for vitamin E synthesis (see the chapter introduction). Under these conditions, however, phenol generates 4-chlorophenol with high selectivity, even after 24-hr reaction times.² In contrast, a more electron rich phenol, 2,6-dimethylphenol, starts to produce the quinone after only 2 h (eq 3.10). Two intermediates appear before any quinone is produced: 4-chloro-2,6-dimethylphenol and 4-acetoxy-2,6-dimethylphenol (Figure 3.15). Once both intermediates are formed they seem to be consumed at a similar rate

and 2,6-dimethylquinone is produced. Identification of the intermediates was verified by isolation from the reaction.

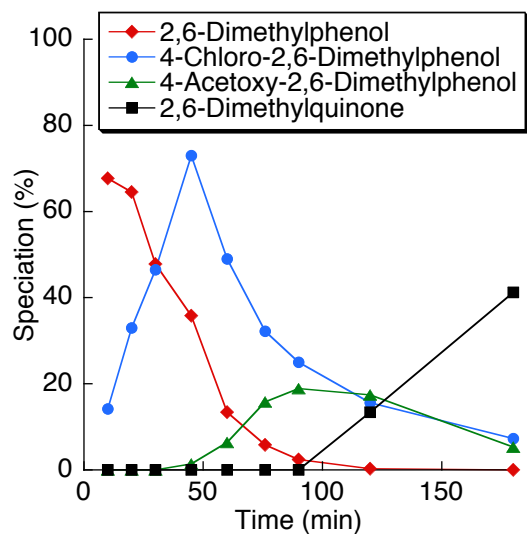
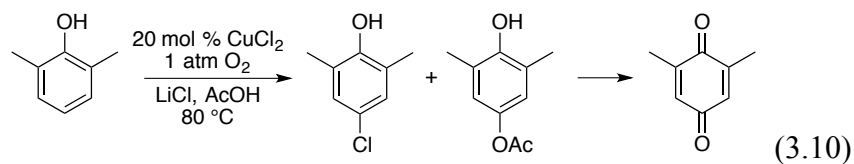


Figure 3.15. Oxidation of 2,6-dimethylphenol produces two intermediates, 4-chloro- and 4-acetoxy-2,6-dimethylphenol, before 2,6-dimethylquinone is formed. Conditions: CuCl_2 (20 mol %), substrate (1 equiv, 300 mM), LiCl (600 mM), 80 °C in AcOH. The intermediates are not yet quantitatively analyzed, as they have not yet been isolated analytically pure for GC calibration.

3.6. Proposed Mechanisms.

3.6.1. 1,3-Dimethoxybenzene Chlorination.

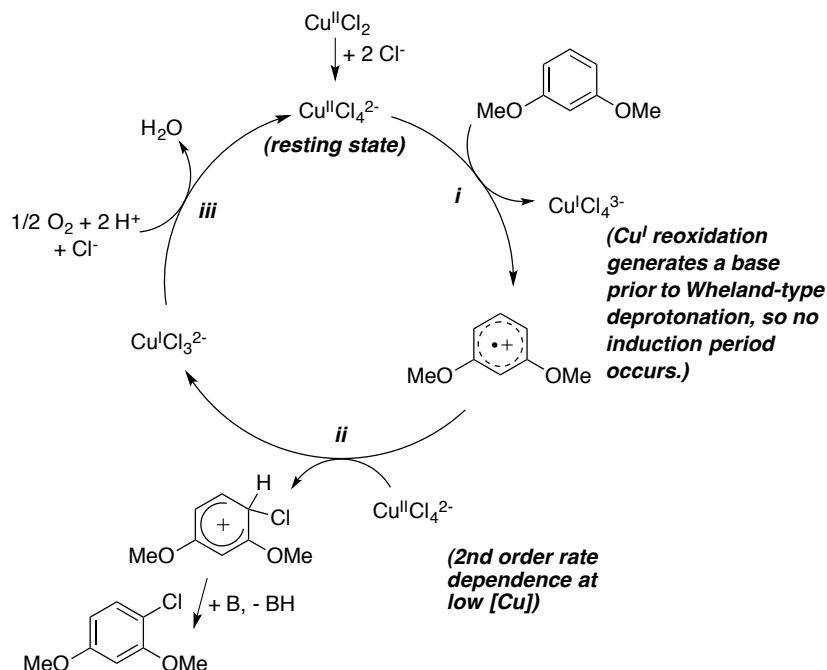
The oxidative chlorination of 1,3-dimethoxybenzene was found to be mixed 2nd/1st order in CuCl_2 concentration (2nd order at low concentration, 1st order at higher concentration), saturating in substrate concentration, and zero order in O_2 concentration. Reaction rate is accelerated by increasing LiCl concentration (~3 equiv relative to Cu), beyond which additional

LiCl inhibits the reaction. Spectroscopic studies of the reaction solution indicated that the catalyst resting state is CuCl_4^{2-} . Additionally, rapid H/D exchange of aryl protons in AcOD (with and without Cu) indicate that 1,3-dimethoxybenzene has high electrophilic reactivity.

Based on this mechanistic information, the proposed mechanism for 1,3-dimethoxybenzene oxidation is (*i*) a single-electron-transfer to $\text{Cu}^{\text{II}}\text{Cl}_4^{2-}$ to yield the aryl-radical-cation, followed by (*ii*) chloride transfer from a second equivalent of $\text{Cu}^{\text{II}}\text{Cl}_4^{2-}$ to yield the aryl-cation Wheland-type intermediate and $\text{Cu}^{\text{I}}\text{Cl}_3^{2-}$ (Scheme 3.7). $\text{Cu}^{\text{I}}\text{Cl}_3^{2-}$ may be reoxidized (*iii*) by O_2 . In off-cycle steps, $\text{Cu}^{\text{II}}\text{Cl}_4^{2-}$ is generated from CuCl_2 and the Wheland-type intermediate is deprotonated to yield the final product.

This proposal may explain key observations. In this mechanism, Cu^{I} reoxidation effectively generates a base (by production of H_2O_2 or H_2O) before deprotonation occurs, so no base-dependent induction period is observed. The mixed $2^{\text{nd}}/1^{\text{st}}$ order dependence on Cu concentration is also explained by this mechanism. At higher Cu concentration, only the 1^{st} order dependence in oxidation to the aryl-radical-cation (*i*) is observed, and chloride transfer (*ii*) is relatively fast. At lower Cu concentration, the chloride transfer step contributes to the rate of the reaction and a 2^{nd} order dependence is observed. Generation of $\text{Cu}^{\text{II}}\text{Cl}_4^{2-}$ from CuCl_2 and Cl^- may explain the [LiCl] dependence.

Scheme 3.7. Proposed Mechanism for Cu-Catalyzed Aerobic Oxidative Chlorination of 1,3-Dimethoxybenzene.



3.6.2. Phenol Chlorination.

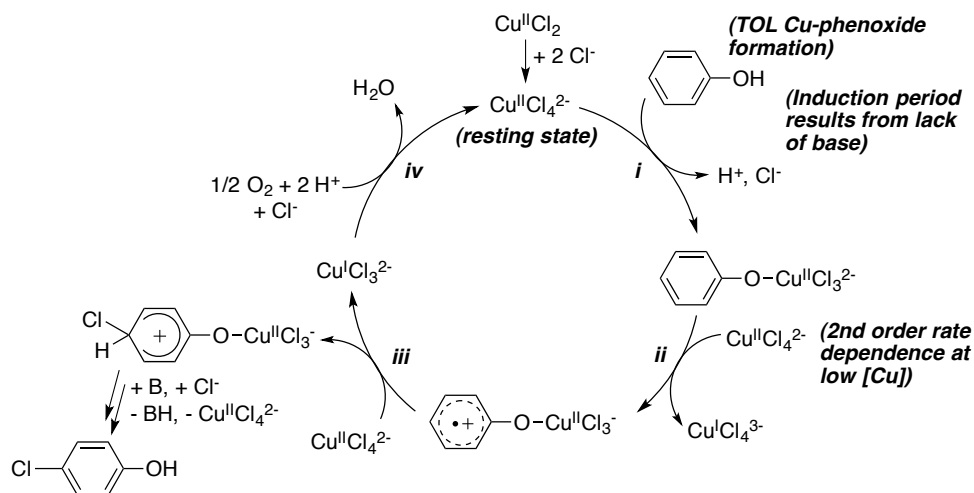
The oxidative chlorination of phenol was found to be mixed $2^{\text{nd}}/1^{\text{st}}$ order in CuCl_2 concentration (2^{nd} order at low concentration, 1^{st} order at higher concentration), saturating in LiCl concentration, 1^{st} order in substrate concentration, and zero order in O_2 concentration. Spectroscopic studies of the reaction solution indicated that the catalyst resting state is CuCl_4^{2-} . Phenol did not undergo H/D exchange in the absence of Cu, and with Cu, only chlorination occurred.

Based on this mechanistic information, the proposed mechanism for phenol oxidation is (i) generation of a Cu^{II} -phenoxide, (ii) a single-electron-transfer to a second equivalent of $\text{Cu}^{\text{II}}\text{Cl}_4^{2-}$ to yield the Cu^{II} -phenoxy-radical-cation, and (iii) chloride transfer from a third

equivalent of $\text{Cu}^{\text{II}}\text{Cl}_4^{2-}$ to yield the Cu^{II} -phenoxy-aryl-cation Wheland-type intermediate (Scheme 3.8). $\text{Cu}^{\text{I}}\text{Cl}_3^{2-}$ may be reoxidized (*iv*) by O_2 . In off-cycle steps, $\text{Cu}^{\text{II}}\text{Cl}_4^{2-}$ is generated from CuCl_2 and the the Wheland-type intermediate yields the final product after arene-deprotonation and Cu ligand exchange.

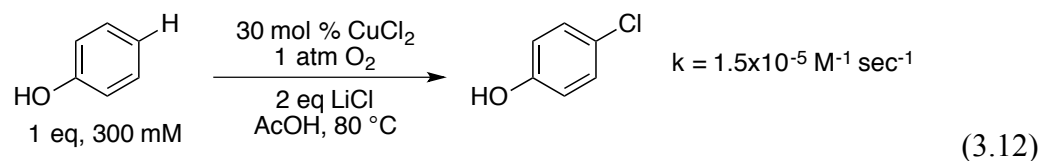
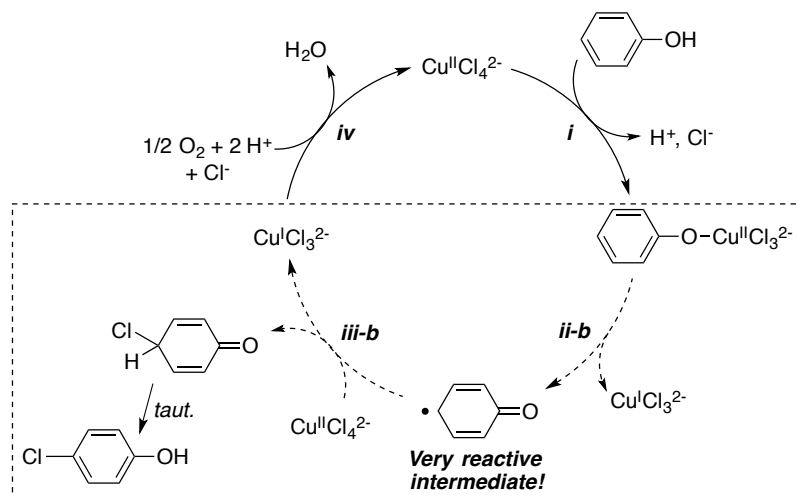
In this mechanism, deprotonation to generate a Cu^{II} -phenoxide must occur before any base has been generated by Cu^{I} reoxidation (by production of H_2O_2 or H_2O), resulting in the observed base-dependent induction period. The mixed $2^{\text{nd}}/1^{\text{st}}$ order dependence on Cu concentration may also explained by this mechanism. At higher Cu concentration, only the 1^{st} order dependence in Cu^{II} -phenoxide generation (*i*) is observed (there is also a 1^{st} order dependence on phenol concentration). At lower Cu concentration, oxidation to the Cu^{II} -phenoxy-radical-cation (*ii*) contributes to the rate of the reaction and a 2^{nd} order dependence is observed. Chloride transfer to the Cu^{II} -phenoxy-radical cation (*iii*) may be fast regardless of Cu concentration. In 1,3-dimethoxybenzene oxidation, the similar step was argued to account for the 2^{nd} order dependence at low Cu (Scheme 3.1), however 1,3-dimethoxybenzene shows H/D exchange under the reaction conditions in AcOD. Phenol does not show H/D exchange under the reaction conditions, which may indicate that chlorination is fast.

Scheme 3.8. Proposed Mechanism for Cu-Catalyzed Aerobic Oxidative Chlorination of Phenol.



The proposed mechanism for phenol oxidation, involving intermolecular single-electron transfer (*ii*) to form a Cu^{II}-phenoxyl-radical-cation intermediate, is different from common proposals for phenol oxidation (see chapter introduction). A more traditional mechanistic proposal would show the key step involving an intramolecular oxidation (*ii-b*) to generate a phenoxyl radical and Cu^ICl₃²⁻ (Scheme 3.9). The phenoxyl radical would abstract a chloride from a second equivalent of Cu^{II}Cl₄²⁻ (*iii-b*) and tautomerization would yield the final product.

Observation of a 2nd order dependence on Cu at low Cu concentration seems unlikely in this mechanism due to the high reactivity of phenoxyl radicals.¹⁷ The rate of reaction of a phenoxyl radical with CuCl₂ to form a complex “Y” has been observed to be on the order of 10⁸ M⁻¹ sec⁻¹ (eq 3.11).¹⁸ In the same study, the rate of the 2-methyl-phenoxyl radical reaction with Cu^{II} was found to be diffusion limited. However, the rate of phenol chlorination is many orders of magnitude slower, on the order of 10⁻⁵ M⁻¹ sec⁻¹ (eq 3.12). Therefore a mechanism involving a phenoxyl radical intermediate (Scheme 3.9) is not proposed for the phenol chlorination.

Scheme 3.9. Phenoxy Radical Mechanism for Phenol Oxidation (Not Proposed).

3.7. Conclusions.

Cu-catalyzed aerobic oxidative chlorination reactions of 1,3-dimethoxybenzene and phenol are proposed to proceed by a similar mechanism with a key aryl-radical-cation intermediate that results from single-electron-oxidation by an exogenous electron-rich copper halide salt. The dimethoxybenzene is quite reactive toward this electrophilic oxidation, but the phenol must be deprotonated to a Cu^{II}-phenoxide before the arene oxidation can occur. This mechanism differs from traditionally proposed mechanisms for phenol and naphthol oxidation

where an intramolecular single-electron-transfer occurs in the Cu^{II}-phenoxide to generate Cu^I and a free phenoxyl radical. This mechanistic proposal is also directly relevant to the industrial process of oxidation of trimethylphenol to the *para*-quinone, a vitamin E precursor. It is demonstrated that while phenol selectively generates 4-chlorophenol under these reaction conditions, an electron-rich dimethylphenol is oxidized to the *para*-quinone through successive *para*-chloro and *para*-acetoxy intermediates.

3.8. Contributions.

Bradford L. Ryland aided in the acquisition and fitting of the EPR spectra.

3.9. Experimental.

3.9.1. General Considerations.

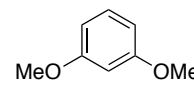
All commercially available compounds were purchased and used as received. ¹H and ¹³C NMR spectra were recorded on Bruker or Varian 300 MHz spectrometers. Chemical shift values are given in parts per million relative to internal TMS (0.00 ppm for ¹H) or CDCl₃ (77.23 ppm for ¹³C). Flash chromatography was performed using SiliaFlash® P60 (Silicycle, particle size 40-63 μm, 230-400 mesh). Gas chromatographic analyses of the reactions were conducted with a Shimadzu GC-17A gas chromatograph with Stabiliwax-DB column, using trimethyl-(phenyl)silane as an internal standard. X-band EPR data were collected using a Bruker EleXsys E500 spectrometer; all spectra were acquired at 145 K using a N₂(l) cryostat under nonsaturating conditions and fit using the W95EPR program.¹⁹

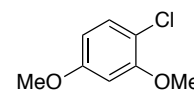
3.9.2. GC Analysis of Reaction Time Courses.

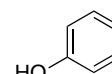
Reactions were run on the Stahl group custom vortexing reactors (2 mL AcOH per rxn). At a timepoint, a 25-uL aliquot of the rxn soln is syringed out of the shaker (getting rid of air bubbles in the needle first) and into a GC vial insert containing 150 uL EtOAc. 100 uL of Ph-TMS standard soln in EtOAc is added and the GC vials are capped, shaken, and analyzed. The rxn appears to stop when diluted in EtOAc and different periods of wait time before analysis (5 min - 20 h) does not appear affect quantitation.

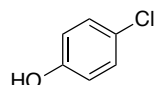
The reaction conditions seem to be corrosive (the stainless steel needles used for reaction aliquot removal loose their polish and become matte after use), so the sensitive gas-uptake manometry setup was not used for reaction rate dependence studies on O₂ partial pressure. Instead, the reaction rate was simply compared under 1 atm O₂ or air, using the custom vortexing multi-well reactors for each experiment.

3.9.3. Characterization.

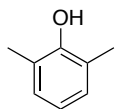
 **1,3-Dimethoxybenzene** is commercially available. ¹H NMR (300 MHz, CDCl₃): δ 7.16-7.11 (m, 1H), 6.49 (d, *J* = 2.4 Hz, 1H), 6.46-6.44 (m, 2H), 3.71 (s, 6H).

 **1-Chloro-2,4-dimethoxybenzene** was compared to the commercially available sample. ¹H NMR (300 MHz, CDCl₃): δ 7.22 (d, *J* = 8.7 Hz, 1H), 6.49 (d, *J* = 2.7 Hz, 1H), 6.41 (dd, *J* = 8.7, 2.7 Hz, 1H), 3.85 (s, 3H), 3.77 (s, 3H).

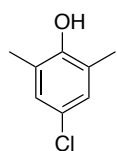
 **Phenol** is commercially available. ¹H NMR (300 Hz, CDCl₃): δ 7.27-7.20 (m, 2H), 6.93-6.88 (m, 1H), 6.85-6.80 (m, 2H).



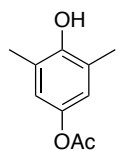
4-Chlorophenol was compared to the commercially available sample. ^1H NMR (300 MHz, CDCl_3): δ 7.19-7.14 (m, 2H), 6.78-6.73 (m, 2H).



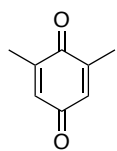
2,6-Dimethylphenol is commercially available. ^1H NMR (300 MHz, CDCl_3): δ 6.97 (d, $J = 7.5$ Hz, 2H), 6.75 (t, $J = 7.5$ Hz, 1H), 4.57 (s, 6H).



4-Chloro-2,6-dimethylphenol is known. ^1H NMR (300 MHz, CDCl_3): δ 6.95 (s, 2H), 2.20 (s, 6H). ^{13}C NMR (75 MHz, CDCl_3): δ 150.95, 128.30, 124.89, 124.77, 16.02.



4-Acetoxy-2,6-dimethylphenol is known. ^1H NMR (300 MHz, CDCl_3): δ 6.68 (s, 2H), 2.26 (s, 3H), 2.20 (s, 6H). ^{13}C NMR (75 MHz, CDCl_3): δ 170.57, 150.16, 143.50, 124.42, 121.30, 21.26, 16.24.



2,6-Dimethylbenzoquinone was compared to the commercially available sample. ^1H NMR (300 MHz, CDCl_3): δ 6.55 (s, 2 H), 2.06 (s, 6 H).

3.10. References and Notes

- Baldenius, K.-U.; von dem Bussche-Hünnefeld, L.; Hilgemann, E.; Hoppe, P.; Stürmer, R. "Vitamins, 4. Vitamin E (Tocopherols, Tocotrienols)." In *Ullmann's Encyclopedia of Industrial Chemistry*; Wiley-VCH Verlag GmbH & Co. KGaA: 2000.

2. (a) Menini, L.; Gusevskaya, E. V. "Novel highly selective catalytic oxychlorination of phenols." *Chem. Commun.* **2006**, 209-211. (b) Menini, L.; Gusevskaya, E. V. "Aerobic oxychlorination of phenols catalyzed by copper(II) chloride." *Appl. Catal. A: Gen.* **2006**, *309*, 122-128.
3. Bussink, J.; van de Grampel, H. T. "Poly(Phenylene) Oxides." In *Ullmann's Encyclopedia of Industrial Chemistry*; Wiley-VCH Verlag GmbH & Co. KGaA: 2000.
4. For a recent comprehensive review, see: Allen, S. E.; Walvoord, R. R.; Padilla-Salinas, R.; Kozlowski, M. C. "Aerobic Copper-Catalyzed Organic Reactions." *Chem. Rev.* **2013**, *113*, 6234-6458.
5. Yang, L.; Lu, Z.; Stahl, S. S. "Regioselective copper-catalyzed chlorination and bromination of arenes with O₂ as the oxidant." *Chem. Commun.* **2009**, 6460-6462.
6. See, for example: (a) Beltrame, P.; Beltrame, P. L.; Carniti, P. "Kinetics and Byproducts of the Liquid-Phase Oxidation of Phenol to *p*-Benzoquinone Catalyzed by CuCl₂." *Ind. Eng. Chem. Prod. Res. Dev.* **1979**, *18*, 208-211. (b) Takehira, K.; Orita, H.; Shimizu, M.; Hayakawa, T. (The State of Japan), "Method for the Preparation of 2,3,5-Trimethylbenzoquinone." EP 369823, **1989**. (c) Shimizu, M.; Watanabe, Y.; Orita, H.; Hayakawa, T.; Takehira, K. "Synthesis of Alkyl Substituted *p*-Benzoquinones from the Corresponding Phenols Using Molecular Oxygen Catalyzed by Copper(II) Chloride-Amine Hydrochloride Systems." *Bull. Chem. Soc. Jpn.* **1992**, *65*, 1522-1526. (d) Thoemel, F.; Hoffmann, W. (BASF Aktiengesellschaft), "Preparation of 2,3,5-Trimethyl-*p*-Benzoquinone." US 4491545, **1991**.

7. Mirica, L. M.; Vance, M.; Rudd, D. J.; Hedman, B.; Hodgson, K. O.; Solomon, E. I.; Stack, T. D. P. "Tyrosinase Reactivity in a Model Complex: An Alternative Hydroxylation Mechanism." *Science* **2005**, *308*, 1890-1892.
8. For a review of the mechanistic debate with emphasis on experimental data corroborating the ionic pathway, see: Gamez, P.; Gupta, S.; Reedijk, J. "Copper-catalyzed oxidative coupling of 2,6-dimethylphenol: A radicalar or an ionic polymerization?" *C. R. Chimie* **2007**, *10*, 295-304.
9. For examples, see: (a) Smrcina, M.; Vyskocil, S.; Maca, B.; Polasek, M.; Claxton, T. A.; Abbott, A. P.; Kocovsky, P. "Selective Cross-Coupling of 2-Naphthol and 2-Naphthylamine Derivatives. A Facile Synthesis of 2,2',3-Trisubstituted and 2,2',3,3'-Tetrasubstituted 1,1'-Binaphthyls." *J. Org. Chem.* **1994**, *59*, 2156-2163. (b) Li, X.; Hewgley, J. B.; Mulrooney, C. A.; Yang, J.; Kozlowski, M. C. "Enantioselective Oxidative Biaryl Coupling Reactions Catalyzed by 1,5-Diazadecalin Metal Complexes: Efficient Formation of Chiral Functionalized BINOL Derivatives." *J. Org. Chem.* **2003**, *68*, 5500-5511. (c) Kitajima, N.; Koda, T.; Iwata, Y.; Morooka, Y. "Reaction aspects of a μ -peroxo binuclear copper(II) complex." *J. Am. Chem. Soc.* **1990**, *112*, 8833-8839.
10. Egami, H.; Matsumoto, K.; Oguma, T.; Kunisu, T.; Katsuki, T. "Enantioenriched Synthesis of C1-Symmetric BINOLs: Iron-Catalyzed Cross-Coupling of 2-Naphthols and Some Mechanistic Insight." *J. Am. Chem. Soc.* **2010**, *132*, 13633-13635.
11. Bansal, S. R.; Nonhebel, D. C.; Mancilla, J. M. "Reactions of copper(II) halides with aromatic compounds-IX: Reactions of 1- and 2-alkoxynaphthalenes." *Tetrahedron* **1973**, *29*, 993-999.

12. Suess, A. M.; Ertem, M. Z.; Cramer, C. J.; Stahl, S. S. "Divergence between Organometallic and Single-Electron-Transfer Mechanisms in Copper(II)-Mediated Aerobic C-H Oxidation." *J. Am. Chem. Soc.* **2013**, *135*, 9797-9804.
13. Use of copper(I) instead of copper(II) increases the rate of alcohol oxidation: Hoover, J. M.; Ryland, B. L.; Stahl, S. S. "Mechanism of Copper(I)/TEMPO-Catalyzed Aerobic Alcohol Oxidation." *J. Am. Chem. Soc.* **2013**, *135*, 2357-2367.
14. Dilution did not appear to disturb reaction speciation; the spectrum simply decreased in overall intensity upon dilution.
15. Eswein, R. P.; Howald, E. S.; Howald, R. A.; Keeton, D. P. "Ion pairs-IV Chlorocuprate equilibria in acetic acid solutions." *J. Inorg. Nucl. Chem.* **1967**, *29*, 437-452.
16. See, for a leading reference: Rahemi, H.; Tayyari, S. F.; Riley, M. J. "Theoretical Studies of the Tetrachlorocuprate(II) Anion: ADF Geometry Optimization, and Calculations of the PES, EPR Parameters, and Vibrational Frequencies." *J. Theor. Comp. Chem.* **2008**, *7*, 53-65.
17. For a summary of phenoxy radical reaction rate constants, including with Cu^{II} (the following reference by Khudyakov et al. is cited), see: Neta, P.; Grodkowski, J. "Rate Constants for Reactions of Phenoxy Radicals in Solution." *J. Phys. Chem. Ref. Data* **2005**, *34*, 109-199.
18. Khudyakov, I. V.; Kuzmin, V. A.; Emanuel, N. M. "Decay kinetics of aryloxy and semiquinone radicals in the presence of copper ions." *Int. J. Chem. Kinet.* **1978**, *10*, 1005-1018.
19. Neese, F. *QCPE Bull.* **1995**, *15*, 5.

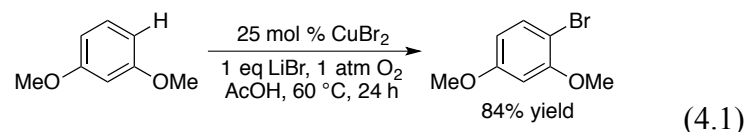
Chapter 4:

Copper-Catalyzed Aerobic Oxidative Bromination of Electron-Rich Arenes

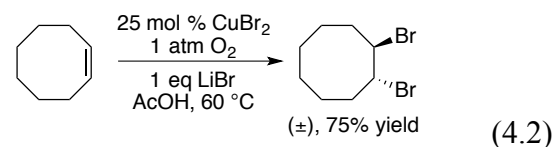
4.1. Introduction.

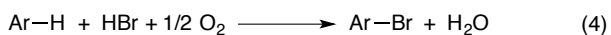
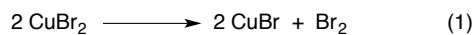
Cu-catalyzed aerobic oxidation procedures are used to halogenate electron-rich substrates, however the mechanism of oxidative bromination may be different from the chlorination mechanism (see Chapter 1). In the previous chapter, a mechanistic study of Cu-catalyzed chlorination of 1,3-dimethoxybenzene and phenol was described. In this chapter, the bromination mechanism is investigated. Arene bromination is carried out under similar reaction conditions with CuCl_2 and LiCl replaced by CuBr_2 and LiBr .

Yang and Stahl reported Cu-catalyzed aerobic bromination of electron-rich methoxy-substituted arenes (eqn 4.1).¹ This reaction proceeds well at lower temperatures than the chlorination reaction (60 °C vs. 100 °C for the chlorination).

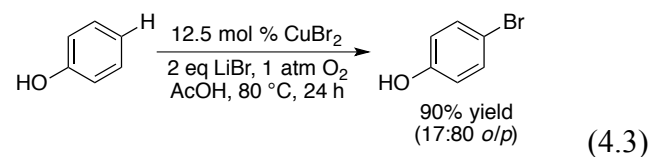


Cis-cyclooctene undergoes dibromination under the same reaction conditions (eqn 4.2). The analogous reaction of cyclooctene with $\text{CuCl}_2/\text{LiCl}$ did not lead to chlorination of the arene. These observations provided the basis for a proposed mechanism in which CuBr_2 disproportionation generates Br_2 and CuBr , and Br_2 brominates the arene (Scheme 4.1). This electrophilic bromination is quite different from the proposed mechanism for chlorination, in which copper chlorides are the active oxidizing and chlorinating reagents in successive steps (see the previous chapter).



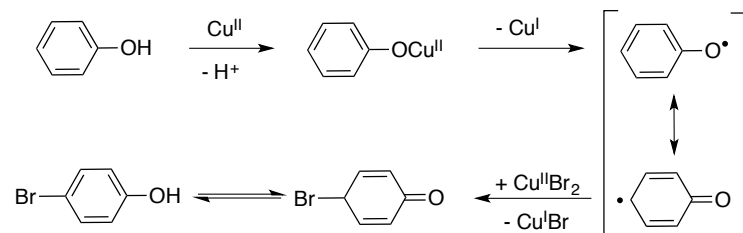
Scheme 4.1. Proposed Mechanism for Arene Bromination Based on CuBr_2 Disproportionation to Generate Br_2 .

Gusevskaya and coworkers reported phenol bromination under similar reaction conditions (eqn 4.3).² The monobromination reaction proceeds in 90% yield after 24 h with 17:80 *ortho/para* selectivity. In contrast, the analogous chlorination reaction is highly *para*-selective.³

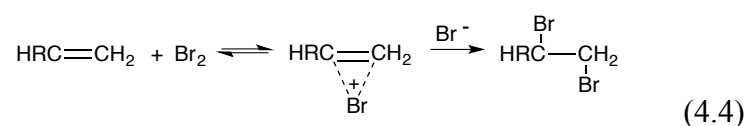


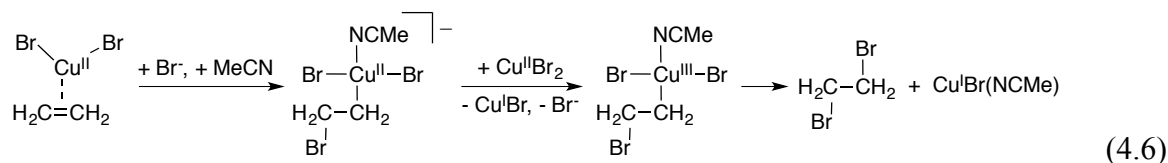
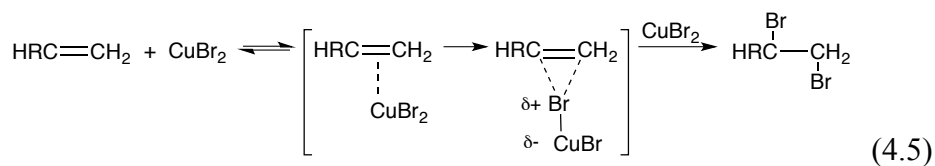
Gusevskaya and coworkers propose a reaction mechanism in which a Cu^{II} -phenoxide is formed and intramolecular electron transfer occurs to generate a phenoxyl radical and Cu^{I} (Scheme 4.2).² The phenoxyl radical then abstracts a bromine atom from CuBr_2 and the bromoarene product is generated after tautomerization. Cu^{I} is aerobically reoxidized to the Cu^{II} catalyst. The authors propose a similar mechanism for phenol chlorination.³

Scheme 4.2. Phenol Oxidative Bromination Mechanism Proposed by Gusevskaya and coworkers.



Alkene bromination by CuBr_2 , such as previously noted for cyclooctene (eqn 4.2) has been reported, though it appears the mechanism is still unclear. One report suggests that Br_2 is generated via disproportionation (as in Scheme 4.1) and is the active brominating reagent (eqn 4.4).⁴ The proposal was based on observation of a second order rate dependence on CuBr_2 concentration and a zero order rate dependence on alkene (allyl alcohol) concentration, suggesting the rate-determining step of the reaction is Br_2 formation. Another study argues that Br_2 is not generated under these conditions and that CuBr_2 forms a bromonium-like complex with the alkene to promote bromination (eqn 4.5).⁵ In this case, the authors observed a second order rate dependence on CuBr_2 concentration and a first order rate dependence on alkene (hexene) concentration, indicating that alkene is involved in the rate-determining step. A more recent study proposed Cu-mediated bromination via an alkyl- Cu^{III} intermediate based on DFT computations and poor reactivity of Br_2 compared to $\text{CuBr}_2/\text{LiBr}$ (eq 4.6).⁶ Based on these reports, it is not certain that the occurrence of alkene bromination can function as a positive indication of the presence of Br_2 in a reaction solution.





In this chapter, mechanistic studies of Cu-catalyzed aerobic oxidative bromination of 1,3-dimethoxybenzene and phenol are performed. The proposed mechanisms are either (1) bromination by Br_2 which is generated by CuBr_2 disproportionation, or (2) bromination by a bromocuprate(II) complex involving the key aryl-radical-cation intermediate similar to that proposed for arene chlorination in the previous chapter. The current mechanistic study is not sufficient for a confident conclusion on the nature of the bromination mechanism. Proposal (1) is favored over (2); however, neither mechanism perfectly fits the observed kinetic features.

4.2. Kinetic Studies.

4.2.1 1,3-Dimethoxybenzene Bromination.

The oxidative bromination of 1,3-dimethoxybenzene catalyzed by CuBr_2 (25 mol %) was reported to proceed to 84% yield in 24 h at 60 °C with 1 equiv 1,3-dimethoxybenzene (300 mM), 1 equiv LiBr , and 1 atm O_2 in AcOH (4.1).¹ To simplify kinetic studies, 2 equiv LiBr (600 mM) were used and because the reaction was quite fast at initial time points it was studied at 30 °C (eqn 4.7). A representative time course for 1,3-dimethoxybenzene bromination shows a short initial non-linear “burst” region (0-10 min, not shown) followed by a region of linear reaction rate (>10 min) (Figure 4.1). This steady state reaction rate of the linear region was analyzed in

the subsequent kinetic studies. This reaction profile is similar to that observed for 1,3-dimethoxybenzene chlorination (previous chapter).

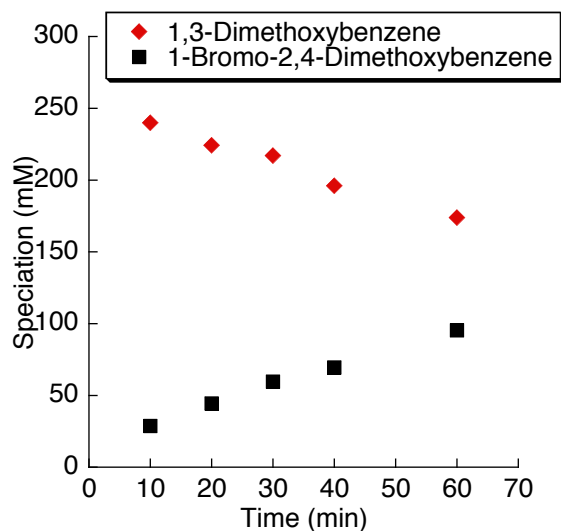
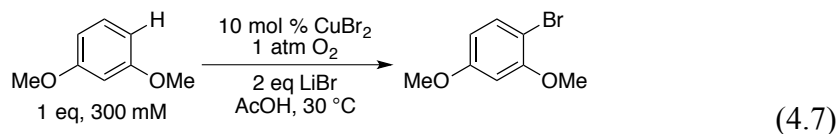


Figure 4.1. A representative timecourse for 1,3-dimethoxybenzene bromination. Conditions: CuBr_2 (25 mol %, 75 mM), 1,3-dimethoxybenzene (1 equiv, 300 mM), LiBr (600 mM), 30 °C in AcOH.

Initial kinetic studies examined the contribution of the reaction components (copper, substrate, LiBr, and O_2) to the steady state reaction rate. In these studies the reaction rate represents the concentration of bromoarene product over time as determined by GC analysis of reaction aliquots. The reaction rate dependence on CuBr_2 concentration shows curvature, and the best fit corresponds to a mixed : 2nd order at low [Cu] and 1st order at high [Cu] (Figure 4.2A). Other 1st and 2nd order fits do not provide the best modeling, though the 1st order fit provides fair modeling (Figure 4.3).

The reaction rate shows a saturation dependence on LiBr concentration (Figure 4.2B).

The reaction rate shows a zero order dependence on 1,3-dimethoxybenzene concentration (Figure 4.2C). Reaction traces for these studies are also shown (Figure 4.4A-C).

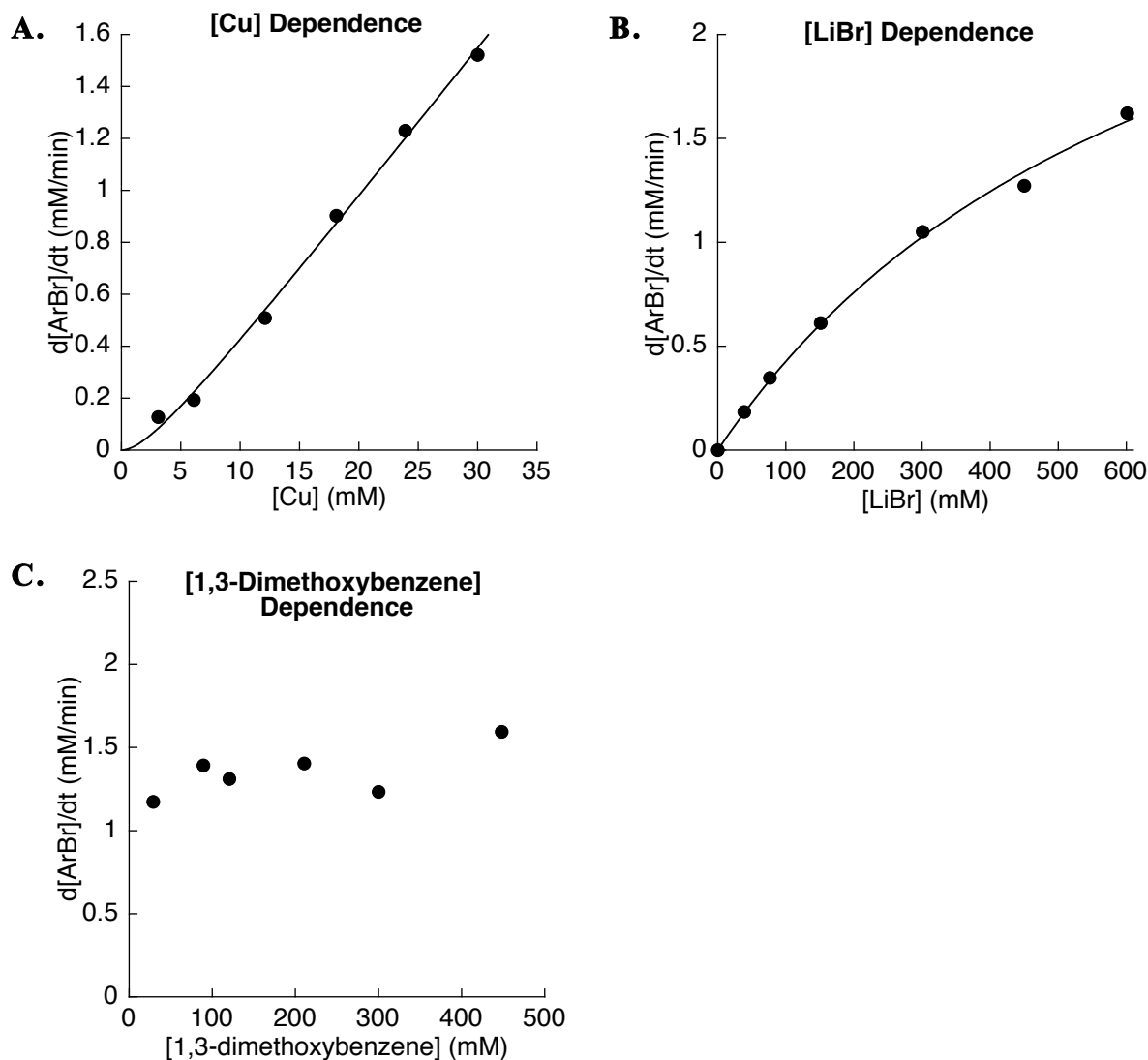


Figure 4.2. Kinetic data from 1,3-dimethoxybenzene bromination assessing the kinetic dependence on (A) $[\text{CuBr}_2]$, (B) $[\text{LiBr}]$, and (C) $[\text{1,3-dimethoxybenzene}]$. Standard reaction conditions: CuBr_2 (30 mol %), 1,3-dimethoxybenzene (1 equiv, 300 mM), LiBr (600 mM), 30°C in AcOH . The curve in (A) is derived from a nonlinear least-squares fit to $d[\text{ArBr}]/dt = c_1[\text{Cu}]^2/(c_2 + c_3[\text{Cu}])$, and in (B), to $d[\text{ArBr}]/dt = c_1[\text{LiBr}]/(c_2 + c_3[\text{LiBr}])$.

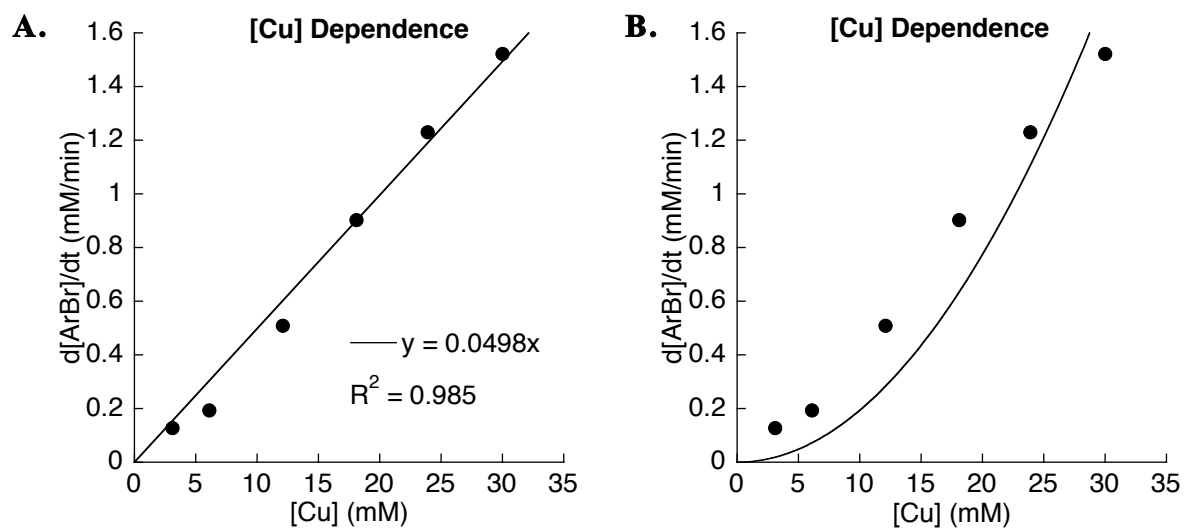


Figure 4.3. (A) 1st order and (B) 2nd order fits of rate dependence on [CuCl₂] do not model the data well. The curve in (B) is derived from a nonlinear least-squares fit to $d[\text{ArBr}]/dt = c_1[\text{Cu}]^2$.

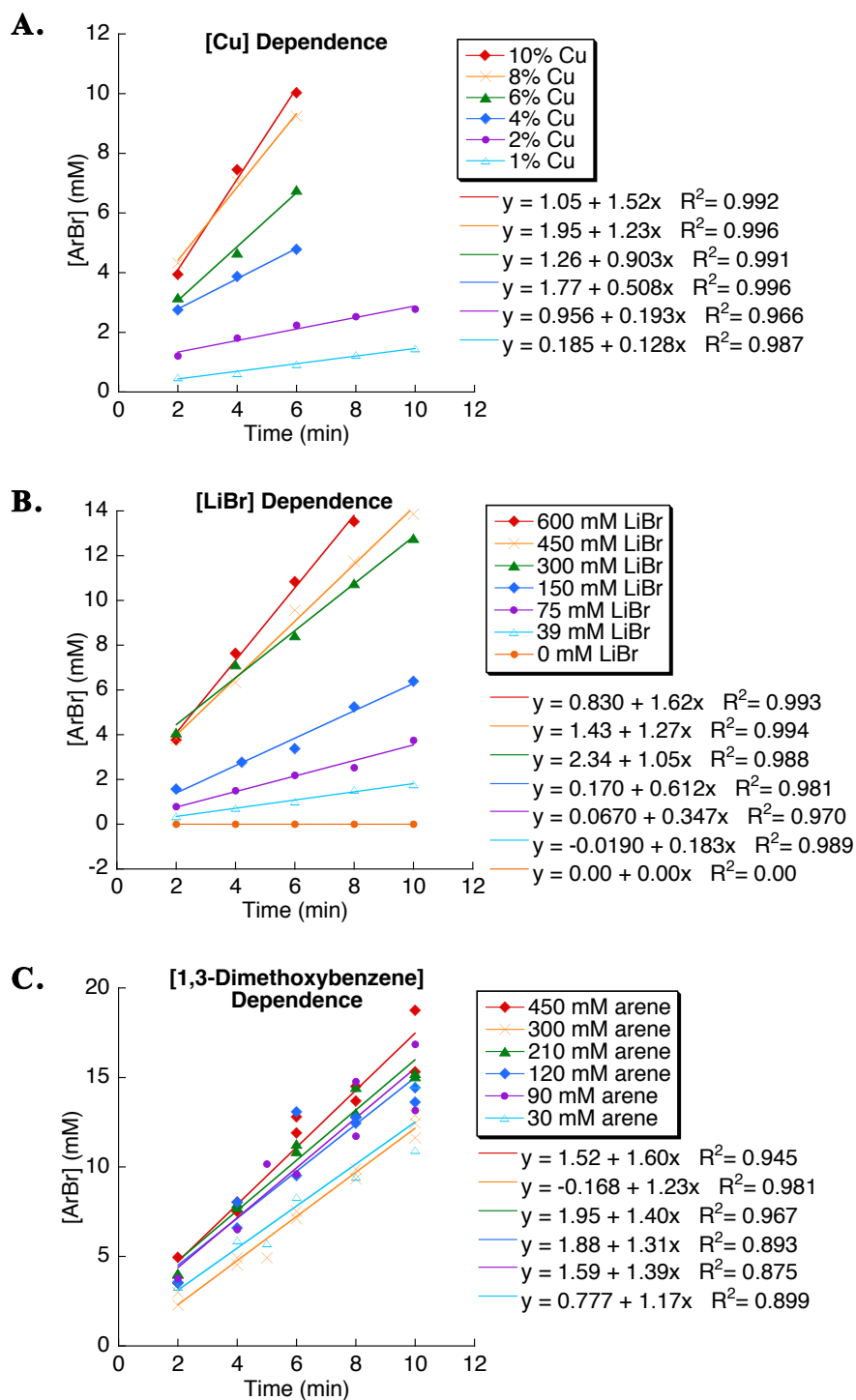


Figure 4.4. Reaction time course dependence plots for (A) $[\text{CuBr}_2]$, (B) $[\text{LiBr}]$, and (C) [1,3-dimethoxybenzene]. Standard reaction conditions: CuBr_2 (30 mol %), 1,3-dimethoxybenzene (1 equiv, 300 mM), LiBr (600 mM), 30 °C in AcOH .

The effect of O₂ partial pressure was studied by comparing the reaction time courses.

The reaction traces under 1 atm O₂ or air exhibit similar profiles (Figure 4.5), suggesting that the reaction has zero order dependence on O₂ concentration.

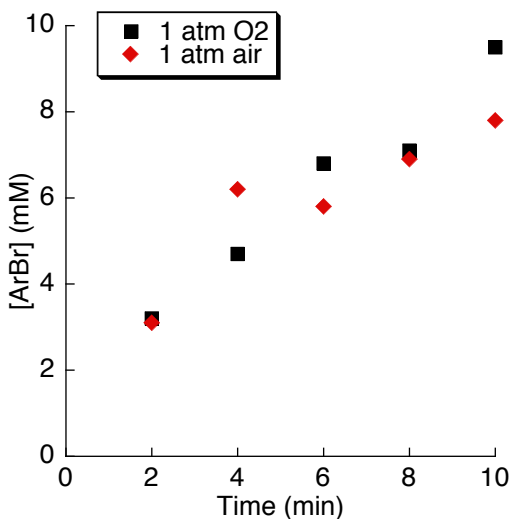


Figure 4.5. Reaction time course plots under 1 atm O₂ or air exhibit similar profiles. Conditions: CuBr₂ (6 mol %), 1,3-dimethoxybenzene (1 equiv, 300 mM), LiBr (600 mM), 30 °C in AcOH.

4.2.2 Phenol Bromination.

The oxidative bromination of phenol catalyzed by CuBr₂ (12.5 mol %) was reported to proceed to 90% yield (17:80 *ortho/para*) in 24 h at 80°C with 1 equiv phenol (40 mM), 2 equiv LiBr, and 1 atm O₂ in AcOH (eqn 4.3).² Kinetic studies of phenol bromination (eqn 4.8) were carried out on the same scale and concentration (300 mM) as the dimethoxybenzene kinetic studies. A representative time course for phenol bromination shows a short initial non-linear “burst” region (<5 min, not pictured) followed by a region of linear reaction rate (>5 min) (Figure 4.6). 4-Bromophenol is initially produced, followed by 2-bromophenol and 2,4-dibromophenol (with corresponding consumption of the mono-brominated species). The linear

region in which 4-bromophenol is primarily produced was used in the following kinetic studies. The phenol bromination time course lacks the induction period that was seen during phenol chlorination (see the previous chapter), and time course shape is similar to the 1,3-dimethoxybenzene chlorination and bromination time courses.

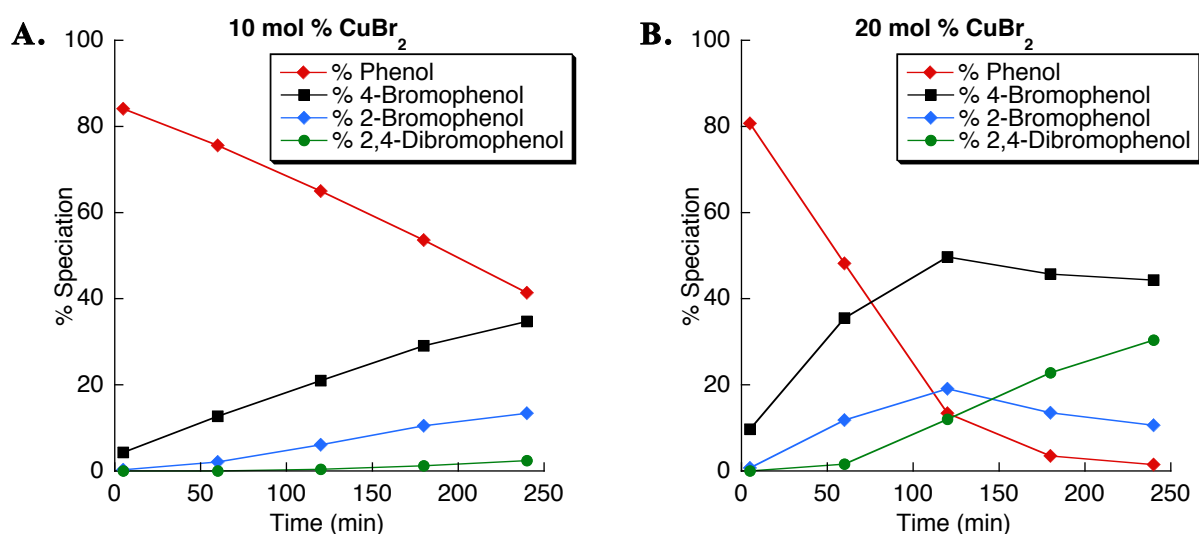
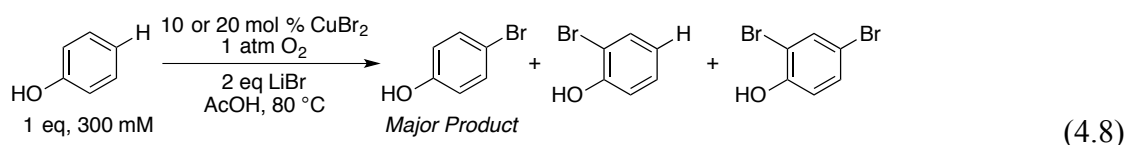


Figure 4.6. A representative timecourse for phenol bromination with (A) 10 mol % CuBr₂ and (B) 20 mol % CuBr₂. 4-Bromophenol is initially produced, followed by 2-bromophenol and 2,4-dibromophenol. Conditions: CuBr₂ (10 or 20 mol %), phenol (1 equiv, 300 mM), LiBr (600 mM), 80 °C in AcOH.

Initial kinetic studies examined the contribution of the reaction components (copper, substrate, LiBr, and O₂) to the steady state reaction rate. In these studies the reaction rate represents the concentration of bromoarene product over time as determined by GC analysis of reaction aliquots. The reaction rate shows a 2nd order dependence on CuBr₂ concentration (Figure

4.7A). A mixed $2^{\text{nd}}/1^{\text{st}}$ order fit cannot be distinguished from the 2^{nd} order fit, but does not provide the simplest modeling due to the increased number of coefficients used in the fit (Figure 4.8).

The reaction rate shows a 1^{st} order dependence on LiBr concentration (Figure 4.7B). The reaction rate shows a saturation dependence on phenol concentration (Figure 4.7C). Reaction time course plots for these studies are also shown (Figure 4.9A-C). Measurement of the reaction rate dependence on phenol concentration is somewhat complicated by the poor selectivity for 4-bromophenol over time. At low initial concentrations of phenol, the desired product 4-bromophenol is consumed quickly and converted to 2,4-bromophenol. Due to this further oxidation of 4-bromophenol, kinetics were monitored by following consumption of phenol over time.

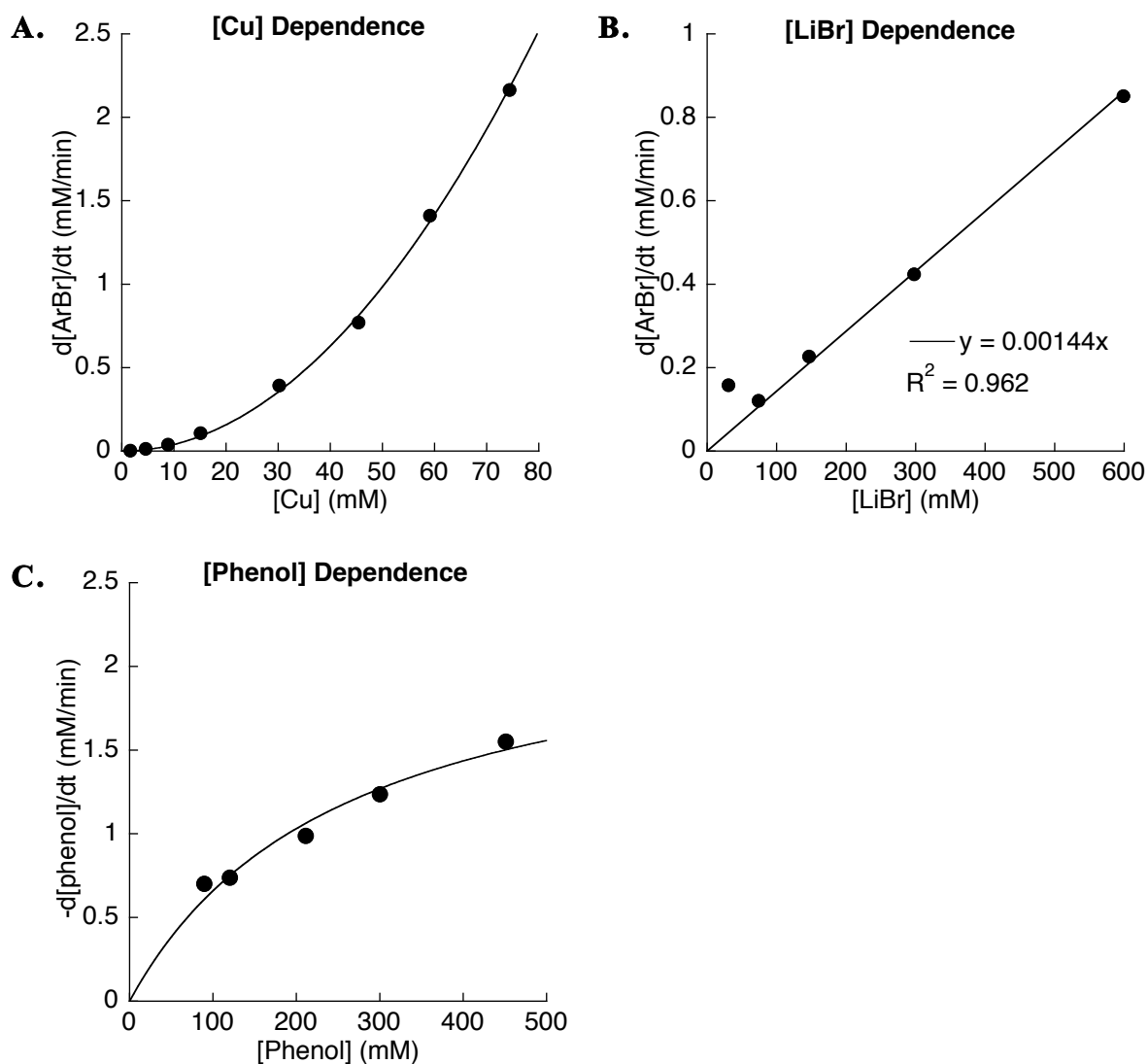


Figure 4.7. Kinetic data from phenol bromination assessing the kinetic dependence on (A) $[\text{CuBr}_2]$, (B) $[\text{LiBr}]$, and (C) $[\text{phenol}]$. Standard reaction conditions: CuBr_2 (20 mol %), phenol (1 equiv, 300 mM), LiBr (600 mM), 80 °C in AcOH . The curve in (A) is derived from a nonlinear least-squares fit to $\text{rate} = c_1[\text{Cu}]^2$.

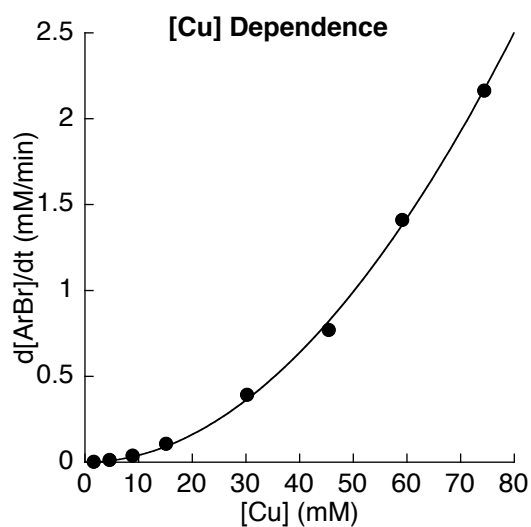


Figure 4.8. A mixed 2nd/1st order dependence on CuBr_2 concentration (2nd order at low $[\text{Cu}]$ and 1st order at high $[\text{Cu}]$) models the data well, but has more variable coefficients than a 2nd order fit. In order to have the simplest fit, the 2nd order fit is chosen as most accurate. The curve is derived from a nonlinear least-squares fit to $\text{rate} = c_1[\text{Cu}]^2/(c_2 + c_3[\text{Cu}])$.

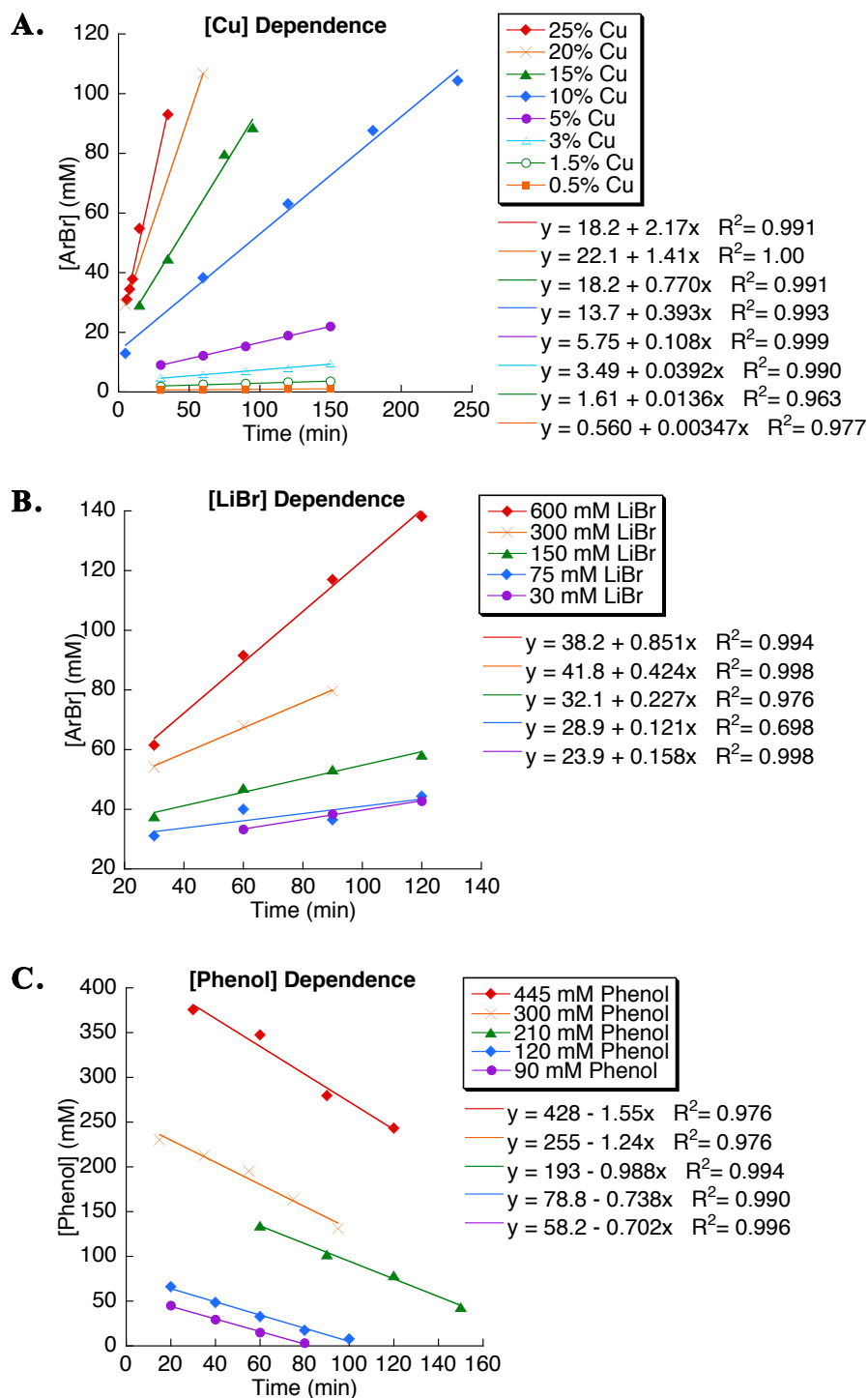


Figure 4.9. Reaction time course dependence plots for (A) $[\text{CuBr}_2]$, (B) $[\text{LiBr}]$, and (C) $[\text{phenol}]$. Standard reaction conditions: CuBr_2 (20 mol %), phenol (1 equiv, 300 mM), LiBr (600 mM), 80°C in AcOH.

The effect of O₂ partial pressure was studied by comparing the reaction time courses.

The reaction traces under 1 atm O₂ or air exhibit similar profiles (Figure 4.10), suggesting that the reaction has zero order dependence on O₂ concentration.

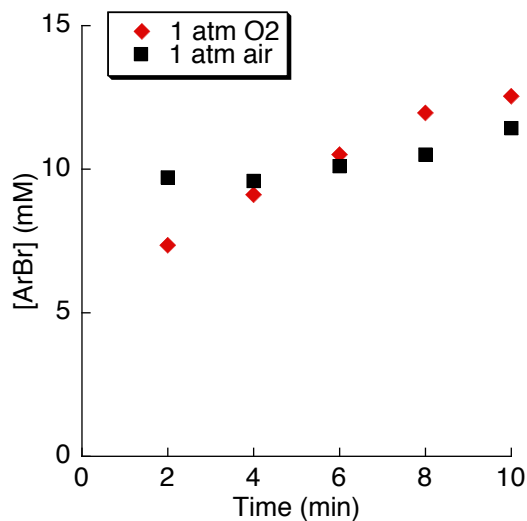
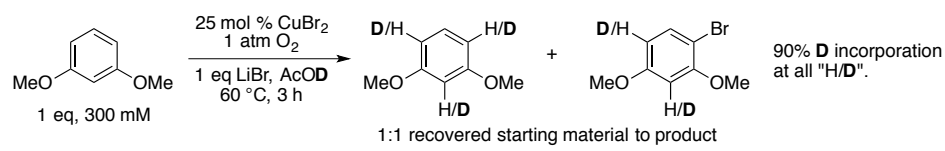


Figure 4.10. Reaction time course plots under 1 atm O₂ or air exhibit similar profiles. Conditions: CuBr₂ (10 mol %), phenol (1 equiv, 300 mM), LiCl (600 mM), 80 °C in AcOH.

4.3. Hydrogen/Deuterium Exchange.

4.3.1 1,3-Dimethoxybenzene Bromination.

1,3-Dimethoxybenzene was submitted to the typical oxidation conditions except that AcOH was replaced with AcOD (eqn 4.9). After 3 h, the reaction was analyzed and there was a 1:1 ratio of recovered starting material to product. At the positions labeled “H/D” (eqn 4.9), in sum there was 90% deuterium incorporation (these peaks overlap in the NMR spectrum and so the sum of deuterium incorporation was evaluated). The non-labeled position *meta* to both methoxy substituents showed no deuterium incorporation, presumably because it is deactivated by the *meta* electron-withdrawing inductive effect of the methoxy substituents.



4.4. Spectroscopic Studies of the Reaction Solution and Catalyst Resting State.

During time course kinetic studies, it was observed that both the 1,3-dimethoxybenzene and phenol reaction solutions appear to be the same emerald green color. A solution of similar concentration of CuBr_2 and LiBr in AcOH appears to be a similar green color. This observation suggests that both reactions may have a similar copper resting state even though phenol has the ability to form Cu -phenoxides and dimethoxybenzene does not have a similar coordinating ability. As elaborated in the following sections, UV-visible and EPR spectroscopy indicate that the catalyst resting state is a bromocuprate(II), most likely the planar CuBr_3^- which is reported to be green. At higher LiBr concentrations or certain other conditions, CuBr_3^- can equilibrate to distorted tetrahedral CuBr_4^{2-} , which is reported to be purple.^{7,8}

Additionally, the observation of green reaction solutions is interesting in that the dimethoxybenzene reaction solutions were originally reported to be red-brown in color, an observation used as part of an argument that Br_2 was produced under the reaction conditions.¹ During these mechanistic studies, the solutions were always emerald green under reaction conditions. The solutions were observed to become red-brown if they were left in the long syringe needle for an extended period of time. Perhaps the stainless steel syringe needle created an anaerobic environment or otherwise reacted with the solution components, causing a color change.⁹

4.4.1. UV-Visible Spectroscopy of 1,3-Dimethoxybenzene and Br₂.

UV-visible spectroscopy was used to compare the phenol and 1,3-dimethoxybenzene reaction solutions to a similar 1:20 CuBr₂/LiBr solution in AcOH (Figure 4.11). The reaction solution was removed from the reactor under turnover and diluted to 3 mM with AcOH.¹⁰ The spectra have identical peaks, except for the organic substrate absorption from 250-300 nm. The spectra agree with reported UV-visible spectra for bromocuprate(II), most likely the planar CuBr₃⁻ (some equilibration between purple tetrahedral CuBr₄²⁻ and planar CuBr₃⁻ may occur).^{7,8}

As generation of Br₂ under the reaction conditions has been proposed,¹ the spectrum of Br₂ in AcOH was also obtained (Figure 4.11). The bromocuprate peaks overlay the Br₂ peak, so if a minimum of Br₂ is generated under the reaction conditions it may not be observable by UV-visible spectroscopy.

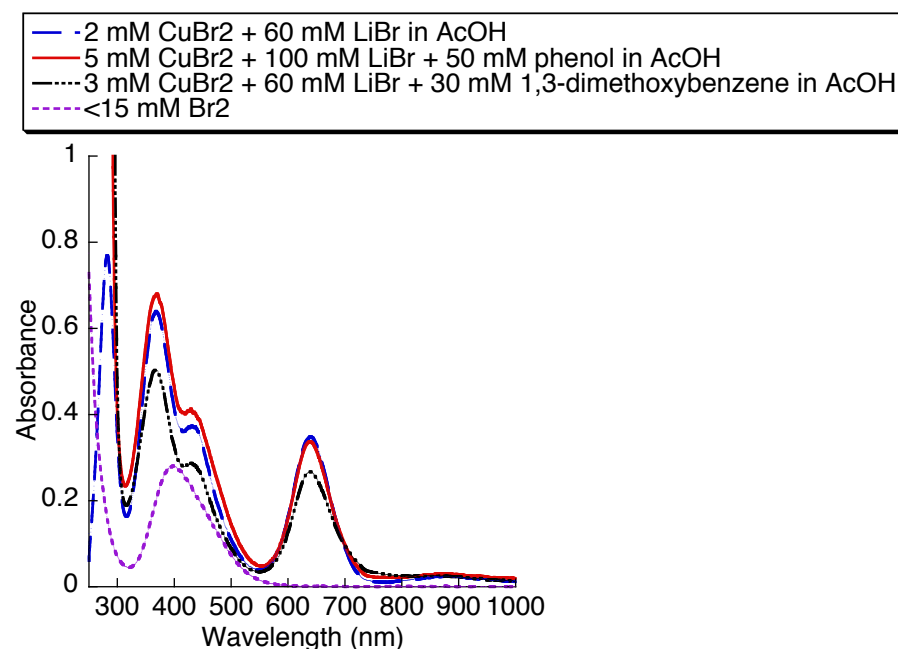


Figure 4.11. UV-visible spectra of the reaction solutions, a CuBr₂ solution, and Br₂ in AcOH.

Spectra of 1:20 $\text{CuBr}_2/\text{LiBr}$, $\text{Cu}(\text{OAc})_2$ and 1:20 $\text{Cu}(\text{OAc})_2/\text{LiBr}$ in AcOH were compared (Figure 4.12). Their UV-visible spectra are quite different, and $\text{Cu}(\text{OAc})_2$ does not appear to be present under the reaction conditions. Additionally, when $\text{Cu}(\text{OAc})_2$ is mixed with excess LiBr it appears to convert to a bromocuprate.

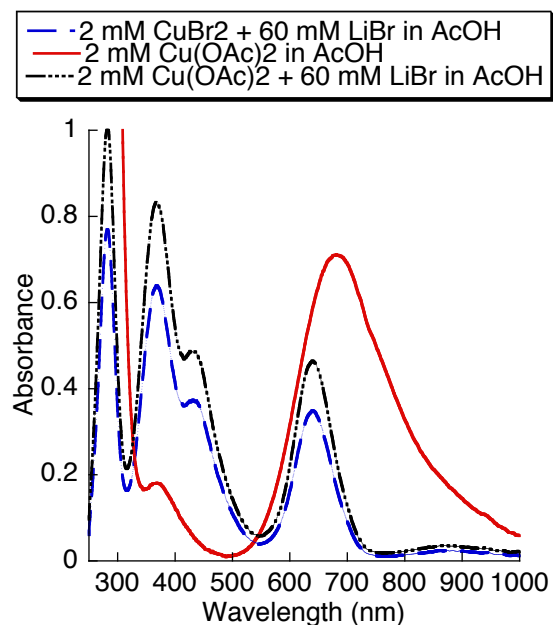


Figure 4.12. UV-visible spectra of 1:20 $\text{CuBr}_2/\text{LiBr}$, $\text{Cu}(\text{OAc})_2$, and 1:20 $\text{Cu}(\text{OAc})_2/\text{LiBr}$ solutions in AcOH .

4.4.2. EPR Spectroscopy of 1,3-Dimethoxybenzene and Phenol Oxidation.

EPR spectroscopy was also used to compare the 1,3-dimethoxybenzene and phenol oxidation reaction solutions with a solution of 1:20 $\text{CuBr}_2/\text{LiBr}$ in AcOH . The reaction solutions (modified to 5 mM concentration) were removed from the reaction vessels under turnover and flash frozen. An independently prepared $\text{CuBr}_2/\text{LiBr}$ solution was also flash frozen. All three of these solutions showed thermochromic behavior, illustrated by the photos of the 5 mM

CuBr_2 /100 mM LiBr solution in AcOH (Figure 4.13). The solutions are emerald green at room temperature and become purple when frozen at either 145 or 77 K.



Figure 4.12. The 5 mM CuBr_2 /100 mM LiBr solution in AcOH shows thermochromic behavior. It is (A) emerald green at room temperature and (B, C) purple when frozen (77 or 145 K).

EPR spectra of the 1,3-dimethoxybenzene and phenol reaction solutions, and the CuBr_2 /excess LiCl solution in AcOH are all isotropic (Figure 4.14). They have identical $g = 2.10$, which agree with literature reports of CuBr_4^{2-} g values.¹¹ The intensities of the spectra are quite different despite the similar Cu concentrations. Tetrabromocuprate(II) materials have been identified as “magnetic spin ladders” where pairs of antiferromagnetically coupled CuBr_4^{2-} centers associate with other pairs in a ladder-like formation.¹² The concentration of antiferromagnetically coupled CuBr_4^{2-} centers may be increased by hydrogen bonding and arene pi stacking,¹¹ so the reduced spectral intensity in the reaction solutions may be caused by a solution environment that favors antiferromagnetic coupling. The presence of antiferromagnetically coupled $\text{Cu}_2(\text{OAc})_4$ paddle-wheel complexes is unlikely based on the UV-visible spectra of the reaction solutions (Figure 4.12).

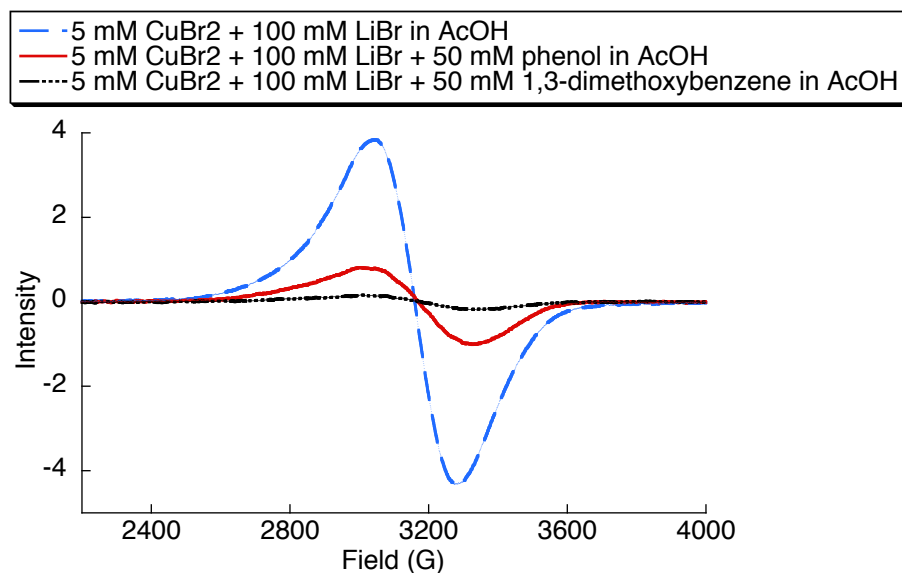


Figure 4.14. X-Band EPR spectra of $\text{CuBr}_2/\text{LiBr}$ in AcOH, the phenol reaction solution, and the 1,3-dimethoxybenzene reaction solution, 145 K. Each spectra is isotropic, fitting $g = 2.10$. Conditions: 5 mM CuCl_2 , 100 mM LiCl , and 0 or 50 mM substrate in AcOH.

4.5. Other Studies Attempting to Address the Possibility of Br_2 Generation.

4.5.1. Reaction Solution Vacuum Transfer and UV-Visible Analysis.

The intense color of the bromocuprate(II) catalyst resting state may obscure any minor concentrations of Br_2 that may be present in the reaction solution, as the Cu UV-visible spectrum completely overlaps the Br_2 spectrum (Figure 4.11). To determine if Br_2 could be isolated, a large-scale dimethoxybenzene reaction was performed (300 mM 1,3-dimethoxybenzene, 10 mL reaction volume) and then the reaction liquid/vapors were vacuum transferred away from the solid copper (eqn 4.10). During the vacuum transfer, no red/purple Br_2 vapors were observed. The reaction solution condensate was colorless and UV-visible analysis showed no Br_2 was present (Figure 4.15). This experiment should be repeated without substrate, as it is possible that substrate may rapidly consume any Br_2 that is generated.

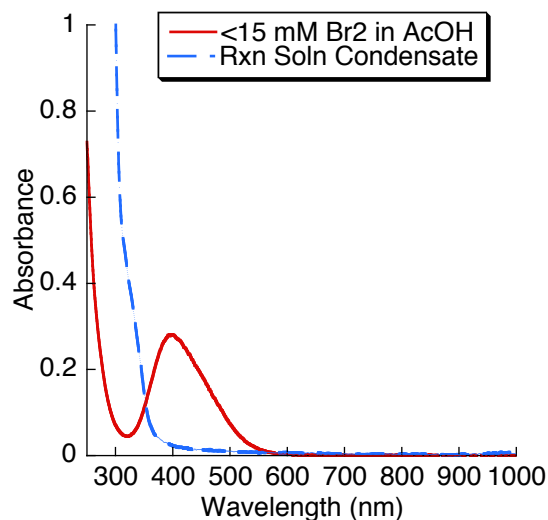
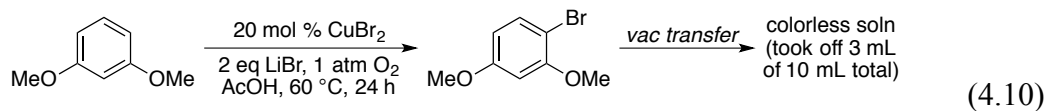
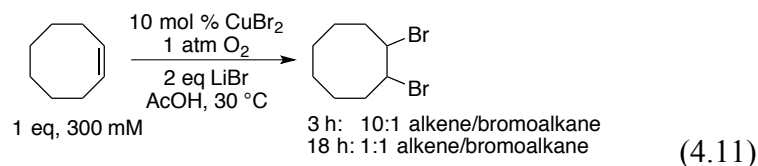


Figure 4.15. UV-visible spectrum of the reaction solution condensate, compared to the Br_2 spectra in AcOH. No Br_2 is apparent in the reaction solution condensate.

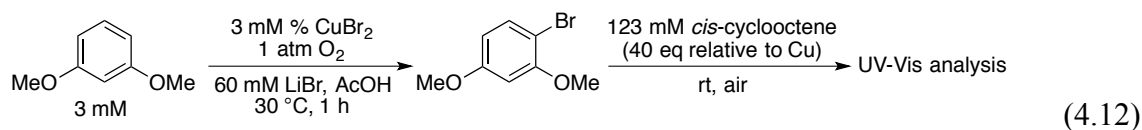
4.5.2. Bromination of Cyclooctene in the Reaction and UV-Visible Analysis.

Yang and Stahl previously reported that bromination of *cis*-cyclooctene catalyzed by CuBr_2 (25 mol %) proceeds to 75% yield in 24 h at 60 °C with 1 equiv *cis*-cyclooctene (300 mM), 1 equiv LiBr, and 1 atm O_2 in AcOH (eqn 4.2).¹ This experiment was repeated under similar conditions, lowering the temperature to 30 °C, the temperature of the kinetic studies. The dibromoalkane was produced in 1:1 ratio with starting material after 17 h (eqn 4.11).



Quenching of the bromination reaction solution UV-visible spectrum by cyclooctene gives some insight into the concentration of Br_2 that might be present in solution. It was

previously noted that the Br₂ peak (400 nm in AcOH) in a UV-visible spectrum overlaps with bromocuprate(II) peaks at 363 and 424 nm (Figure 4.11). The bromocuprate(II) spectrum also shows a strong peak at 634 nm which does not overlap with the Br₂ spectrum. A dimethoxybenzene bromination reaction was performed and then excess *cis*-cyclooctene was added after 1 h, when the reaction would be under turnover conditions (eqn 4.12).



With addition of excess cyclooctene, the reaction solution UV-visible spectrum rapidly decreased in intensity over 10 min (Figure 4.16A). The three distinctive peaks at 363, 424, and 634 nm decay at the same rate (Figure 4.16B, decay of each peak is plotted as % intensity of absorbance, where 100% is the peak height at 0 min and 0% is the peak height at 10 min). If there was a significant concentration of Br₂ in solution and Br₂ was the primary brominating agent, it would be expected that the peaks at 363 and 424 nm, which overlap with the 400 nm Br₂ peak, would decay more rapidly than the Cu peak at 634 nm. The identical decay rate indicates that there is little to no Br₂ present in the reaction solution.

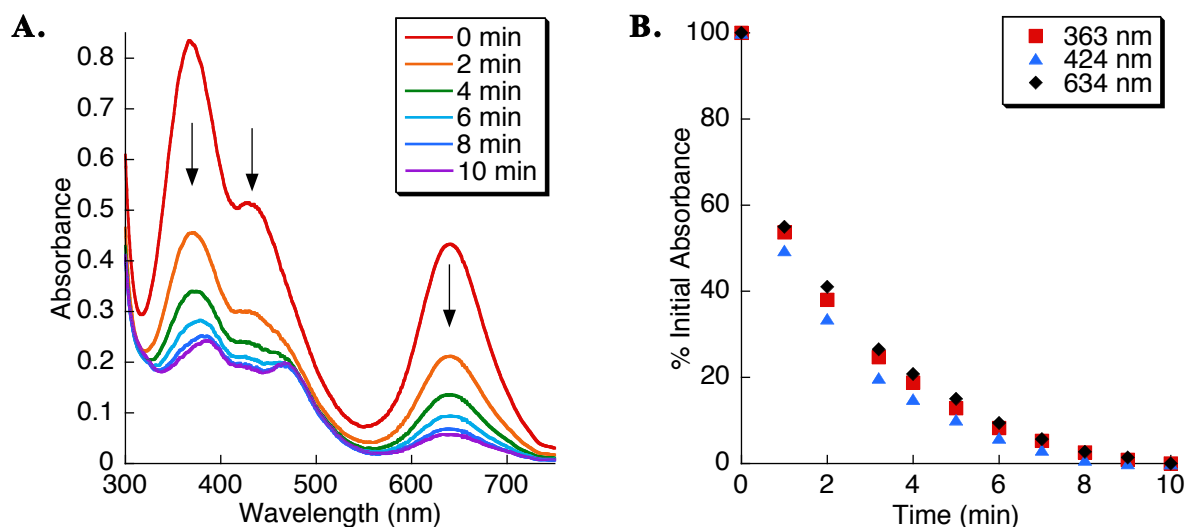


Figure 4.16. (A) The distinctive peaks of the bromination reaction UV-visible spectrum rapidly decay after 40 equiv cyclooctene addition. **(B)** Decay of each peak is plotted as % intensity of absorbance, in which 100% is the peak height at 0 min and 0% is the peak height at 10 min. All three peaks decay at the same rate, indicating that there is little to no Br_2 present in the reaction solution.

4.5.3. Comments on the Previous Experiments.

In the vacuum transfer experiment (section 4.5.1) and the cyclooctene quenching experiment (section 4.5.2), no Br_2 was directly observed. These experiments indicate that a significant concentration of Br_2 does not build up during the course of the reaction. However, these experiments do not indicate that Br_2 is never generated during the reaction. If disproportionation of CuBr_2 to generate Br_2 is slow but reaction of Br_2 with the organic substrate is fast, then little to no Br_2 would be detectable under the catalytic experiments. It has been previously reported that Br_2 can be distilled from a refluxing solution of CuBr_2 in acetonitrile;⁷ however, acetonitrile is known to stabilize Cu^{I} and could promote disproportionation.¹³

4.6. Proposed Mechanisms.

4.6.1 1,3-Dimethoxybenzene Bromination.

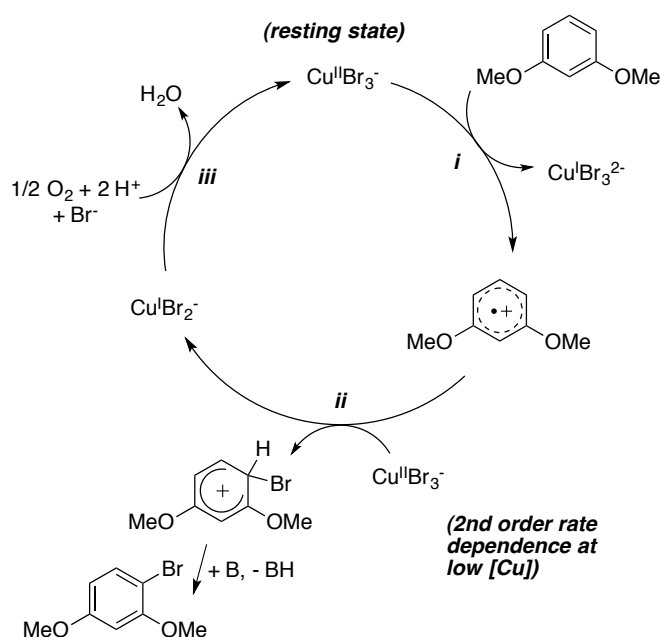
The oxidative bromination of 1,3-dimethoxybenzene was found to be mixed 2nd/1st order in CuBr₂ concentration (2nd order at low concentration, 1st order at higher concentration), saturating in LiBr concentration, zero order in substrate, and zero-order in O₂ concentration. The rate dependence only on CuBr₂ and LiBr indicates that the turnover-limiting step may be a halide exchange or disproportionation step, but not a step involving the substrate or Cu^I reoxidation by O₂. Spectroscopic studies of the reaction solution indicated that the catalyst resting state is a bromocuprate(II). The green color and UV-visible spectrum has been assigned to CuBr₃²⁻, which can equilibrate to the purple distorted tetrahedral CuBr₄²⁻ under certain conditions. Additionally, rapid H/D exchange of aryl protons in AcOD (with and without Cu) indicate that 1,3-dimethoxybenzene has high electrophilic reactivity.

The first order dependence on CuBr₂ (except at low Cu concentrations) may indicate that a CuBr₂ disproportionation mechanism to generate Br₂ is not active. This disproportionation would likely show a second order dependence on Cu as 2 equiv of CuBr₂ are necessary to generate 1 equiv of “Br⁺”. Observation of Br₂ generated under the reaction conditions would of course answer this question, but it is currently unclear if Br₂ is generated under the reaction conditions (see section 4.5.3). Indeed, even if Br₂ were generated it may not be detectable if disproportionation to generate Br₂ is slow but the reaction of Br₂ with the arene is fast.

If dimethoxybenzene bromination is similar to chlorination, the proposed mechanism for 1,3-dimethoxybenzene oxidation is (i) a single-electron-transfer to Cu^{II}Br₃⁻ to yield the aryl-radical-cation, followed by (ii) bromine atom transfer from a second equivalent of Cu^{II}Br₃⁻ to yield the aryl-cation Wheland-type intermediate and Cu^IBr₂⁻ (Scheme 4.3). The Wheland-type

intermediate is ultimately deprotonated, giving the final product. $\text{Cu}^{\text{I}}\text{Br}_2^-$ may be reoxidized by O_2 (**iii**). The mixed $2^{\text{nd}}/1^{\text{st}}$ order dependence on Cu concentration may be explained by this mechanism. At higher Cu concentration, only the 1^{st} order dependence in oxidation to the aryl-radical-cation (**i**) is observed, and bromide transfer (**ii**) is relatively fast. At lower Cu concentration, the bromide transfer step contributes to the rate of the reaction and a 2^{nd} order dependence is observed. However, if step **i** is turnover-limiting, the reaction should show a substrate concentration rate dependence. The observed dependence on only Cu and LiBr concentration is not explained by this mechanism, which does not contain any sort of ligand exchange or other steps solely involving Cu and LiBr.

Scheme 4.3. Proposed Mechanism for Cu-Catalyzed Aerobic Oxidative Chlorination of 1,3-Dimethoxybenzene.



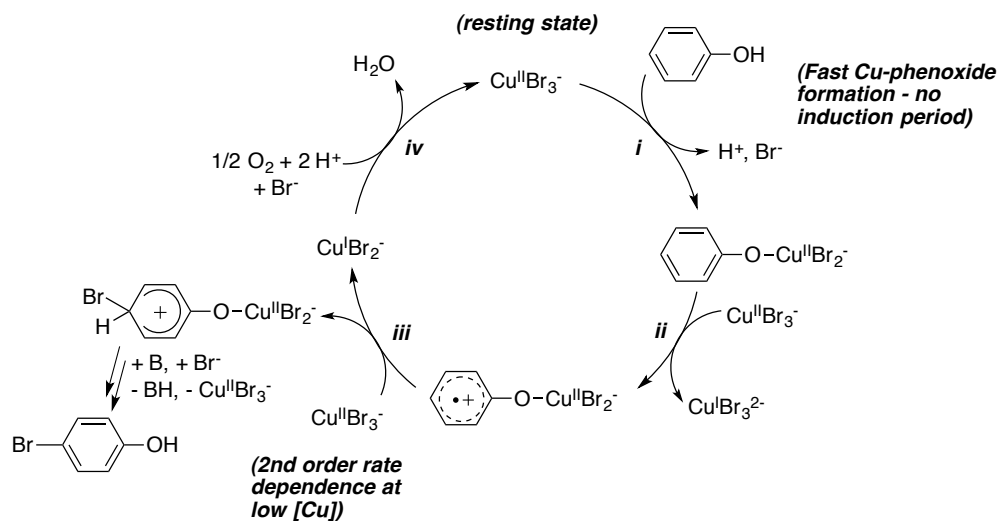
4.6.2 Phenol Bromination.

The oxidative bromination of phenol was found to be 2nd order in CuBr₂ concentration, first order in LiBr concentration, saturating in substrate concentration, and zero order in O₂ concentration. Spectroscopic studies of the reaction solution indicated that the catalyst resting state is a bromocuprate(II). The green color and UV-visible spectrum has been assigned to CuBr₃²⁻, which can equilibrate to the purple distorted tetrahedral CuCl₄²⁻ under certain conditions.

As discussed in the previous section, it is currently unknown if a CuBr₂ disproportionation mechanism to generate Br₂ operates during these reaction conditions. The possible second order dependence on CuBr₂ may favor this mechanism as the disproportionation would likely show a second order dependence on Cu as 2 equiv of CuBr₂ are necessary to generate 1 equiv of “Br⁺”.

If Br₂ is not generated and phenol bromination is similar to chlorination, the proposed mechanism for phenol oxidation is *(i)* generation of a Cu^{II}-phenoxide, *(ii)* a single-electron-transfer to a second equivalent of Cu^{II}Br₃⁻ to yield the Cu^{II}-phenoxy-radical-cation, and *(iii)* bromide transfer from a third equivalent of Cu^{II}Br₃⁻ to yield the Cu^{II}-phenoxy-aryl-cation Wheland-type intermediate (Scheme 4.4). The Wheland-type intermediate is ultimately deprotonated and can exchange off of Cu, giving the final product. Cu^IBr₂⁻ may be reoxidized by O₂ *(iv)*. Unlike phenol chlorination, generation of the Cu^{II}-phenoxide may be fast as no base-dependent induction period is observed. The 2nd order dependence on Cu concentration may also be explained by this mechanism if the oxidation *(ii)* and bromine transfer *(iii)* steps are slow.

Scheme 4.4. Proposed Mechanism for Cu-Catalyzed Aerobic Oxidative Chlorination of Phenol.



4.7 Conclusions.

The current mechanistic study is not sufficient for a confident conclusion on the nature of the bromination mechanism. The proposed mechanisms are either (1) bromination by Br_2 which is generated by CuBr_2 disproportionation, or (2) bromination by a bromocuprate(II) complex involving the key aryl-radical-cation intermediate similar to that proposed for arene chlorination in the previous chapter. However, neither mechanism perfectly fits the observed kinetic features.

4.8 Contributions.

Bradford L. Ryland aided in the acquisition and fitting of the EPR spectra.

4.9. Experimental.

4.9.1. General Considerations.

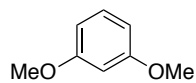
All commercially available compounds were purchased and used as received. ^1H and ^{13}C NMR spectra were recorded on Bruker or Varian 300 MHz spectrometers. Chemical shift values are given in parts per million relative to internal TMS (0.00 ppm for ^1H) or CDCl_3 (77.23 ppm for ^{13}C). Flash chromatography was performed using SiliaFlash® P60 (Silicycle, particle size 40-63 μm , 230-400 mesh). Gas chromatographic analyses of the reactions were conducted with a Shimadzu GC-17A gas chromatograph with Stabilwax-DB column, using trimethyl-(phenyl)silane as an internal standard. X-band EPR data were collected using a Bruker EleXsys E500 spectrometer; all spectra were acquired at 145 K using a $\text{N}_2(\text{l})$ cryostat under nonsaturating conditions and fit using the W95EPR program.¹⁴

4.9.2. GC Analysis of Reaction Time Courses.

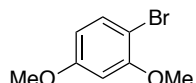
Reactions were run on the Stahl group custom vortexing reactors (2 mL AcOH per rxn). At a timepoint, a 25- μL aliquot of the rxn soln is syringed out of the shaker (getting rid of air bubbles in the needle first) and into a GC vial insert containing 150 μL EtOAc. 100 μL of Ph-TMS standard soln in EtOAc is added and the GC vials are capped, shaken, and analyzed. The rxn appears to stop when diluted in EtOAc and different periods of wait time before analysis (5 min - 20 h) does not appear affect quantitation.

4.9.3. Characterization.

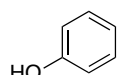
To separate products from the reaction mixture, the reaction mixture was diluted with 10 mL water and 10 mL CH_2Cl_2 . The organic layer was washed with saturated Na_2CO_3 (15 mL) and brine solution (15 mL). The organic layer was dried over MgSO_4 and concentrated under vacuum. The residue was purified by column chromatography.



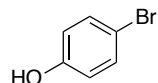
1,3-Dimethoxybenzene is commercially available. ^1H NMR: (300 MHz, CDCl_3) δ 7.16-7.11 (m, 1H), 6.49 (d, $J = 2.4$ Hz, 1H), 6.46-6.44 (m, 2H), 3.71 (s, 6H).



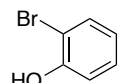
1-Bromo-2,4-dimethoxybenzene was compared to the commercially available sample. ^1H NMR: (300 Hz, CDCl_3): δ 7.40 (d, $J = 8.7$ Hz, 1H), 6.48 (d, $J = 2.8$ Hz, 1H), 6.39 (dd, $J = 8.9, 2.5$ Hz, 1H), 3.86 (s, 3H), 3.79 (s, 3H).



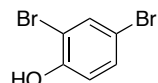
Phenol is commercially available. ^1H NMR: (300 Hz, CDCl_3): δ 7.27-7.20 (m, 2 H), 6.93-6.88 (m, 1 H), 6.85-6.80 (m, 2 H).



4-Bromophenol was compared to the commercially available sample. ^1H NMR: (300 Hz, CDCl_3): δ 7.35-7.30 (m, 2 H), 6.74-6.69 (m, 2 H).



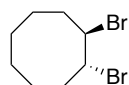
2-Bromophenol is known. ^1H NMR: (300 Hz, CDCl_3): δ 7.47-7.44 (m, 1 H), 7.24-7.19 (m, 1 H), 7.03-7.00 (m, 1 H), 6.82-6.78 (m, 1 H).



2,4-Dibromophenol is known. ^1H NMR: (300 Hz, CDCl_3): δ 7.60-7.59 (m, 1 H), 7.25-7.22 (m, 1 H), 6.85-6.82 (m, 1 H).



Cis-Cyclooctene is commercially available. ^1H NMR: (300 Hz, CDCl_3): δ 5.67-5.57 (m, 2 H), 2.14 (br s, 4 H), 1.49 (br s, 8 H).



Trans-1,2-Dibromocyclooctane agrees with the previous report.¹ ¹H NMR: (300 Hz, CDCl₃): δ 4.62-4.55 (m, 2 H), 2.47-2.37 (m, 2 H), 2.13-2.06 (m, 2 H), 1.87-1.83 (m, 2 H), 1.71-1.45 (m, 6 H).

4.10. References and Notes.

1. Yang, L.; Lu, Z.; Stahl, S. S. "Regioselective copper-catalyzed chlorination and bromination of arenes with O₂ as the oxidant." *Chem. Commun.* **2009**, 6460-6462.
2. (a) Menini, L.; Parreira, L. A.; Gusevskaya, E. V. "A practical highly selective oxybromination of phenols with dioxygen." *Tetrahedron Lett.* **2007**, *48*, 6401-6404.
3. (a) Menini, L.; Gusevskaya, E. V. "Novel highly selective catalytic oxychlorination of phenols." *Chem. Commun.* **2006**, 209-211. (b) Menini, L.; Gusevskaya, E. V. "Aerobic oxychlorination of phenols catalyzed by copper(II) chloride." *Appl. Catal. A: Gen.* **2006**, *309*, 122-128.
4. Castro, C. E.; Gaughan, E. J.; Owsley, D. C. "Cupric Halide Halogenations." *J. Org. Chem.* **1965**, *30*, 587-592.
5. Koyano, T. "On the Mechanism of Bromination of Olefins with Cupric Bromide." *Bull. Chem. Soc. Jpn.* **1971**, *44*, 1158-1160.
6. Rodebaugh, R.; Debenham, J. S.; Fraser-Reid, B.; Snyder, J. P. "Bromination of Alkenyl Glycosides with Copper(II) Bromide and Lithium Bromide: Synthesis, Mechanism, and DFT Calculations." *J. Org. Chem.* **1999**, *64*, 1758-1761.
7. (a) Barnes, J. C.; Hume, D. N. "Copper(II) Bromide Complexes. I. A Spectrophotometric Study." *Inorg. Chem.* **1963**, *2*, 444-448. (b) Khan, M. A.; Meullemeestre, J.; Schwing, M. J.;

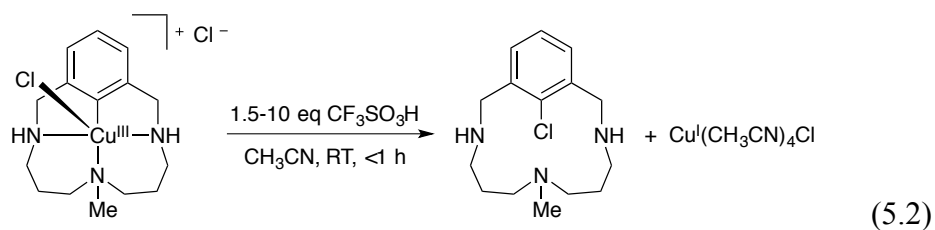
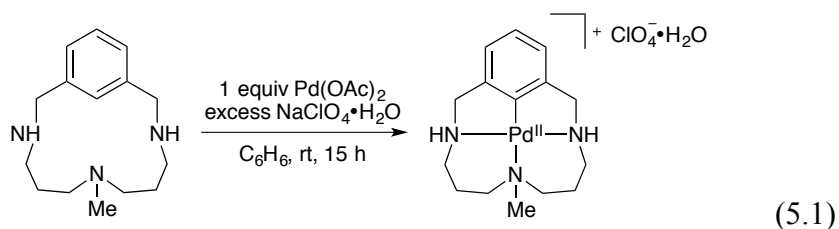
- Vierling, F. "Theoretical aspects of an equilibrium study in the non-dissociating molecular solvent acetic acid." *Polyhedron* **1990**, *9*, 2613-2617.
8. Eswein, R. P.; Howald, E. S.; Howald, R. A.; Keeton, D. P. "Ion pairs-IV Chlorocuprate equilibria in acetic acid solutions." *J. Inorg. Nucl. Chem.* **1967**, *29*, 437-452.
 9. For example, other group members working to adapt Cu^I/TEMPO-catalyzed aerobic alcohol oxidations to flow reactors have observed that catalyst solutions stored in stainless steel HPLC pumps lose activity. Glass-lined HPLC pumps must be used for the catalyst solution to remain active.
 10. Dilution did not appear to disturb reaction speciation; the spectrum simply decreased in overall intensity upon dilution.
 11. For a leading reference, see: Luque, A.; Sertucha, J.; Castillo, O.; Roman, P. "Crystal packing and physical properties of pyridinium tetrabromocuprate(II) complexes assembled via hydrogen bonds and aromatic stacking interactions." *New J. Chem.* **2001**, *25*, 1208-1214.
 12. For a leading reference, see: Watson, B. C.; Kotov, V. N.; Meisel, M. W.; Hall, D. W.; Granroth, G. E.; Montfrooij, W. T.; Nagler, S. E.; Jensen, D. A.; Backov, R.; Petruska, M. A.; Fanucci, G. E.; Talham, D. R. "Magnetic Spin Ladder (C₅H₁₂N)₂CuBr₄: High-Field Magnetization and Scaling near Quantum Criticality." *Phys. Rev. Lett.* **2001**, *86*, 5168-5171.
 13. Zuberbüler, A. D. "Interaction of Cu^I Complexes with Dioxygen." In *Metal Ions in Biological Systems, Vol. 5*; Marcel Dekker, **1976**, 325-368.
 14. Neese, F. *QCPE Bull.* **1995**, *15*, 5.

Chapter 5:

Synthesis of Novel Aryl-Pd^{IV} Triazamacrocyclic Complexes
and Comparison to Analogous Aryl-Cu^{III} Complexes

5.1. Introduction.

In 1986, Hiraki and coworkers reported synthesis and palladation of a triazamacrocyclic ligand to form an aryl-Pd^{II} complex (eq 5.1).¹ In 2002, Ribas, Llobet, Stack, and coworkers reported that an aryl-Cu^{III} complex could be formed from the same ligand.² Further studies by Stahl, Ribas, and coworkers demonstrated that the aryl-Cu^{III} complex was a kinetically competent intermediate in Cu-catalyzed arene C-O and C-N bond formation.³ Formation of aryl-Cu^{III}-halide complexes and reductive elimination of aryl halides was also demonstrated (5.2).⁴ In contrast to the aryl-Cu^{III} complex, the aryl-Pd^{II} complex did not undergo further oxidation in the presence of nucleophiles and O₂.⁵ Further examination of aryl-Pd complex was carried out to compare the reactivity of Pd and Cu in the same ligand environment.



This chapter presents a summary of the reactivity of the aryl-Pd^{II} complex. A variety of novel aryl-Pd^{IV} complexes were synthesized using methods similar to those used by Sanford and coworkers.⁶ These complexes did not show facile reductive elimination, unlike the analogous aryl-Cu^{III} complexes. Intriguingly, radical species are implicated in the formation of the aryl-Pd^{IV} complexes and electrochemical analysis of the aryl-Pd^{II} complex indicates it undergoes one-electron oxidation rather than simultaneous two-electron oxidation. Since the completion of this

study (ca. 2009), aryl-Pd^{III} complexes have been demonstrated to be intermediates in Pd-catalyzed arene C-H functionalization reactions.⁷

5.2. Synthesis of Novel Aryl-Pd^{IV} Triazamacrocyclic Complexes.

The [aryl-Pd^{II}]⁺BF₄⁻ complex **2** was synthesized with an alternate tetrafluoroborate counterion instead of the shock-sensitive perchlorate counterion (eq 5.3). X-ray analysis of the colorless crystals of **2** indicates the Pd environment is square planar and the macrocyclic ring lies in plane with the arene (Figure 5.1).

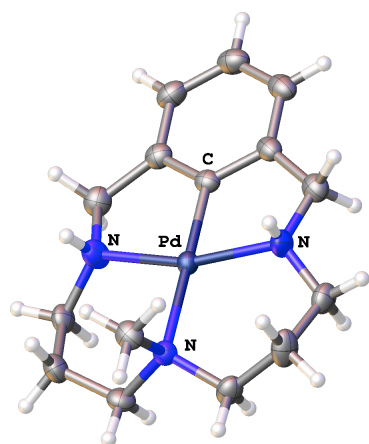
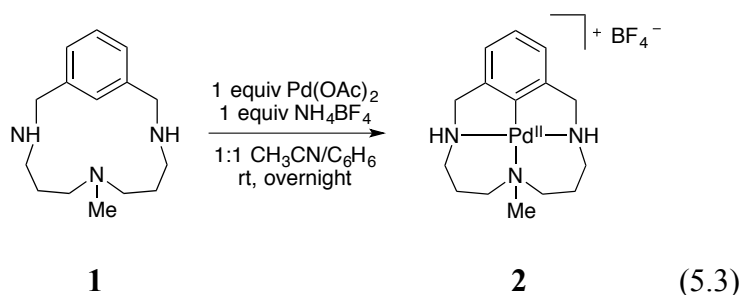


Figure 5.1. Structure of [aryl-Pd^{II}]⁺BF₄⁻ complex **2** determined by X-ray crystallography. Counterion (BF₄⁻) not shown.

A solution of **2** was treated with 1 equiv PhICl_2 and the solution immediately changed from colorless to yellow-orange (eq 5.4). The product was determined to be the octahedral [aryl- $\text{Pd}^{\text{IV}}\text{Cl}_2$] BF_4 complex **3** with axial chloride ligands by X-ray analysis (Figure 5.2).

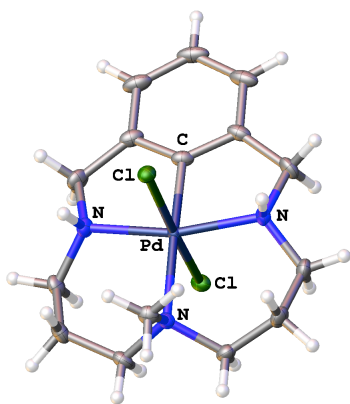
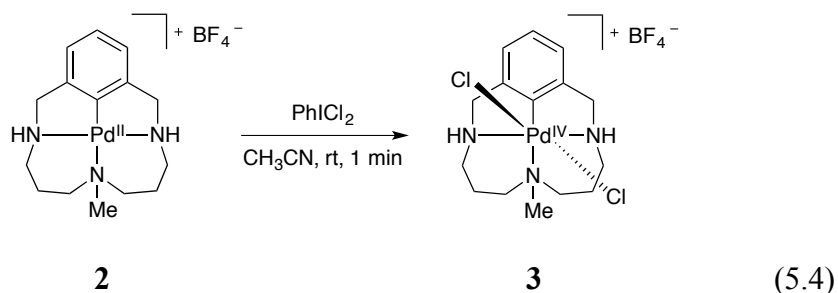


Figure 5.2. Structure of [aryl- $\text{Pd}^{\text{IV}}\text{Cl}_2$] BF_4 complex **3** determined by X-ray crystallography. Counterion (BF_4^-) not shown.

A solution of **2** was treated with 1 equiv *N*-chlorosuccinimide (NCS) and the solution immediately changed from colorless to yellow-orange (eq 5.5). A crystal of the product was determined to be the octahedral [aryl- $\text{Pd}^{\text{II}}(\text{NCS})$] BF_4 complex **4** by X-ray analysis (Figure 5.3). However, NMR spectra of a re-dissolved sample of a majority of crystals from the reaction indicated that the [aryl- $\text{Pd}^{\text{IV}}\text{Cl}_2$] BF_4 complex **3** was the major product.

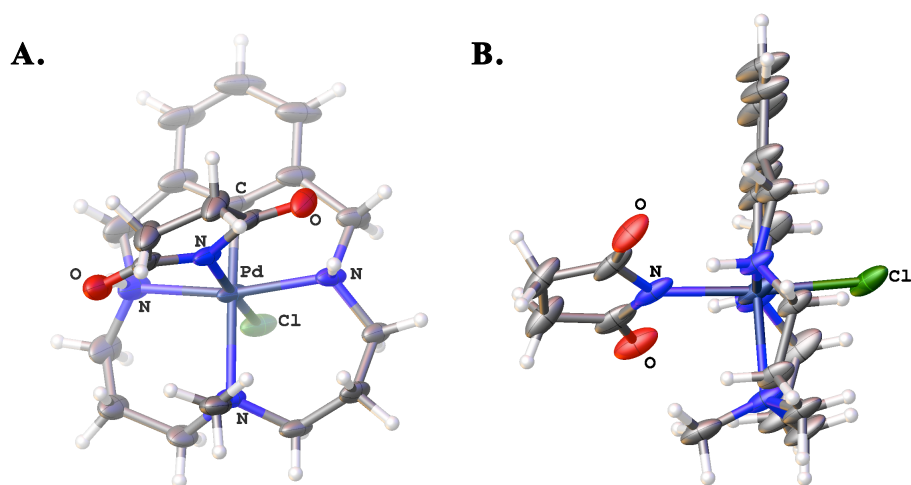
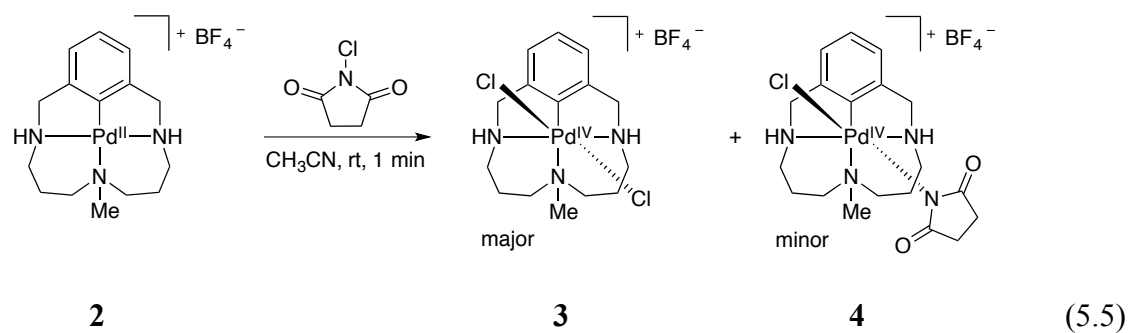
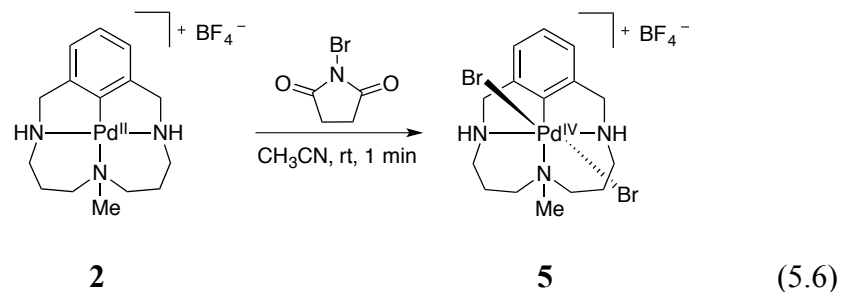


Figure 5.3. Structure of [aryl-Pd^{IV}(NCS)]BF₄ complex **4** determined by X-ray crystallography. **(A)** Front and **(B)** side views. Counterion (BF₄⁻) not shown.

A solution of **2** was treated with 1 equiv *N*-bromosuccinimide (NBS) and the solution immediately changed from colorless to purple (eq 5.6). A crystal of the product was determined to be the octahedral [aryl-Pd^{IV}Br₂]₂BF₄ complex **5** by X-ray analysis (Figure 5.3). NMR spectra of a majority of crystals from the reaction indicated **5** was generated as the major species.



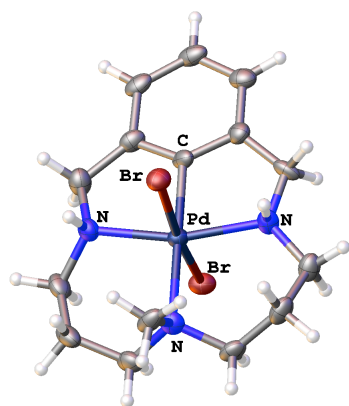
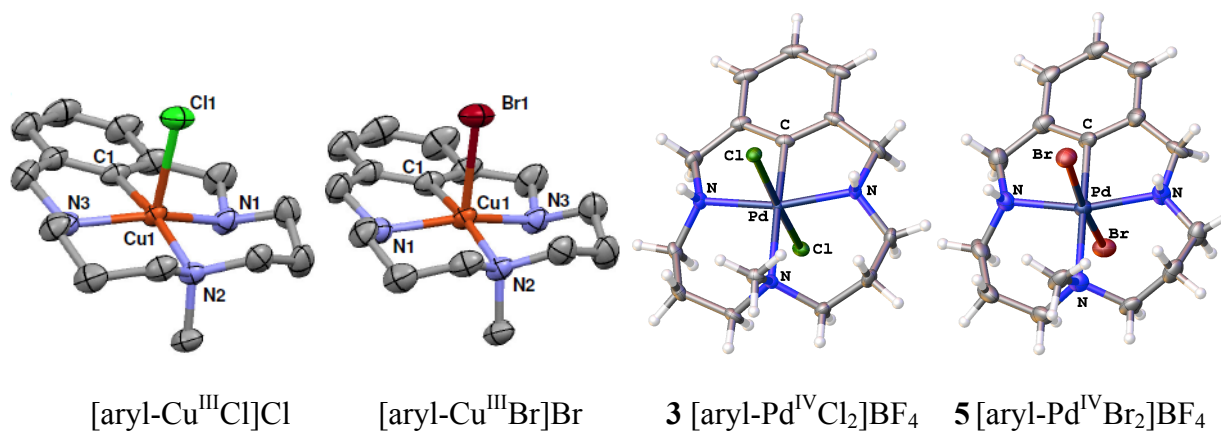


Figure 5.4. Structure of [aryl-Pd^{IV}Br₂]BF₄ complex **5** determined by X-ray crystallography. Counterion (BF₄⁻) not shown.

5.3. Comparison of Aryl-Pd^{IV} and Aryl-Cu^{III} Triazamacrocyclic Complexes.

Halide-ligated aryl-Pd^{IV} and aryl-Cu^{III} complexes of the triazamacrocyclic ligand have been isolated (Table 5.1). These complexes have fairly similar bond lengths and bond angles. The effective ionic radii of Cu^{III} and Pd^{IV} are fairly similar, 54 and 61.5 pm respectively.⁸ The major difference is that the aryl-Pd^{IV} complexes are octahedral with two axial halide ligands while the aryl-Cu^{III} complexes are square pyramidal with a second non-coordinated halide counterion. The structural difference may be attributed to the electron count of the ions: the d⁶ Pd^{IV} ion would strongly favor an octahedral coordination environment. The d⁸ Cu^{III} ion favors square planar or square pyramidal coordination environments.

Table 5.1. Comparison of Aryl-Pd^{IV} and Aryl-Cu^{III} Triazamacrocyclic Complexes.

(Å, °)	[aryl-Cu ^{III} Cl]Cl	[aryl-Cu ^{III} Br]Br	3 [aryl-Pd ^{IV} Cl ₂]BF ₄	5 [aryl-Pd ^{IV} Br ₂]BF ₄
M-X	2.455	2.600	2.3049	2.447
N1-M	1.972	1.974	2.0706	2.051
N2-M	2.037	2.034	2.0668	2.166
N3-M	1.971	1.974	2.2304	2.057
C-M	1.908	1.914	1.9462	1.901
C-M-N1	82.58	82.52	83.79	84.4
C-M-N3	81.78	81.71	83.55	84.6
N1-M-N2	95.07	95.17	96.88	88.4
N2-M-N3	96.89	96.99	96.02	102.7
C1-M-N2	169.38	169.5	177.30	172.5
N1-M-N3	155.7	155.8	166.28	167.9

5.4. Lack of Reductive Elimination from [Aryl-Pd^{IV}Cl₂]BF₄.

The [aryl-Cu^{III}Cl]Cl complex underwent facile reductive elimination to form a carbon-chlorine bond when treated with CF₃SO₃H in CH₃CN at room temperature (eq 5.2). The [aryl-Pd^{IV}Cl₂]BF₄ complex **3** was subjected to these conditions, and no change in the complex was observed using NMR spectroscopy. Up to 48 equiv CF₃SO₃H were added while heating to 70°C for over 5 hours; no reactivity occurred under these more forcing conditions.

5.5. One-Electron Oxidation of [Aryl-Pd^{II}]₂BF₄.

5.5.1. Observation of an EPR-Active Species During [Aryl-Pd^{IV}(NCS)]BF₄ Synthesis.

The [aryl-Pd^{IV}(NCS)]BF₄ **4** complex could not be cleanly synthesized or isolated from the [aryl-Pd^{IV}Cl₂]₂BF₄ complex **3**. During attempted optimization, it was noted that the crude reaction mixture for the production of **3** plus **4** showed line-broadening in the ¹H NMR spectrum, as would be expected from a radical or unpaired spin.

When the mixture was examined by X-band EPR spectroscopy, an isotropic signal with $g = 2.006$ was observed (Figure 5.5). This g value is close to that of the free electron, indicating that the signal is likely due to an organic radical. NCS is a likely source of an organic radical. However, a palladium(III) complex has been analyzed which has a similar isotropic signal with g of 2.01.⁹ The observed signal was quantified by comparison to Cu(ClO₄)₂•6H₂O and was determined to account for only a trace of the mass present in the sample. Assuming the mass of the EPR active species was approximately 440 g/mol (a value intermediate between the molecular weights of the palladium(II) and palladium(IV) complexes) and that the sample mass was composed entirely of the EPR active species (which is certainly not true but a useful assumption for comparison), it was calculated that the signal was only 0.0037% of what would be expected, not accounting for any response factor difference between the observed species and the copper standard.

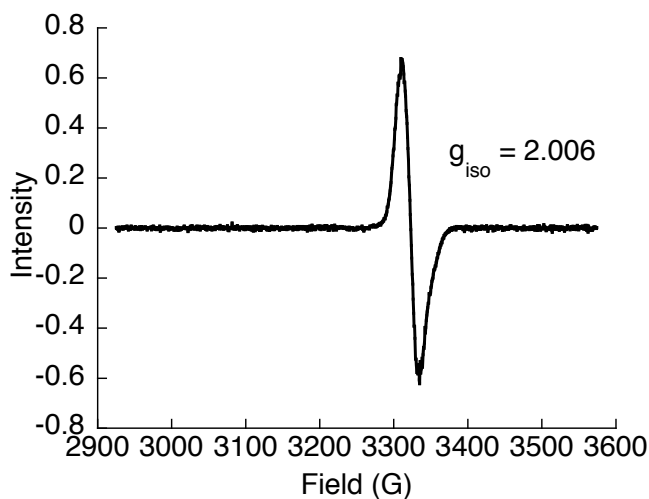


Figure 5.5. Isotropic EPR spectrum ($g_{\text{iso}} = 2.006$) derived from crude mixture of **3**, **4**, **2** in CH_3CN , 77 K.

5.5.2. One-Electron Oxidation of $[\text{Aryl-Pd}^{\text{II}}]\text{BF}_4$ by Cyclic Voltammetry.

The $[\text{aryl-Pd}^{\text{II}}]\text{BF}_4$ complex **2** was analyzed using cyclic voltammetry to determine if either a one electron or two electron oxidation of the complex preferentially occurred. An irreversible oxidation peak was observed at 1.35 V vs. Ag/AgCl (Figure 5.6). The oxidation peak was quantified using 1 equiv ferrocene. The $[\text{aryl-Pd}^{\text{II}}]\text{BF}_4$ oxidation peak at 1.35 V is roughly the same intensity as the ferrocene oxidation peak at 0.35 V, indicating that it corresponds to a one-electron oxidation (Figure 5.6). This data indicates that ligand- or metal-based radical such as that seen in the previous section (from the crude product mixture generating **3** plus **4**) can be accessed from oxidation of **2** alone.

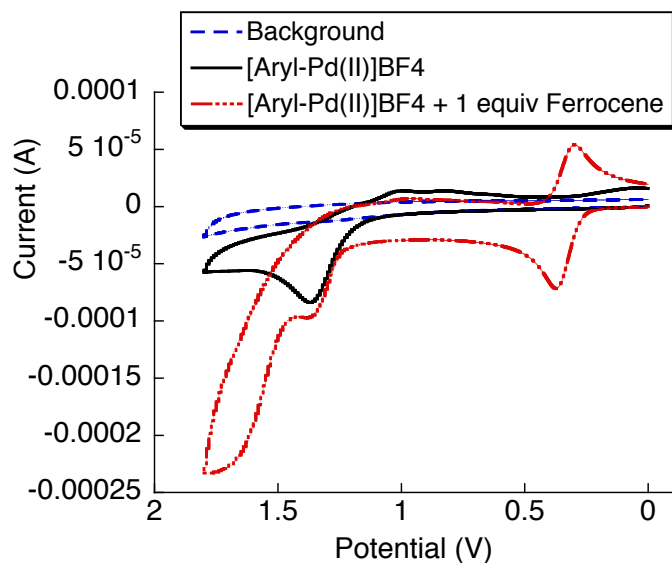


Figure 5.6. Cyclic voltammetry indicates that [aryl-Pd^{II}] BF_4 complex **2** undergoes one-electron oxidation. Analysis vs. Ag/AgCl in CH_3CN , 200 mV/s, 0.1 M LiClO_4 , 1 mmol/L **2** and ferrocene.

5.5.3. Controlled Potential Electrolysis of [Aryl-Pd^{II}] BF_4 and EPR Spectroscopy.

In an attempt to analyze the one-electron oxidized species of **2**, controlled potential electrolysis (CPE) of a solution of **2** in CH_3CN under argon was carried out at a higher potential than the one-electron oxidation potential (1098 mV vs. Ag/AgTBAPF₆ in CH_3CN). During the electrolysis the colorless solution of **2** turned yellow-orange. The solution from CPE of **2** was transferred to a degassed EPR tube and frozen in liquid nitrogen. An EPR spectrum was obtained with $g = 2.006$, though the spectrum has significant noise (Figure 5.7). The signal was quantified to be only a trace of the material present. This may indicate that the one-electron oxidized species of **2** was not stable after it was generated and decomposed during the lengthy CPE.

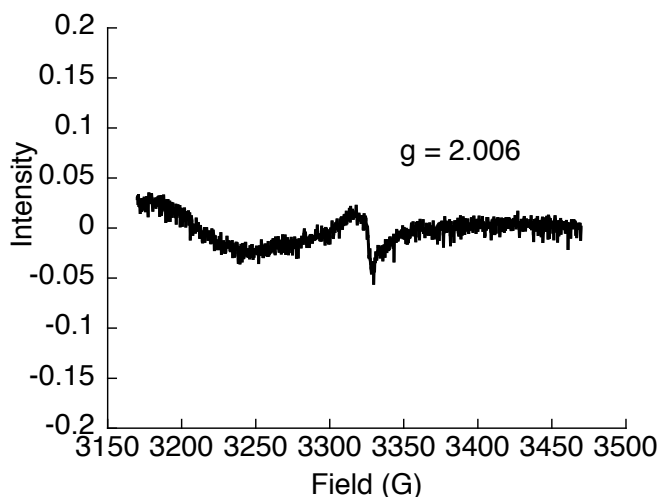


Figure 5.7. EPR spectrum obtained after controlled potential electrolysis of **2**, CH₃CN, 77 K.

5.6. Conclusions.

An [aryl-Pd^{II}]BF₄ complex **2** was synthesized and oxidized to a variety of aryl-Pd^{IV} complexes. If PhICl₂ was used as the oxidant, an octahedral [aryl-Pd^{IV}Cl₂]BF₄ **3** complex with axial chloride ligands was cleanly generated. If NCS was used as the oxidant, a mix of the [aryl-Pd^{IV}Cl₂]BF₄ **3** complex and an [aryl-Pd^{IV}(NCS)]BF₄ **4** complex, resulting from *trans*-oxidative addition, was formed. If NBS was used as the oxidant, the [aryl-Pd^{IV}Br₂]BF₄ **5** complex with axial Br ligands was formed. These complexes are analogous to previously reported aryl-Cu^{III} complexes, however, when investigated, **3** did not undergo the facile reductive elimination observed with the Cu complexes.

It is unusual that use of NCS and NBS oxidants results in a majority of the [aryl-Pd^{IV}Cl₂]BF₄ and [aryl-Pd^{IV}Br₂]BF₄ complexes rather than yielding complexes resulting from oxidative addition of the nitrogen-halogen bond.⁶ The products suggest that Cl₂ and Br₂ may be formed in the reaction mixtures, or that there is some radical reactivity. An isotropic radical

species was observed in the NCS-oxidant reaction mixture. It is uncertain whether the signal belongs to an organic or Pd radical species.

The involvement of a radical aryl-Pd^{III} species is possible given the results of electrochemical analysis of the [aryl-Pd^{II}]BF₄ complex **2**. Cyclic voltammetry measurements indicated that **2** displays an irreversible one-electron oxidation wave. Controlled potential electrolysis followed by EPR spectroscopy demonstrated an isotropic radical species is formed, though signal-to-noise was low, perhaps due to decomposition of the radical species. Since the time of this work (ca. 2009), the involvement of Pd^{III} in C-H bond functionalization has been demonstrated.⁷

The triazamacrocyclic ligand is functionalized in a facile manner using aerobic Cu-catalyzed methods.^{3,4} In contrast, oxidation of aryl-Pd^{II} to higher oxidation states does not occur under O₂, and once oxidation to aryl-Pd^{IV} is achieved, reductive elimination does not easily occur. The behavior of aryl-Pd in this system serves to underscore the benefits of using Cu catalysts, linked with O₂ oxidant, to functionalize arene C-H bonds.

5.7. Contributions.

The X-ray crystal structures were obtained and solved by Ilia A. Guzei and Lara C. Spencer. Amanda E. King first synthesized the [aryl-Pd^{II}]ClO₄ complex and shared a synthesis method with Alison M. Suess. Lauren M. Huffman provided initial triazamacrocyclic ligand samples and shared a synthesis method with Alison M. Suess.

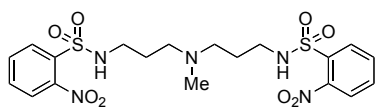
5.8. Experimental.

5.8.1. General Considerations.

All commercially available compounds were purchased and used as received. Solvents were anhydrous and stored under nitrogen or were dried over alumina columns prior to use. ^1H and ^{13}C NMR spectra were recorded on Bruker or Varian 300 MHz spectrometers. Chemical shift values are given in parts per million relative to internal TMS (0.00 ppm for ^1H) or CDCl_3 (77.23 ppm for ^{13}C). Flash chromatography was performed using SiliaFlash® P60 (Silicycle, particle size 40-63 μm , 230-400 mesh). Except where otherwise noted, electrochemical experiments were performed using a BASinc Potentiostat a glassy carbon working electrode, a Ag/AgCl reference electrode, and a platinum counter-electrode. X-band EPR data were collected using a Bruker EleXsys E500 spectrometer; all spectra were acquired at 77 K using a $\text{N}_2(\text{l})$ finger dewar under nonsaturating conditions.

5.8.2. Synthesis of the Triazamacrocyclic Arene.

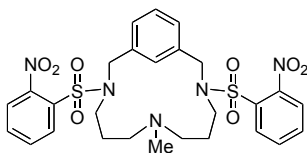
The triazamacrocyclic arene was synthesized in three steps according to a literature procedure (reference to Huffman paper) with the modifications described below.



Protection of the linear triamine. 3,3'-Diamino-*N*-

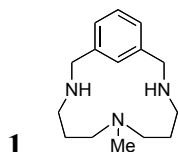
methylpropylamine (4.36 g, 30 mmol) was dissolved in CH_2Cl_2 (100 mL) and Et_3N (9 mL, 65 mmol) and cooled to 0°C in a 250-mL round bottom flask equipped with stir bar. 2-Nitrobenzenesulfonyl chloride (13.30 g, 60 mmol) was dissolved in CH_2Cl_2 (100 mL) and added dropwise to the reaction mixture over 30-60 min. After the addition was complete, the mixture was allowed to warm to room temperature and stirred an additional 5 hours. The reaction mixture was then washed with water and brine, dried over MgSO_4 , and evaporated to dryness. The

resultant viscous yellow oil was isolated and was placed under vacuum for several hours to remove excess Et₃N. The oil was then used in the next step without further purification (crude yield = 15.5 g, 100% yield).



Macrocyclization. The protected linear triamine (15.5 g, 30

mmol) and Cs₂CO₃ (20.2 g, 62 mmol) were suspended in 600 mL of anhydrous DMF in a 1-L round bottom flask equipped with stir bar and allowed to stir for 10 minutes. α,α' -Dibromo-*m*-xylene (7.92 g, 30 mmol) was added over 10 minutes and the reaction mixture was allowed to stir for 3-4 days at room temperature. The solvent was then removed under vacuum and the residue dissolved in CHCl₃ and water. The layers were separated, and the organic layer was washed with brine, dried over MgSO₄, and the solvent removed under vacuum. An off-white powder was isolated after complete removal of solvent under vacuum (8.0 g, 41% yield).

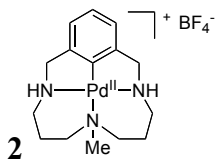


1 *Deprotection to the triazamacrocyclic arene 1.* The protected

triazamacrocyclic arene (2.5 g, 4.0 mmol) was added to a dry 250-mL round bottom flask with stir bar and the flask was purged with N₂. LiOH (0.774 g, 32.3 mmol) was added to a second dry 250-mL round bottom flask with stir bar and the flask was purged with N₂. Anhydrous DMF (50 mL) was added via cannula to each flask. Thioglycolic acid (1.12 mL, 16.2 mmol) was added to the flask containing the LiOH suspension via syringe and allowed to stir for 5 minutes. The solution containing the protected triazamacrocyclic arene was transferred via cannula into the flask containing the LiOH suspension and the reaction mixture was allowed to stir under N₂ for five hours at room temperature. The reaction mixture was then diluted with 100 mL CH₂Cl₂ and

washed with 2M NaOH aqueous solution and brine. The solvent was removed under vacuum and the residue was purified via column chromatography on silica with a mobile phase of CH_2Cl_2 that had been used to extract aqueous NH_4OH then dried with MgSO_4 . A white crystalline powder was isolated (0.54 g, 54% yield). ^1H NMR (300 MHz, CDCl_3): δ 7.62 (s, 1H), 7.19 (app. t, $J = 7.7$ Hz, 2 H), 7.02 (d, $J = 7.4$ Hz, 2 H), 3.90 (s, 4 H), 2.57 (app. t, $J = 6.1$ Hz, 4 H), 2.41 (app. t, $J = 5.9$ Hz, 4 H), 1.99 (s, 3 H), 1.62 (q, $J = 5.8$ Hz, 4 H).

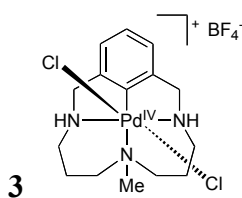
5.8.3. Synthesis of the Aryl-Palladium(II) Triazamacrocyclic Complex.



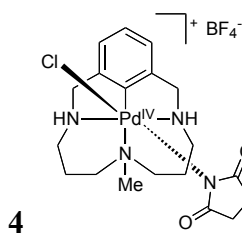
The triazamacrocyclic arene **1** (0.099 g, 0.400 mmol) was dissolved in 20 mL CH_3CN . $\text{Pd}(\text{OAc})_2$ (0.0898 g, 0.400 mmol) was added to the solution of **1** as a brown solution/suspension in 20 mL CH_3CN . Upon addition the solution turned opaque and yellow in color. Benzene (40 mL) was added and the solution turned clear yellow. NaBF_4 (0.066 g, 0.60 mmol) was added and the reaction mixture was allowed to stir overnight until the solution was colorless (excess NaBF_4 remained suspended in solution). The excess NaBF_4 was then filtered off and solvent was removed from the filtrate under vacuum. The residue was reconstituted in 12 mL CH_3CN , 63 mL Et_2O was added, and the mixture was cooled in a freezer for a day. White powder was isolated as a precipitate. ^1H NMR (300 MHz, CD_3CN): δ 6.95 (dd, $J = 7.9, 7.1$ Hz, 1 H), 6.79 (d, $J = 7.6$ Hz, 2 H), 4.88 (br s, 2 H), 4.86 (dd, $J = 15.8, 6.5$ Hz, 2 H), 4.00 (dd, $J = 16, 7.8$ Hz, 2 H), 3.17-3.10 (m, 2 H), 3.07-2.97 (m, 2 H), 2.91-2.78 (m, 2 H), 2.51-2.45 (m, 2 H), 2.46 (s, 3 H), 1.92-1.80 (m, 4 H). Crystal structure obtained; see supporting information.

5.8.4. Synthesis of Aryl-Palladium(IV) Triazamacrocyclic Complexes.

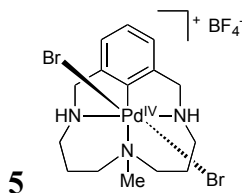
The aryl-palladium(II) triazamacrocyclic complex **2** (0.0260 g, 0.059 mmol) dissolved in 10 mL CH₃CN. The chosen oxidant (0.059 mmol) was added and the solution immediately turned from clear to the color described below. After stirring for at least 20 minutes, the solutions were diluted somewhat and allowed to crystallize with Et₂O vapor diffusion over a week.



results from addition of PhICl₂. The reaction solution turns orange; crystals of **3** are orange. This species is also formed from addition of *N*-chlorosuccinimide. Crystal structure obtained from reaction with PhICl₂; see supporting information. ¹H NMR (300 MHz, CD₃CN): δ 7.18-8.08 (m, 3 H), 6.61 (br s, 2 H), 4.54-4.34 (m, 4 H), 3.48-3.35 (m, 4 H), 2.89-2.84 (m, 2 H), 2.63 (s, 3 H), 2.62-2.57 (m, 2 H).



results from addition of *N*-chlorosuccinimide. The reaction solution turns orange; crystals of **4** are orange. A yellow powder also precipitates out and has a trace isotropic EPR signal. Crystal structure obtained, see supporting information.



results from addition of *N*-bromosuccinimide. The reaction solution turns burgundy; crystals of **5** are burgundy. Crystal structure obtained, see supporting information. ¹H NMR (300 MHz, CD₃CN): δ 7.10-6.99 (m, 3 H), 6.75 (br s, 2 H), 4.62-4.55 (m,

2 H), 4.41-4.33 (m, 2 H), 3.63-3.50 (m, 4 H), 3.08-3.05 (m, 2 H), 2.81 (s, 3 H), 2.67-2.61 (m, 2 H), 2.02-1.94 (m, 4 H).

5.9. References and Notes.

1. Hiraki, K.; Tsutsumida, J.; Fuchita, Y. "Synthesis and Cyclopalladation of a Macrocyclic Triamine, 7-Methyl-3,7,11-Triazabicyclo[11,3,1]Heptadeca-1(17),13,15-Triene." *Chem. Lett.* **1986**, *15*, 337-340.
2. Ribas, X.; Jackson, D. A.; Donnadieu, B.; Mahía, J.; Parella, T.; Xifra, R.; Hedman, B.; Hodgson, K. O.; Llobet, A.; Stack, T. D. P. "Aryl C–H Activation by Cu^{II} To Form an Organometallic Aryl–Cu^{III} Species: A Novel Twist on Copper Disproportionation." *Angew. Chem. Int. Ed.* **2002**, *41*, 2991-2994.
3. (a) Huffman, L. M.; Stahl, S. S. "Carbon–Nitrogen Bond Formation Involving Well-Defined Aryl–Copper(III) Complexes." *J. Am. Chem. Soc.* **2008**, *130*, 9196-9197. (b) King, A. E.; Huffman, L. M.; Casitas, A.; Costas, M.; Ribas, X.; Stahl, S. S. "Copper-Catalyzed Aerobic Oxidative Functionalization of an Arene C–H Bond: Evidence for an Aryl-Copper(III) Intermediate." *J. Am. Chem. Soc.* **2010**, *132*, 12068-12073.
4. Casitas, A.; King, A. E.; Parella, T.; Costas, M.; Stahl, S. S.; Ribas, X. "Direct observation of Cu^I/Cu^{III} redox steps relevant to Ullmann-type coupling reactions." *Chem. Sci.* **2010**, 326-330.
5. Experiment performed by Amanda E. King.
6. (a) Dick, A. R.; Hull, K. L.; Sanford, M. S. "A Highly Selective Catalytic Method for the Oxidative Functionalization of C-H Bonds." *J. Am. Chem. Soc.* **2004**, *126*, 2300-2301. (b) Whitfield, S. R.; Sanford, M. S. "Reactivity of Pd(II) Complexes with Electrophilic

Chlorinating Reagents: Isolation of Pd(IV) Products and Observation of C-Cl Bond-Forming Reductive Elimination." *J. Am. Chem. Soc.* **2007**, *129*, 15142-15143.

7. For examples, see the following and references therein: (a) Mirica, L. M.; Khusnutdinova, J. R. "Structure and electronic properties of Pd(III) complexes." *Coord. Chem. Rev.* **2013**, *257*, 299-314. (b) Powers, D. C.; Lee, E.; Ariafard, A.; Sanford, M. S.; Yates, B. F.; Canty, A. J.; Ritter, T. "Connecting Binuclear Pd(III) and Mononuclear Pd(IV) Chemistry by Pd-Pd Bond Cleavage." *J. Am. Chem. Soc.* **2012**, *134*, 12002-12009.
8. Greenwood, N. N.; Earnshaw, A. *Chemistry of the Elements*, Oxford: Elsevier Ltd., **1997**.
9. Berry, J. F.; Bill, E.; Bothe, E.; Cotton, F. A.; Dalal, N. S.; Ibragimov, S. A.; Kaur, N.; Liu, C. Y.; Murillo, C. A.; Nellutla, S.; North, J. M.; Villagrán, D. "A Fractional Bond Order of 1/2 in Pd₂⁵⁺ Formamidinate Species; The Value of Very High-Field EPR Spectra." *J. Am. Chem. Soc.* **2007**, *129*, 1393-1401.

Appendix 1:

NMR Spectra for
Divergence between Organometallic and
Single-Electron-Transfer Mechanisms in Copper(II)-Mediated
Aerobic C–H Oxidation

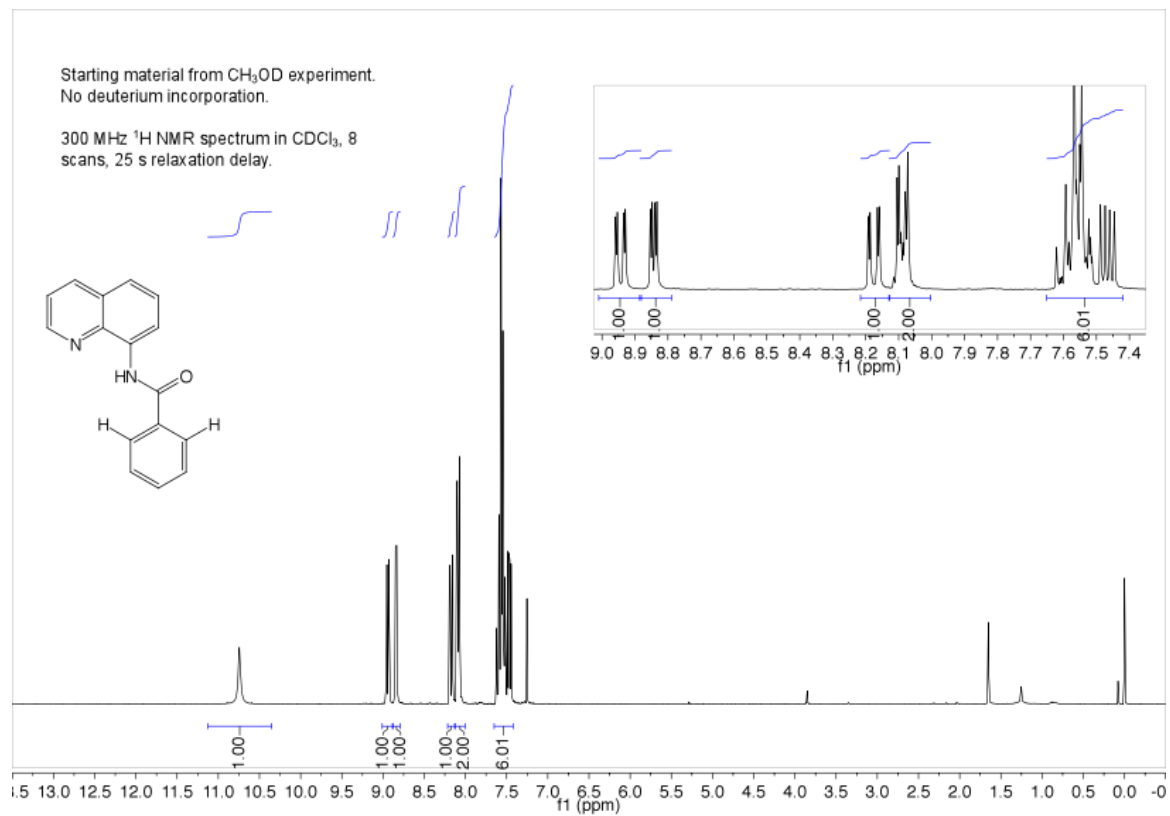
Spectra for Section 2.3.2. Deuteration and Isotope Effect Experiments for Benzamide**Methoxylation:**

Figure A2.1. No deuterium incorporation was observed in starting material **2a**.

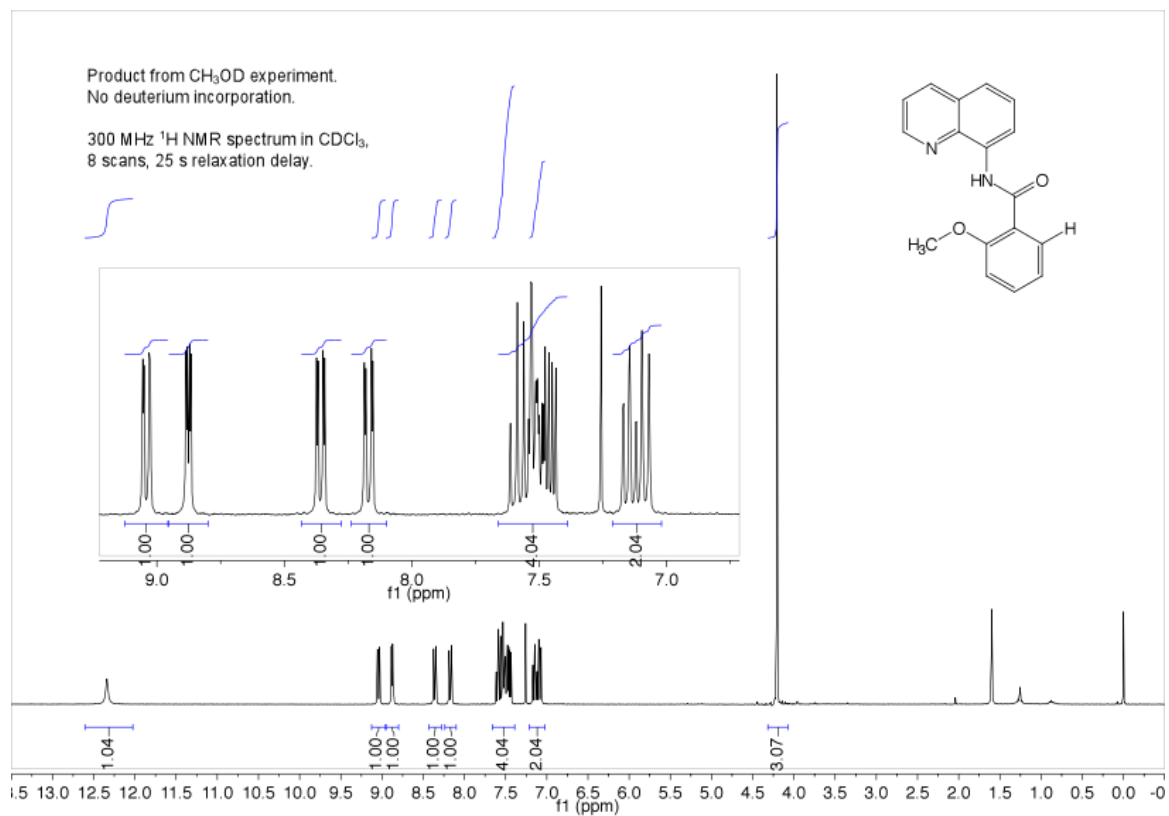


Figure A2.2. No deuterium incorporation was observed in product **3a**.

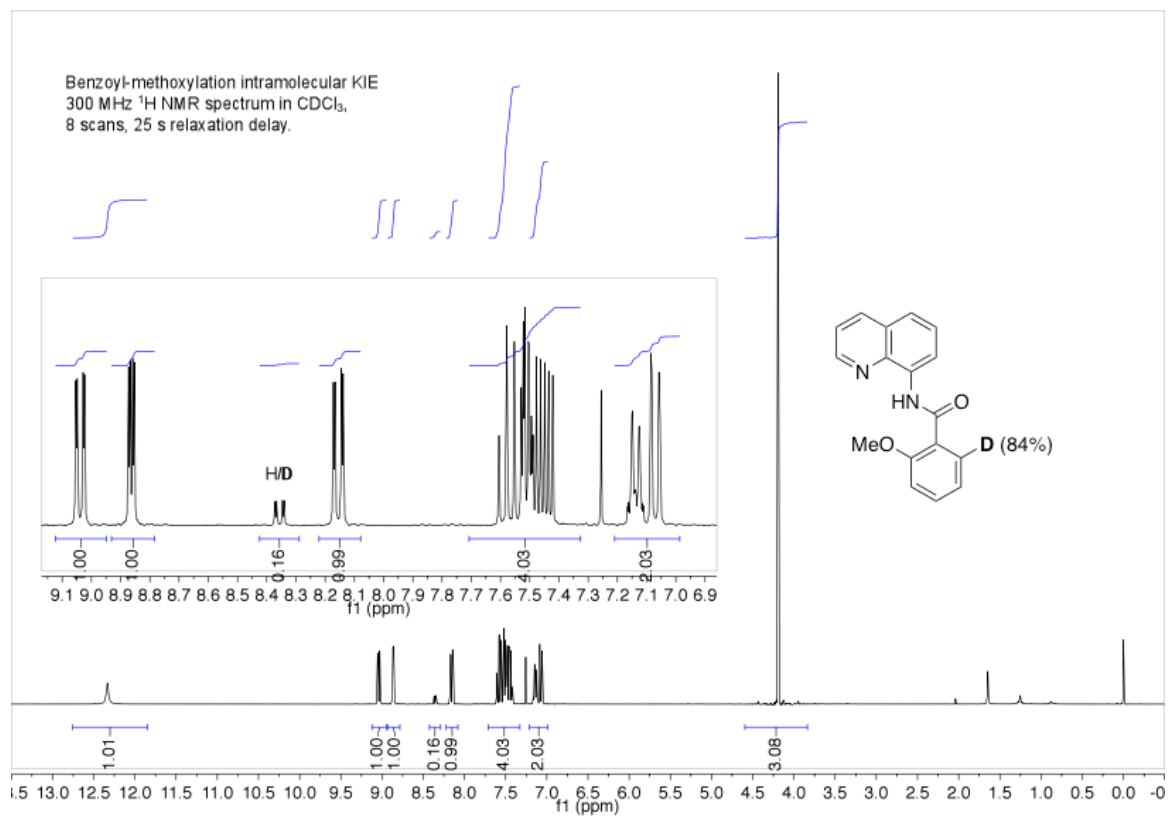


Figure A2.3. ^1H NMR spectrum of product from the intramolecular KIE experiment.

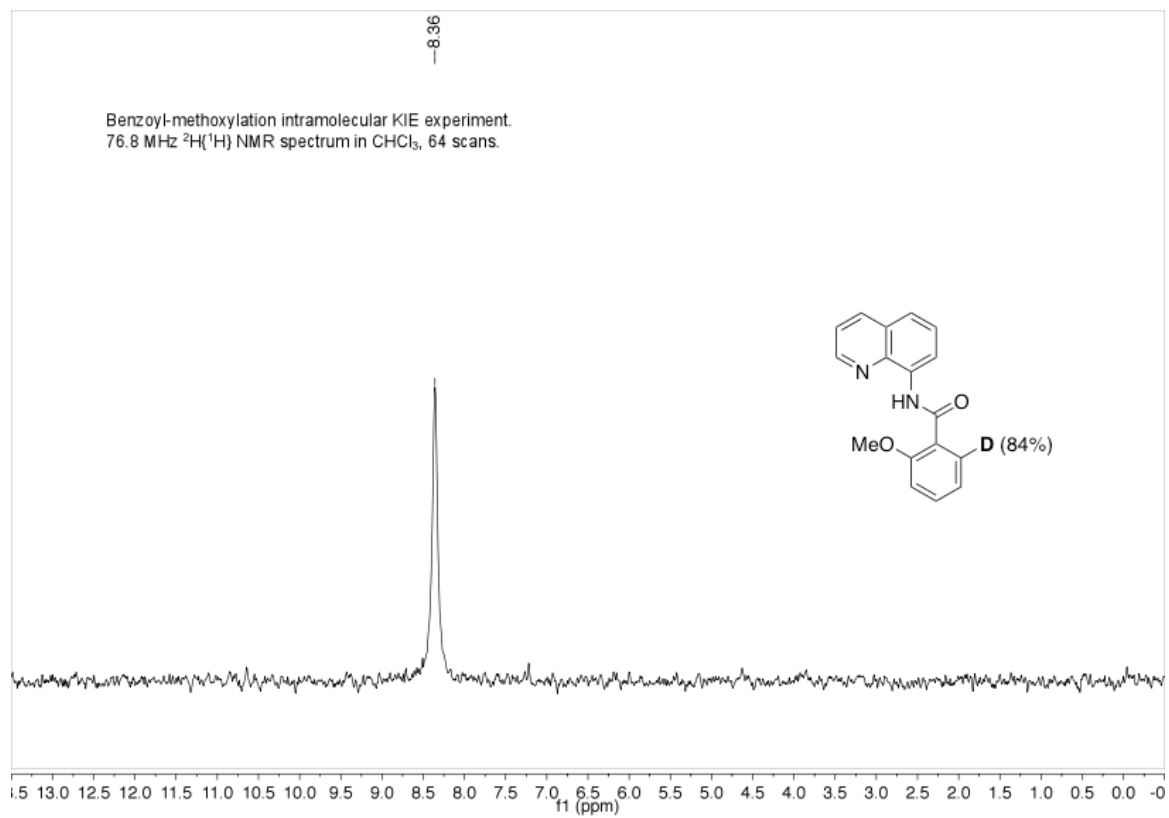


Figure A2.4. $^2\text{H}\{^1\text{H}\}$ NMR spectrum of product from the intramolecular KIE experiment.

Spectra for Section 2.x.x. Deuteration and Isotope Effect Experiments for Quinoline

Chlorination:

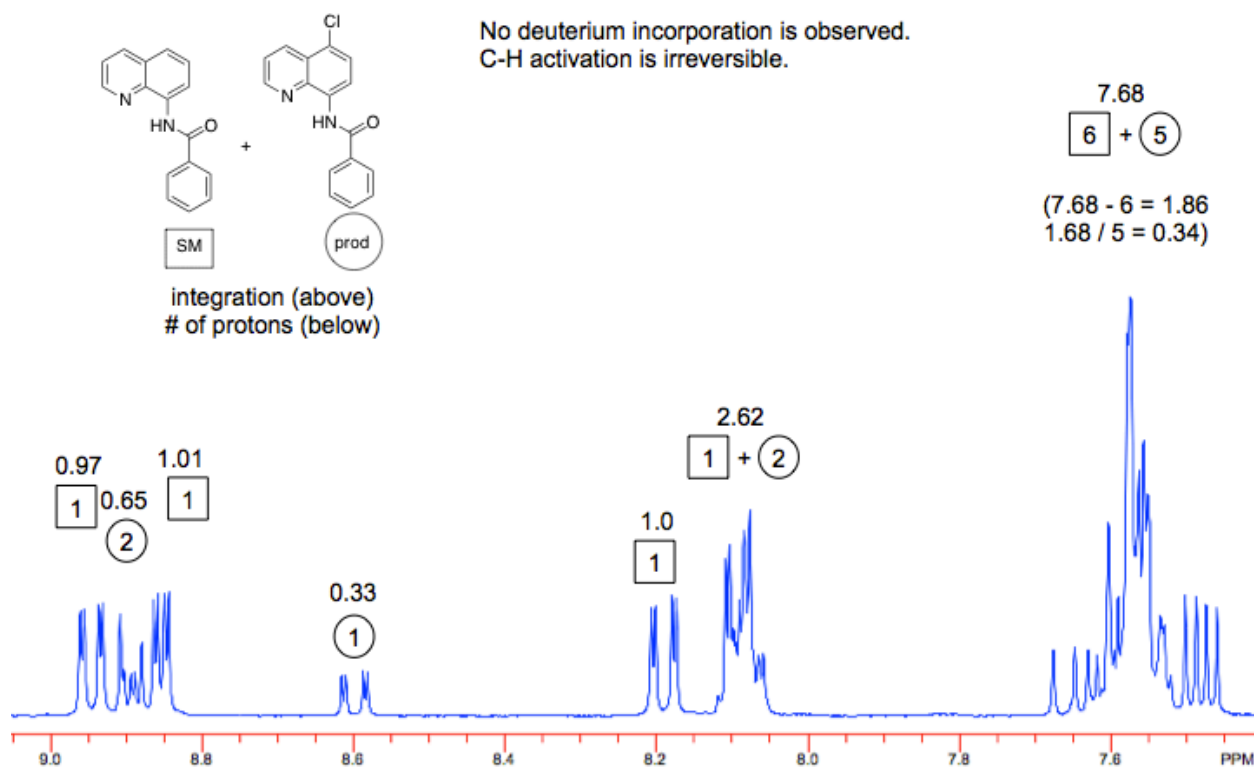


Figure A2.5. No deuterium incorporation was observed in the combination of starting material **2a** or product **3a** (aryl region is shown). Starting material protons each integrate to 1.0 area, and product protons each integrate to 0.33 area.

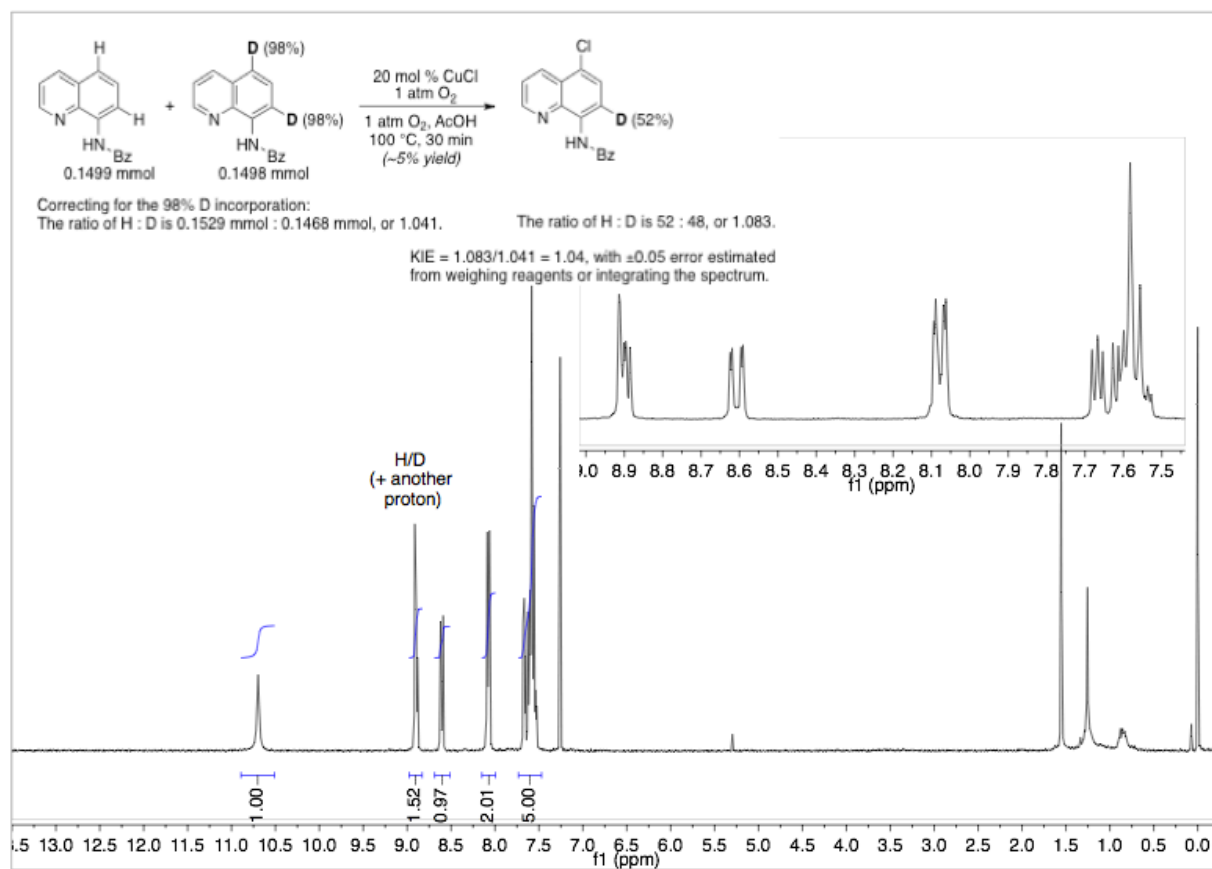
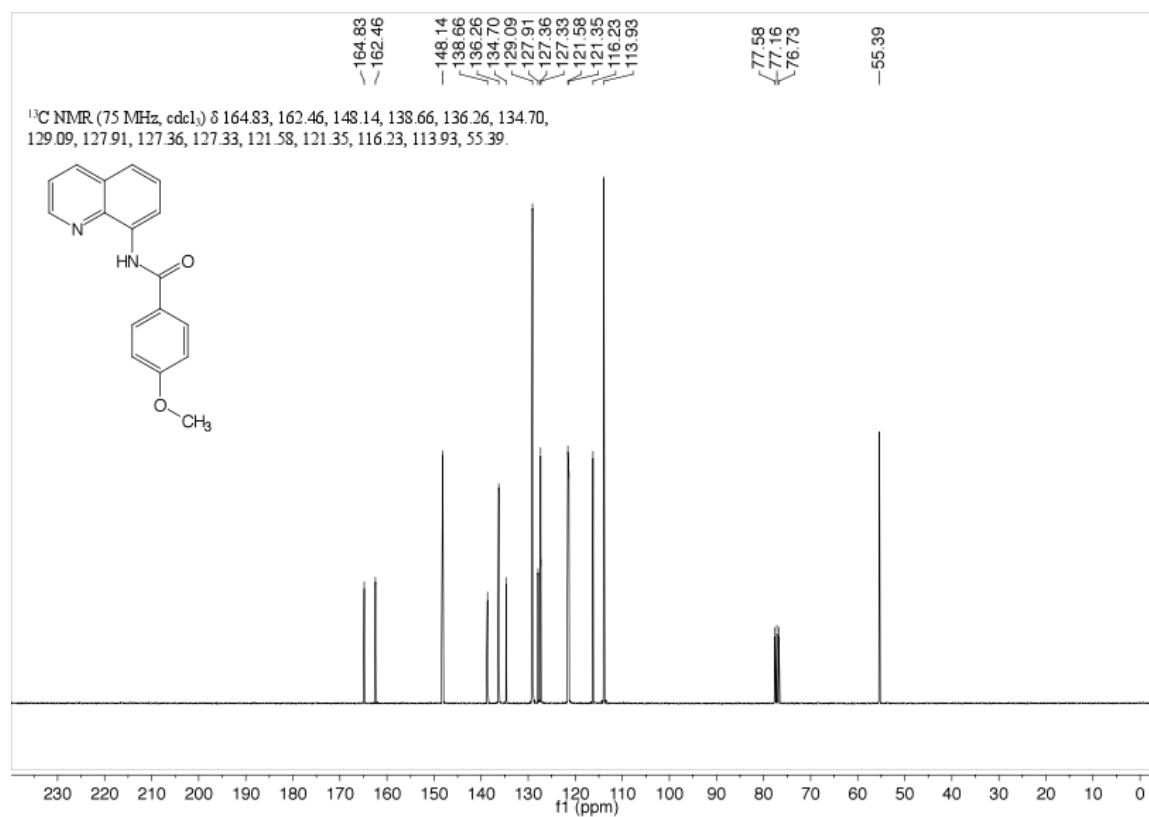
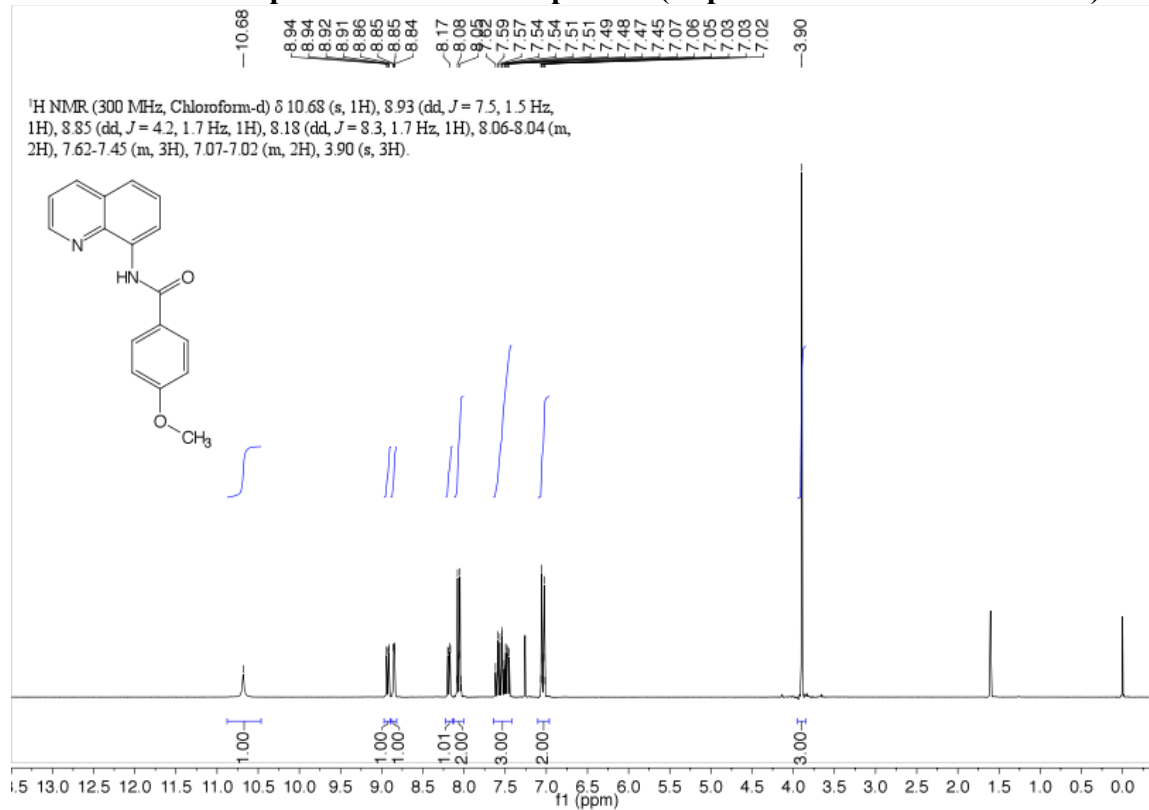
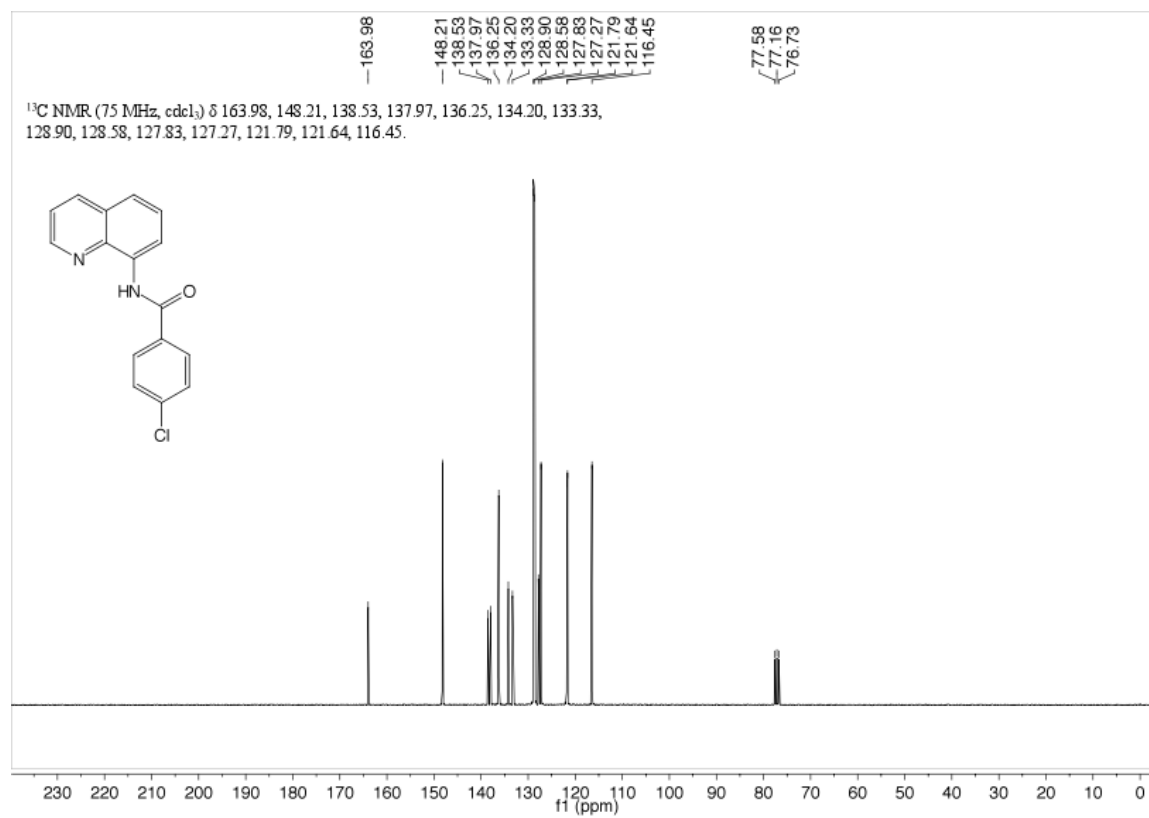
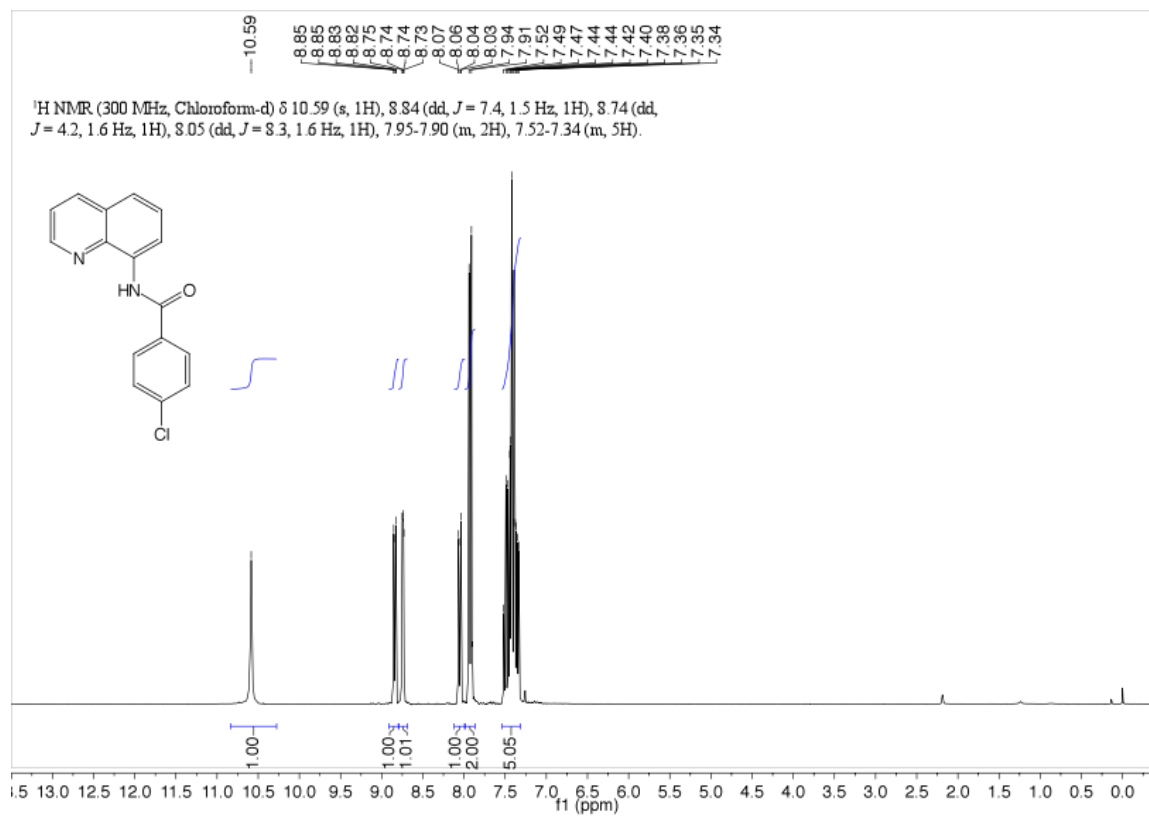
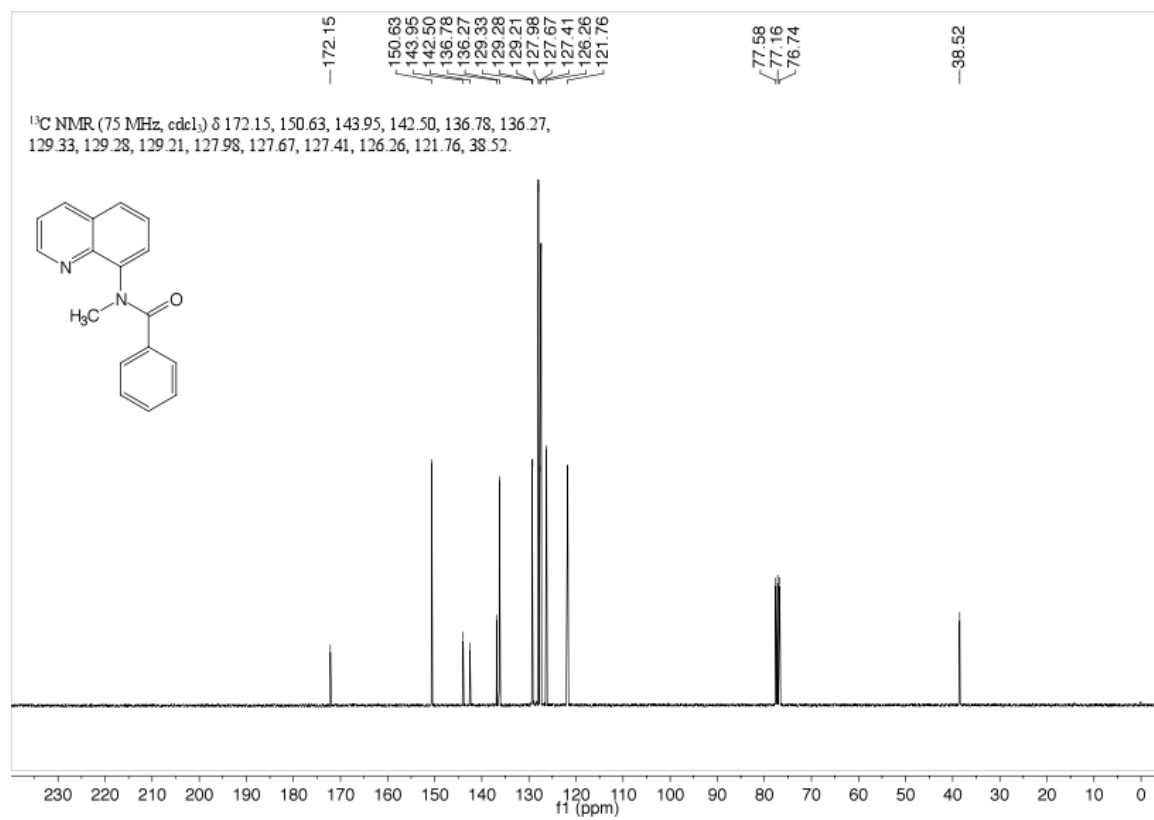
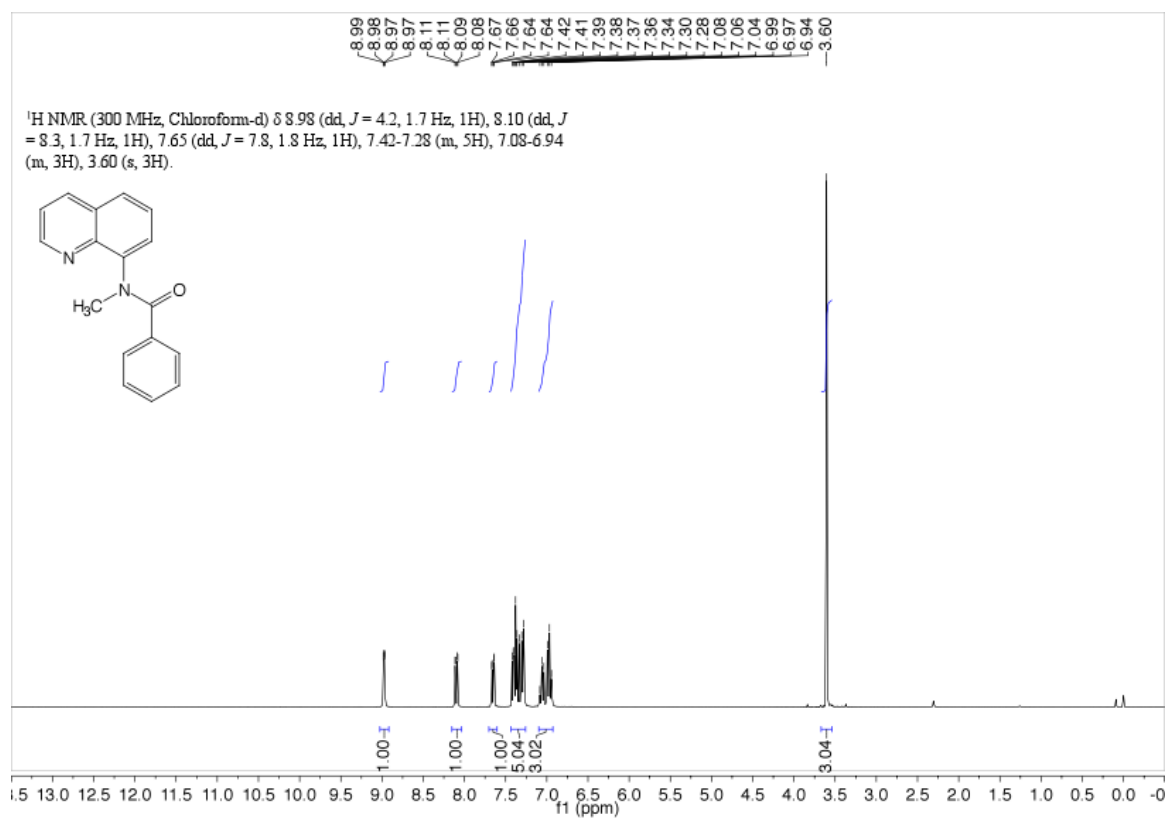
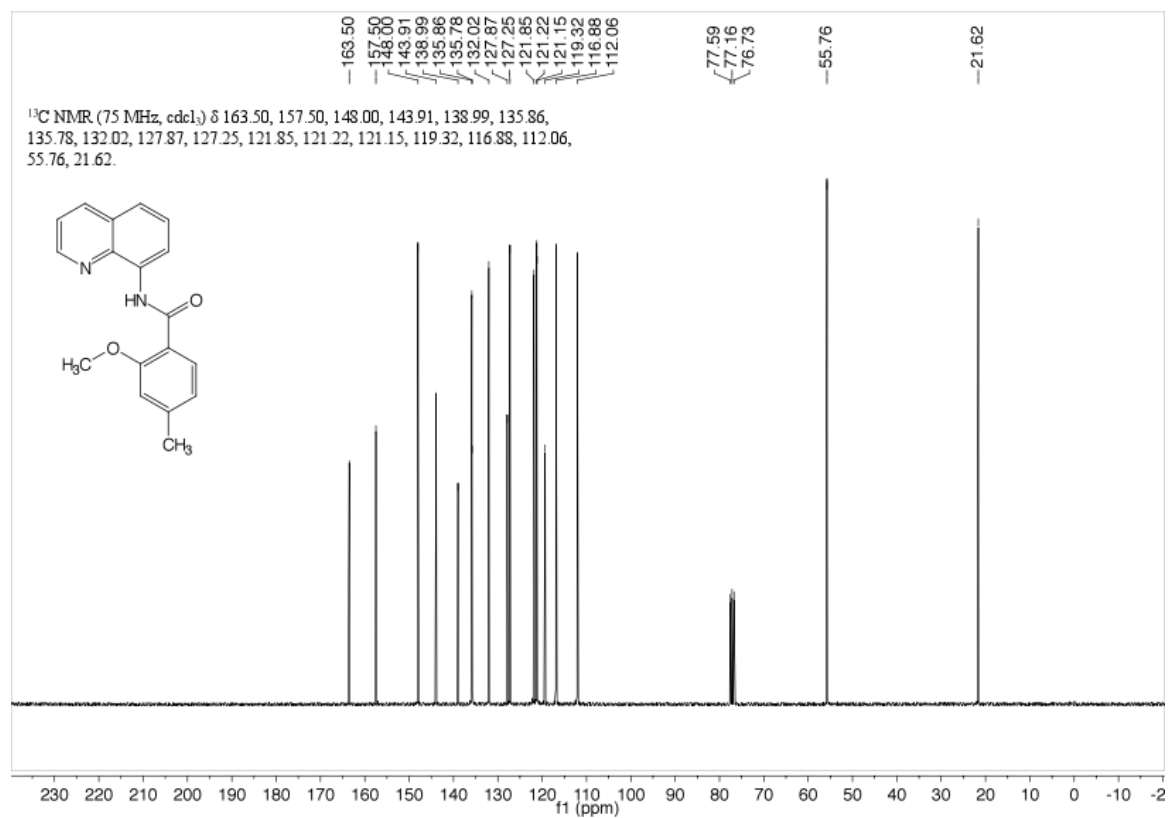
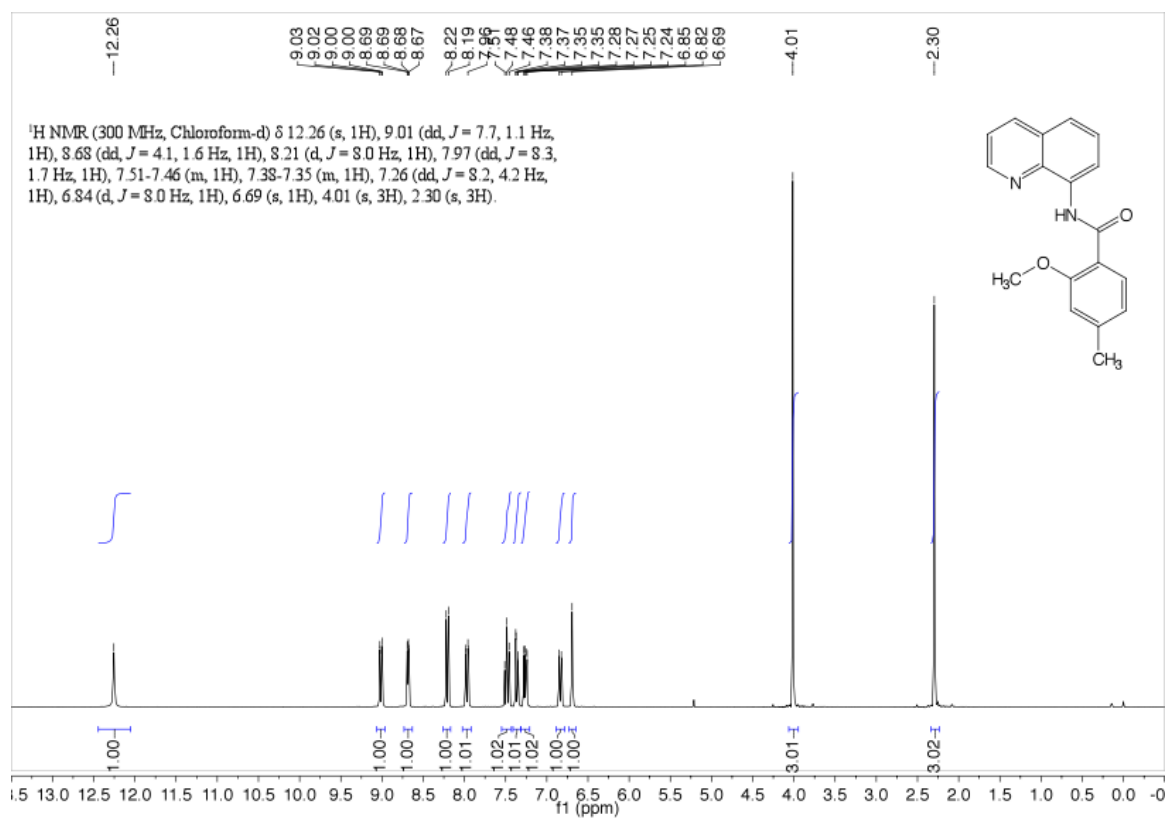


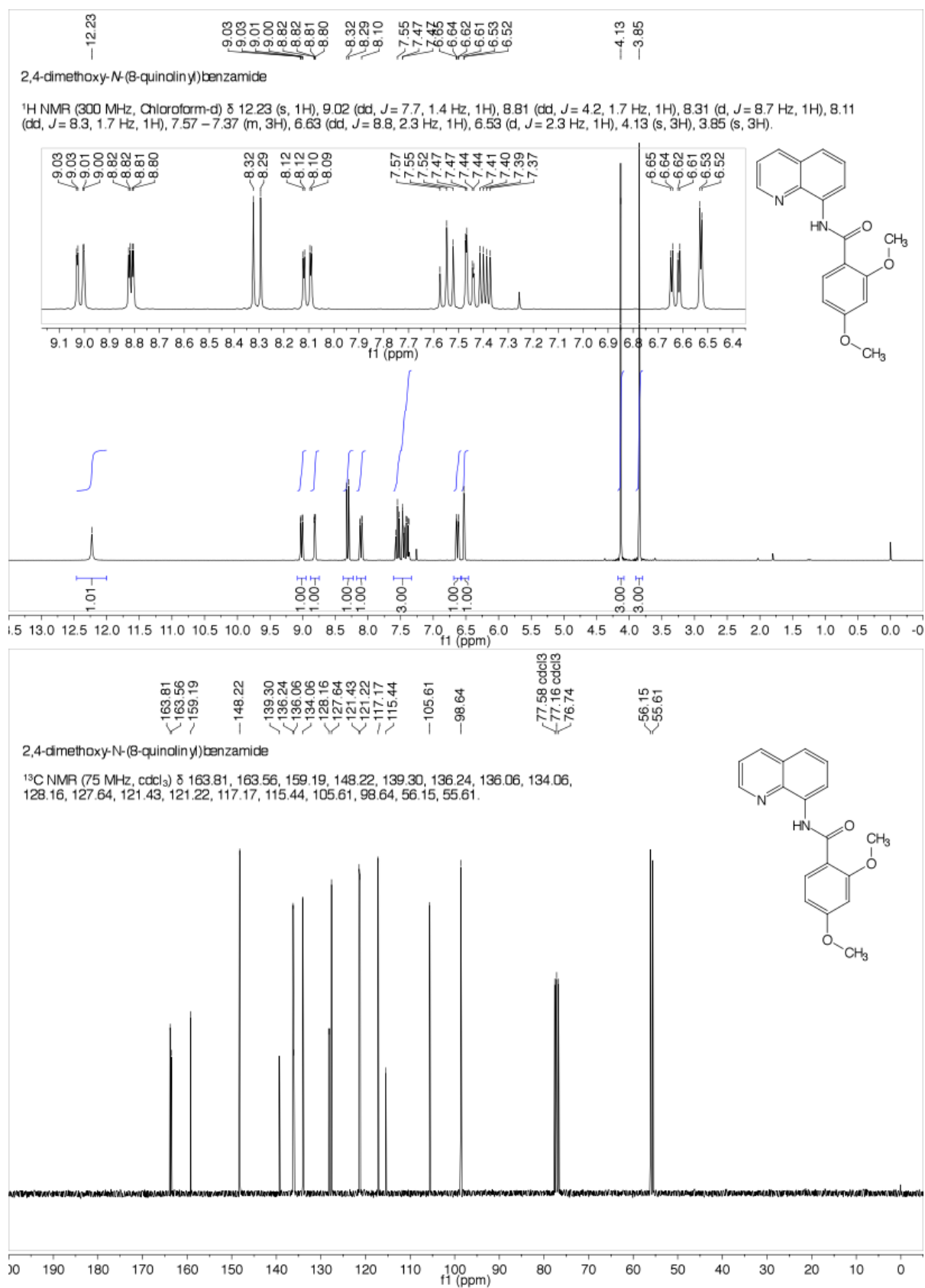
Figure A2.6. ^1H NMR spectrum of product of the intermolecular competition KIE experiment and determination of the KIE value.

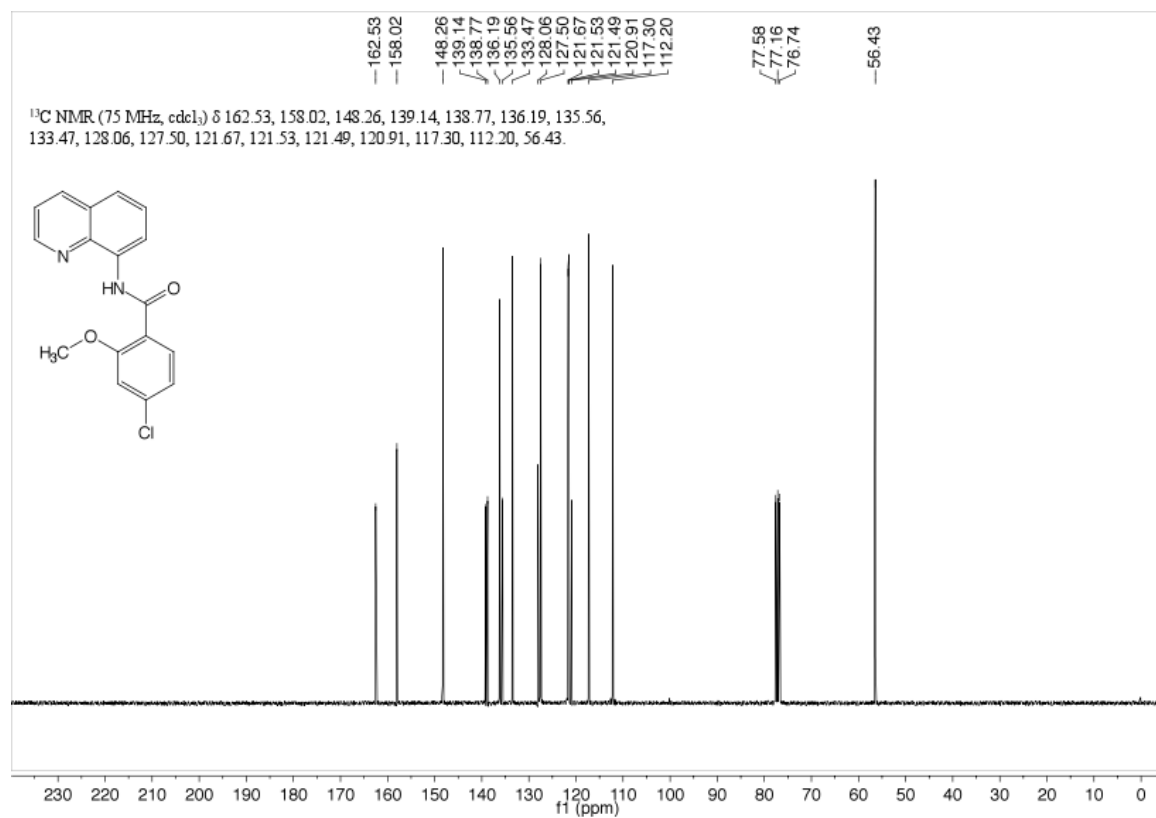
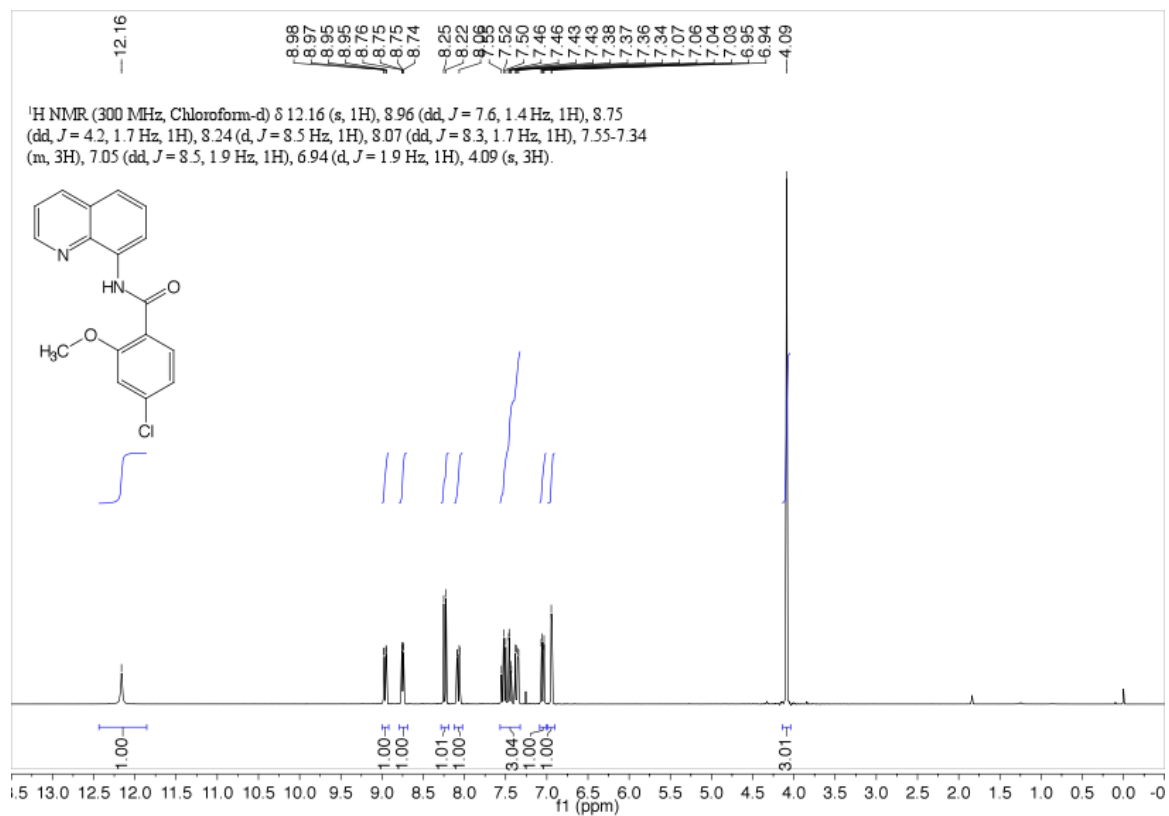
^1H and ^{13}C NMR Spectra of Novel Compounds (Experimental Sections 2.10.7-9):

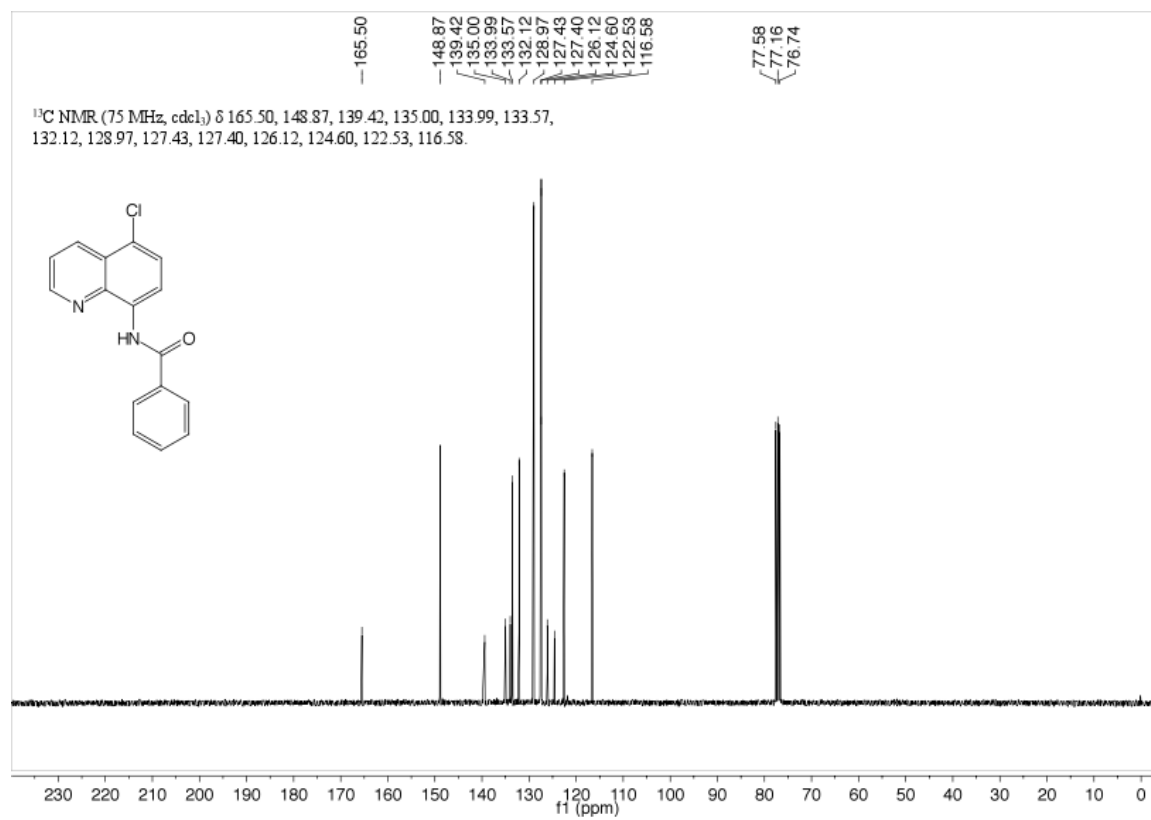
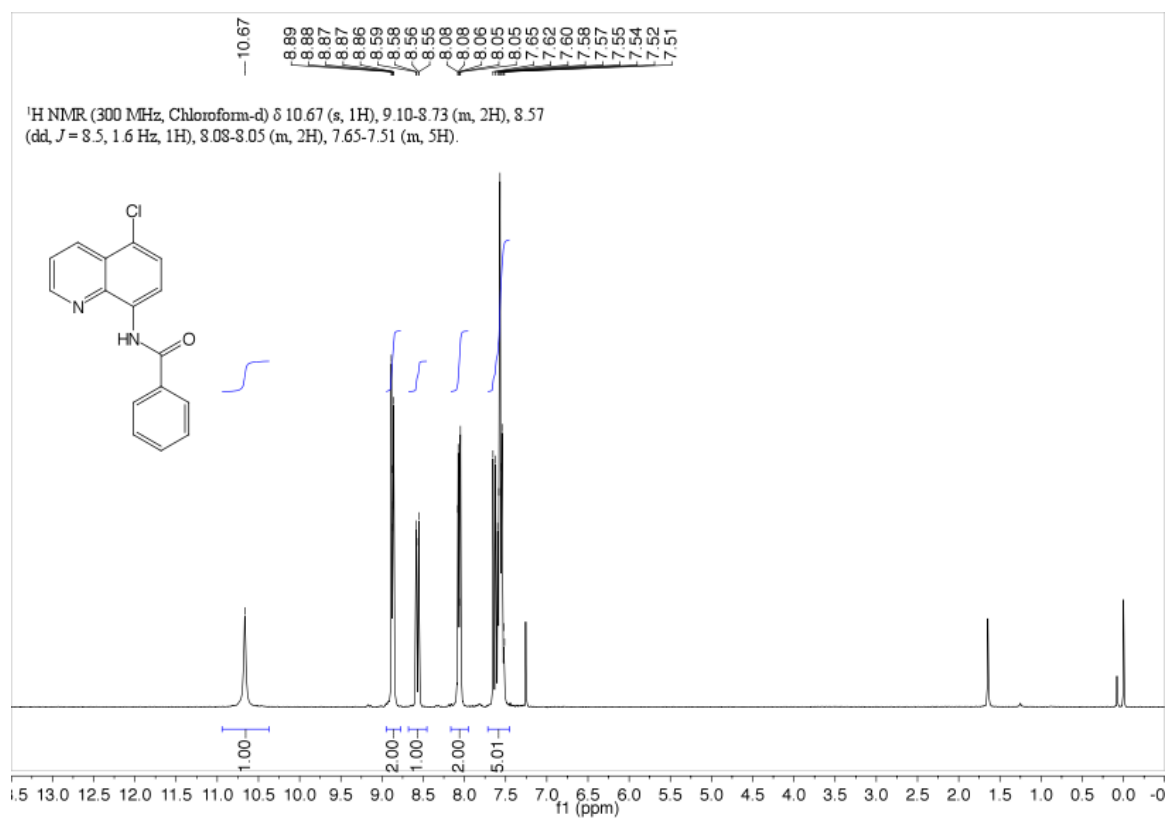




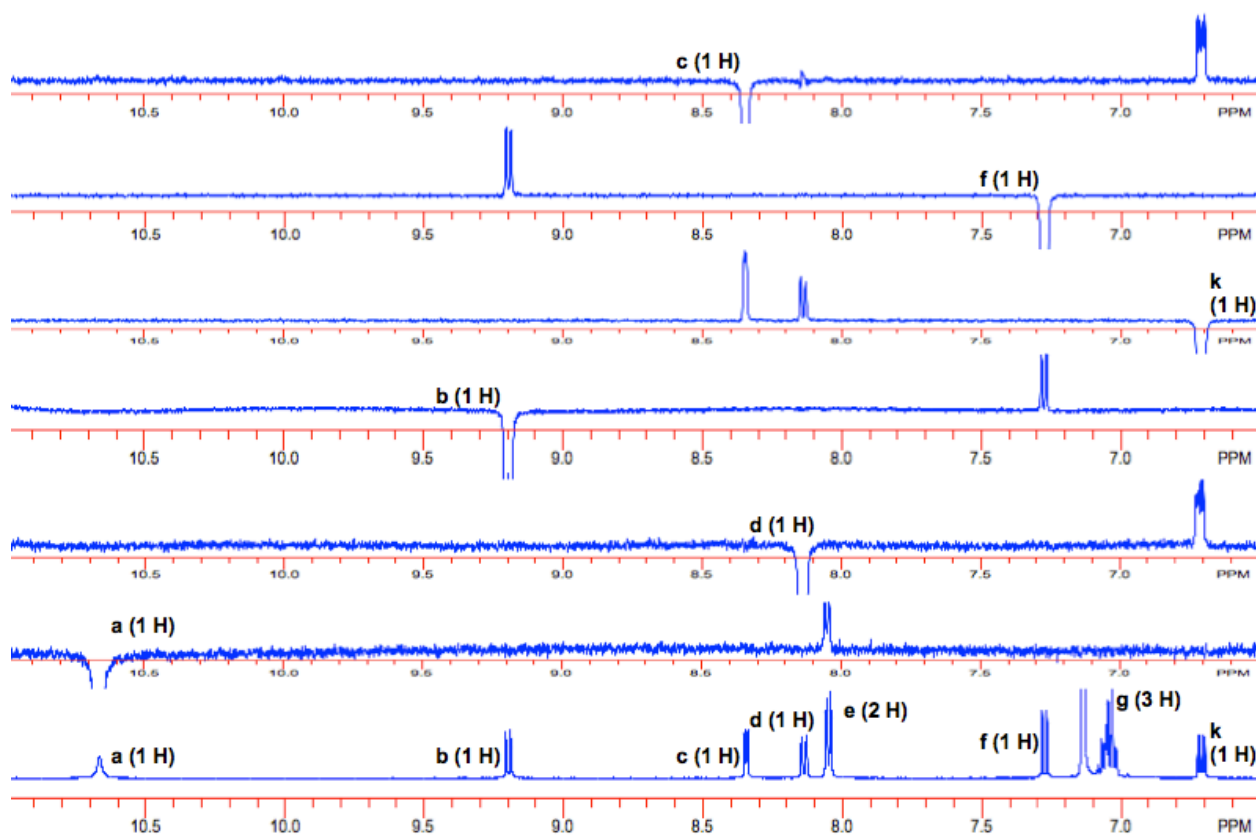
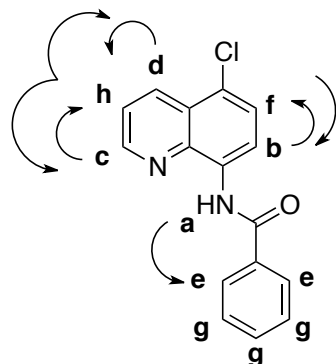




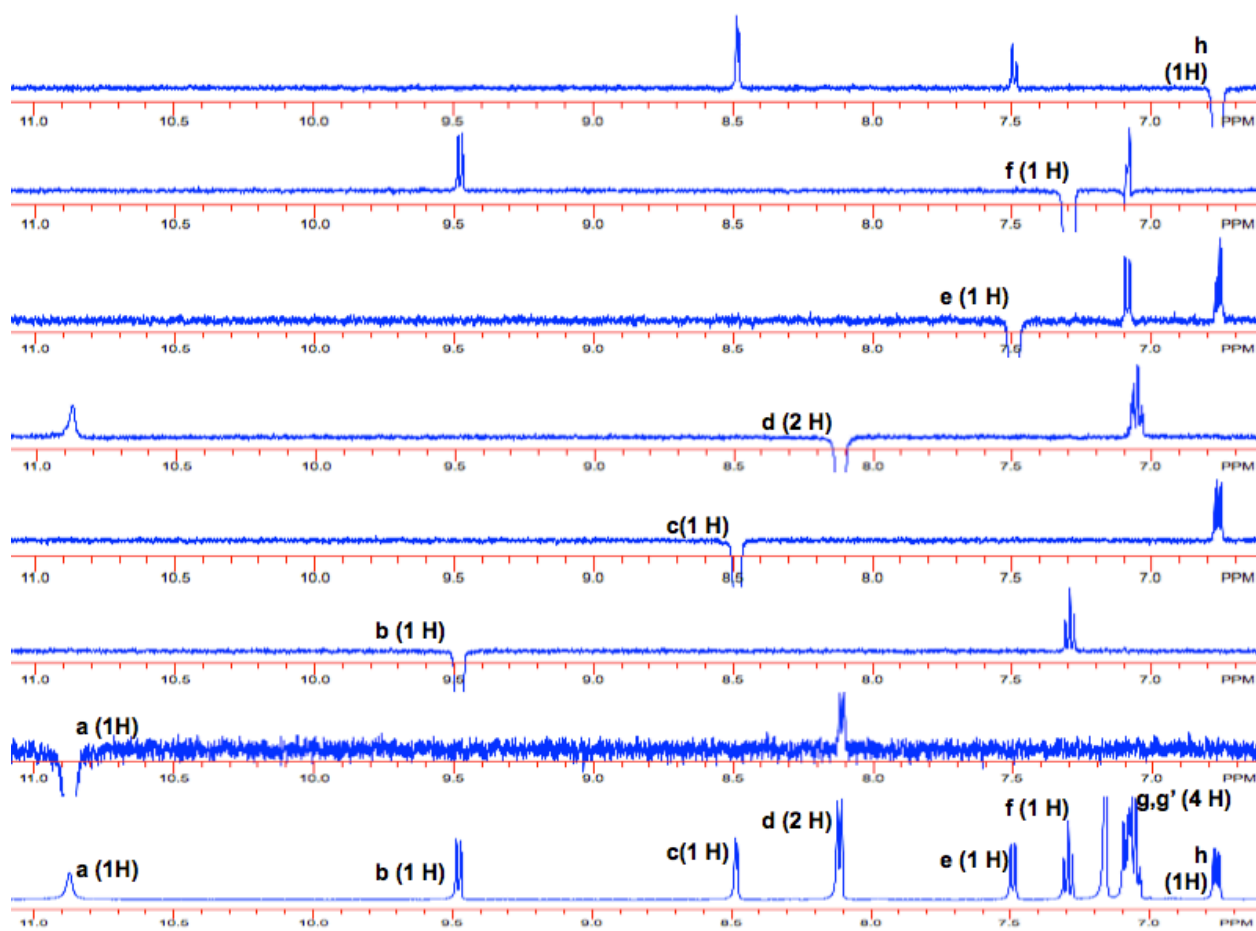
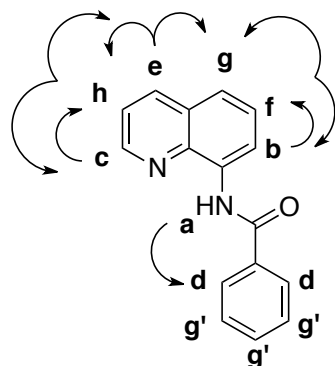


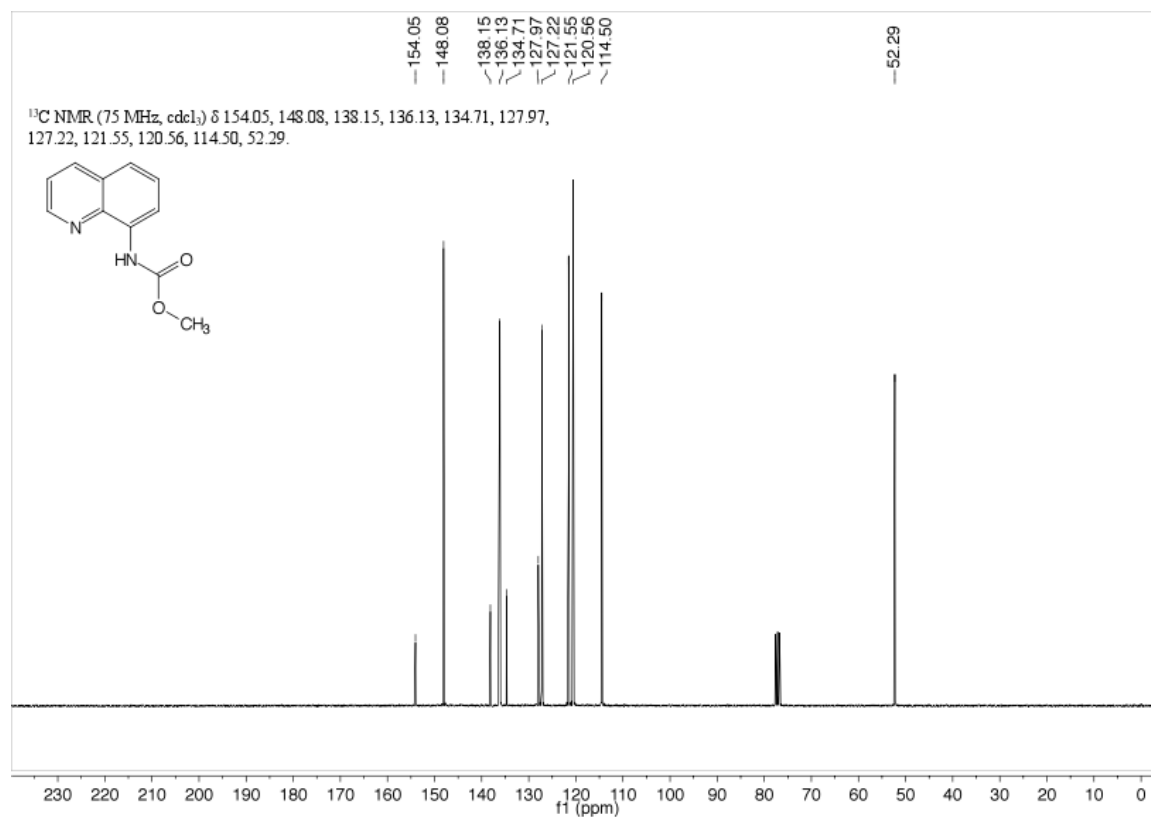
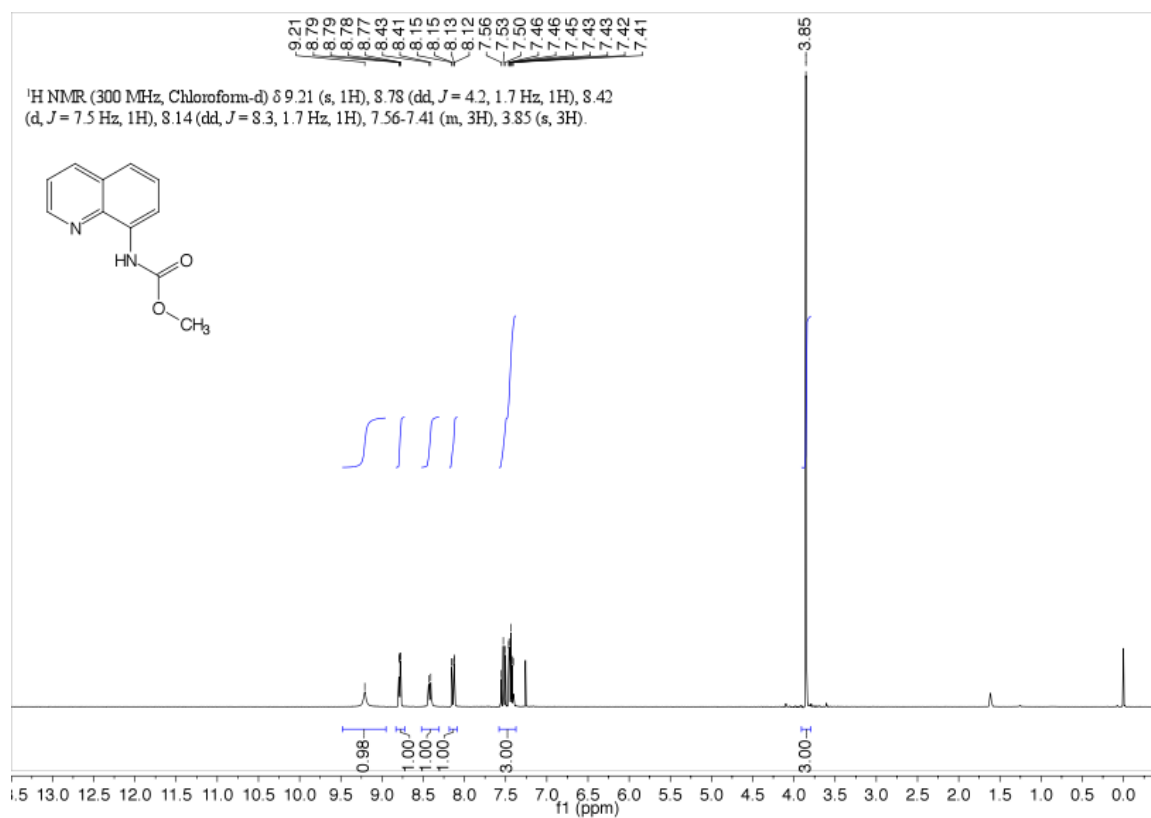


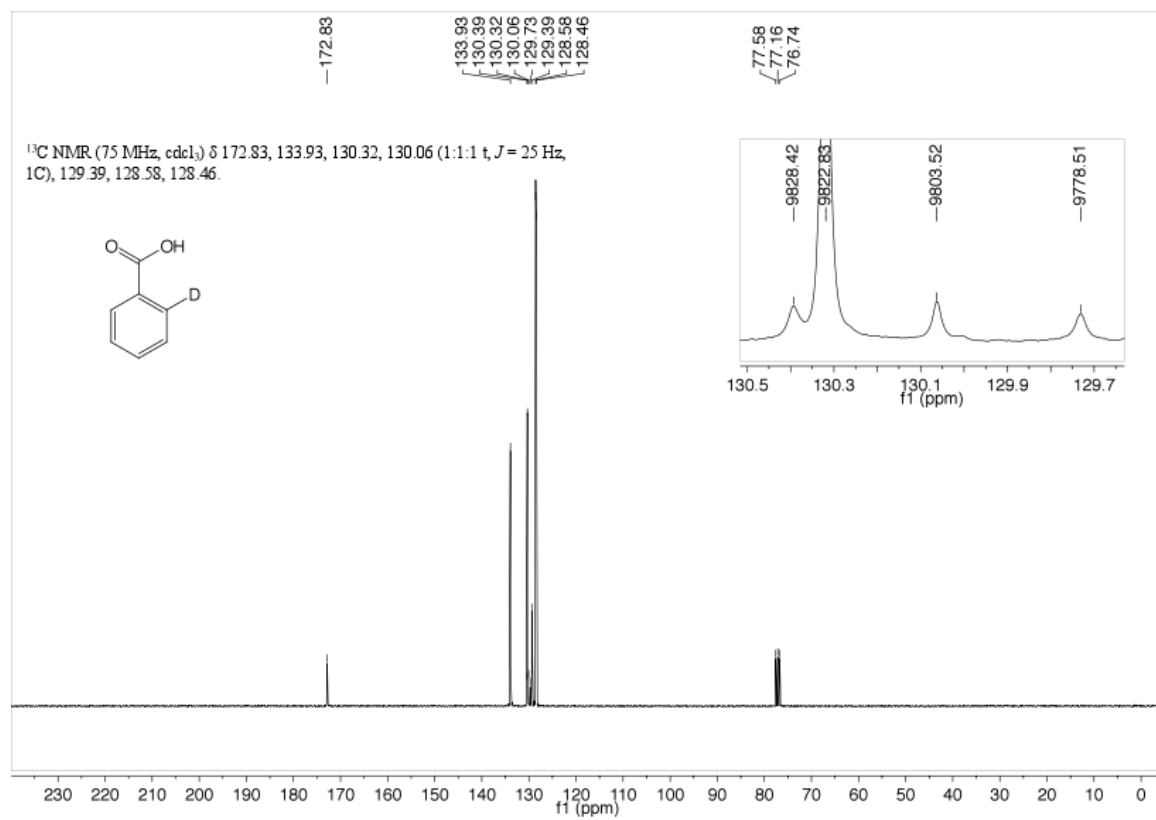
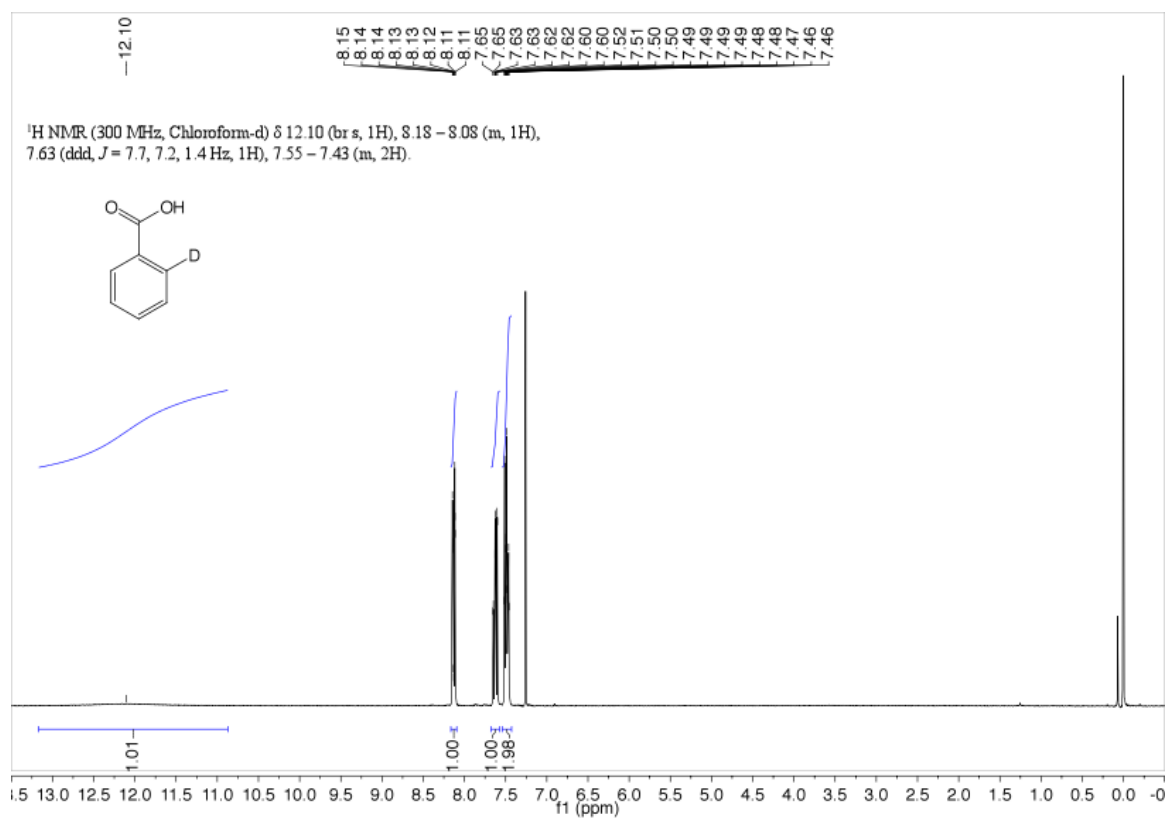
1D nOe NMR experiment on *N*-(5-chloro-8-quinoliny)benzamide product (compare to 1D nOe of the substrate below).

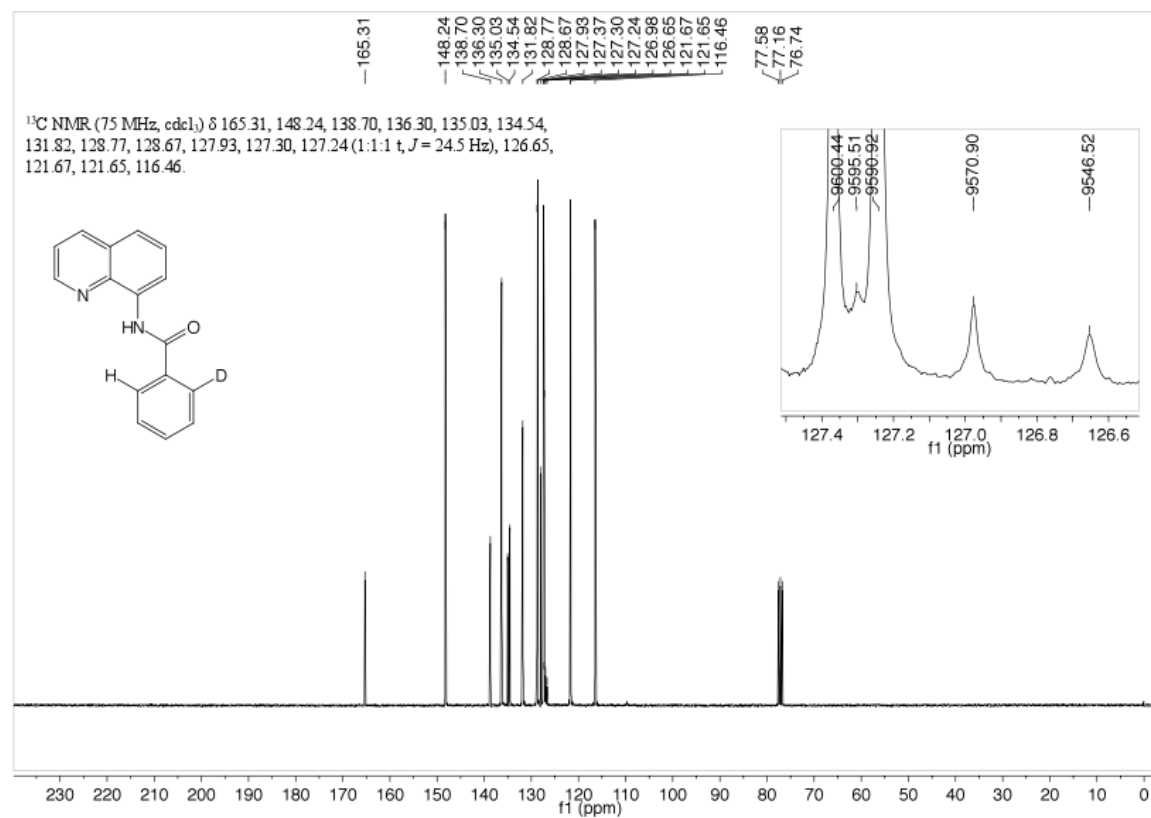
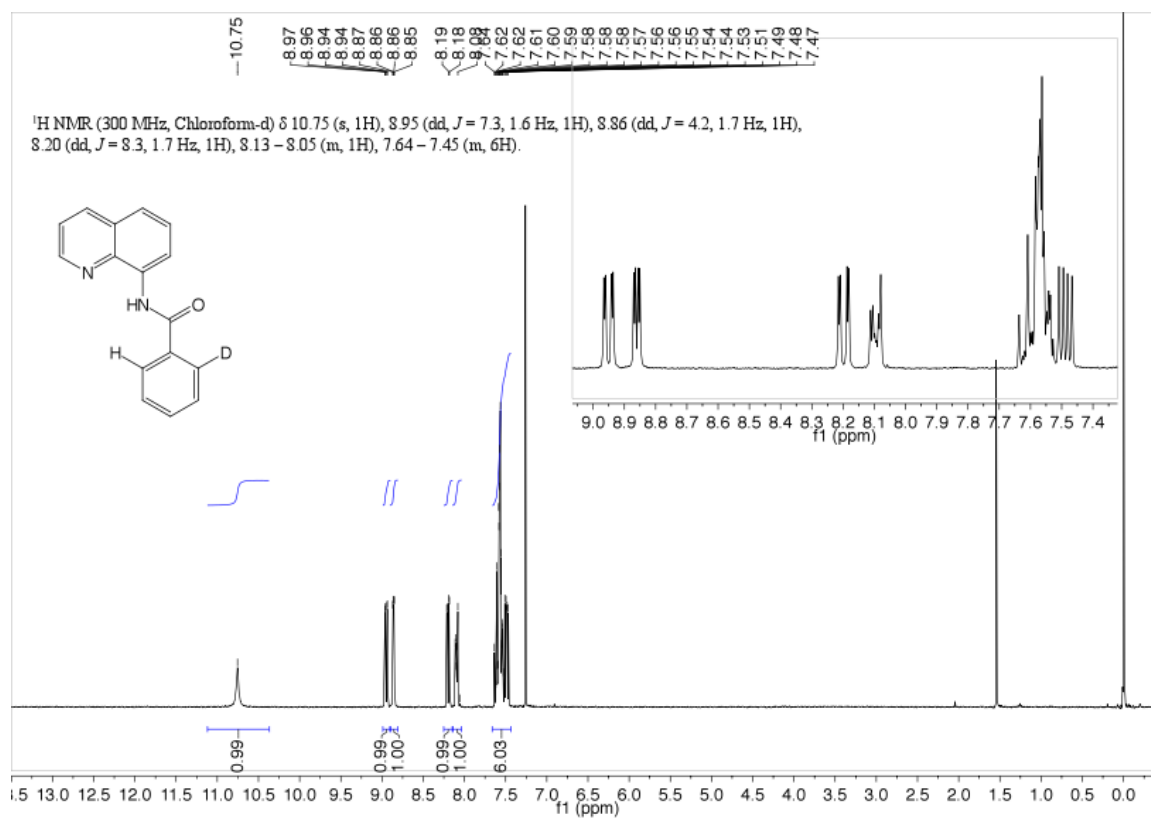


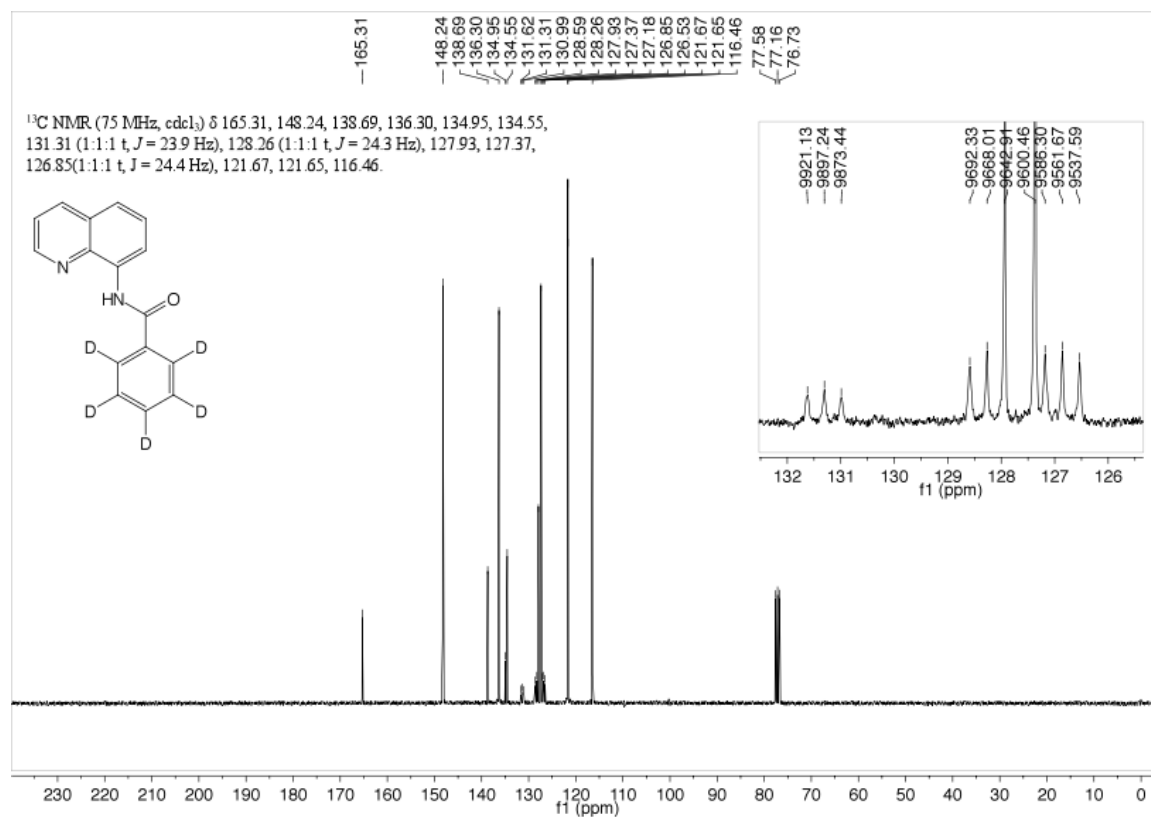
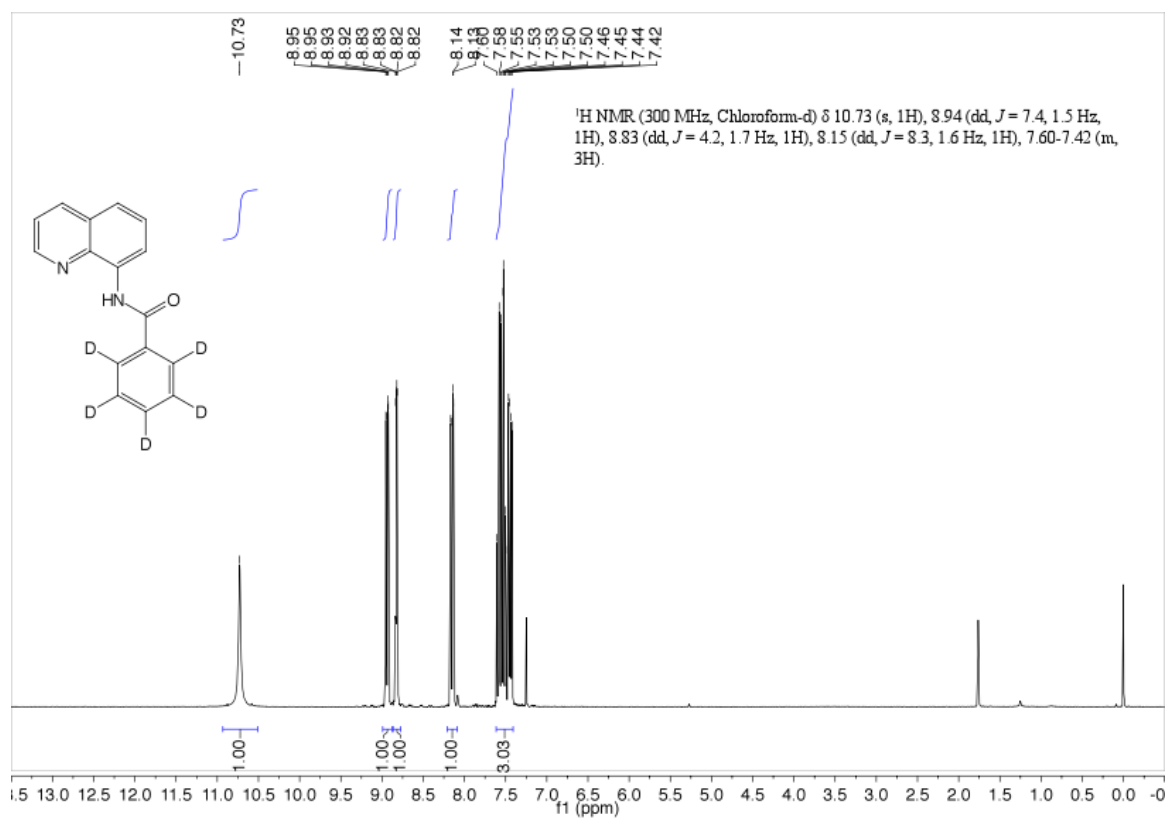
1D nOe experiment on *N*-(8-quinoliny)benzamide substrate.

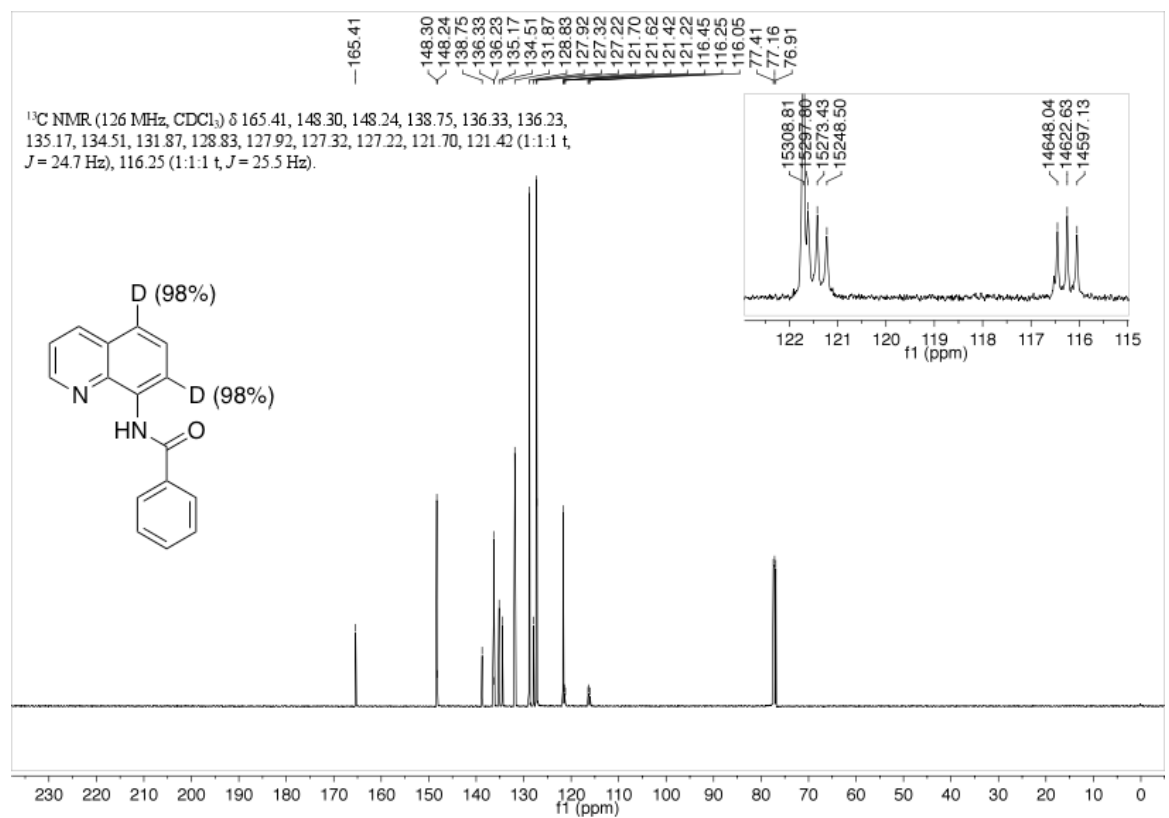
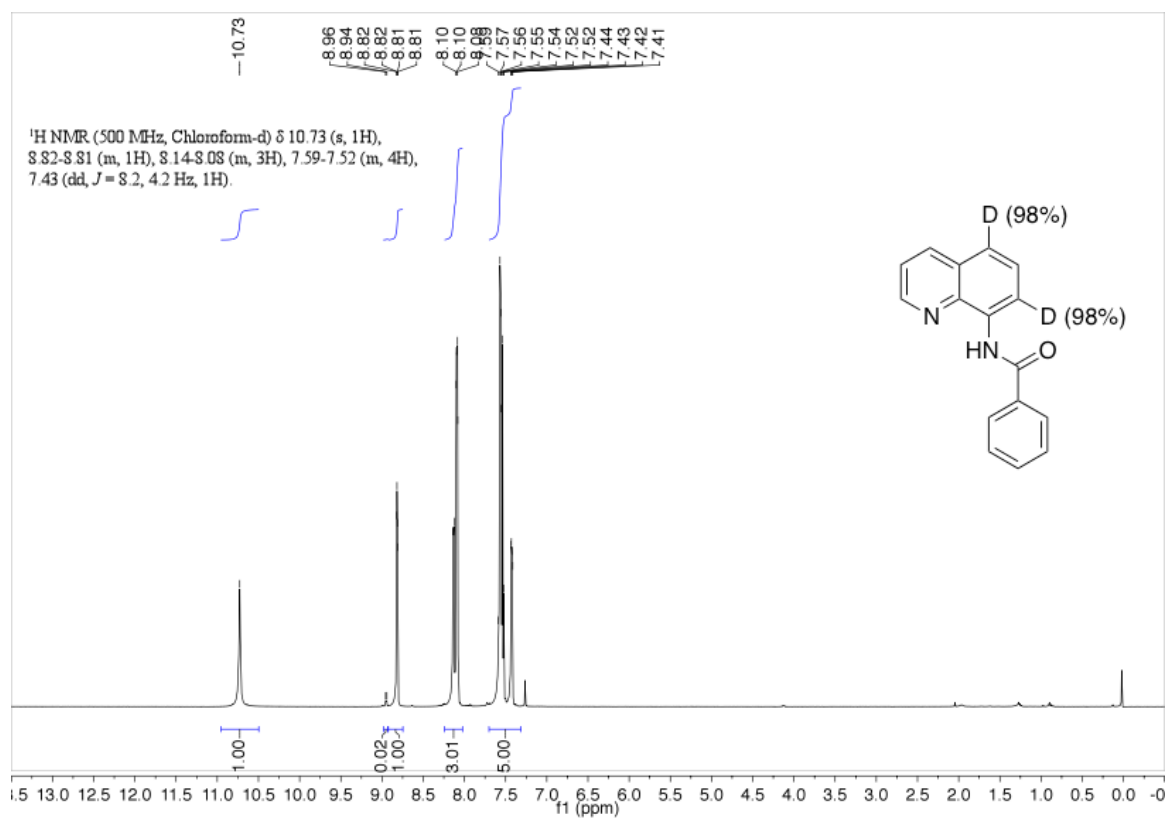












Appendix 2:

Other Transformations of *N*-(8-Quinoliny)benzamide
and Similar Substrates

A2.1. Directed Benzamide Methoxylation of 3-Substituted and 3,5-Disubstituted *N*-(8-Quinoliny)benzamide Derivatives.

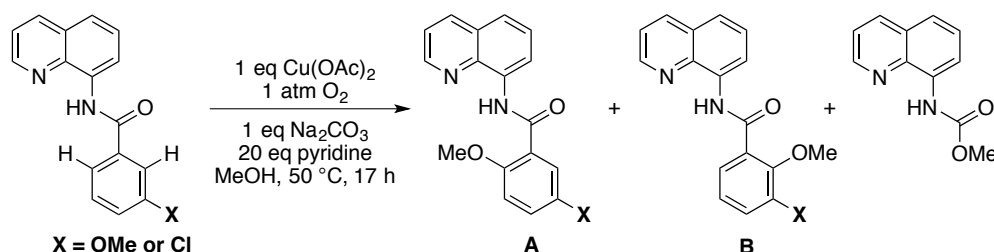
In the development of mechanistic studies discussed in Chapter 2, 3-substituted and 3,5-disubstituted *N*-(8-quinoliny)benzamide derivatives were synthesized and studied in the directed methoxylation. The problems encountered with these substrates led to the use of the 4-substituted *N*-(8-quinoliny)benzamide derivatives used in the final mechanistic studies.

The 3-substituted *N*-(8-quinoliny)benzamide derivatives were designed assuming that only the C-H bond *para* to the electronically-varying substituent would be oxidized. However, mono-methoxylation of the substrate took place in varying ratios at either C-H bond *ortho* to the directing group, despite one of those positions being significantly more sterically-hindered (Table A2.1). This result is unusual; in the more well-explored directed C-H functionalizations with Pd, similar steric hindrance results in functionalization of only the less-sterically hindered C-H bond *ortho* to the directing group.¹ However, recent non-aerobic reports utilizing the amidoquinoline directing group indicate that Cu allows access to the more-sterically hindered site.²

The ratio of the position of C-H methoxylation varied under reaction conditions with and without pyridine (Table A2.1, “**A:B**”). Pyridine is added to the typical reaction conditions because it was discovered during initial reaction screening that pyridine aids dissolution of the substrates into the reaction mixture, allowing higher product yields for substrates that are poorly soluble in MeOH. Without pyridine (Table A2.1, entries 2, 5), methoxylation was more selective for the less sterically-hindered position **A**. With pyridine (Table A2.1, entries 3, 6), methoxylation was more selective for the more sterically-hindered position **B**. The origin of this

selectivity difference is unknown, but presumably depends on differences in copper ligation in the C-H activation transition state caused by the lack or presence of pyridine.

Table A2.1. Lack of selectivity in directed methoxylation of electron-rich and electron-poor benzamide groups of 3-substituted *N*-(8-quinolinyl)-benzamides.



Entry	X	Cu	Base (1 eq)	Pyridine (eq)	% RSM	% A+B	A:B	% Carbamate
1	OMe	1 eq Cu(OAc) ₂	none	none	87.6	0.0	N/A	0.0
2	OMe	1 eq Cu(OAc) ₂	Na ₂ CO ₃	none	24.4	38.7	1.32:1	1.9
3	OMe	1 eq Cu(OAc) ₂	Na ₂ CO ₃	20	0.0	28.2	1:2.35	6.2
4	Cl	1 eq Cu(OAc) ₂	none	none	87.6	0.0	N/A	0.0
5	Cl	1 eq Cu(OAc) ₂	Na ₂ CO ₃	none	33.9	33.0	8.42:1	4.1
6	Cl	1 eq Cu(OAc) ₂	Na ₂ CO ₃	20	0.0	62.4	1:2.52	7.3

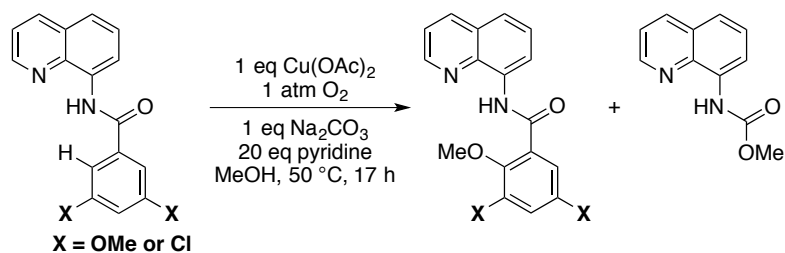
Conditions: 50 mM substrate, 50 mM Cu, 50 mM base in 1 mL MeOH, Stahl group custom vortexing reactors. Yields from ¹H NMR spectroscopy; 1,4-bis(trimethylsilyl)benzene internal standard.

The poor selectivity for the position *para* to the electronically-varying substituent and the pyridine-dependent selectivity variance would complicate mechanistic study, so alternative substitution patterns were tested.

The 3,5-substituted *N*-(8-quinolinyl)benzamide derivatives were designed such that both C-H bonds *ortho* to the directing group would be equivalent. Without pyridine in the reaction conditions, these substrates are only minimally soluble and show little reactivity (Table A2.2, entries 1,3). With pyridine, solubility improves and product yield increases (Table A2.2, entries

2,4). However, even with pyridine, these substrates are not fully soluble under the reaction conditions and are thus unsuitable for mechanistic study. Ultimately, 4-substituted *N*-(8-quinolinyl)benzamide derivatives were selected for the mechanistic study in the previous chapter. The 4-substituted substrates have equivalent C-H bonds *ortho* to the directing group and proved to be fully soluble under the reaction conditions.

Table A2.2. Lack of selectivity in directed methoxylation of electron-rich and electron-poor benzamide groups of *N*-(8-quinolinyl)-3-substituted-benzamides.



Entry	X	Cu	Base (1 eq)	Pyridine (eq)	% RSM	% Product	% Carbamate
1	OMe	1 eq Cu(OAc) ₂	none	none	56.3	4.1	0.0
2	OMe	1 eq Cu(OAc) ₂	Na ₂ CO ₃	20	0.0	15.1	0.0
3	Cl	1 eq Cu(OAc) ₂	none	none	82.9	2.8	0.0
4	Cl	1 eq Cu(OAc) ₂	Na ₂ CO ₃	20	29.9	44.4	1.8

Conditions: 50 mM substrate, 50 mM Cu, 50 mM base in 1 mL MeOH, Stahl group custom vortexing reactors. Yields from ¹H NMR spectroscopy; 1,4-bis(trimethylsilyl)benzene internal standard.

A2.2. Isolation and Analysis of Crystalline Copper(II)-Amidate Complexes from *N*-(8-Quinolinyl)benzamide, Including Observation of Oxidase Reactivity.

Attempts were made to generate a discrete 1 equiv copper-1 equiv substrate complex for mechanistic studies. Literature reports demonstrated crystallographically-analyzed complexes from a similar pyridine-amidoquinoline ligand³ (Figure A2.1A) and a pyridine-amide ligand⁴

(Figure A2.1B) were synthesized by room temperature or reflux mixing of the respective amide ligand with $\text{Cu}(\text{OAc})_2 \cdot \text{H}_2\text{O}$ in methanol.

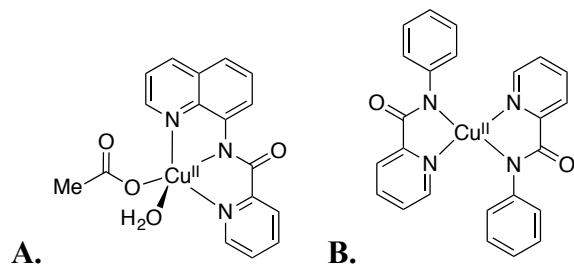


Figure A2.1. Crystallographically-analyzed literature copper(II) amidate complexes with (A) a similar pyridine-amidoquinoline ligand and (B) a pyridine-amide ligand.

Unfortunately, crystallization of a similar complex from the reaction mixture was unsuccessful. $\text{Cu}(\text{OAc})_2$ (0.10 mmol, 0.0182 g), *N*-(8-quinolinyl)benzamide (0.05 mmol, 0.0139 g), and Cs_2CO_3 (0.05 mmol, 0.0163 g) were added to 1 mL of the typical 5:1 methanol/pyridine solvent mixture and heated in a test tube under 1 atm O_2 at 50 °C for 30 min, then filtered. The filtrate was set up for Et_2O vapor diffusion. There was a minor amount of small, irregular dark green crystals that were not suitable for X-ray crystallography. The major species was the pyridine-capped copper acetate paddlewheel $\text{Cu}_2(\text{OAc})_4(\text{py})_2$ (Figure A2.2). These crystals are blue-green dichroic in color and have a flat rectangular shape with polygonal edges. The large size of these crystals suggests that the paddlewheel is a favorable solid-state structure.

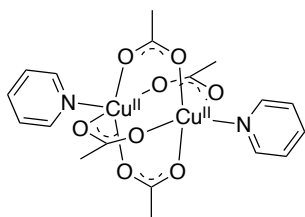


Figure A2.2. $\text{Cu}_2(\text{OAc})_4(\text{py})_2$ chemical structure drawing.

A crystallization solution similar to the reaction solution but lacking Cs_2CO_3 yielded a 1 equiv copper-1 equiv substrate complex, but the substrate underwent C-H oxidase reactivity and crystallized as the copper-phenoxide. $\text{Cu}(\text{OAc})_2$ (0.2 mmol, 0.0365 g) and pyridine (4 mmol, 0.324 mL) were added to 1 mL methanol, giving a deep blue solution. *N*-(8-quinolinyl)benzamide (0.2 mmol, 0.497 g) was dissolved in 1 mL methanol and this solution was added to the $\text{Cu}(\text{OAc})_2$ solution, which turned dark green. The solution was refluxed under air for 2 h. Two types of crystals resulted from Et_2O vapor diffusion crystallization of the solution. The major species was the pyridine-capped copper acetate paddlewheel, $\text{Cu}_2(\text{OAc})_4(\text{py})_2$. The minor species was the neutral copper(II) phenoxide amidate (Figure A2.3) resulting from C-H oxidation. These crystals are dark green, small and irregular with a spiky coating. Crystals from one crystallization vial were dried and manually separated. The $\text{Cu}_2(\text{OAc})_4(\text{py})_2$ crystals represented 59.8 mol % of the initial copper starting material, and the phenoxide crystals represented only 1.2 mol % copper.

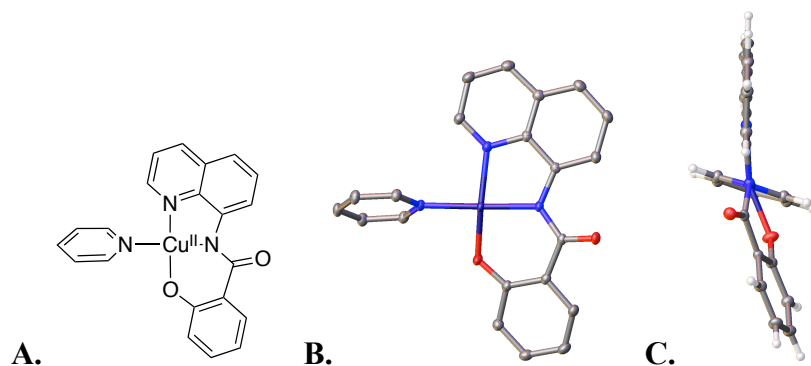


Figure A2.3. Copper(II)-phenoxide complex crystallized after methanol reflux. (A) Chemical structure drawing, (B) crystal structure, front view, (C) crystal structure, side view.

A bis-ligated bis-amidate complex was isolated when the reflux solvent was changed to acetone. $\text{Cu}(\text{OAc})_2$ (0.2 mmol, 0.0365 g) was added to 1 mL acetone, minimally dissolving to yield a light blue solution with undissolved blue $\text{Cu}(\text{OAc})_2$ powder. *N*-(8-quinoliny)benzamide (0.2 mmol, 0.497 g) was dissolved in 1 mL acetone and this soln was added to the $\text{Cu}(\text{OAc})_2$ solution, which turned brown. The solution was refluxed for 2 h, filtered, and the filtrate was set up for Et_2O vapor diffusion crystallization. The crystallization yielded small dark crystals (the crystallographers describe the color as red), green powder precipitate, and green mother liquor. X-ray analysis of the crystals demonstrated that a neutral bis-ligated copper(II) bis-amidate complex had been formed (Figure A2.4).

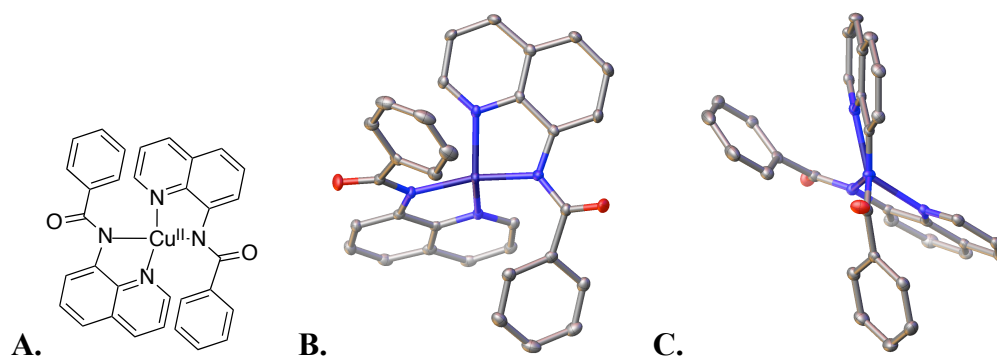


Figure A2.4. Bis-ligated copper(II) bis-amidate complex crystallized after acetone reflux. (A) Chemical structure drawing, (B) crystal structure, front view, (C) crystal structure, side view.

Generation of a 1 eq copper-1 eq substrate complex was attempted using the sodium amidate salt of *N*-(8-quinoliny)benzamide; however, unfortunately, only an insoluble copper species was obtained from this method. To make the sodium amidate, NaH (0.0366 mmol, 0.8788 mg) was placed in a septum-sealed flask under N_2 atmosphere. *N*-(8-quinoliny)benzamide (0.0403 mmol, 10.0 mg) was dissolved in 3 mL Et_2O ; this soln was syringed into the flask containing NaH. After 2 h, the vial was opened, 3-5 mL of hexane was

added to further precipitate the salt, and the yellow precipitate sodium *N*-(8-quinolinyl)benzamidate salt was filtered, dried under vacuum, and stored in a desiccator. (AMS2030) When the sodium amidate salt is dissolved in various solvents (DMSO, CH₂Cl₂, Et₂O) it appears to be rapidly protonated (¹H NMR analysis shows the amide N-H peak).

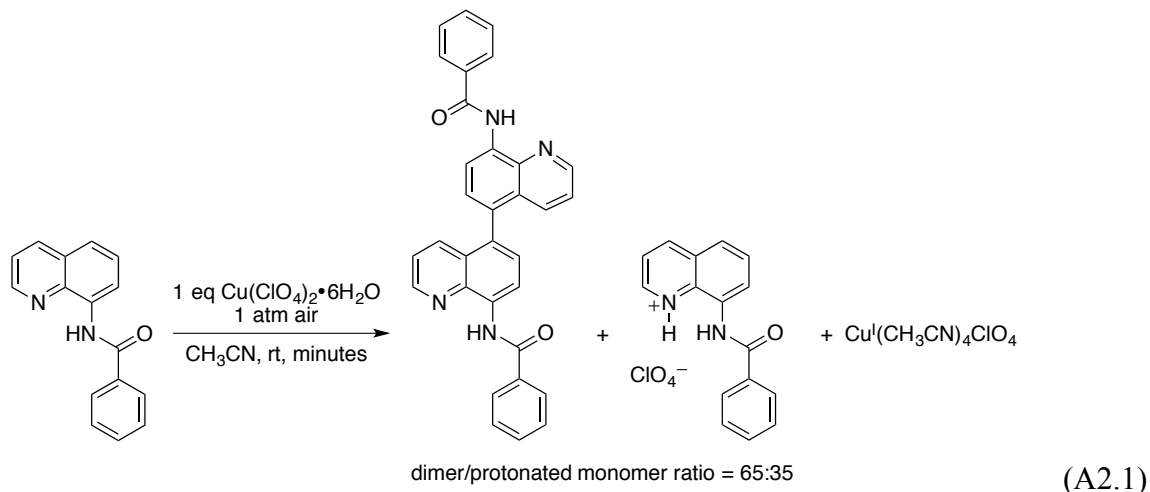
CuCl₂ was added to CH₂Cl₂ (it did not dissolve). Sodium *N*-(8-quinolinyl)benzamidate was added, and over the course of 2 h the reaction solution turned cloudy white (possible precipitation of NaCl) and the CuCl₂ powder at the bottom of the solution turned dark olive green. The dark green copper materials could not be dissolved (CH₂Cl₂, MeOH, acetone, H₂O, toluene, THF, Et₂O, hexane, DMF, and DMSO were tested).

A2.3. *N*-(8-Quinolinyl)benzamide C-C Homocoupling in the Presence of Cu(ClO₄)₂.

A C-C homocoupling reaction occurs when *N*-(8-quinolinyl)benzamide is mixed with 1 equiv Cu(ClO₄)₂ in CH₃CN at ambient conditions (eq A2.1). The dimer structure was proposed after NMR and ESI-MS analysis. The protonated monomer and Cu^I(CH₃CN)₄ClO₄ were determined by X-ray crystallography after Et₂O vapor diffusion crystallization of the reaction mixture. When the organics are separated from Cu with a basic work up, the dimer and monomer starting material may be extracted together; analysis reveals a 65:35 ratio of these species, respectively.

Color change may give insight into the mechanism of this reaction. When the substrate and Cu(ClO₄)₂ are mixed in CH₃CN, the solution turns briefly dark green, then almost immediately red. In minutes, the reaction solution fades to colorless, and then slowly turns light green. During formation of the triazamacrocyclic aryl-Cu^{III}, Huffman noted that when the arene and Cu^{II} are mixed, the reaction solution turns briefly dark green then red, the color of the aryl-

Cu^{III} complex.⁵ $\text{Cu}^{\text{I}}(\text{CH}_3\text{CN})_4\text{ClO}_4$ is colorless under N_2 but slowly turns light green when exposed to O_2 . This color change sequence may be indicative of an aryl- Cu^{III} intermediate.



A2.4. *N*-(8-Quinoliny)benzamide Bromination, Methoxylation and Dimerization in Methanol.

N-(8-quinoliny)benzamide was subjected to Cu-mediated methoxylation conditions with CuBr_2 and a complex mixture of products formed, including brominated, methoxylated, and dimerized products (eq A2.2). Products were analyzed by NMR spectroscopy and ESI-MS. A time course of the reaction indicates that brominated products appear then are consumed (Figure A2.5). Methoxylated products appear as the yield of the brominated products peaks. This result contrasts with the previous study; when CuCl_2 was used, chlorinated and methoxylated products formed, but no dimerization occurred (see chapter 2).

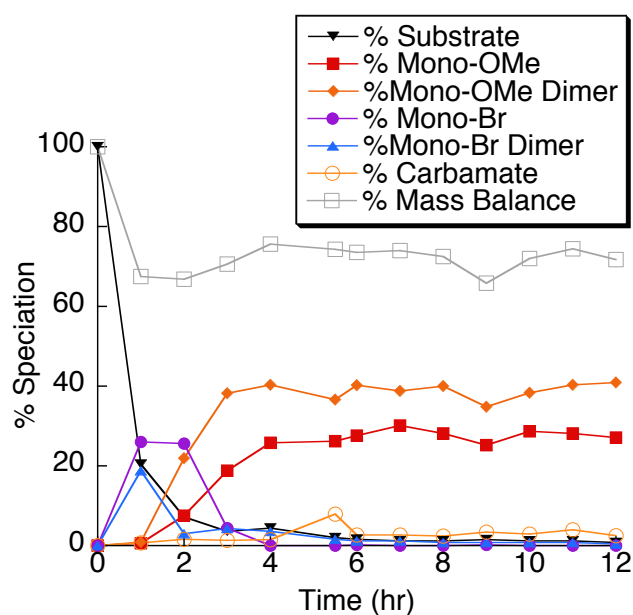
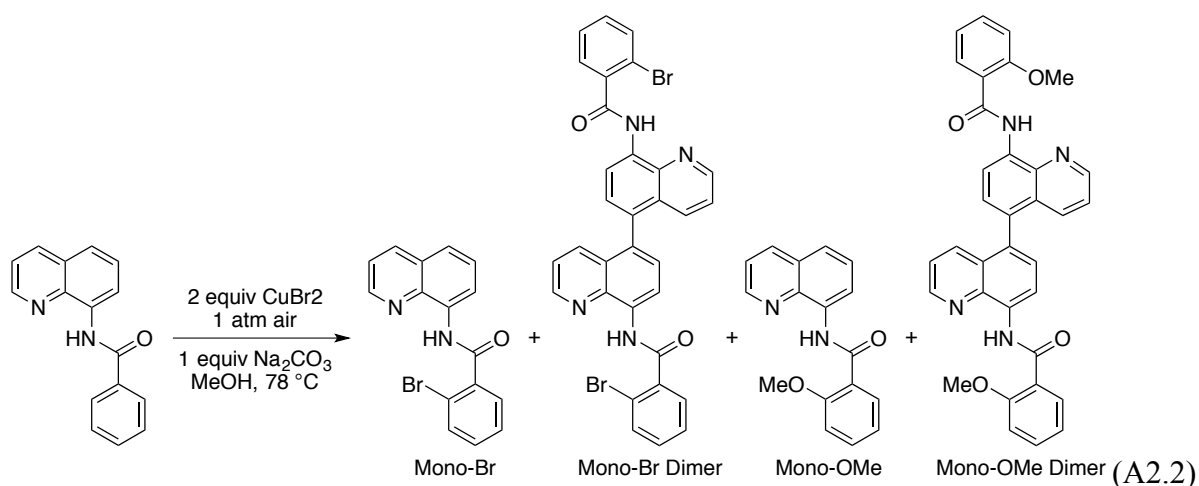


Figure A2.5. Time course of *N*-(8-quinoliny)benzamide bromination, methoxylation, and dimerization in methanol. Conditions: 50 mM substrate, 100 mM CuBr₂, 50 mM Na₂CO₃ in MeOH, 1 atm air, 78 °C.

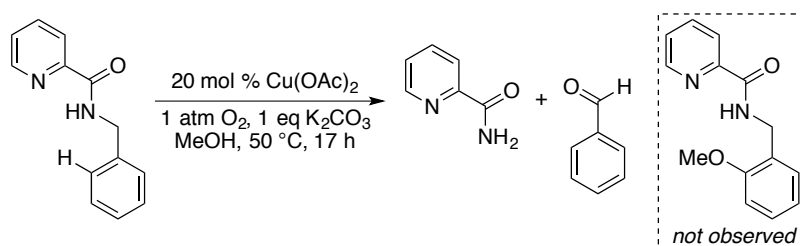
A2.5. Reactivity of Other Directing-Group-Containing Substrates.

After early success with stoichiometric Cu^{II}-mediated methoxylation of *N*-(8-quinoliny)benzamide, few other directing groups were examined. Though Pd-catalyzed C-H

oxidation can be carried out with a variety of directing groups, the 8-amidoquinoline directing group seems to be the best directing group to use with copper.⁶

A substrate with a pyridine-containing directing group, *N*-(phenylmethyl)-2-pyridinecarboxamide, was synthesized and tested under methoxylation reaction conditions (Table A2.3). Without copper, the substrate was stable under the reaction conditions (entry 1), however with 20 mol % $\text{Cu}(\text{OAc})_2$ debenzoylation occurred to yield 2-pyridinecarboxamide and benzaldehyde (entry 2). There is precedent for such debenzoylation; room-temperature photolysis of a pyridinecarboxamidate-ligated copper complex resulted in a similar debenzoylation.⁷ Debenzoylation of *N*-benzylamides has also been demonstrated at high temperature using a copper(II) tris(triflyl)methide catalyst.⁸ With 1 eq $\text{Cu}(\text{OAc})_2$, a majority of the substrate was recovered after work-up and only a few line-broadened peaks were visible in the ^1H NMR spectrum, indicating some substrate may have remained chelated to copper (entry 3-4).

Table A2.3. Reaction utilizing a pyridine-containing directing group resulted in debenzoylation rather than the desired directed methoxylation.



Entry	$\text{Cu}(\text{OAc})_2$	Base (1 eq)	Pyridine (eq)	% RSM	% 2-Pyridine-carboxamide
1	none	K_2CO_3	none	98.1	0.0
2	20 mol %	K_2CO_3	none	8.4	66.0
3	1 eq	K_2CO_3	none	64.9	0.0
4	1 eq	K_2CO_3	20	97.7	0.0

Conditions: 50 mM substrate, 0-50 mM Cu, 50 mM base in 1 mL MeOH, Stahl group custom vortexing reactors. Yields from ^1H NMR spectroscopy; 1,4-bis(trimethylsilyl)benzene internal standard.

In order to avoid debenzoylation, a pyridine-containing directing group with a dimethyl-protected benzylic position was synthesized. This substrate was unreactive under the methoxylation reaction conditions (Table A2.4).

Table A2.4. Reaction utilizing a pyridine-containing directing group with a protected benzylic position did not result in the desired directed methoxylation.



Entry	Cu(OAc) ₂	Base (1 eq)	Pyridine (eq)	% RSM	% 2-Pyridine-carboxamide
1	20 mol %	K ₂ CO ₃	20	100	0.0
2	1 eq	K ₂ CO ₃	20	87.8	0.0

Conditions: 50 mM substrate, 10-50 mM Cu, 50 mM base in 1 mL MeOH, Stahl group custom vortexing reactors. Yields from ¹H NMR spectroscopy; 1,4-bis(trimethylsilyl)benzene internal standard.

To synthesize the protected substrate, benzonitrile (0.082 mL, 0.8 mmol) and THF (2 mL, from solvent system) were added to a microwave tube with stir bar. Methylmagnesium bromide (0.93 mL, 2.8 mmol) was added to the reaction mixture and the tube was capped and microwaved at 100 °C, 200 W for 10 min. The reaction mixture turned light yellow-green. Titanium isopropoxide (0.25 mL, 0.8 mmol) was added to the reaction mixture, which immediately turned red and gelled. The tube was recapped and microwaved at 50 °C, 200 W for 1 h. The reaction mixture turned black. The reaction mixture was filtered through Celite with 30 mL CH₂Cl₂, washed in a separatory funnel with brine (2x 20 mL), dried with MgSO₄, and filtered. 2 M HCl in Et₂O (0.5 mL) was added to form the ammonium chloride, and the organic

layer was rotovapped to an offwhite powder: α,α -dimethylbenzylammonium chloride, 0.10 g, 73% yield. This procedure was adapted from a literature reference.⁹

2-Picolinic acid (0.1509 g, 1.22 mmol) was suspended in THF (4 mL, from the solvent system), then cooled to -21 °C (5x(33 g NaCl + 81 g ice)). Triethylamine (0.175 mL, 0.122 mmol) and then ethyl chloroformate (0.12 mL, 1.22 mmol) were added to the reaction solution and stirred for 30 min. Meanwhile, α,α -dimethylbenzylammonium chloride freebased in a mixture of THF and concentrated KOH solution. The THF containing α,α -dimethylbenzylamine was dried with MgSO₄ and filtered. The amine solution was added dropwise to the acid reaction solution, which was allowed to stir overnight while the solution warmed. The reaction mixture was filtered, rotovapped, and reconstituted in EtOAc, washed (3x 2 M NaOH, 2x 1 M HCl, 1x brine) in a separatory funnel, dried with MgSO₄, filtered, and rotovapped onto silica gel after determining column conditions by TLC. The amide product, *N*-(1-methyl-1-phenylethyl)-2-pyridinecarboxamide, was separated on a EtOAc/hexanes gradient silica gel column: 0.1903 g, 65% yield. Procedure from the benzylamine analogue: Liang *et al.* *Org. Lett.* **2009**, *11*, 5726-5729.

A2.6. Contributions.

Ahn T. Nguyen synthesized *N*-(phenylmethyl)-2-pyridinecarboxamide under the mentorship of Alison M. Sues.

A2.7. References and Notes

1. (a) Zaitsev, V. G.; Shabashov, D.; Daugulis, O. "Highly Regioselective Arylation of sp³ C-H Bonds Catalyzed by Palladium Acetate." *J. Am. Chem. Soc.* **2005**, *127*, 13154-13155. (b)

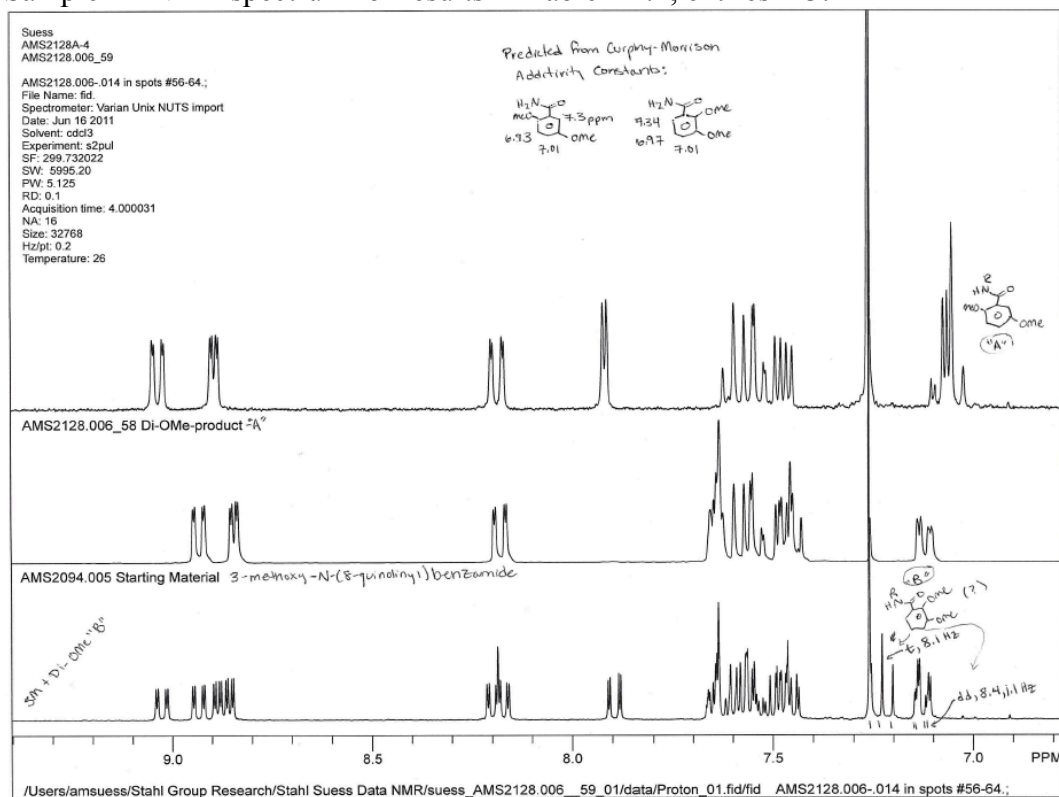
- Daugulis, O.; Do, H.-Q.; Shabashov, D. "Palladium- and Copper-Catalyzed Arylation of Carbon-Hydrogen Bonds." *Acc. Chem. Res.* **2009**, *42*, 1074-1086. (c) Lyons, T. W.; Sanford, M. S. "Palladium-Catalyzed Ligand-Directed C-H Functionalization Reactions." *Chem. Rev.* **2010**, *110*, 1147-1169.
2. (a) Truong, T.; Klimovica, K.; Daugulis, O. "Copper-Catalyzed, Directing Group-Assisted Fluorination of Arene and Heteroarene C-H Bonds." *J. Am. Chem. Soc.* **2013**, *135*, 9342-9345. (b) Nishino, M.; Hirano, K.; Satoh, T.; Miura, M. "Copper-Mediated C-H/C-H Biaryl Coupling of Benzoic Acid Derivatives and 1,3-Azoles." *Angew. Chem. Int. Ed.* **2013**, *52*, 4457-4461. (c) Tran, L. D.; Popov, I.; Daugulis, O. "Copper-Promoted Sulfenylation of sp² C-H Bonds." *J. Am. Chem. Soc.* **2012**, *134*, 18237-18240.
3. Zhang, J.; Ke, X.; Tu, C.; Lin, J.; Ding, J.; Lin, L.; Fun, H.-K.; You, X.; Guo, Z. "Novel Cu(II)-quinoline carboxamide complexes: Structural characterization, cytotoxicity and reactivity towards 5'-GMP." *BioMetals* **2003**, *16*, 485-496.
4. (a) Patra, A. K.; Ray, M.; Mukherjee, R. "Synthesis, crystal structure and properties of trigonal bipyramidal [M(L⁵)₂(H₂O)]•H₂O complexes [M=cobalt(II) (*S*=3/2) or copper(II) (*S*=1/2); HL⁵=*N*-(2-chloro-6-methylphenyl)pyridine-2-carboxamide]." *J. Chem. Soc., Dalton Trans.* **1999**, 2461-2466. (b) Ray, M.; Mukherjee, R.; Richardson, J. F.; Mashuta, M. S.; Buchanan, R. M. "Control of the Stereochemistry of Four-co-ordinate Copper(II) Complexes by Pyridinecarboxamide Ligands: Crystal Structure, Spectral and Redox Properties" *J. Chem. Soc., Dalton Trans.* **1994**, 965-969.
5. Huffman, L. M.; Stahl, S. S. "Carbon-Nitrogen Bond Formation Involving Well-Defined Aryl-Copper(III) Complexes." *J. Am. Chem. Soc.* **2008**, *130*, 9196-9197.

6. Miura and coworkers screen a variety of directing groups developing a Cu^{II}-mediated C-C coupling reaction; they suggest 8-amidoquinoline is the best due to its bidentate nature and relatively acid N-H bond: see reference 4b. Nishino, M.; Hirano, K.; Satoh, T.; Miura, M. "Copper-Mediated C-H/C-H Biaryl Coupling of Benzoic Acid Derivatives and 1,3-Azoles." *Angew. Chem. Int. Ed.* **2013**, *52*, 4457-4461.
7. Ciesinski, K. L.; Haas, K. L.; Dickens, M. G.; Tesema, Y. T.; Franz, K. J. "A Photolabile Ligand for Light-Activated Release of Caged Copper." *J. Am. Chem. Soc.* **2008**, *130*, 12246-12247.
8. Ishihara, K.; Hiraiwa, Y.; Yamamoto, H. "Homogeneous Debenzylation Using Extremely Active Catalysts: Tris(triflyl)methane, Scandium(III) Tris(triflyl)methide, and Copper(II) Tris(triflyl)methide." *Synlett* **2000**, *1*, 80-82.
9. Wang, R.; Gregg, B. T.; Zhang, W.; Golden, K. C.; Quinn, J. F.; Cui, P.; Tymoshenko, D. O. "Rapid Ti(Oi-Pr)₄ facilitated synthesis of α,α,α -trisubstituted primary amines by the addition of Grignard reagents to nitriles under microwave heating conditions." *Tetrahedron Lett.* **2009**, *50*, 7070-7073.

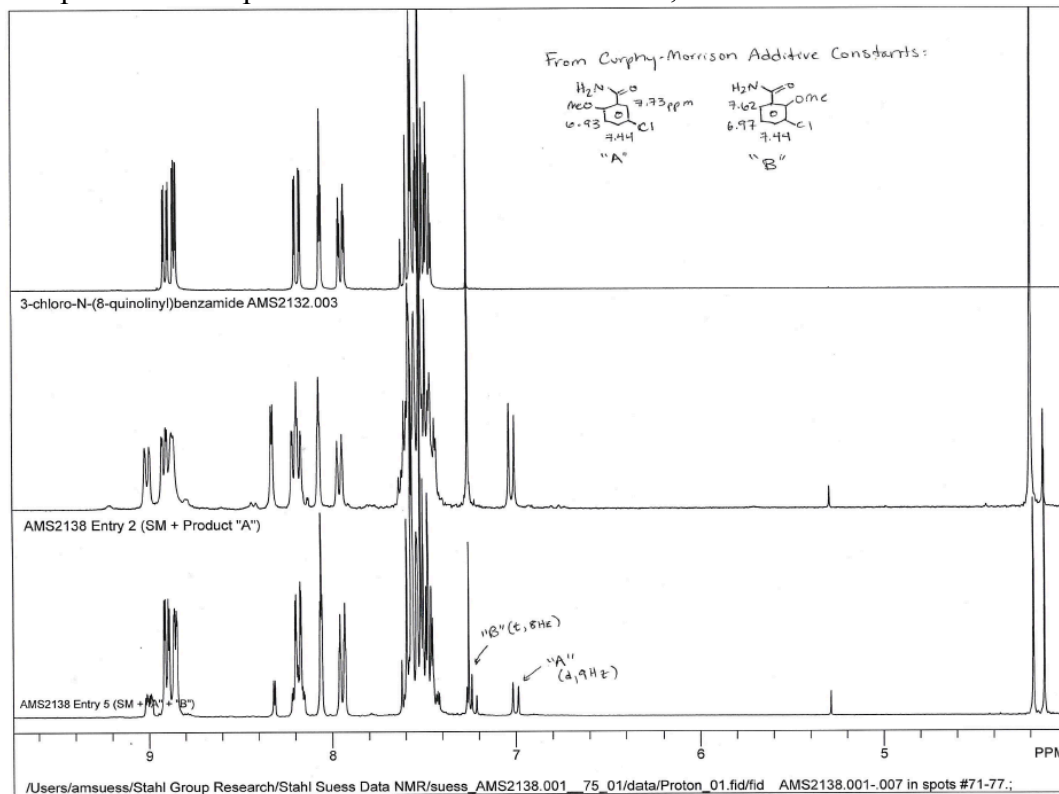
Appendix 3:

NMR Spectra and Crystal Structure Data for Appendix 2

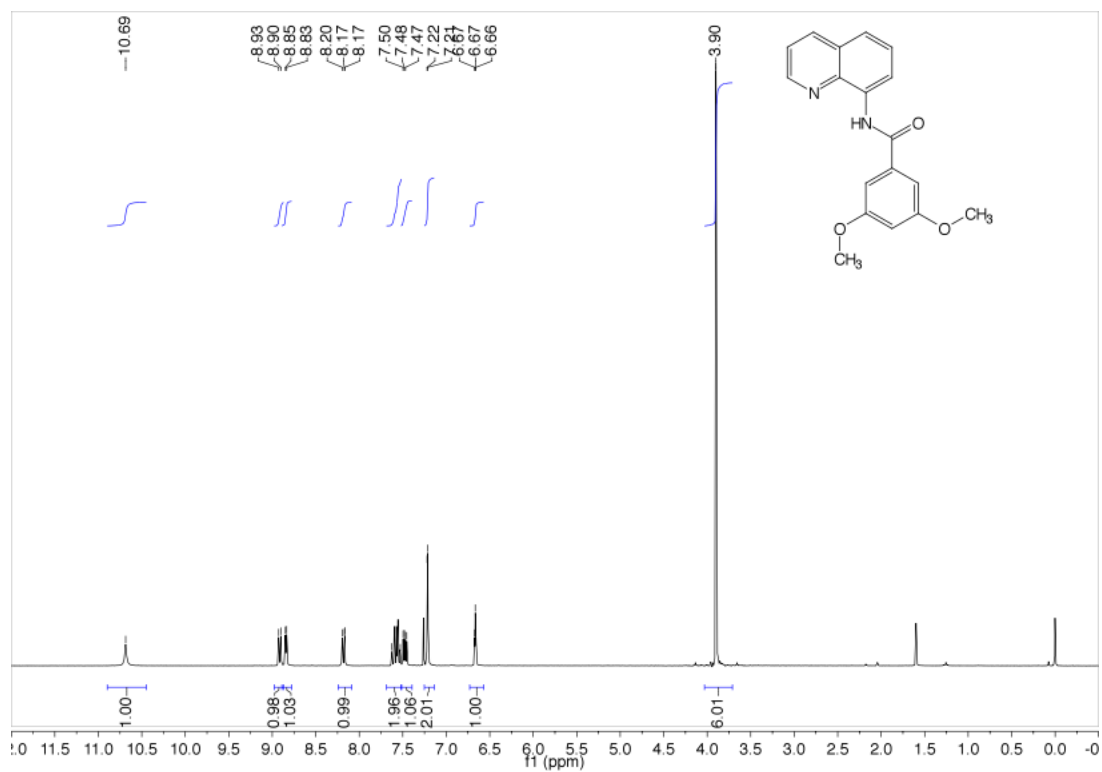
Sample ^1H NMR spectrum for results in Table A2.1, entries 1-3:



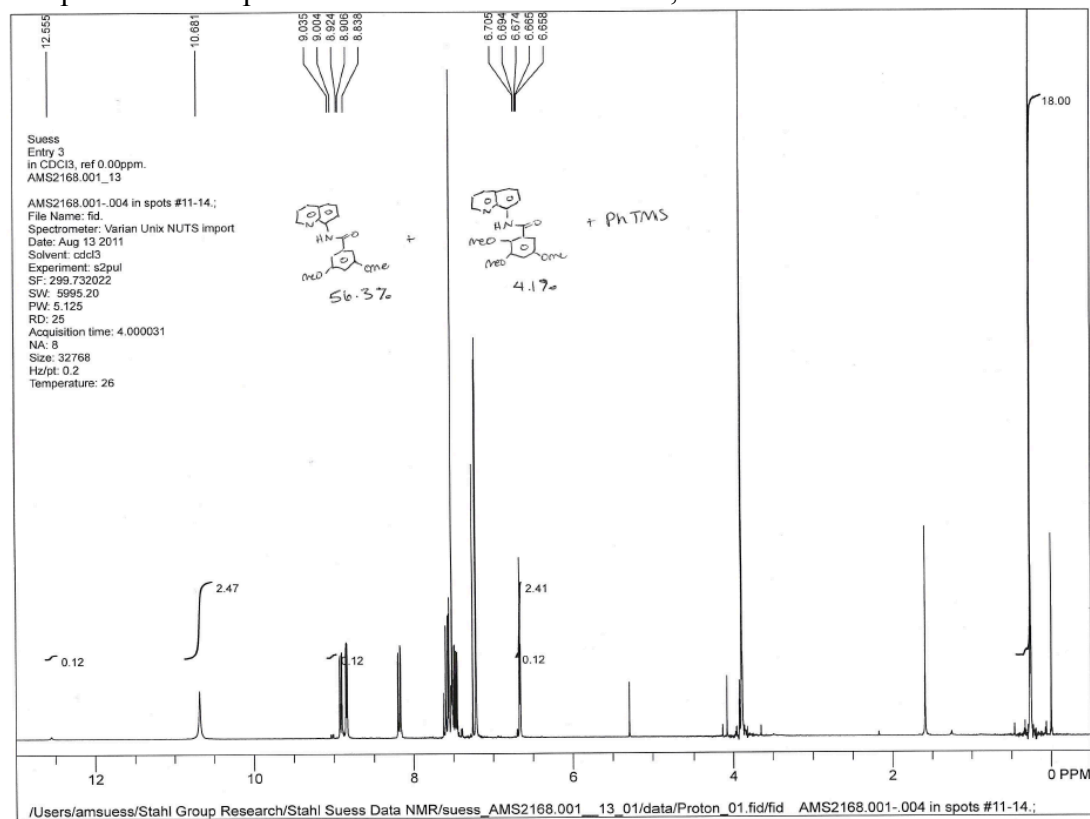
Sample ^1H NMR spectrum for results in Table A2.1, entries 4-6:



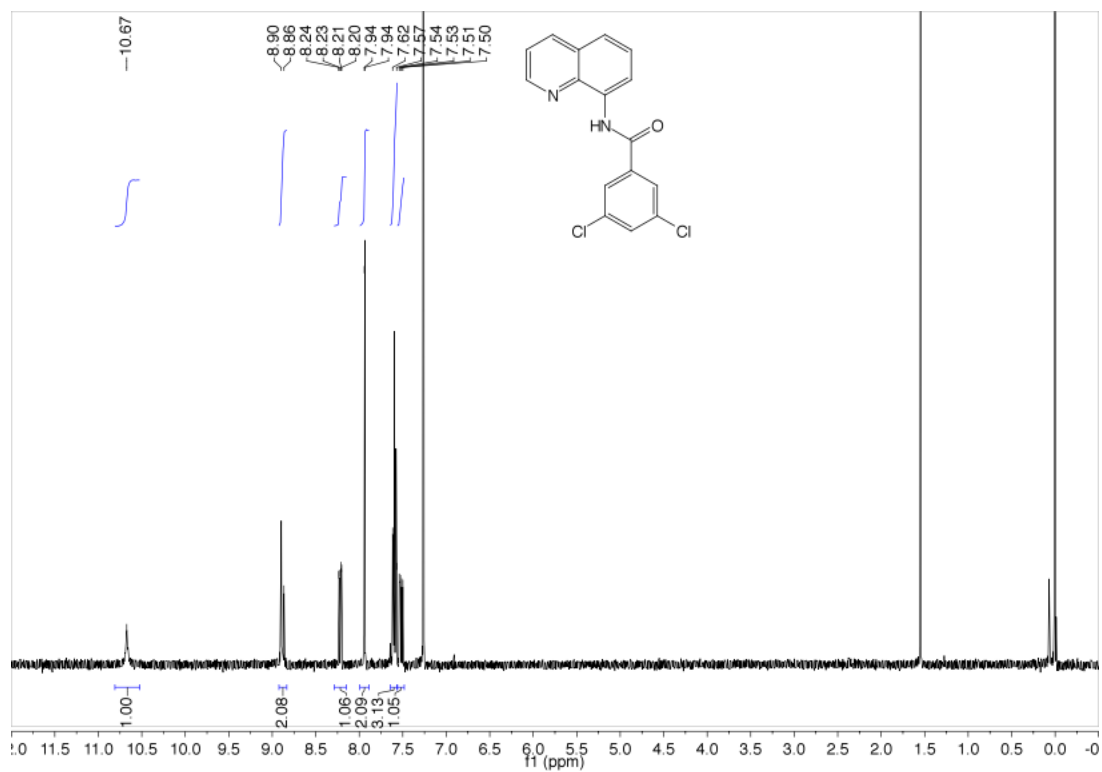
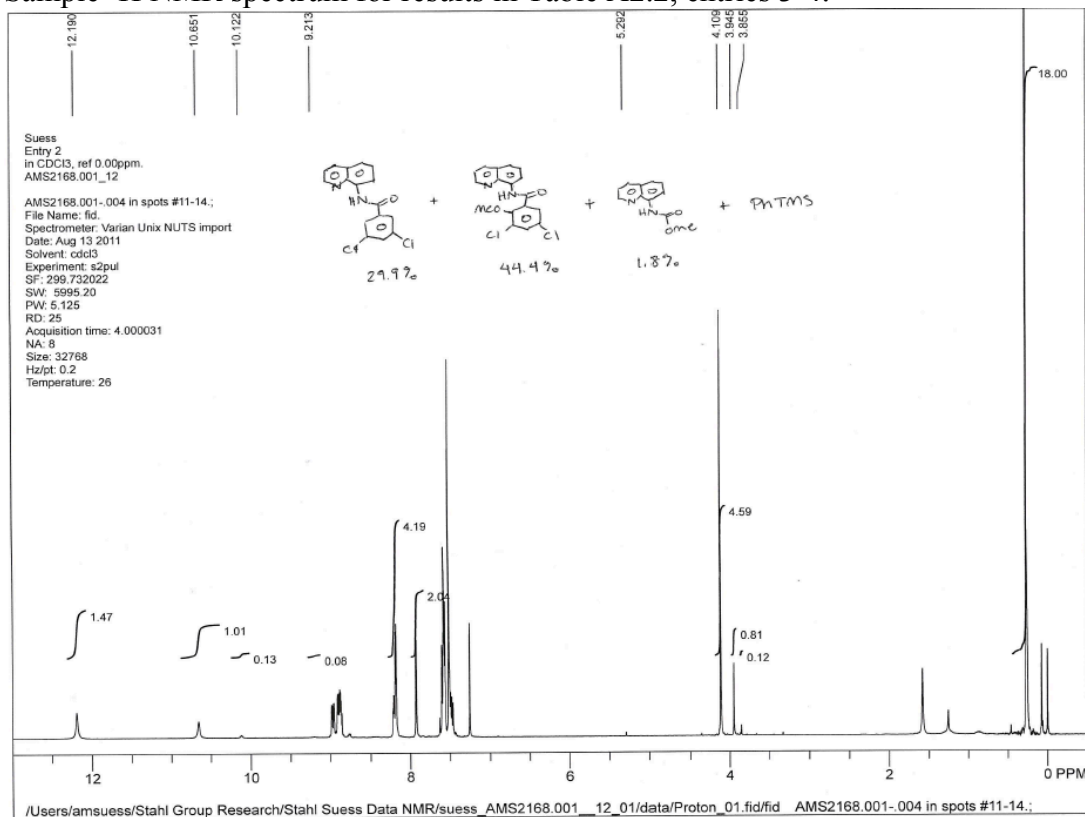
^1H NMR spectrum of 3,5-dimethoxy-N-(8-quinolinyl)benzamide (Table A2.2):

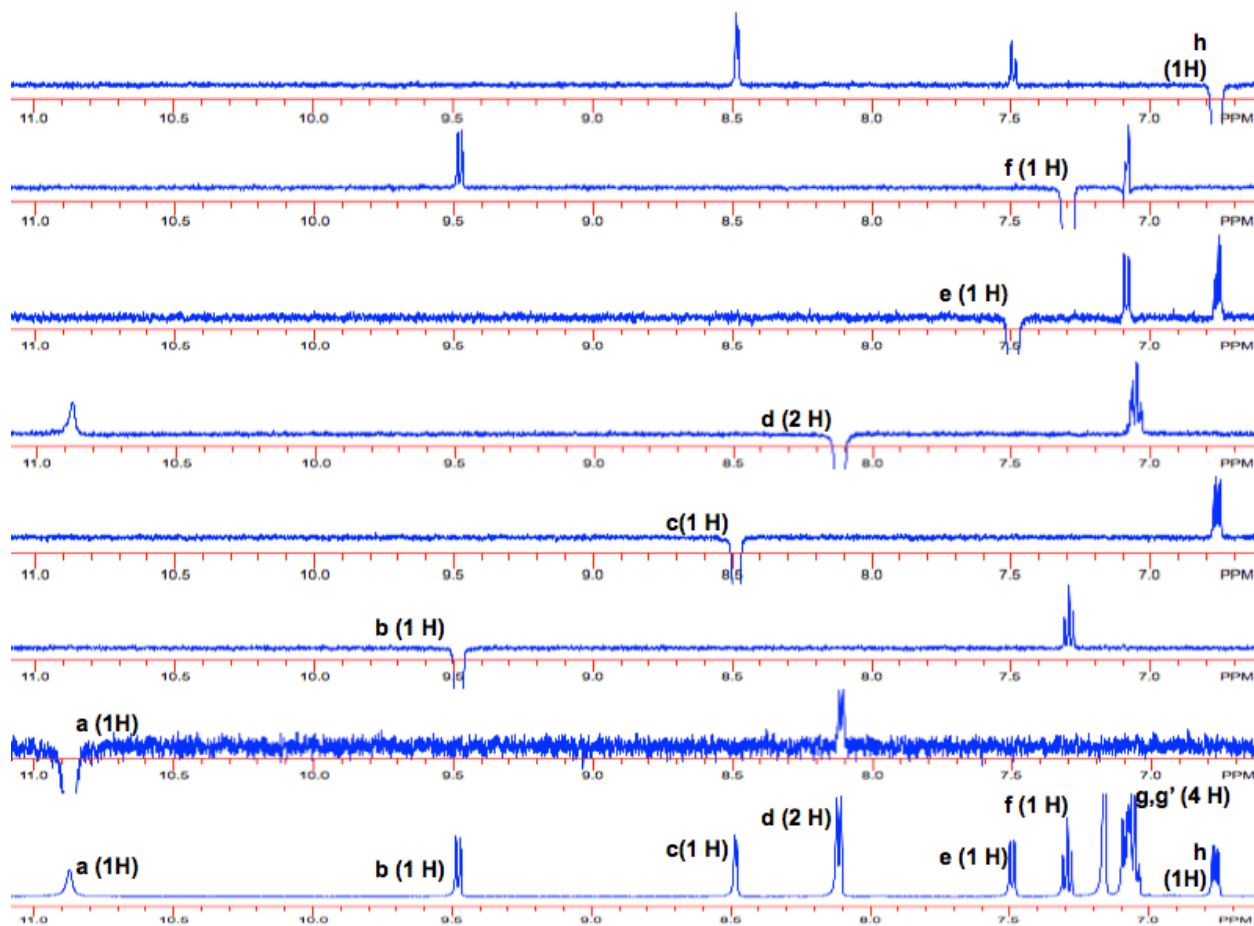
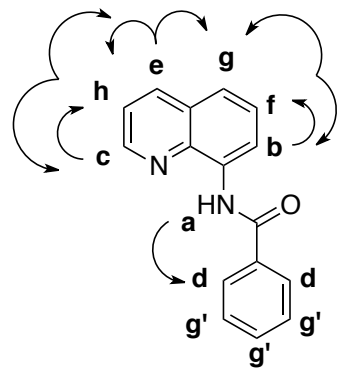


Sample ^1H NMR spectrum for results in Table A2.2, entries 1-2:

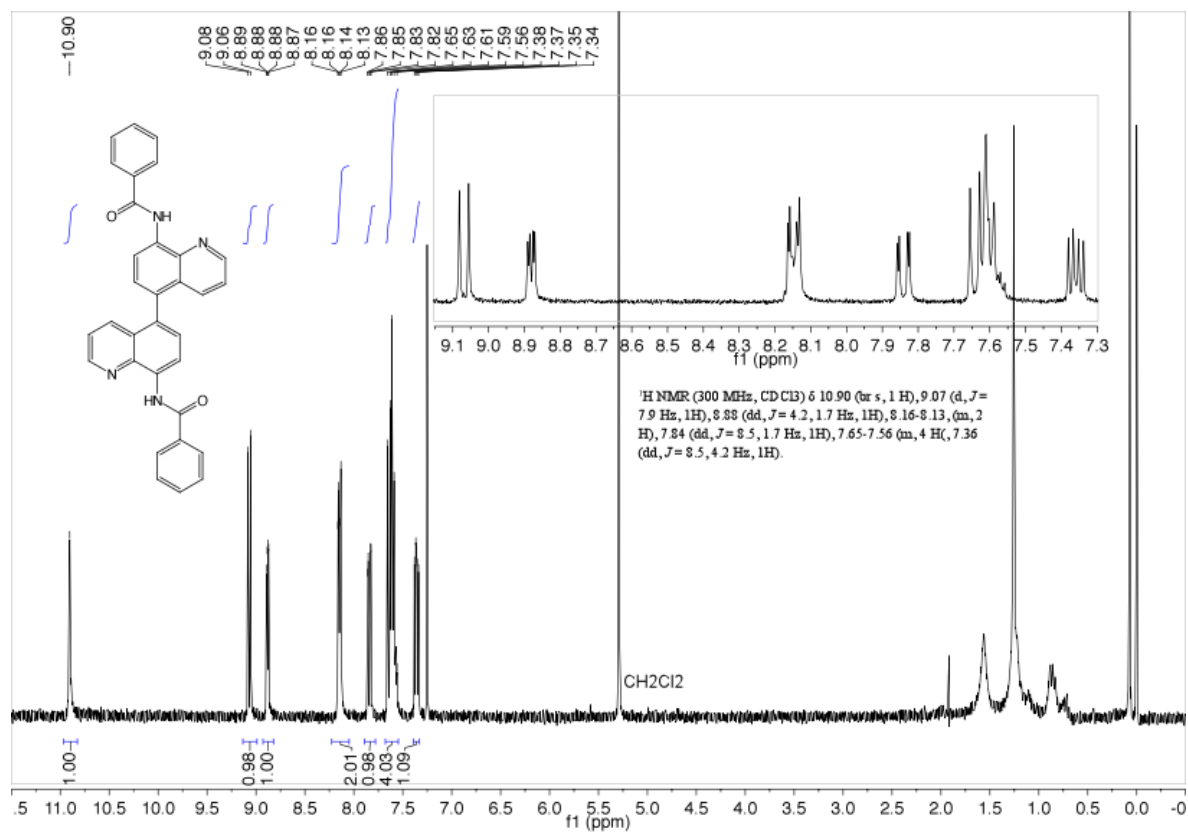


^1H NMR spectrum of 3,5-dichloro-N-(8-quinolinyl)benzamide (Table A2.2):

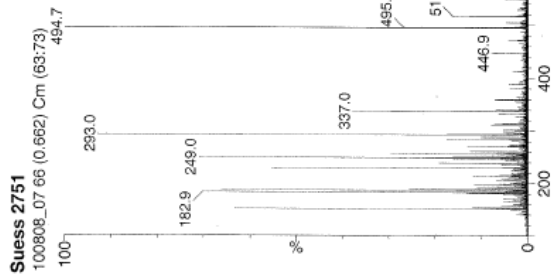
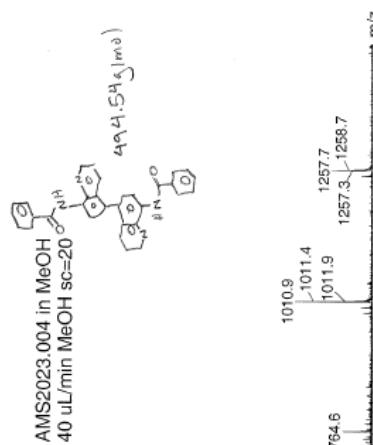
Sample ^1H NMR spectrum for results in Table A2.2, entries 3-4:1D nOe experiment on *N*-(8-quinolinyl)benzamide substrate.



Compared to *N*-(8-quinolinyl)benzamide, the homocoupled product shows changes: (1) Peak b, 9.07 ppm in the product, has lost the *meta* coupling and is a d instead of dd. (2) Peak f has shifted to overlap with the g' peaks. (3) Peak g is gone due to C-C coupling.

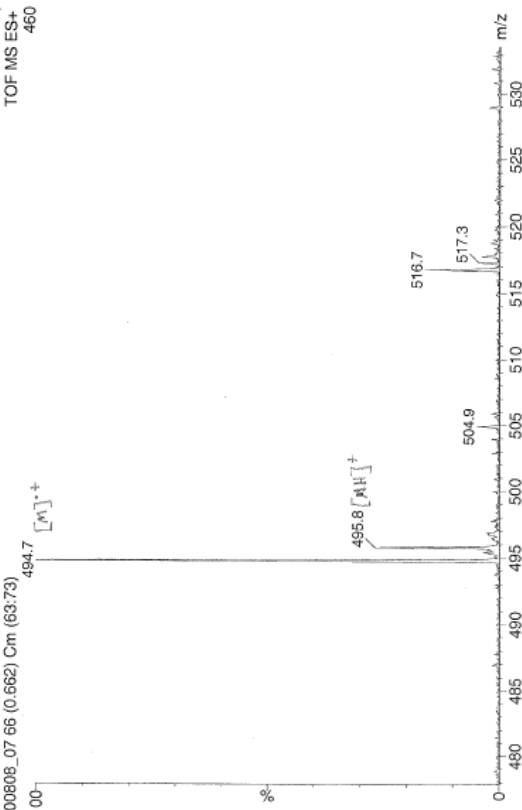


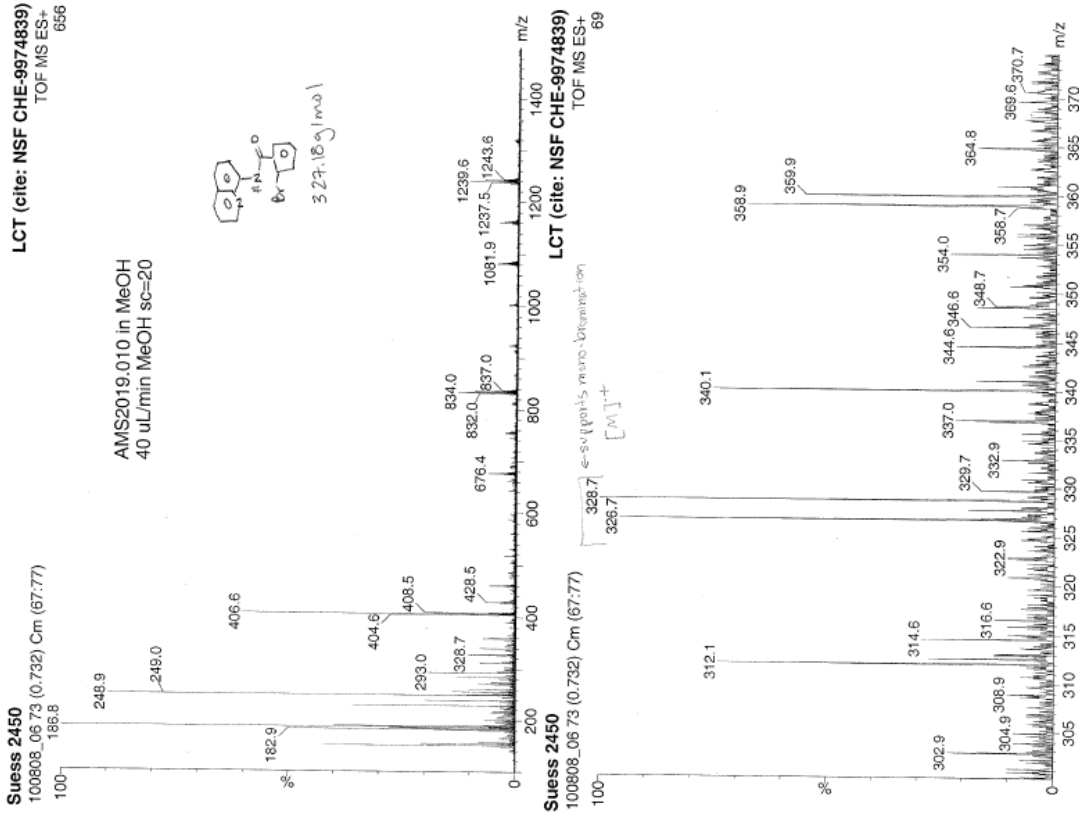
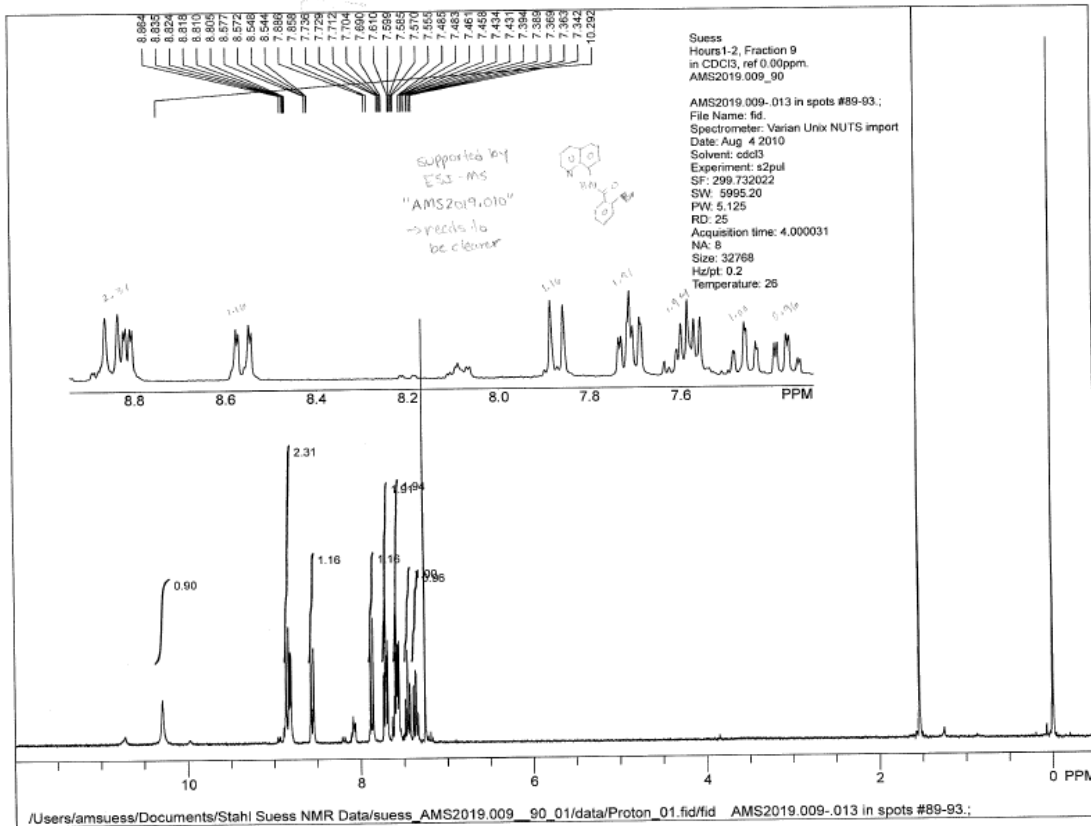
LCT (cite: NSF CHE-9974839)
TOF MS ES+
460

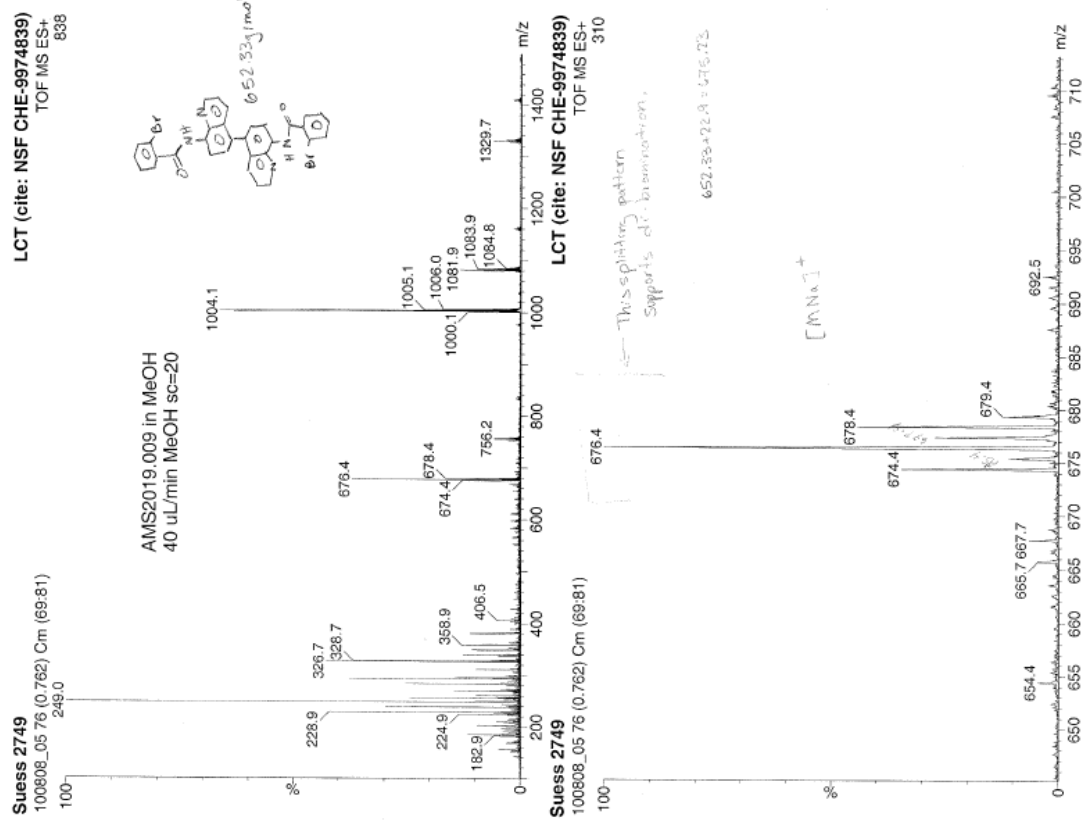
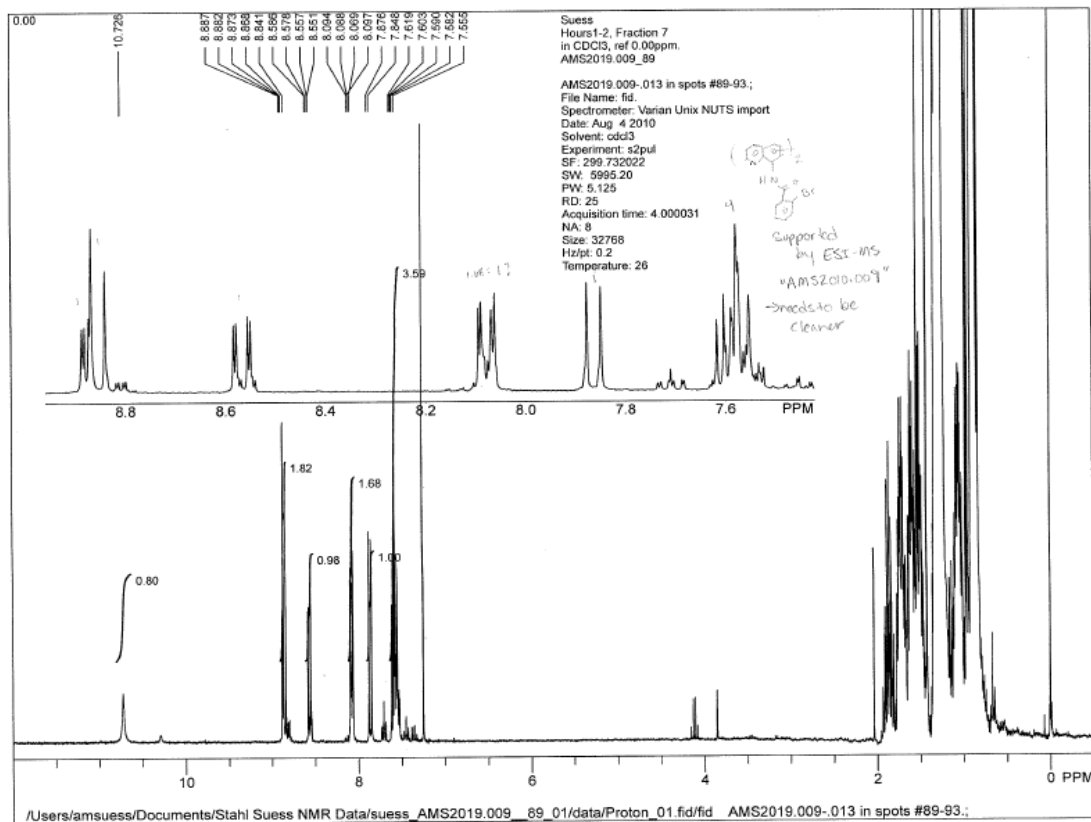


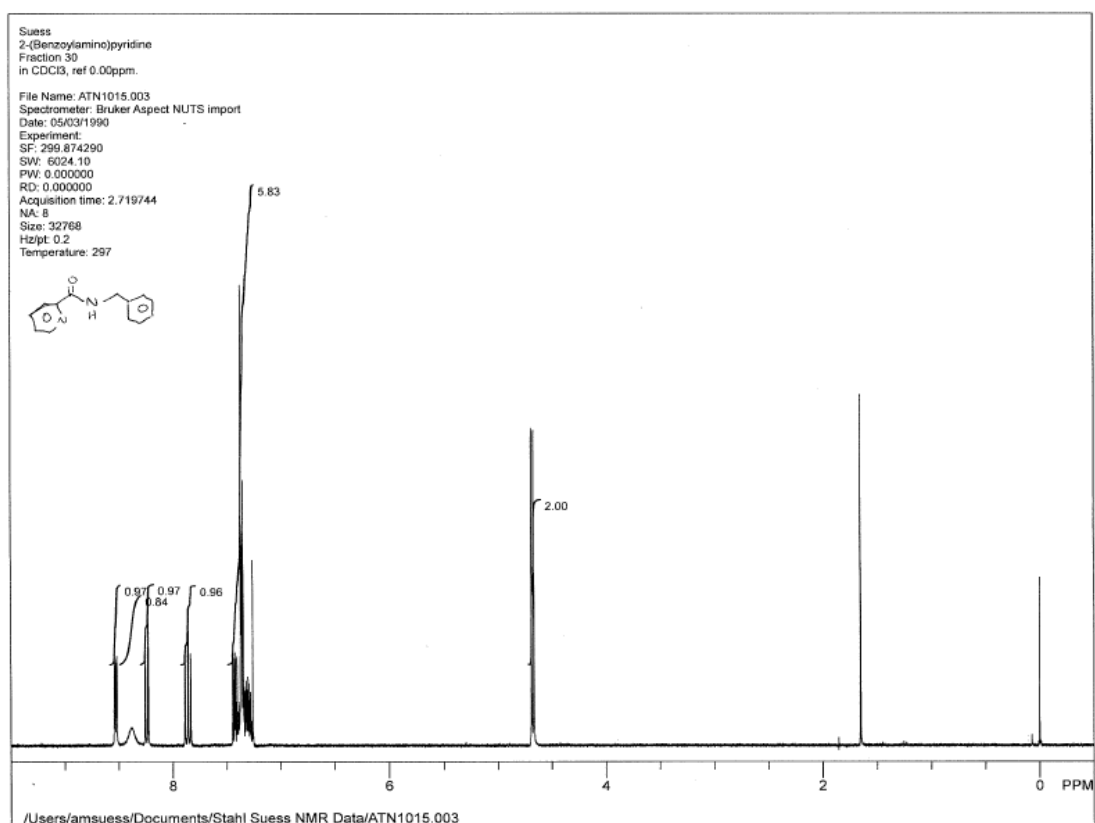
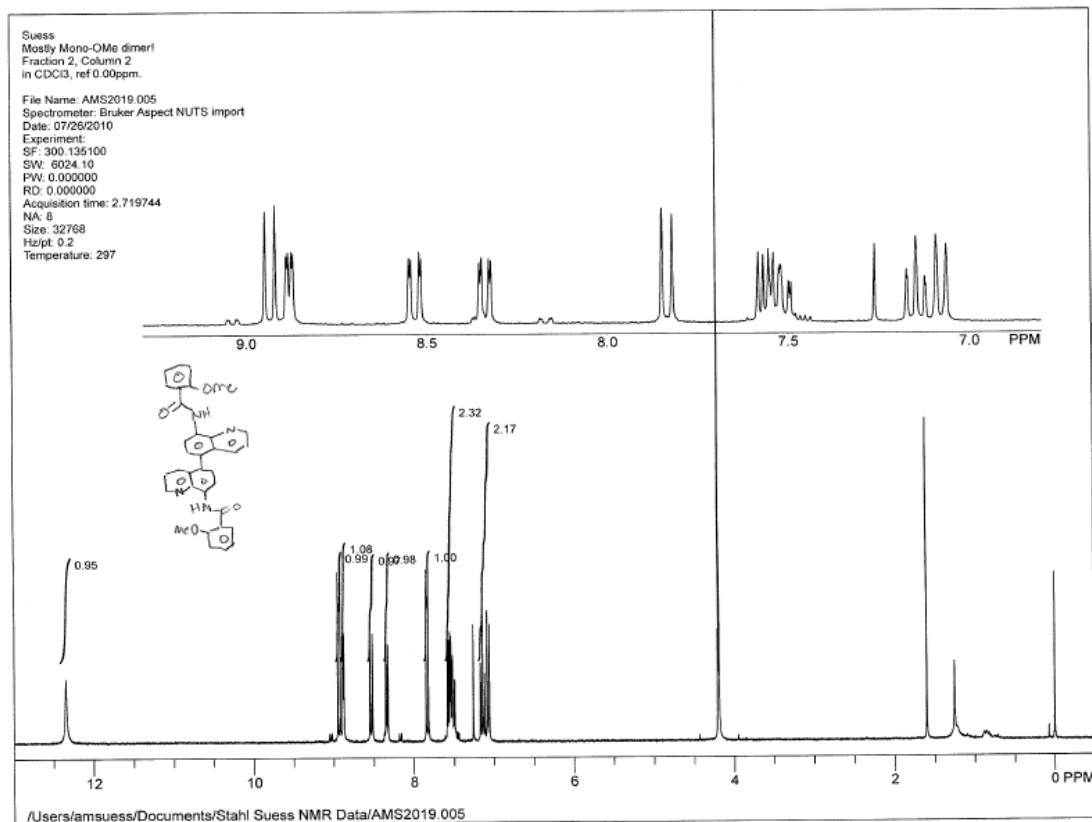
LCT (cite: NSF CHE-9974839)
TOF MS ES+
460

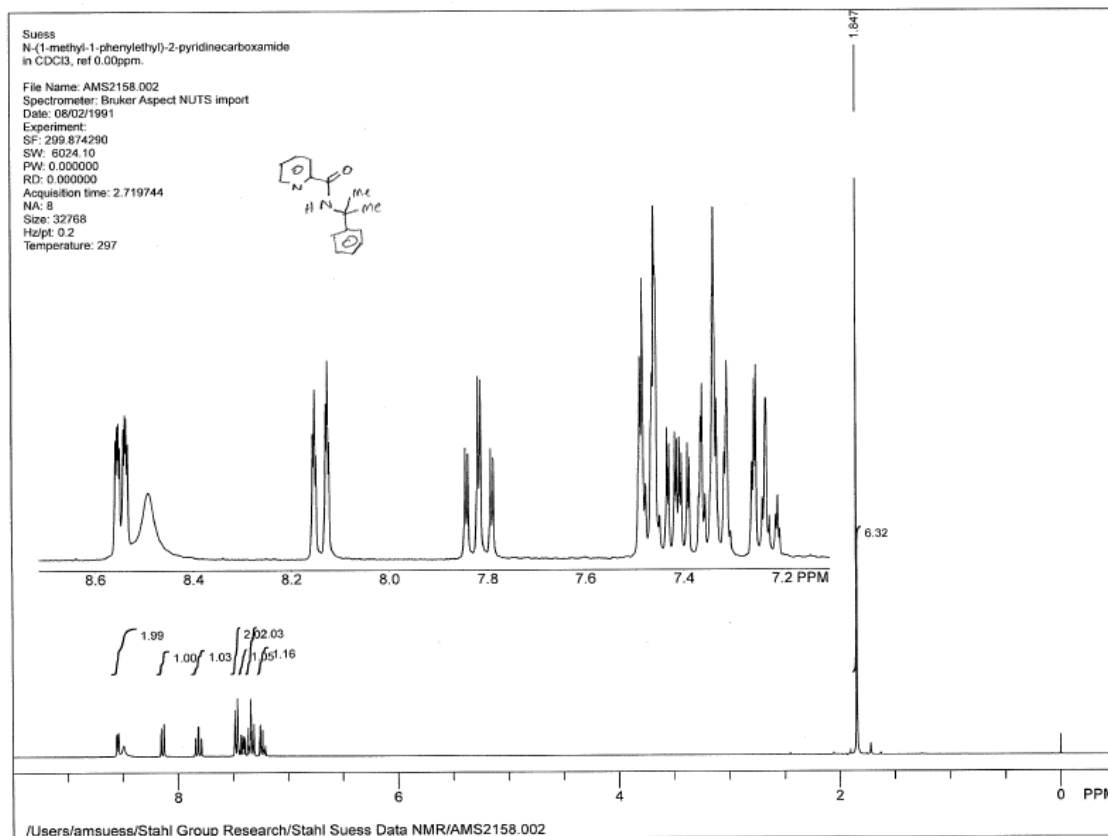
Suess 2751
100808_07.66 (0.662) Cm (63:73)
494.7











X-Ray Structure Data for *N*-(8-Quinoliny)benzamide Cu-Phenoxide, “Stahl 110”:

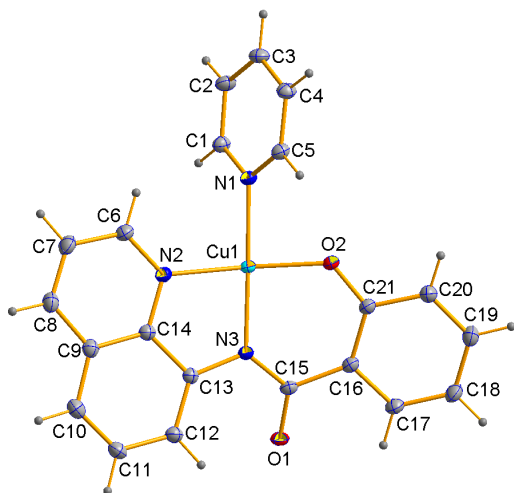


Figure 1. A molecular drawing of stahl110.

Data Collection

A green crystal with approximate dimensions 0.21 x 0.17 x 0.12 mm³ was selected under oil under ambient conditions and attached to the tip of a MiTeGen MicroMount©. The crystal was mounted in a stream of cold nitrogen at 100(1) K and centered in the X-ray beam by using a video camera.

The crystal evaluation and data collection were performed on a Bruker Quazar SMART APEXII diffractometer with Mo K_α ($\lambda = 0.71073 \text{ \AA}$) radiation and the diffractometer to crystal distance of 4.97 cm.

The initial cell constants were obtained from three series of ω scans at different starting angles. Each series consisted of 12 frames collected at intervals of 0.5° in a 10° range about ω with the exposure time of 5 second per frame. The reflections were successfully indexed by an automated indexing routine built in the APEXII program suite. The final cell constants were calculated from a set of 9915 strong reflections from the actual data collection.

The data were collected by using the full sphere data collection routine to survey the reciprocal space to the extent of a full sphere to a resolution of 0.72 Å. A total of 19640 data

were harvested by collecting 6 sets of frames with 0.4° scans in ω and ϕ with exposure times of 13 sec per frame. These highly redundant datasets were corrected for Lorentz and polarization effects. The absorption correction was based on fitting a function to the empirical transmission surface as sampled by multiple equivalent measurements.¹

Structure Solution and Refinement

The systematic absences in the diffraction data were consistent for the space groups $P\bar{1}$ and $P1$. The E -statistics strongly suggested the centrosymmetric space group $P\bar{1}$ that yielded chemically reasonable and computationally stable results of refinement.^{2,3}

A successful solution by the direct methods provided most non-hydrogen atoms from the E -map. The remaining non-hydrogen atoms were located in an alternating series of least-squares cycles and difference Fourier maps. All non-hydrogen atoms were refined with anisotropic displacement coefficients. All hydrogen atoms were included in the structure factor calculations at idealized positions and were allowed to ride on the neighboring atoms with relative isotropic displacement coefficients.

The final least-squares refinement of 244 parameters against 4568 data resulted in residuals R (based on F^2 for $I \geq 2\sigma$) and wR (based on F^2 for all data) of 0.0248 and 0.0692, respectively. The molecular diagram is drawn with 50% probability ellipsoids.⁴

Table 1. Crystal data and structure refinement for stahl110.

Identification code	stahl110	
Empirical formula	C ₂₁ H ₁₅ CuN ₃ O ₂	
Formula weight	404.90	
Temperature	100(2) K	
Wavelength	0.71073 Å	
Crystal system	Triclinic	
Space group	P1	
Unit cell dimensions	a = 8.6311(2) Å	α = 71.5910(10)°.
	b = 8.8889(2) Å	β = 86.1890(10)°.
	c = 11.2764(3) Å	γ = 86.8910(10)°.
Volume	818.54(3) Å ³	
Z	2	
Density (calculated)	1.643 Mg/m ³	
Absorption coefficient	1.357 mm ⁻¹	
F(000)	414	
Crystal size	0.21 x 0.17 x 0.12 mm ³	
Theta range for data collection	2.37 to 29.58°.	
Index ranges	-11 ≤ h ≤ 11, -12 ≤ k ≤ 12, -15 ≤ l ≤ 15	
Reflections collected	19640	
Independent reflections	4568 [R(int) = 0.0191]	
Completeness to theta = 25.00°	99.6 %	
Absorption correction	Analytical with SADABS	
Max. and min. transmission	0.8541 and 0.7637	
Refinement method	Full-matrix least-squares on F ²	
Data / restraints / parameters	4568 / 0 / 244	
Goodness-of-fit on F ²	1.057	
Final R indices [I > 2σ(I)]	R1 = 0.0248, wR2 = 0.0682	
R indices (all data)	R1 = 0.0266, wR2 = 0.0692	
Largest diff. peak and hole	0.498 and -0.296 e.Å ⁻³	

Table 2. Atomic coordinates ($\times 10^4$) and equivalent isotropic displacement parameters ($\text{\AA}^2 \times 10^3$) for stahl110. $U(\text{eq})$ is defined as one third of the trace of the orthogonalized U^{ij} tensor.

	x	y	z	$U(\text{eq})$
Cu(1)	2754(1)	4492(1)	4267(1)	13(1)
O(1)	-383(1)	6784(1)	6021(1)	17(1)
O(2)	3421(1)	3519(1)	5905(1)	20(1)
N(1)	4033(1)	2801(1)	3778(1)	14(1)
N(2)	2625(1)	5978(1)	2521(1)	14(1)
N(3)	1520(1)	6165(1)	4705(1)	13(1)
C(1)	3478(2)	1866(2)	3183(1)	17(1)
C(2)	4371(2)	653(2)	2927(1)	19(1)
C(3)	5896(2)	386(2)	3297(1)	19(1)
C(4)	6469(2)	1365(2)	3896(1)	18(1)
C(5)	5506(2)	2551(2)	4125(1)	16(1)
C(6)	3243(2)	5815(2)	1457(1)	18(1)
C(7)	3131(2)	7011(2)	298(1)	21(1)
C(8)	2374(2)	8412(2)	256(1)	20(1)
C(9)	1666(2)	8620(2)	1370(1)	17(1)
C(10)	832(2)	10016(2)	1402(1)	19(1)
C(11)	176(2)	10107(2)	2521(1)	19(1)
C(12)	314(2)	8848(2)	3647(1)	17(1)
C(13)	1149(2)	7458(2)	3667(1)	13(1)
C(14)	1820(2)	7353(2)	2497(1)	14(1)
C(15)	810(2)	5994(2)	5850(1)	13(1)
C(16)	1538(2)	4853(2)	6961(1)	14(1)
C(17)	967(2)	4955(2)	8128(1)	18(1)
C(18)	1598(2)	4066(2)	9238(1)	21(1)
C(19)	2856(2)	3026(2)	9200(1)	20(1)
C(20)	3437(2)	2882(2)	8072(1)	17(1)
C(21)	2796(2)	3774(2)	6922(1)	15(1)

Table 3. Bond lengths [Å] and angles [°] for stahl110.

Cu(1)-O(2)	1.8898(11)	C(7)-H(7)	0.9500
Cu(1)-N(3)	1.9534(11)	C(8)-C(9)	1.421(2)
Cu(1)-N(2)	2.0009(12)	C(8)-H(8)	0.9500
Cu(1)-N(1)	2.0108(12)	C(9)-C(10)	1.410(2)
O(1)-C(15)	1.2532(17)	C(9)-C(14)	1.4154(19)
O(2)-C(21)	1.3131(16)	C(10)-C(11)	1.372(2)
N(1)-C(5)	1.3414(18)	C(10)-H(10)	0.9500
N(1)-C(1)	1.3454(18)	C(11)-C(12)	1.410(2)
N(2)-C(6)	1.3263(18)	C(11)-H(11)	0.9500
N(2)-C(14)	1.3669(18)	C(12)-C(13)	1.3908(19)
N(3)-C(15)	1.3581(17)	C(12)-H(12)	0.9500
N(3)-C(13)	1.3979(17)	C(13)-C(14)	1.4335(19)
C(1)-C(2)	1.384(2)	C(15)-C(16)	1.4927(19)
C(1)-H(1)	0.9500	C(16)-C(17)	1.4035(18)
C(2)-C(3)	1.392(2)	C(16)-C(21)	1.4168(19)
C(2)-H(2)	0.9500	C(17)-C(18)	1.381(2)
C(3)-C(4)	1.386(2)	C(17)-H(17)	0.9500
C(3)-H(3)	0.9500	C(18)-C(19)	1.394(2)
C(4)-C(5)	1.385(2)	C(18)-H(18)	0.9500
C(4)-H(4)	0.9500	C(19)-C(20)	1.377(2)
C(5)-H(5)	0.9500	C(19)-H(19)	0.9500
C(6)-C(7)	1.405(2)	C(20)-C(21)	1.4198(19)
C(6)-H(6)	0.9500	C(20)-H(20)	0.9500
C(7)-C(8)	1.363(2)		
O(2)-Cu(1)-N(3)	94.16(5)	N(1)-C(5)-H(5)	118.8
O(2)-Cu(1)-N(2)	161.11(5)	C(4)-C(5)-H(5)	118.8
N(3)-Cu(1)-N(2)	83.52(5)	N(2)-C(6)-C(7)	122.90(14)
O(2)-Cu(1)-N(1)	86.90(5)	N(2)-C(6)-H(6)	118.6
N(3)-Cu(1)-N(1)	178.77(5)	C(7)-C(6)-H(6)	118.6
N(2)-Cu(1)-N(1)	95.28(5)	C(8)-C(7)-C(6)	119.13(14)
C(21)-O(2)-Cu(1)	125.48(9)	C(8)-C(7)-H(7)	120.4
C(5)-N(1)-C(1)	118.57(12)	C(6)-C(7)-H(7)	120.4
C(5)-N(1)-Cu(1)	117.38(9)	C(7)-C(8)-C(9)	119.70(14)
C(1)-N(1)-Cu(1)	123.96(10)	C(7)-C(8)-H(8)	120.1
C(6)-N(2)-C(14)	119.10(12)	C(9)-C(8)-H(8)	120.1
C(6)-N(2)-Cu(1)	129.24(10)	C(10)-C(9)-C(14)	119.07(13)
C(14)-N(2)-Cu(1)	111.61(9)	C(10)-C(9)-C(8)	123.28(13)
C(15)-N(3)-C(13)	121.07(12)	C(14)-C(9)-C(8)	117.66(13)
C(15)-N(3)-Cu(1)	124.32(9)	C(11)-C(10)-C(9)	119.27(13)
C(13)-N(3)-Cu(1)	113.32(9)	C(11)-C(10)-H(10)	120.4
N(1)-C(1)-C(2)	122.22(13)	C(9)-C(10)-H(10)	120.4
N(1)-C(1)-H(1)	118.9	C(10)-C(11)-C(12)	122.07(14)
C(2)-C(1)-H(1)	118.9	C(10)-C(11)-H(11)	119.0
C(1)-C(2)-C(3)	119.15(13)	C(12)-C(11)-H(11)	119.0
C(1)-C(2)-H(2)	120.4	C(13)-C(12)-C(11)	120.80(13)
C(3)-C(2)-H(2)	120.4	C(13)-C(12)-H(12)	119.6
C(4)-C(3)-C(2)	118.43(13)	C(11)-C(12)-H(12)	119.6
C(4)-C(3)-H(3)	120.8	C(12)-C(13)-N(3)	128.22(13)
C(2)-C(3)-H(3)	120.8	C(12)-C(13)-C(14)	117.21(12)
C(5)-C(4)-C(3)	119.24(13)	N(3)-C(13)-C(14)	114.42(12)
C(5)-C(4)-H(4)	120.4	N(2)-C(14)-C(9)	121.48(13)
C(3)-C(4)-H(4)	120.4	N(2)-C(14)-C(13)	116.96(12)
N(1)-C(5)-C(4)	122.37(13)	C(9)-C(14)-C(13)	121.56(13)

O(1)-C(15)-N(3)	123.49(13)	C(19)-C(18)-H(18)	120.6
O(1)-C(15)-C(16)	118.74(12)	C(20)-C(19)-C(18)	120.12(14)
N(3)-C(15)-C(16)	117.71(12)	C(20)-C(19)-H(19)	119.9
C(17)-C(16)-C(21)	118.65(13)	C(18)-C(19)-H(19)	119.9
C(17)-C(16)-C(15)	115.60(12)	C(19)-C(20)-C(21)	121.96(14)
C(21)-C(16)-C(15)	125.62(12)	C(19)-C(20)-H(20)	119.0
C(18)-C(17)-C(16)	122.61(14)	C(21)-C(20)-H(20)	119.0
C(18)-C(17)-H(17)	118.7	O(2)-C(21)-C(16)	125.41(13)
C(16)-C(17)-H(17)	118.7	O(2)-C(21)-C(20)	116.81(13)
C(17)-C(18)-C(19)	118.86(13)	C(16)-C(21)-C(20)	117.78(12)
C(17)-C(18)-H(18)	120.6		

Symmetry transformations used to generate equivalent atoms:

Table 4. Anisotropic displacement parameters ($\text{\AA}^2 \times 10^3$) for stahl110. The anisotropic displacement factor exponent takes the form: $-2\pi^2 [h^2 a^{*2} U^{11} + \dots + 2 h k a^* b^* U^{12}]$

	U^{11}	U^{22}	U^{33}	U^{23}	U^{13}	U^{12}
Cu(1)	14(1)	13(1)	13(1)	-6(1)	0(1)	3(1)
O(1)	15(1)	17(1)	19(1)	-8(1)	2(1)	3(1)
O(2)	24(1)	22(1)	14(1)	-8(1)	-1(1)	10(1)
N(1)	15(1)	14(1)	14(1)	-6(1)	1(1)	2(1)
N(2)	14(1)	15(1)	15(1)	-6(1)	0(1)	0(1)
N(3)	13(1)	13(1)	14(1)	-6(1)	0(1)	1(1)
C(1)	15(1)	19(1)	18(1)	-9(1)	-2(1)	1(1)
C(2)	19(1)	19(1)	23(1)	-12(1)	-1(1)	1(1)
C(3)	19(1)	17(1)	23(1)	-9(1)	2(1)	3(1)
C(4)	14(1)	21(1)	21(1)	-9(1)	-1(1)	2(1)
C(5)	15(1)	19(1)	18(1)	-9(1)	0(1)	0(1)
C(6)	19(1)	20(1)	16(1)	-8(1)	1(1)	1(1)
C(7)	22(1)	26(1)	14(1)	-7(1)	2(1)	0(1)
C(8)	19(1)	24(1)	15(1)	-3(1)	-1(1)	-1(1)
C(9)	15(1)	18(1)	16(1)	-5(1)	-2(1)	-1(1)
C(10)	18(1)	17(1)	20(1)	-3(1)	-4(1)	1(1)
C(11)	18(1)	15(1)	23(1)	-5(1)	-4(1)	2(1)
C(12)	17(1)	16(1)	19(1)	-7(1)	-1(1)	1(1)
C(13)	12(1)	14(1)	15(1)	-5(1)	-2(1)	-1(1)
C(14)	12(1)	15(1)	16(1)	-6(1)	-2(1)	0(1)
C(15)	13(1)	14(1)	16(1)	-7(1)	1(1)	-1(1)
C(16)	14(1)	14(1)	14(1)	-6(1)	1(1)	-2(1)
C(17)	17(1)	20(1)	17(1)	-8(1)	2(1)	1(1)
C(18)	23(1)	27(1)	14(1)	-8(1)	2(1)	0(1)
C(19)	21(1)	23(1)	14(1)	-4(1)	-1(1)	-2(1)
C(20)	18(1)	18(1)	17(1)	-6(1)	-2(1)	2(1)
C(21)	16(1)	15(1)	14(1)	-6(1)	0(1)	0(1)

Table 5. Hydrogen coordinates ($\times 10^4$) and isotropic displacement parameters ($\text{\AA}^2 \times 10^{-3}$) for stahl110.

	x	y	z	U(eq)
H(1)	2438	2043	2929	20
H(2)	3950	11	2504	23
H(3)	6528	-448	3142	23
H(4)	7510	1223	4146	22
H(5)	5903	3211	4543	20
H(6)	3784	4848	1480	21
H(7)	3578	6845	-445	25
H(8)	2320	9246	-516	24
H(10)	724	10884	657	23
H(11)	-389	11049	2537	22
H(12)	-170	8950	4400	20
H(17)	113	5666	8156	21
H(18)	1183	4160	10014	25
H(19)	3312	2415	9954	24
H(20)	4291	2164	8064	21

Table 6. Torsion angles [°] for stahl110.

N(3)-Cu(1)-O(2)-C(21)	15.74(12)	N(3)-C(13)-C(14)-N(2)	4.89(17)
N(2)-Cu(1)-O(2)-C(21)	97.86(18)	C(12)-C(13)-C(14)-C(9)	1.12(19)
N(1)-Cu(1)-O(2)-C(21)	-164.89(12)	N(3)-C(13)-C(14)-C(9)	-174.72(12)
O(2)-Cu(1)-N(1)-C(5)	-49.74(11)	C(13)-N(3)-C(15)-O(1)	13.0(2)
N(3)-Cu(1)-N(1)-C(5)	100(2)	Cu(1)-N(3)-C(15)-O(1)	-153.15(11)
N(2)-Cu(1)-N(1)-C(5)	111.44(11)	C(13)-N(3)-C(15)-C(16)	-164.23(12)
O(2)-Cu(1)-N(1)-C(1)	126.90(12)	Cu(1)-N(3)-C(15)-C(16)	29.61(16)
N(3)-Cu(1)-N(1)-C(1)	-84(2)	O(1)-C(15)-C(16)-C(17)	-10.31(18)
N(2)-Cu(1)-N(1)-C(1)	-71.91(12)	N(3)-C(15)-C(16)-C(17)	167.06(12)
O(2)-Cu(1)-N(2)-C(6)	94.64(18)	O(1)-C(15)-C(16)-C(21)	173.93(13)
N(3)-Cu(1)-N(2)-C(6)	178.52(13)	N(3)-C(15)-C(16)-C(21)	-8.7(2)
N(1)-Cu(1)-N(2)-C(6)	-1.23(13)	C(21)-C(16)-C(17)-C(18)	1.0(2)
O(2)-Cu(1)-N(2)-C(14)	-82.66(17)	C(15)-C(16)-C(17)-C(18)	-175.05(13)
N(3)-Cu(1)-N(2)-C(14)	1.22(9)	C(16)-C(17)-C(18)-C(19)	0.2(2)
N(1)-Cu(1)-N(2)-C(14)	-178.52(9)	C(17)-C(18)-C(19)-C(20)	-0.8(2)
O(2)-Cu(1)-N(3)-C(15)	-30.36(11)	C(18)-C(19)-C(20)-C(21)	0.3(2)
N(2)-Cu(1)-N(3)-C(15)	168.47(11)	Cu(1)-O(2)-C(21)-C(16)	-1.7(2)
N(1)-Cu(1)-N(3)-C(15)	-180(100)	Cu(1)-O(2)-C(21)-C(20)	177.88(10)
O(2)-Cu(1)-N(3)-C(13)	162.54(9)	C(17)-C(16)-C(21)-O(2)	178.01(13)
N(2)-Cu(1)-N(3)-C(13)	1.37(9)	C(15)-C(16)-C(21)-O(2)	-6.3(2)
N(1)-Cu(1)-N(3)-C(13)	13(2)	C(17)-C(16)-C(21)-C(20)	-1.5(2)
C(5)-N(1)-C(1)-C(2)	0.5(2)	C(15)-C(16)-C(21)-C(20)	174.10(13)
Cu(1)-N(1)-C(1)-C(2)	-176.15(11)	C(19)-C(20)-C(21)-O(2)	-178.66(14)
N(1)-C(1)-C(2)-C(3)	0.1(2)	C(19)-C(20)-C(21)-C(16)	0.9(2)
C(1)-C(2)-C(3)-C(4)	-0.9(2)		
C(2)-C(3)-C(4)-C(5)	1.1(2)		
C(1)-N(1)-C(5)-C(4)	-0.2(2)		
Cu(1)-N(1)-C(5)-C(4)	176.63(11)		
C(3)-C(4)-C(5)-N(1)	-0.6(2)		
C(14)-N(2)-C(6)-C(7)	1.1(2)		
Cu(1)-N(2)-C(6)-C(7)	-176.01(11)		
N(2)-C(6)-C(7)-C(8)	0.8(2)		
C(6)-C(7)-C(8)-C(9)	-2.2(2)		
C(7)-C(8)-C(9)-C(10)	-178.48(14)		
C(7)-C(8)-C(9)-C(14)	1.7(2)		
C(14)-C(9)-C(10)-C(11)	-0.7(2)		
C(8)-C(9)-C(10)-C(11)	179.49(14)		
C(9)-C(10)-C(11)-C(12)	0.2(2)		
C(10)-C(11)-C(12)-C(13)	0.9(2)		
C(11)-C(12)-C(13)-N(3)	173.61(13)		
C(11)-C(12)-C(13)-C(14)	-1.6(2)		
C(15)-N(3)-C(13)-C(12)	13.5(2)		
Cu(1)-N(3)-C(13)-C(12)	-178.94(12)		
C(15)-N(3)-C(13)-C(14)	-171.23(12)		
Cu(1)-N(3)-C(13)-C(14)	-3.66(14)		
C(6)-N(2)-C(14)-C(9)	-1.6(2)		
Cu(1)-N(2)-C(14)-C(9)	175.98(10)		
C(6)-N(2)-C(14)-C(13)	178.77(12)		
Cu(1)-N(2)-C(14)-C(13)	-3.63(15)		
C(10)-C(9)-C(14)-N(2)	-179.60(13)		
C(8)-C(9)-C(14)-N(2)	0.2(2)		
C(10)-C(9)-C(14)-C(13)	0.0(2)		
C(8)-C(9)-C(14)-C(13)	179.84(13)		
C(12)-C(13)-C(14)-N(2)	-179.27(12)		

Symmetry transformations used to generate equivalent atoms:

X-Ray Structure Data for *N*-(8-Quinoliny)benzamide Cu-Dimer, “Stahl 114”:

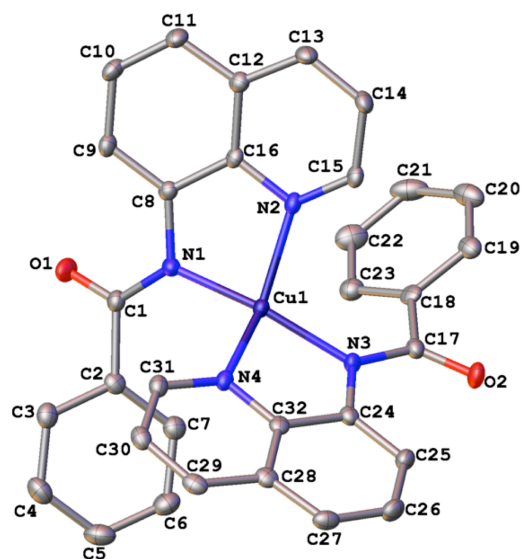


Figure 1. A molecular drawing of Stahl114. All H atoms are omitted.

Data Collection

A red crystal with approximate dimensions 0.18 x 0.14 x 0.10 mm³ was selected under oil under ambient conditions and attached to the tip of a MiTeGen MicroMount©. The crystal was mounted in a stream of cold nitrogen at 100(1) K and centered in the X-ray beam by using a video camera. The crystal evaluation and data collection were performed on a Bruker Quazar SMART APEXII diffractometer with Mo K_α ($\lambda = 0.71073 \text{ \AA}$) radiation and the diffractometer to crystal distance of 4.95 cm.

The initial cell constants were obtained from three series of ω scans at different starting angles. Each series consisted of 12 frames collected at intervals of 0.5° in a 6° range about ω with the exposure time of 10 seconds per frame. The reflections were successfully indexed by an automated indexing routine built in the APEXII program suite. The final cell constants were calculated from a set of 4615 strong reflections from the actual data collection.

The data were collected by using the full sphere data collection routine to survey the reciprocal space to the extent of a full sphere to a resolution of 0.70 Å. A total of 14359 data

were harvested by collecting 4 sets of frames with 0.5° scans in ω and ϕ with exposure times of 20 sec per frame. These highly redundant datasets were corrected for Lorentz and polarization effects. The absorption correction was based on fitting a function to the empirical transmission surface as sampled by multiple equivalent measurements.¹

Structure Solution and Refinement

The systematic absences in the diffraction data were consistent for the space groups $P\bar{1}$ and $P1$. The E -statistics suggested the centrosymmetric space group $P\bar{1}$ that yielded chemically reasonable and computationally stable results of refinement.^{2,3,5}

A successful solution by charge-flipping provided all non-hydrogen atoms from the E -map. All non-hydrogen atoms were refined with anisotropic displacement coefficients. All hydrogen atoms were included in the structure factor calculation at idealized positions and were allowed to ride on the neighboring atoms with relative isotropic displacement coefficients.

The final least-squares refinement of 352 parameters against 4680 data resulted in residuals R (based on F^2 for $I \geq 2\sigma$) and wR (based on F^2 for all data) of 0.0368 and 0.0916, respectively. The final difference Fourier map was featureless. The molecular diagram is drawn with 50% probability ellipsoids.

Table 1. Crystal data and structure refinement for stahl114.

Identification code	stahl114	
Empirical formula	$C_{32} H_{22} Cu N_4 O_2$	
Formula weight	558.08	
Temperature	100(2) K	
Wavelength	0.71073 Å	
Crystal system	Triclinic	
Space group	$P\bar{1}$	
Unit cell dimensions	a = 9.8016(18) Å	$\alpha = 79.882(4)^\circ$.
	b = 10.3701(19) Å	$\beta = 69.549(2)^\circ$.
	c = 13.947(3) Å	$\gamma = 67.155(2)^\circ$.
Volume	1222.8(4) Å ³	
Z	2	
Density (calculated)	1.516 Mg/m ³	
Absorption coefficient	0.933 mm ⁻¹	
F(000)	574	
Crystal size	0.18 x 0.14 x 0.10 mm ³	
Theta range for data collection	1.56 to 25.84°.	
Index ranges	-12 ≤ h ≤ 12, -12 ≤ k ≤ 12, -17 ≤ l ≤ 17	
Reflections collected	14359	
Independent reflections	4680 [R(int) = 0.0378]	
Completeness to theta = 25.00°	99.6 %	
Absorption correction	Numerical with SADABS	
Max. and min. transmission	0.9125 and 0.8500	
Refinement method	Full-matrix least-squares on F ²	
Data / restraints / parameters	4680 / 0 / 352	
Goodness-of-fit on F ²	0.985	
Final R indices [I > 2σ(I)]	R1 = 0.0368, wR2 = 0.0847	
R indices (all data)	R1 = 0.0501, wR2 = 0.0916	
Largest diff. peak and hole	0.583 and -0.593 e.Å ⁻³	

Table 2. Atomic coordinates ($\times 10^4$) and equivalent isotropic displacement parameters ($\text{\AA}^2 \times 10^3$) for stahl114. $U(\text{eq})$ is defined as one third of the trace of the orthogonalized U^{ij} tensor.

	x	y	z	U(eq)
Cu(1)	900(1)	2111(1)	7898(1)	13(1)
O(1)	1367(2)	260(2)	5351(1)	22(1)
O(2)	2110(2)	4762(2)	9076(1)	22(1)
N(1)	558(2)	1417(2)	6829(2)	14(1)
N(2)	-1188(2)	3598(2)	7986(2)	14(1)
N(3)	1789(2)	2883(2)	8616(2)	14(1)
N(4)	1648(2)	368(2)	8716(2)	14(1)
C(1)	1609(3)	490(3)	6102(2)	15(1)
C(2)	3180(3)	-355(3)	6236(2)	16(1)
C(3)	3731(3)	-1784(3)	6074(2)	19(1)
C(4)	5181(3)	-2645(3)	6150(2)	24(1)
C(5)	6104(3)	-2091(3)	6382(2)	26(1)
C(6)	5577(3)	-684(3)	6537(2)	24(1)
C(7)	4114(3)	190(3)	6466(2)	18(1)
C(8)	-990(3)	2066(3)	6814(2)	14(1)
C(9)	-1741(3)	1654(3)	6308(2)	16(1)
C(10)	-3325(3)	2397(3)	6400(2)	19(1)
C(11)	-4203(3)	3529(3)	6995(2)	18(1)
C(12)	-3511(3)	3964(3)	7550(2)	16(1)
C(13)	-4334(3)	5073(3)	8222(2)	18(1)
C(14)	-3581(3)	5409(3)	8752(2)	18(1)
C(15)	-1993(3)	4640(3)	8612(2)	15(1)
C(16)	-1910(3)	3240(3)	7446(2)	13(1)
C(17)	1789(3)	4209(3)	8503(2)	16(1)
C(18)	1339(3)	5082(3)	7607(2)	16(1)
C(19)	475(3)	6507(3)	7742(2)	20(1)
C(20)	-10(3)	7366(3)	6964(2)	28(1)
C(21)	377(3)	6829(3)	6022(2)	30(1)
C(22)	1272(3)	5435(3)	5863(2)	27(1)
C(23)	1748(3)	4559(3)	6650(2)	20(1)
C(24)	2282(3)	1944(3)	9390(2)	14(1)
C(25)	2817(3)	2173(3)	10120(2)	18(1)
C(26)	3265(3)	1114(3)	10850(2)	21(1)
C(27)	3234(3)	-191(3)	10868(2)	19(1)
C(28)	2718(3)	-488(3)	10128(2)	16(1)
C(29)	2666(3)	-1805(3)	10055(2)	18(1)
C(30)	2067(3)	-1995(3)	9360(2)	18(1)
C(31)	1557(3)	-868(3)	8700(2)	16(1)
C(32)	2222(3)	585(3)	9416(2)	14(1)

Table 3. Bond lengths [Å] and angles [°] for stahl114.

Cu(1)-N(1)	1.941(2)	C(12)-C(13)	1.408(4)
Cu(1)-N(3)	1.959(2)	C(12)-C(16)	1.418(3)
Cu(1)-N(4)	1.984(2)	C(13)-C(14)	1.373(4)
Cu(1)-N(2)	2.006(2)	C(13)-H(13)	0.9500
O(1)-C(1)	1.231(3)	C(14)-C(15)	1.405(3)
O(2)-C(17)	1.243(3)	C(14)-H(14)	0.9500
N(1)-C(1)	1.362(3)	C(15)-H(15)	0.9500
N(1)-C(8)	1.407(3)	C(17)-C(18)	1.501(4)
N(2)-C(15)	1.320(3)	C(18)-C(23)	1.396(4)
N(2)-C(16)	1.371(3)	C(18)-C(19)	1.397(4)
N(3)-C(17)	1.356(3)	C(19)-C(20)	1.376(4)
N(3)-C(24)	1.406(3)	C(19)-H(19)	0.9500
N(4)-C(31)	1.323(3)	C(20)-C(21)	1.388(5)
N(4)-C(32)	1.371(3)	C(20)-H(20)	0.9500
C(1)-C(2)	1.506(3)	C(21)-C(22)	1.378(4)
C(2)-C(7)	1.389(4)	C(21)-H(21)	0.9500
C(2)-C(3)	1.396(4)	C(22)-C(23)	1.387(4)
C(3)-C(4)	1.383(4)	C(22)-H(22)	0.9500
C(3)-H(3)	0.9500	C(23)-H(23)	0.9500
C(4)-C(5)	1.387(4)	C(24)-C(25)	1.387(4)
C(4)-H(4)	0.9500	C(24)-C(32)	1.426(3)
C(5)-C(6)	1.375(4)	C(25)-C(26)	1.407(4)
C(5)-H(5)	0.9500	C(25)-H(25)	0.9500
C(6)-C(7)	1.395(4)	C(26)-C(27)	1.361(4)
C(6)-H(6)	0.9500	C(26)-H(26)	0.9500
C(7)-H(7)	0.9500	C(27)-C(28)	1.419(4)
C(8)-C(9)	1.391(3)	C(27)-H(27)	0.9500
C(8)-C(16)	1.429(3)	C(28)-C(29)	1.408(4)
C(9)-C(10)	1.410(4)	C(28)-C(32)	1.411(4)
C(9)-H(9)	0.9500	C(29)-C(30)	1.371(4)
C(10)-C(11)	1.366(4)	C(29)-H(29)	0.9500
C(10)-H(10)	0.9500	C(30)-C(31)	1.397(4)
C(11)-C(12)	1.411(4)	C(30)-H(30)	0.9500
C(11)-H(11)	0.9500	C(31)-H(31)	0.9500
N(1)-Cu(1)-N(3)	162.03(8)	O(1)-C(1)-C(2)	116.9(2)
N(1)-Cu(1)-N(4)	102.03(9)	N(1)-C(1)-C(2)	117.9(2)
N(3)-Cu(1)-N(4)	84.14(9)	C(7)-C(2)-C(3)	119.0(2)
N(1)-Cu(1)-N(2)	84.15(8)	C(7)-C(2)-C(1)	125.0(2)
N(3)-Cu(1)-N(2)	103.70(8)	C(3)-C(2)-C(1)	115.9(2)
N(4)-Cu(1)-N(2)	134.49(8)	C(4)-C(3)-C(2)	120.4(2)
C(1)-N(1)-C(8)	119.4(2)	C(4)-C(3)-H(3)	119.8
C(1)-N(1)-Cu(1)	128.80(17)	C(2)-C(3)-H(3)	119.8
C(8)-N(1)-Cu(1)	111.72(16)	C(3)-C(4)-C(5)	120.2(3)
C(15)-N(2)-C(16)	119.5(2)	C(3)-C(4)-H(4)	119.9
C(15)-N(2)-Cu(1)	128.82(17)	C(5)-C(4)-H(4)	119.9
C(16)-N(2)-Cu(1)	110.22(16)	C(6)-C(5)-C(4)	119.9(3)
C(17)-N(3)-C(24)	121.3(2)	C(6)-C(5)-H(5)	120.0
C(17)-N(3)-Cu(1)	126.50(17)	C(4)-C(5)-H(5)	120.0
C(24)-N(3)-Cu(1)	111.75(15)	C(5)-C(6)-C(7)	120.2(3)
C(31)-N(4)-C(32)	119.9(2)	C(5)-C(6)-H(6)	119.9
C(31)-N(4)-Cu(1)	128.46(18)	C(7)-C(6)-H(6)	119.9
C(32)-N(4)-Cu(1)	111.52(16)	C(2)-C(7)-C(6)	120.3(2)
O(1)-C(1)-N(1)	125.2(2)	C(2)-C(7)-H(7)	119.9

C(6)-C(7)-H(7)	119.9	C(19)-C(20)-H(20)	119.9
C(9)-C(8)-N(1)	127.8(2)	C(21)-C(20)-H(20)	119.9
C(9)-C(8)-C(16)	116.9(2)	C(22)-C(21)-C(20)	119.7(3)
N(1)-C(8)-C(16)	115.2(2)	C(22)-C(21)-H(21)	120.1
C(8)-C(9)-C(10)	120.9(2)	C(20)-C(21)-H(21)	120.1
C(8)-C(9)-H(9)	119.6	C(21)-C(22)-C(23)	120.3(3)
C(10)-C(9)-H(9)	119.6	C(21)-C(22)-H(22)	119.8
C(11)-C(10)-C(9)	122.4(2)	C(23)-C(22)-H(22)	119.8
C(11)-C(10)-H(10)	118.8	C(22)-C(23)-C(18)	120.4(3)
C(9)-C(10)-H(10)	118.8	C(22)-C(23)-H(23)	119.8
C(10)-C(11)-C(12)	119.1(2)	C(18)-C(23)-H(23)	119.8
C(10)-C(11)-H(11)	120.5	C(25)-C(24)-N(3)	128.3(2)
C(12)-C(11)-H(11)	120.5	C(25)-C(24)-C(32)	116.6(2)
C(13)-C(12)-C(11)	123.4(2)	N(3)-C(24)-C(32)	115.1(2)
C(13)-C(12)-C(16)	117.7(2)	C(24)-C(25)-C(26)	121.3(2)
C(11)-C(12)-C(16)	118.9(2)	C(24)-C(25)-H(25)	119.4
C(14)-C(13)-C(12)	119.7(2)	C(26)-C(25)-H(25)	119.4
C(14)-C(13)-H(13)	120.1	C(27)-C(26)-C(25)	122.4(2)
C(12)-C(13)-H(13)	120.1	C(27)-C(26)-H(26)	118.8
C(13)-C(14)-C(15)	119.4(2)	C(25)-C(26)-H(26)	118.8
C(13)-C(14)-H(14)	120.3	C(26)-C(27)-C(28)	118.6(2)
C(15)-C(14)-H(14)	120.3	C(26)-C(27)-H(27)	120.7
N(2)-C(15)-C(14)	122.4(2)	C(28)-C(27)-H(27)	120.7
N(2)-C(15)-H(15)	118.8	C(29)-C(28)-C(32)	117.1(2)
C(14)-C(15)-H(15)	118.8	C(29)-C(28)-C(27)	123.9(2)
N(2)-C(16)-C(12)	121.3(2)	C(32)-C(28)-C(27)	119.0(2)
N(2)-C(16)-C(8)	116.7(2)	C(30)-C(29)-C(28)	120.7(2)
C(12)-C(16)-C(8)	121.9(2)	C(30)-C(29)-H(29)	119.6
O(2)-C(17)-N(3)	126.0(2)	C(28)-C(29)-H(29)	119.6
O(2)-C(17)-C(18)	117.7(2)	C(29)-C(30)-C(31)	118.7(2)
N(3)-C(17)-C(18)	116.4(2)	C(29)-C(30)-H(30)	120.7
C(23)-C(18)-C(19)	118.4(2)	C(31)-C(30)-H(30)	120.7
C(23)-C(18)-C(17)	124.0(2)	N(4)-C(31)-C(30)	122.4(2)
C(19)-C(18)-C(17)	117.6(2)	N(4)-C(31)-H(31)	118.8
C(20)-C(19)-C(18)	120.9(3)	C(30)-C(31)-H(31)	118.8
C(20)-C(19)-H(19)	119.6	N(4)-C(32)-C(28)	121.2(2)
C(18)-C(19)-H(19)	119.6	N(4)-C(32)-C(24)	116.8(2)
C(19)-C(20)-C(21)	120.2(3)	C(28)-C(32)-C(24)	122.1(2)

Symmetry transformations used to generate equivalent atoms:

Table 4. Anisotropic displacement parameters ($\text{\AA}^2 \times 10^3$) for stahl114. The anisotropic displacement factor exponent takes the form: $-2\pi^2 [h^2 a^{*2} U^{11} + \dots + 2 h k a^* b^* U^{12}]$

	U^{11}	U^{22}	U^{33}	U^{23}	U^{13}	U^{12}
Cu(1)	14(1)	13(1)	16(1)	-2(1)	-5(1)	-5(1)
O(1)	20(1)	29(1)	19(1)	-12(1)	-6(1)	-5(1)
O(2)	28(1)	17(1)	27(1)	-4(1)	-12(1)	-11(1)
N(1)	12(1)	13(1)	18(1)	-3(1)	-4(1)	-4(1)
N(2)	15(1)	15(1)	14(1)	-2(1)	-3(1)	-9(1)
N(3)	16(1)	12(1)	16(1)	-2(1)	-6(1)	-5(1)
N(4)	13(1)	16(1)	13(1)	-4(1)	-2(1)	-7(1)
C(1)	16(1)	15(1)	16(1)	-3(1)	-4(1)	-7(1)
C(2)	15(1)	17(1)	12(1)	-1(1)	-1(1)	-6(1)
C(3)	20(1)	21(1)	17(1)	-4(1)	-2(1)	-10(1)
C(4)	25(2)	16(1)	26(2)	-1(1)	-4(1)	-5(1)
C(5)	17(1)	26(2)	30(2)	5(1)	-8(1)	-5(1)
C(6)	18(1)	30(2)	24(2)	0(1)	-6(1)	-11(1)
C(7)	18(1)	20(1)	16(1)	-2(1)	-2(1)	-8(1)
C(8)	14(1)	13(1)	15(1)	1(1)	-5(1)	-6(1)
C(9)	18(1)	18(1)	15(1)	-4(1)	-4(1)	-8(1)
C(10)	17(1)	26(2)	18(1)	-2(1)	-7(1)	-11(1)
C(11)	13(1)	22(1)	22(1)	-3(1)	-6(1)	-6(1)
C(12)	15(1)	16(1)	18(1)	0(1)	-4(1)	-8(1)
C(13)	11(1)	17(1)	25(1)	-3(1)	-5(1)	-4(1)
C(14)	14(1)	14(1)	22(1)	-7(1)	-1(1)	-4(1)
C(15)	16(1)	14(1)	16(1)	-2(1)	-3(1)	-9(1)
C(16)	15(1)	14(1)	14(1)	1(1)	-4(1)	-8(1)
C(17)	13(1)	14(1)	20(1)	-4(1)	-3(1)	-5(1)
C(18)	12(1)	18(1)	23(1)	1(1)	-5(1)	-10(1)
C(19)	16(1)	18(1)	26(2)	0(1)	-4(1)	-8(1)
C(20)	19(1)	19(1)	40(2)	7(1)	-7(1)	-8(1)
C(21)	18(1)	39(2)	29(2)	15(1)	-9(1)	-12(1)
C(22)	22(2)	38(2)	19(2)	4(1)	-3(1)	-13(1)
C(23)	17(1)	22(1)	22(1)	0(1)	-5(1)	-9(1)
C(24)	11(1)	13(1)	17(1)	-3(1)	-1(1)	-4(1)
C(25)	16(1)	18(1)	20(1)	-5(1)	-6(1)	-6(1)
C(26)	20(1)	27(2)	20(1)	-5(1)	-9(1)	-8(1)
C(27)	15(1)	24(1)	14(1)	2(1)	-4(1)	-4(1)
C(28)	11(1)	18(1)	15(1)	-1(1)	1(1)	-5(1)
C(29)	12(1)	16(1)	18(1)	2(1)	0(1)	-5(1)
C(30)	15(1)	15(1)	20(1)	-3(1)	0(1)	-7(1)
C(31)	15(1)	17(1)	17(1)	-4(1)	-1(1)	-7(1)
C(32)	9(1)	16(1)	15(1)	-4(1)	1(1)	-4(1)

Table 5. Hydrogen coordinates ($\times 10^4$) and isotropic displacement parameters ($\text{\AA}^2 \times 10^{-3}$) for stahl114.

	x	y	z	U(eq)
H(3)	3108	-2168	5910	23
H(4)	5545	-3617	6044	29
H(5)	7100	-2684	6433	31
H(6)	6212	-305	6693	28
H(7)	3755	1161	6574	22
H(9)	-1178	863	5895	20
H(10)	-3799	2099	6035	22
H(11)	-5264	4016	7034	22
H(13)	-5407	5587	8309	22
H(14)	-4127	6154	9208	21
H(15)	-1481	4879	8982	18
H(19)	220	6888	8381	24
H(20)	-612	8330	7071	33
H(21)	26	7419	5488	36
H(22)	1564	5072	5212	33
H(23)	2356	3597	6536	24
H(25)	2881	3061	10128	21
H(26)	3601	1318	11349	25
H(27)	3552	-889	11366	22
H(29)	3051	-2570	10493	21
H(30)	2000	-2875	9327	21
H(31)	1130	-993	8223	19

Table 6. Torsion angles [°] for stahl114.

N(3)-Cu(1)-N(1)-C(1)	46.8(4)	Cu(1)-N(2)-C(15)-C(14)	-164.93(19)
N(4)-Cu(1)-N(1)-C(1)	-61.8(2)	C(13)-C(14)-C(15)-N(2)	0.1(4)
N(2)-Cu(1)-N(1)-C(1)	163.9(2)	C(15)-N(2)-C(16)-C(12)	-0.3(3)
N(3)-Cu(1)-N(1)-C(8)	-129.3(3)	Cu(1)-N(2)-C(16)-C(12)	167.26(18)
N(4)-Cu(1)-N(1)-C(8)	122.13(16)	C(15)-N(2)-C(16)-C(8)	-177.4(2)
N(2)-Cu(1)-N(1)-C(8)	-12.17(16)	Cu(1)-N(2)-C(16)-C(8)	-9.9(3)
N(1)-Cu(1)-N(2)-C(15)	178.2(2)	C(13)-C(12)-C(16)-N(2)	0.5(4)
N(3)-Cu(1)-N(2)-C(15)	-18.2(2)	C(11)-C(12)-C(16)-N(2)	-178.5(2)
N(4)-Cu(1)-N(2)-C(15)	77.1(2)	C(13)-C(12)-C(16)-C(8)	177.5(2)
N(1)-Cu(1)-N(2)-C(16)	12.17(16)	C(11)-C(12)-C(16)-C(8)	-1.4(4)
N(3)-Cu(1)-N(2)-C(16)	175.75(16)	C(9)-C(8)-C(16)-N(2)	176.7(2)
N(4)-Cu(1)-N(2)-C(16)	-88.96(19)	N(1)-C(8)-C(16)-N(2)	0.1(3)
N(1)-Cu(1)-N(3)-C(17)	68.9(4)	C(9)-C(8)-C(16)-C(12)	-0.4(4)
N(4)-Cu(1)-N(3)-C(17)	-179.8(2)	N(1)-C(8)-C(16)-C(12)	-177.0(2)
N(2)-Cu(1)-N(3)-C(17)	-45.4(2)	C(24)-N(3)-C(17)-O(2)	-4.8(4)
N(1)-Cu(1)-N(3)-C(24)	-118.8(3)	Cu(1)-N(3)-C(17)-O(2)	166.84(19)
N(4)-Cu(1)-N(3)-C(24)	-7.53(16)	C(24)-N(3)-C(17)-C(18)	176.1(2)
N(2)-Cu(1)-N(3)-C(24)	126.90(16)	Cu(1)-N(3)-C(17)-C(18)	-12.3(3)
N(1)-Cu(1)-N(4)-C(31)	-15.4(2)	O(2)-C(17)-C(18)-C(23)	143.6(3)
N(3)-Cu(1)-N(4)-C(31)	-178.3(2)	N(3)-C(17)-C(18)-C(23)	-37.2(3)
N(2)-Cu(1)-N(4)-C(31)	78.3(2)	O(2)-C(17)-C(18)-C(19)	-35.6(3)
N(1)-Cu(1)-N(4)-C(32)	169.32(16)	N(3)-C(17)-C(18)-C(19)	143.7(2)
N(3)-Cu(1)-N(4)-C(32)	6.42(16)	C(23)-C(18)-C(19)-C(20)	2.3(4)
N(2)-Cu(1)-N(4)-C(32)	-97.05(18)	C(17)-C(18)-C(19)-C(20)	-178.5(2)
C(8)-N(1)-C(1)-O(1)	7.8(4)	C(18)-C(19)-C(20)-C(21)	-1.1(4)
Cu(1)-N(1)-C(1)-O(1)	-168.02(19)	C(19)-C(20)-C(21)-C(22)	-1.1(4)
C(8)-N(1)-C(1)-C(2)	-170.4(2)	C(20)-C(21)-C(22)-C(23)	1.9(4)
Cu(1)-N(1)-C(1)-C(2)	13.8(3)	C(21)-C(22)-C(23)-C(18)	-0.6(4)
O(1)-C(1)-C(2)-C(7)	133.4(3)	C(19)-C(18)-C(23)-C(22)	-1.5(4)
N(1)-C(1)-C(2)-C(7)	-48.3(3)	C(17)-C(18)-C(23)-C(22)	179.4(2)
O(1)-C(1)-C(2)-C(3)	-44.0(3)	C(17)-N(3)-C(24)-C(25)	-0.1(4)
N(1)-C(1)-C(2)-C(3)	134.3(2)	Cu(1)-N(3)-C(24)-C(25)	-172.8(2)
C(7)-C(2)-C(3)-C(4)	0.6(4)	C(17)-N(3)-C(24)-C(32)	-179.9(2)
C(1)-C(2)-C(3)-C(4)	178.2(2)	Cu(1)-N(3)-C(24)-C(32)	7.4(3)
C(2)-C(3)-C(4)-C(5)	-0.5(4)	N(3)-C(24)-C(25)-C(26)	179.8(2)
C(3)-C(4)-C(5)-C(6)	0.1(4)	C(32)-C(24)-C(25)-C(26)	-0.4(4)
C(4)-C(5)-C(6)-C(7)	0.2(4)	C(24)-C(25)-C(26)-C(27)	1.5(4)
C(3)-C(2)-C(7)-C(6)	-0.3(4)	C(25)-C(26)-C(27)-C(28)	-0.6(4)
C(1)-C(2)-C(7)-C(6)	-177.7(2)	C(26)-C(27)-C(28)-C(29)	178.6(2)
C(5)-C(6)-C(7)-C(2)	-0.1(4)	C(26)-C(27)-C(28)-C(32)	-1.4(4)
C(1)-N(1)-C(8)-C(9)	17.5(4)	C(32)-C(28)-C(29)-C(30)	-3.9(4)
Cu(1)-N(1)-C(8)-C(9)	-166.0(2)	C(27)-C(28)-C(29)-C(30)	176.1(2)
C(1)-N(1)-C(8)-C(16)	-166.3(2)	C(28)-C(29)-C(30)-C(31)	2.2(4)
Cu(1)-N(1)-C(8)-C(16)	10.1(3)	C(32)-N(4)-C(31)-C(30)	-1.7(4)
N(1)-C(8)-C(9)-C(10)	177.8(2)	Cu(1)-N(4)-C(31)-C(30)	-176.70(18)
C(16)-C(8)-C(9)-C(10)	1.7(4)	C(29)-C(30)-C(31)-N(4)	0.8(4)
C(8)-C(9)-C(10)-C(11)	-1.1(4)	C(31)-N(4)-C(32)-C(28)	-0.2(3)
C(9)-C(10)-C(11)-C(12)	-0.9(4)	Cu(1)-N(4)-C(32)-C(28)	175.56(18)
C(10)-C(11)-C(12)-C(13)	-176.8(2)	C(31)-N(4)-C(32)-C(24)	-179.8(2)
C(10)-C(11)-C(12)-C(16)	2.1(4)	Cu(1)-N(4)-C(32)-C(24)	-4.1(3)
C(11)-C(12)-C(13)-C(14)	178.5(2)	C(29)-C(28)-C(32)-N(4)	3.0(3)
C(16)-C(12)-C(13)-C(14)	-0.4(4)	C(27)-C(28)-C(32)-N(4)	-177.1(2)
C(12)-C(13)-C(14)-C(15)	0.1(4)	C(29)-C(28)-C(32)-C(24)	-177.4(2)
C(16)-N(2)-C(15)-C(14)	0.0(4)	C(27)-C(28)-C(32)-C(24)	2.6(4)

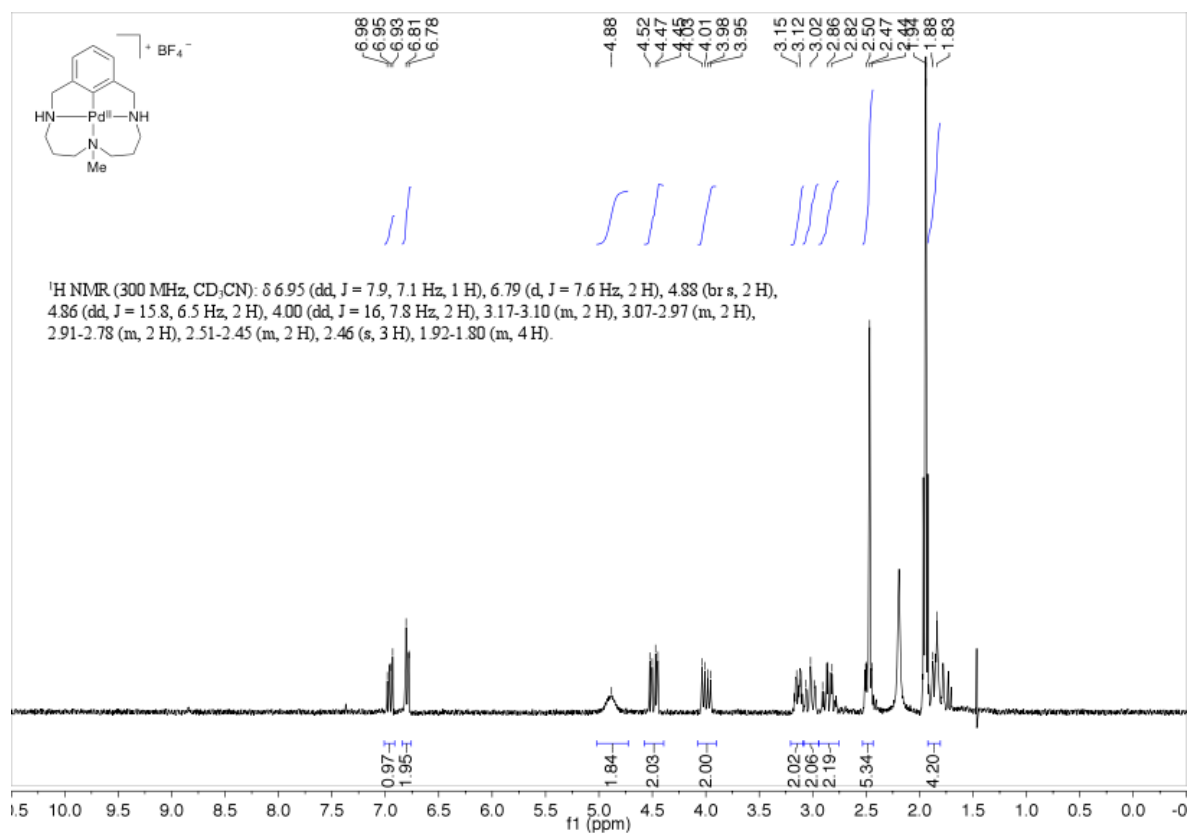
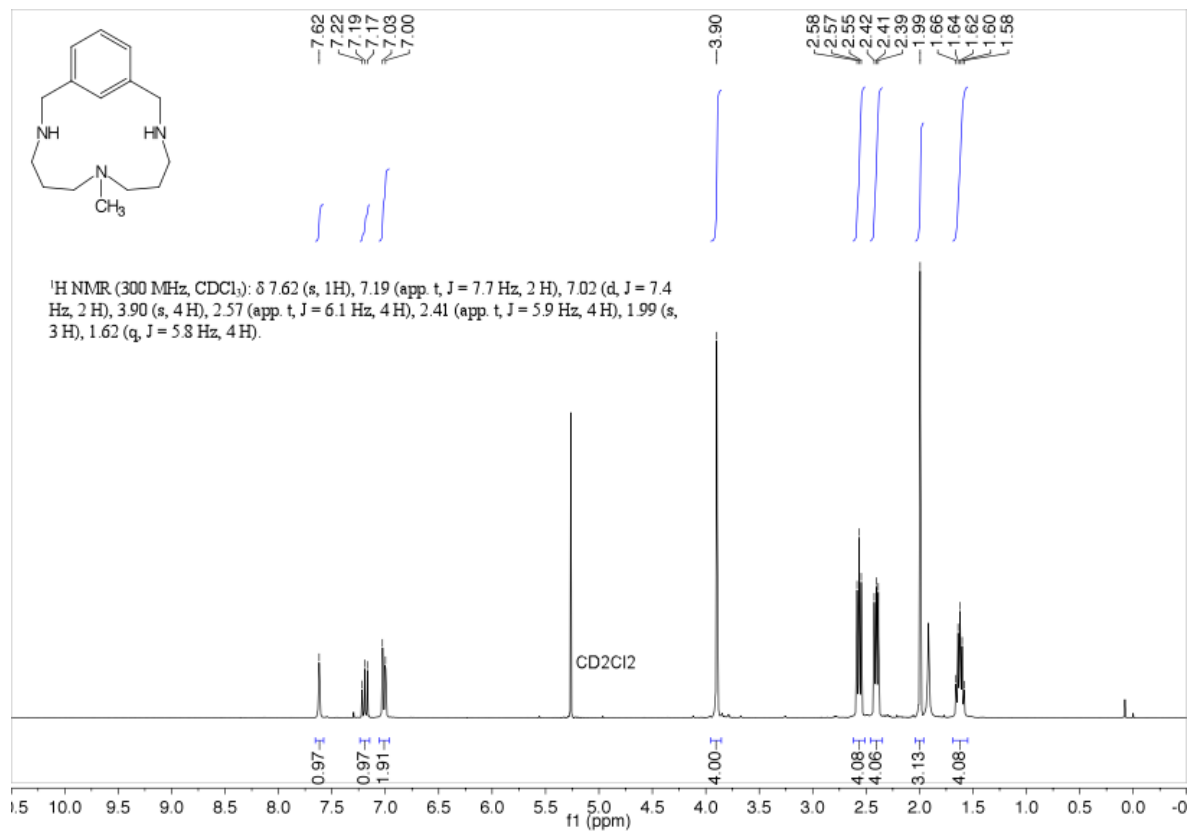
C(25)-C(24)-C(32)-N(4)	178.0(2)
N(3)-C(24)-C(32)-N(4)	-2.2(3)
C(25)-C(24)-C(32)-C(28)	-1.6(4)
N(3)-C(24)-C(32)-C(28)	178.2(2)

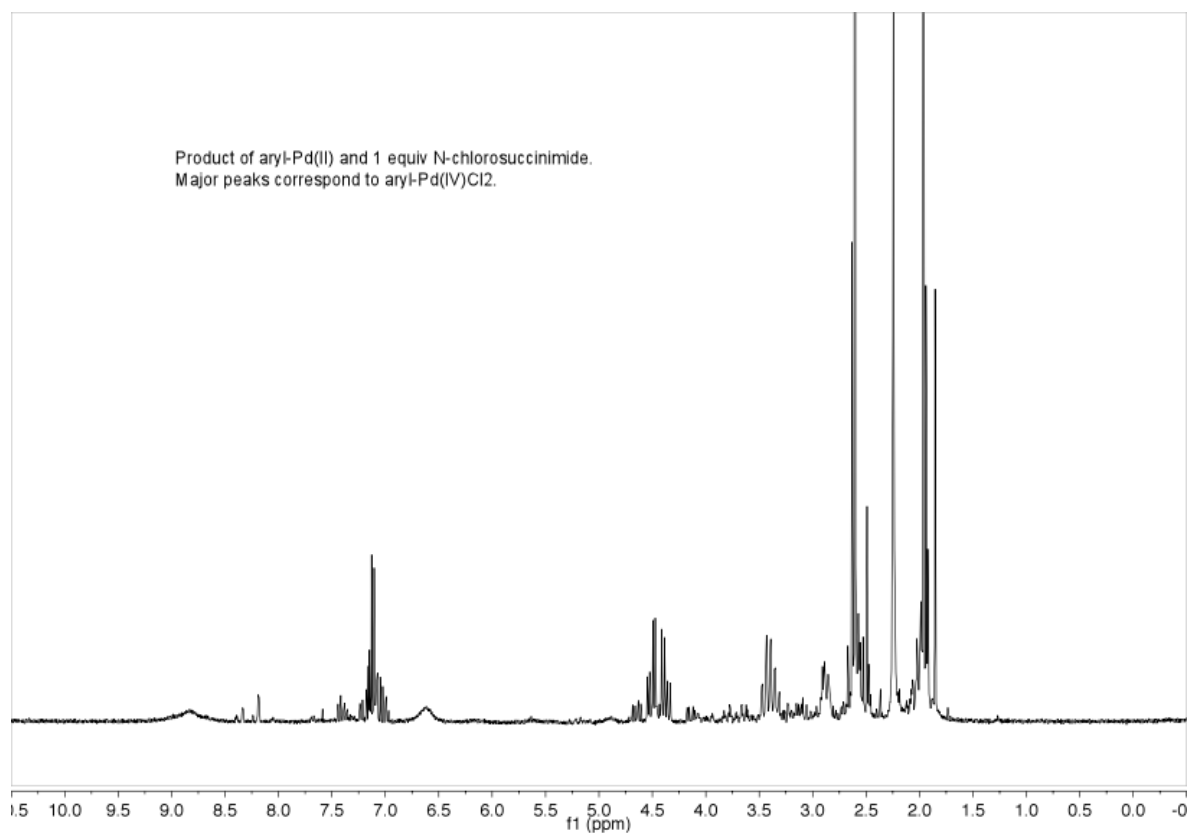
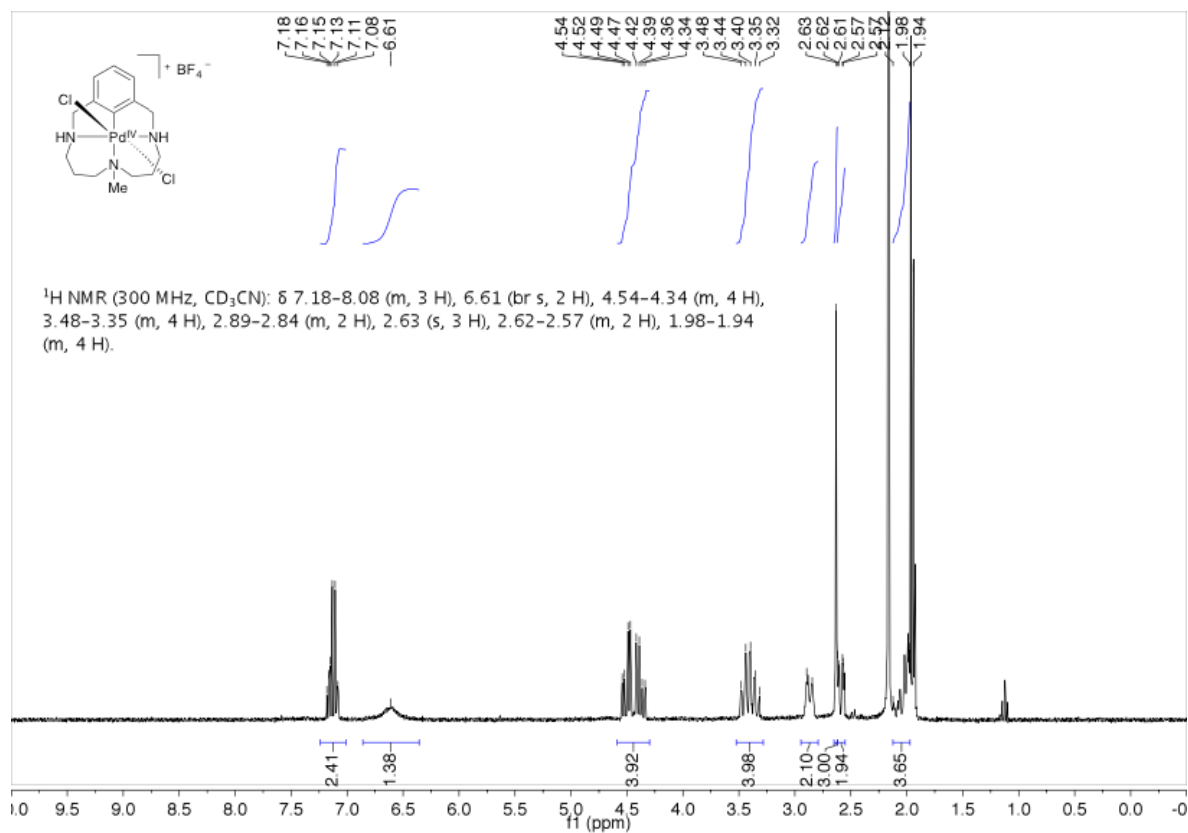
References and Notes:

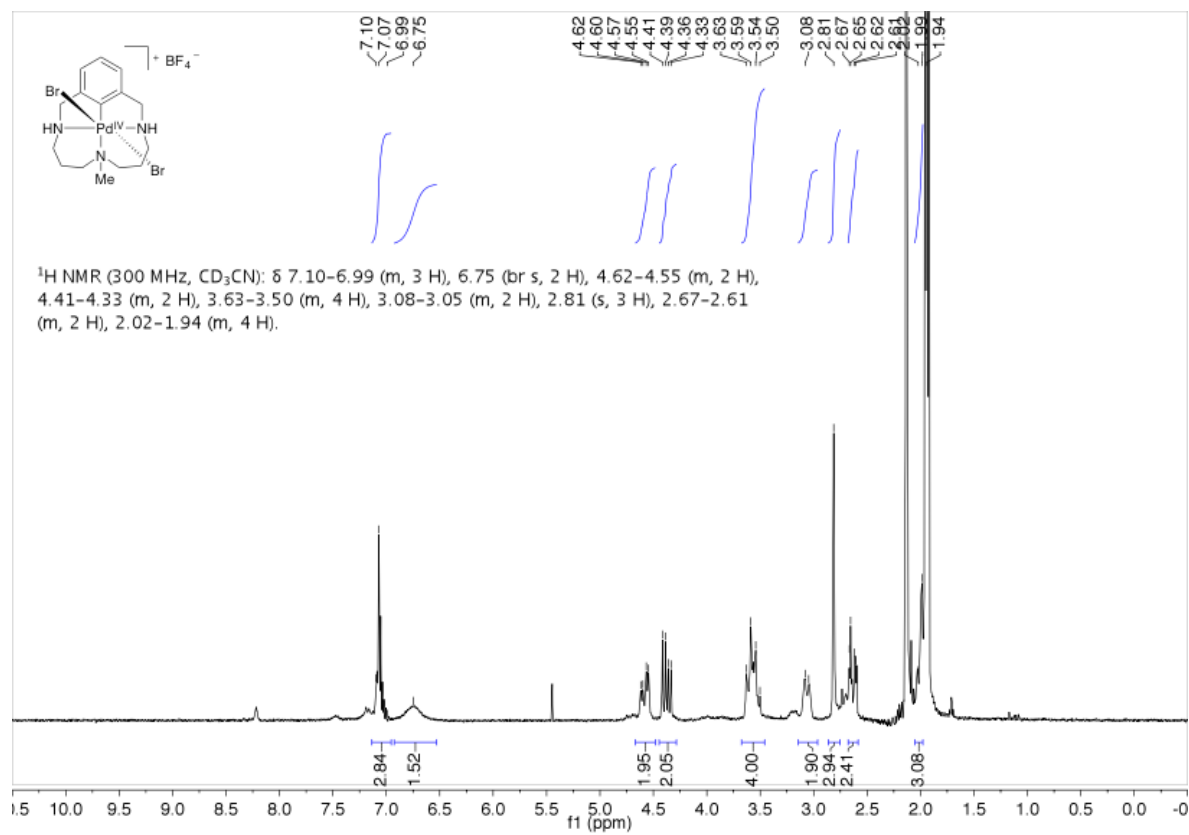
1. Bruker-AXS. (2009) APEX2, SADABS, and SAINT Software Reference Manuals. Bruker-AXS, Madison, Wisconsin, USA.
2. Sheldrick, G. M. (2008) SHELXL. *Acta Cryst.* **A64**, 112-122.
3. Guzei, I.A. (2006-2008). Internal laboratory computer programs "Inserter", "FCF_filter", "Modicifer".
4. Pennington, W.T. (1999) *J. Appl. Cryst.* **32**(5), 1028-1029.
5. Dolomanov, O.V.; Bourhis, L.J.; Gildea, R.J.; Howard, J.A.K.; Puschmann, H. "OLEX2: a complete structure solution, refinement and analysis program". *J. Appl. Cryst.* (2009) **42**, 339-341.

Appendix 4:

NMR Spectra and Crystal Structure Data for
Novel Aryl-Palladium(IV) Triazamacrocyclic Complexes







X-Ray Crystal Structure Data for Aryl-Pd^{II} Complex 2, “Stahl92”.

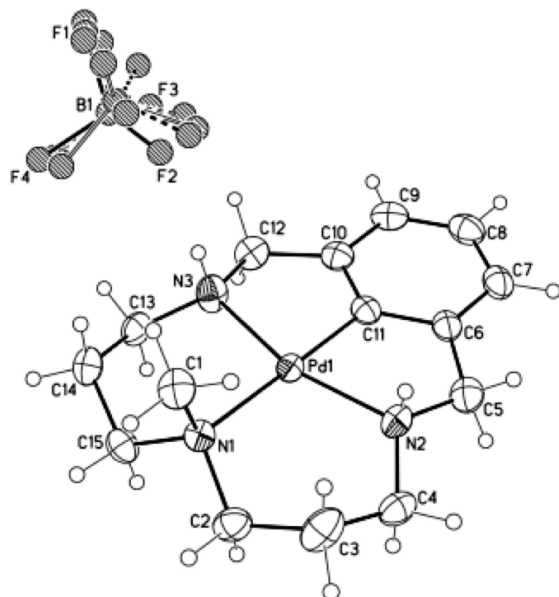


Figure 1. A molecular drawing of Stahl92. All four positions of the disordered BF_4^- anion are shown.

Data Collection

A yellow crystal with approximate dimensions $0.19 \times 0.16 \times 0.09 \text{ mm}^3$ was selected under oil under ambient conditions and attached to the tip of a MiTeGen MicroMount©. The crystal was mounted in a stream of cold nitrogen at 100(1) K and centered in the X-ray beam by using a video camera.

The crystal evaluation and data collection were performed on a Bruker SMART APEXII diffractometer with $\text{Cu K}\alpha$ ($\lambda = 1.54178 \text{ \AA}$) radiation and the diffractometer to crystal distance of 4.03 cm. Bruker SMART APEXII diffractometer with $\text{Cu K}\alpha$ ($\lambda = 1.54178 \text{ \AA}$) radiation and the diffractometer to crystal distance of 4.03 cm

The initial cell constants were obtained from three series of ω scans at different starting angles. Each series consisted of 41 frames collected at intervals of 0.6° in a 25° range about ω with the exposure time of 10 seconds per frame. The reflections were successfully indexed by an automated indexing routine built in the APEXII program. The final cell constants were calculated from a set of 9905 strong reflections from the actual data collection.

The data were collected by using the full sphere data collection routine to survey the reciprocal space to the extent of a full sphere to a resolution of 0.82 \AA . A total of 25958 data were harvested by collecting 15 sets of frames with 0.5° scans in ω with an exposure time 60-90 sec per frame. These highly redundant datasets were corrected for Lorentz and polarization effects. The absorption correction was based on fitting a function to the empirical transmission surface as sampled by multiple equivalent measurements.¹

Structure Solution and Refinement

The systematic absences in the diffraction data were uniquely consistent for the space group $P2_1/n$ that yielded chemically reasonable and computationally stable results of refinement.²⁻⁴

A successful solution by the direct methods provided most non-hydrogen atoms from the E -map. The remaining non-hydrogen atoms were located in an alternating series of least-squares cycles and difference Fourier maps. All non-hydrogen atoms were refined with anisotropic displacement coefficients unless specified otherwise. All hydrogen atoms were included in the structure factor calculation at idealized positions and were allowed to ride on the neighboring atoms with relative isotropic displacement coefficients.

The BF_4^- anion is disordered over four positions in a $31.1(3) : 30.2(4) : 28.8(4) : 9.8(4)$ ratio and was refined with restraints and constraints.

The final least-squares refinement of 240 parameters against 3245 data resulted in residuals R (based on F^2 for $I \geq 2\sigma$) and wR (based on F^2 for all data) of 0.0316 and 0.0778, respectively. The final difference Fourier map was featureless.

The molecular diagram is drawn with 50% probability ellipsoids.

Table 1. Crystal data and structure refinement for stahl92.

Identification code	stahl92	
Empirical formula	C ₁₅ H ₂₄ B F ₄ N ₃ Pd	
Formula weight	439.58	
Temperature	100(1) K	
Wavelength	1.54178 Å	
Crystal system	Monoclinic	
Space group	P2 ₁ /c	
Unit cell dimensions	a = 11.4049(4) Å	α = 90°.
	b = 15.2544(6) Å	β = 116.964(2)°.
	c = 10.9571(4) Å	γ = 90°.
Volume	1699.03(11) Å ³	
Z	4	
Density (calculated)	1.718 Mg/m ³	
Absorption coefficient	9.209 mm ⁻¹	
F(000)	888	
Crystal size	0.19 x 0.16 x 0.09 mm ³	
Theta range for data collection	4.35 to 71.12°.	
Index ranges	-13 ≤ h ≤ 13, -18 ≤ k ≤ 18, -12 ≤ l ≤ 13	
Reflections collected	25958	
Independent reflections	3245 [R(int) = 0.0315]	
Completeness to theta = 71.12°	98.8 %	
Absorption correction	Numerical with SADABS	
Max. and min. transmission	0.4979 and 0.2806	
Refinement method	Full-matrix least-squares on F ²	
Data / restraints / parameters	3245 / 41 / 240	
Goodness-of-fit on F ²	1.066	
Final R indices [I > 2σ(I)]	R1 = 0.0316, wR2 = 0.0758	
R indices (all data)	R1 = 0.0347, wR2 = 0.0778	
Largest diff. peak and hole	1.032 and -0.626 e.Å ⁻³	

Table 2. Atomic coordinates ($\times 10^4$) and equivalent isotropic displacement parameters ($\text{\AA}^2 \times 10^3$) for stahl92. $U(\text{eq})$ is defined as one third of the trace of the orthogonalized U^{ij} tensor.

	x	y	z	$U(\text{eq})$
Pd(1)	1297(1)	3817(1)	1304(1)	21(1)
N(1)	3266(3)	4236(2)	1849(3)	23(1)
N(2)	858(4)	4717(2)	2408(4)	43(1)
N(3)	1258(3)	2732(2)	159(3)	33(1)
C(1)	4218(4)	3765(3)	3082(4)	32(1)
C(2)	3384(4)	5202(2)	2112(4)	33(1)
C(3)	2952(4)	5521(3)	3168(4)	40(1)
C(4)	1479(4)	5570(2)	2695(4)	33(1)
C(5)	-466(4)	4674(3)	2191(4)	32(1)
C(6)	-1146(3)	3876(2)	1422(4)	27(1)
C(7)	-2394(4)	3566(3)	1156(4)	33(1)
C(8)	-2890(4)	2833(3)	328(4)	37(1)
C(9)	-2193(4)	2394(2)	-251(4)	34(1)
C(10)	-947(3)	2698(2)	12(4)	28(1)
C(11)	-452(3)	3428(2)	850(3)	24(1)
C(12)	-79(4)	2353(3)	-579(4)	32(1)
C(13)	1968(4)	2820(2)	-670(4)	30(1)
C(14)	3372(4)	3122(3)	152(4)	32(1)
C(15)	3588(4)	4064(2)	691(4)	29(1)
B(1)	2754(5)	656(3)	1353(5)	33(1)
F(1)	3217(7)	-123(4)	2059(8)	43(1)
F(2)	2844(8)	1321(4)	2250(7)	43(1)
F(3)	1449(5)	552(6)	396(6)	43(1)
F(4)	3497(7)	874(5)	688(8)	43(1)
B(1A)	2787(5)	588(3)	1611(5)	33(1)
F(1A)	3712(6)	385(5)	2933(6)	43(1)
F(2A)	1803(7)	1096(4)	1662(8)	43(1)
F(3A)	2241(8)	-185(4)	919(7)	43(1)
F(4A)	3390(8)	1044(5)	956(8)	43(1)
B(1B)	2583(5)	558(4)	1374(6)	33(1)
F(1B)	3474(7)	2(5)	2355(8)	43(1)
F(2B)	2199(9)	1192(5)	2025(8)	43(1)
F(3B)	1493(7)	86(5)	479(7)	43(1)
F(4B)	3158(9)	951(6)	638(9)	43(1)
B(1C)	2639(13)	552(9)	1334(13)	33(1)
F(1C)	2720(20)	-355(9)	1390(20)	43(1)
F(2C)	3404(18)	891(15)	2629(17)	43(1)
F(3C)	1344(14)	811(14)	880(20)	43(1)
F(4C)	3090(20)	858(15)	430(20)	43(1)

Table 3. Bond lengths [Å] and angles [°] for stahl92.

Pd(1)-C(11)	1.918(3)	C(8)-H(8)	0.9500
Pd(1)-N(2)	2.037(3)	C(9)-C(10)	1.396(5)
Pd(1)-N(3)	2.064(3)	C(9)-H(9)	0.9500
Pd(1)-N(1)	2.142(3)	C(10)-C(11)	1.389(5)
N(1)-C(1)	1.480(4)	C(10)-C(12)	1.502(5)
N(1)-C(2)	1.496(4)	C(12)-H(12A)	0.9900
N(1)-C(15)	1.496(4)	C(12)-H(12B)	0.9900
N(2)-C(5)	1.419(5)	C(13)-C(14)	1.510(5)
N(2)-C(4)	1.446(5)	C(13)-H(13B)	0.9900
N(2)-H(2)	0.9300	C(13)-H(13A)	0.9900
N(3)-C(13)	1.472(5)	C(14)-C(15)	1.531(5)
N(3)-C(12)	1.482(5)	C(14)-H(14B)	0.9900
N(3)-H(3)	0.9300	C(14)-H(14A)	0.9900
C(1)-H(1C)	0.9800	C(15)-H(15B)	0.9900
C(1)-H(1A)	0.9800	C(15)-H(15A)	0.9900
C(1)-H(1B)	0.9800	B(1)-F(2)	1.385(3)
C(2)-C(3)	1.528(6)	B(1)-F(1)	1.385(3)
C(2)-H(2A)	0.9900	B(1)-F(4)	1.385(3)
C(2)-H(2B)	0.9900	B(1)-F(3)	1.386(3)
C(3)-C(4)	1.518(6)	B(1A)-F(4A)	1.385(3)
C(3)-H(3A)	0.9900	B(1A)-F(1A)	1.386(3)
C(3)-H(3B)	0.9900	B(1A)-F(2A)	1.386(3)
C(4)-H(4B)	0.9900	B(1A)-F(3A)	1.387(3)
C(4)-H(4A)	0.9900	B(1B)-F(1B)	1.385(3)
C(5)-C(6)	1.484(5)	B(1B)-F(4B)	1.385(3)
C(5)-H(5B)	0.9900	B(1B)-F(3B)	1.385(3)
C(5)-H(5A)	0.9900	B(1B)-F(2B)	1.385(3)
C(6)-C(11)	1.392(5)	B(1C)-F(2C)	1.385(3)
C(6)-C(7)	1.399(5)	B(1C)-F(1C)	1.385(3)
C(7)-C(8)	1.389(6)	B(1C)-F(4C)	1.385(3)
C(7)-H(7)	0.9500	B(1C)-F(3C)	1.386(3)
C(8)-C(9)	1.392(6)		
C(11)-Pd(1)-N(2)	81.71(15)	C(13)-N(3)-H(3)	104.2
C(11)-Pd(1)-N(3)	82.02(14)	C(12)-N(3)-H(3)	104.2
N(2)-Pd(1)-N(3)	163.29(13)	Pd(1)-N(3)-H(3)	104.2
C(11)-Pd(1)-N(1)	178.81(12)	N(1)-C(1)-H(1C)	109.5
N(2)-Pd(1)-N(1)	98.16(12)	N(1)-C(1)-H(1A)	109.5
N(3)-Pd(1)-N(1)	98.02(11)	H(1C)-C(1)-H(1A)	109.5
C(1)-N(1)-C(2)	109.7(3)	N(1)-C(1)-H(1B)	109.5
C(1)-N(1)-C(15)	109.2(3)	H(1C)-C(1)-H(1B)	109.5
C(2)-N(1)-C(15)	107.5(3)	H(1A)-C(1)-H(1B)	109.5
C(1)-N(1)-Pd(1)	110.6(2)	N(1)-C(2)-C(3)	115.3(3)
C(2)-N(1)-Pd(1)	109.8(2)	N(1)-C(2)-H(2A)	108.4
C(15)-N(1)-Pd(1)	109.9(2)	C(3)-C(2)-H(2A)	108.4
C(5)-N(2)-C(4)	117.2(3)	N(1)-C(2)-H(2B)	108.4
C(5)-N(2)-Pd(1)	113.5(3)	C(3)-C(2)-H(2B)	108.4
C(4)-N(2)-Pd(1)	120.5(3)	H(2A)-C(2)-H(2B)	107.5
C(5)-N(2)-H(2)	100.0	C(4)-C(3)-C(2)	116.3(3)
C(4)-N(2)-H(2)	100.0	C(4)-C(3)-H(3A)	108.2
Pd(1)-N(2)-H(2)	100.0	C(2)-C(3)-H(3A)	108.2
C(13)-N(3)-C(12)	114.6(3)	C(4)-C(3)-H(3B)	108.2
C(13)-N(3)-Pd(1)	115.8(2)	C(2)-C(3)-H(3B)	108.2
C(12)-N(3)-Pd(1)	112.2(2)	H(3A)-C(3)-H(3B)	107.4

N(2)-C(4)-C(3)	112.8(3)	N(3)-C(13)-H(13A)	109.0
N(2)-C(4)-H(4B)	109.0	C(14)-C(13)-H(13A)	109.0
C(3)-C(4)-H(4B)	109.0	H(13B)-C(13)-H(13A)	107.8
N(2)-C(4)-H(4A)	109.0	C(13)-C(14)-C(15)	117.2(3)
C(3)-C(4)-H(4A)	109.0	C(13)-C(14)-H(14B)	108.0
H(4B)-C(4)-H(4A)	107.8	C(15)-C(14)-H(14B)	108.0
N(2)-C(5)-C(6)	112.0(3)	C(13)-C(14)-H(14A)	108.0
N(2)-C(5)-H(5B)	109.2	C(15)-C(14)-H(14A)	108.0
C(6)-C(5)-H(5B)	109.2	H(14B)-C(14)-H(14A)	107.2
N(2)-C(5)-H(5A)	109.2	N(1)-C(15)-C(14)	115.7(3)
C(6)-C(5)-H(5A)	109.2	N(1)-C(15)-H(15B)	108.4
H(5B)-C(5)-H(5A)	107.9	C(14)-C(15)-H(15B)	108.4
C(11)-C(6)-C(7)	118.2(3)	N(1)-C(15)-H(15A)	108.4
C(11)-C(6)-C(5)	113.6(3)	C(14)-C(15)-H(15A)	108.4
C(7)-C(6)-C(5)	128.0(3)	H(15B)-C(15)-H(15A)	107.4
C(8)-C(7)-C(6)	118.9(4)	F(2)-B(1)-F(1)	110.2(3)
C(8)-C(7)-H(7)	120.6	F(2)-B(1)-F(4)	109.3(3)
C(6)-C(7)-H(7)	120.6	F(1)-B(1)-F(4)	109.3(3)
C(7)-C(8)-C(9)	122.5(4)	F(2)-B(1)-F(3)	109.2(3)
C(7)-C(8)-H(8)	118.8	F(1)-B(1)-F(3)	109.4(3)
C(9)-C(8)-H(8)	118.8	F(4)-B(1)-F(3)	109.4(3)
C(8)-C(9)-C(10)	119.0(4)	F(4A)-B(1A)-F(1A)	109.4(3)
C(8)-C(9)-H(9)	120.5	F(4A)-B(1A)-F(2A)	109.9(3)
C(10)-C(9)-H(9)	120.5	F(1A)-B(1A)-F(2A)	109.2(3)
C(11)-C(10)-C(9)	118.2(3)	F(4A)-B(1A)-F(3A)	110.5(3)
C(11)-C(10)-C(12)	114.6(3)	F(1A)-B(1A)-F(3A)	108.8(3)
C(9)-C(10)-C(12)	127.1(3)	F(2A)-B(1A)-F(3A)	109.1(3)
C(10)-C(11)-C(6)	123.2(3)	F(1B)-B(1B)-F(4B)	110.1(3)
C(10)-C(11)-Pd(1)	118.9(3)	F(1B)-B(1B)-F(3B)	109.7(3)
C(6)-C(11)-Pd(1)	117.9(3)	F(4B)-B(1B)-F(3B)	108.8(3)
N(3)-C(12)-C(10)	110.1(3)	F(1B)-B(1B)-F(2B)	108.6(3)
N(3)-C(12)-H(12A)	109.6	F(4B)-B(1B)-F(2B)	109.9(3)
C(10)-C(12)-H(12A)	109.6	F(3B)-B(1B)-F(2B)	109.6(3)
N(3)-C(12)-H(12B)	109.6	F(2C)-B(1C)-F(1C)	109.3(3)
C(10)-C(12)-H(12B)	109.6	F(2C)-B(1C)-F(4C)	109.7(3)
H(12A)-C(12)-H(12B)	108.1	F(1C)-B(1C)-F(4C)	109.3(3)
N(3)-C(13)-C(14)	113.0(3)	F(2C)-B(1C)-F(3C)	109.5(3)
N(3)-C(13)-H(13B)	109.0	F(1C)-B(1C)-F(3C)	109.7(3)
C(14)-C(13)-H(13B)	109.0	F(4C)-B(1C)-F(3C)	109.3(3)

Symmetry transformations used to generate equivalent atoms:

Table 4. Anisotropic displacement parameters ($\text{\AA}^2 \times 10^3$) for stahl92. The anisotropic displacement factor exponent takes the form: $-2\pi^2 [h^2 a^{*2} U^{11} + \dots + 2 h k a^* b^* U^{12}]$

	U ¹¹	U ²²	U ³³	U ²³	U ¹³	U ¹²
Pd(1)	22(1)	22(1)	18(1)	1(1)	9(1)	2(1)
N(1)	23(1)	26(1)	19(1)	1(1)	7(1)	2(1)
N(2)	56(2)	26(2)	67(2)	-10(2)	45(2)	-3(2)
N(3)	33(2)	39(2)	29(2)	-13(1)	15(1)	-6(1)
C(1)	27(2)	39(2)	24(2)	5(2)	8(2)	6(2)
C(2)	28(2)	27(2)	37(2)	-4(2)	10(2)	-3(2)
C(3)	36(2)	37(2)	35(2)	-13(2)	5(2)	2(2)
C(4)	42(2)	25(2)	28(2)	-4(1)	14(2)	1(2)
C(5)	31(2)	35(2)	29(2)	6(2)	13(2)	7(2)
C(6)	27(2)	30(2)	26(2)	9(1)	13(2)	7(1)
C(7)	32(2)	39(2)	33(2)	12(2)	18(2)	8(2)
C(8)	27(2)	38(2)	41(2)	10(2)	13(2)	-1(2)
C(9)	33(2)	29(2)	32(2)	3(2)	8(2)	-4(2)
C(10)	26(2)	28(2)	25(2)	6(1)	8(1)	2(1)
C(11)	23(2)	27(2)	22(2)	6(1)	9(1)	2(1)
C(12)	30(2)	34(2)	26(2)	-1(2)	7(2)	1(2)
C(13)	37(2)	29(2)	25(2)	-5(1)	16(2)	4(2)
C(14)	32(2)	37(2)	31(2)	-3(2)	17(2)	5(2)
C(15)	31(2)	35(2)	24(2)	3(2)	15(2)	-1(2)

Table 5. Hydrogen coordinates ($\times 10^4$) and isotropic displacement parameters ($\text{\AA}^2 \times 10^{-3}$) for stahl92.

	x	y	z	U(eq)
H(2)	1282	4465	3273	52
H(3)	1732	2310	809	40
H(1C)	5111	3966	3318	48
H(1A)	4155	3134	2898	48
H(1B)	4019	3883	3848	48
H(2A)	2850	5508	1236	40
H(2B)	4313	5374	2424	40
H(3A)	3340	5127	3972	49
H(3B)	3328	6112	3479	49
H(4B)	1318	5860	3413	39
H(4A)	1072	5935	1858	39
H(5B)	-945	5200	1676	38
H(5A)	-480	4678	3088	38
H(7)	-2894	3853	1534	40
H(8)	-3737	2622	150	44
H(9)	-2561	1895	-815	40
H(12A)	-28	1706	-500	38
H(12B)	-460	2507	-1562	38
H(13B)	1496	3246	-1417	35
H(13A)	1965	2248	-1096	35
H(14B)	3829	3051	-425	39
H(14A)	3806	2723	946	39
H(15B)	4521	4220	993	35
H(15A)	3046	4459	-76	35

Table 6. Torsion angles [°] for stahl92.

C(11)-Pd(1)-N(1)-C(1)	7(6)		
N(2)-Pd(1)-N(1)-C(1)	90.7(2)	C(5)-C(6)-C(7)-C(8)	175.5(3)
N(3)-Pd(1)-N(1)-C(1)	-85.1(2)	C(6)-C(7)-C(8)-C(9)	-0.1(6)
C(11)-Pd(1)-N(1)-C(2)	-114(6)	C(7)-C(8)-C(9)-C(10)	0.2(6)
N(2)-Pd(1)-N(1)-C(2)	-30.6(2)	C(8)-C(9)-C(10)-C(11)	0.4(5)
N(3)-Pd(1)-N(1)-C(2)	153.6(2)	C(8)-C(9)-C(10)-C(12)	-176.0(3)
C(11)-Pd(1)-N(1)-C(15)	128(6)	C(9)-C(10)-C(11)-C(6)	-1.0(5)
N(2)-Pd(1)-N(1)-C(15)	-148.6(2)	C(12)-C(10)-C(11)-C(6)	175.8(3)
N(3)-Pd(1)-N(1)-C(15)	35.5(2)	C(9)-C(10)-C(11)-Pd(1)	176.6(3)
C(11)-Pd(1)-N(2)-C(5)	-6.1(3)	C(12)-C(10)-C(11)-Pd(1)	-6.6(4)
N(3)-Pd(1)-N(2)-C(5)	-19.4(7)	C(7)-C(6)-C(11)-C(10)	1.1(5)
N(1)-Pd(1)-N(2)-C(5)	175.1(3)	C(5)-C(6)-C(11)-C(10)	-175.5(3)
C(11)-Pd(1)-N(2)-C(4)	-152.7(3)	C(7)-C(6)-C(11)-Pd(1)	-176.6(3)
N(3)-Pd(1)-N(2)-C(4)	-166.0(4)	C(5)-C(6)-C(11)-Pd(1)	6.9(4)
N(1)-Pd(1)-N(2)-C(4)	28.5(3)	N(2)-Pd(1)-C(11)-C(10)	-178.4(3)
C(11)-Pd(1)-N(3)-C(13)	144.6(3)	N(3)-Pd(1)-C(11)-C(10)	-2.2(3)
N(2)-Pd(1)-N(3)-C(13)	158.0(5)	N(1)-Pd(1)-C(11)-C(10)	-95(6)
N(1)-Pd(1)-N(3)-C(13)	-36.6(3)	N(2)-Pd(1)-C(11)-C(6)	-0.6(3)
C(11)-Pd(1)-N(3)-C(12)	10.4(2)	N(3)-Pd(1)-C(11)-C(6)	175.6(3)
N(2)-Pd(1)-N(3)-C(12)	23.8(7)	N(1)-Pd(1)-C(11)-C(6)	83(6)
N(1)-Pd(1)-N(3)-C(12)	-170.8(2)	C(13)-N(3)-C(12)-C(10)	-150.8(3)
C(1)-N(1)-C(2)-C(3)	-67.5(4)	Pd(1)-N(3)-C(12)-C(10)	-16.0(4)
C(15)-N(1)-C(2)-C(3)	173.9(3)	C(11)-C(10)-C(12)-N(3)	14.7(4)
Pd(1)-N(1)-C(2)-C(3)	54.3(3)	C(9)-C(10)-C(12)-N(3)	-168.8(3)
N(1)-C(2)-C(3)-C(4)	-76.0(4)	C(12)-N(3)-C(13)-C(14)	-174.1(3)
C(5)-N(2)-C(4)-C(3)	169.3(3)	Pd(1)-N(3)-C(13)-C(14)	52.8(4)
Pd(1)-N(2)-C(4)-C(3)	-45.3(4)	N(3)-C(13)-C(14)-C(15)	-69.0(4)
C(2)-C(3)-C(4)-N(2)	66.6(5)	C(1)-N(1)-C(15)-C(14)	67.7(4)
C(4)-N(2)-C(5)-C(6)	158.8(3)	C(2)-N(1)-C(15)-C(14)	-173.3(3)
Pd(1)-N(2)-C(5)-C(6)	11.1(4)	Pd(1)-N(1)-C(15)-C(14)	-53.8(3)
N(2)-C(5)-C(6)-C(11)	-11.6(4)	C(13)-C(14)-C(15)-N(1)	72.5(4)
N(2)-C(5)-C(6)-C(7)	172.3(4)		
C(11)-C(6)-C(7)-C(8)	-0.5(5)		

Symmetry transformations used to generate equivalent atoms:

Table 7. Hydrogen bonds for stahl92 [\AA and $^\circ$].

D-H...A	d(D-H)	d(H...A)	d(D...A)	\angle (DHA)
N(3)-H(3)...F(2)	0.93	2.14	3.065(9)	177.9
N(3)-H(3)...F(2B)	0.93	2.08	2.978(9)	161.7

Symmetry transformations used to generate equivalent atoms:

X-Ray Crystal Structure Data for Aryl-Pd^{IV}Cl₂ Complex 3, “Stahl90”.

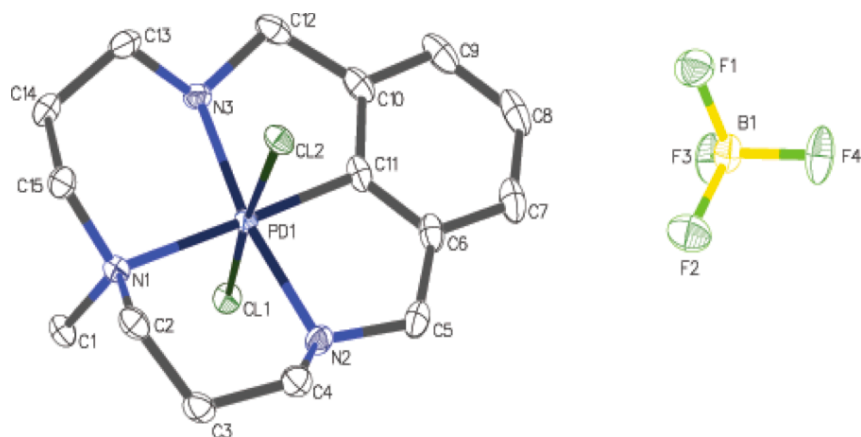


Figure 1. A molecular drawing of Stahl90. All H atoms are omitted.

Data Collection

A red crystal with approximate dimensions 0.27 x 0.23 x 0.22 mm³ was selected under oil under ambient conditions and attached to the tip of a MiTeGen MicroMount[®]. The crystal was mounted in a stream of cold nitrogen at 100(1) K and centered in the X-ray beam by using a video camera.

The crystal evaluation and data collection were performed on a Bruker Quazar APEXII diffractometer with Mo K_α ($\lambda = 0.71073 \text{ \AA}$) radiation and the diffractometer to crystal distance of 4.03 cm.

The initial cell constants were obtained from three series of ω scans at different starting angles. Each series consisted of 36 frames collected at intervals of 0.5° in a 18° range about ω with the exposure time of 1 seconds per frame. The reflections were successfully indexed by an automated indexing routine built in the APEXII program. The final cell constants were calculated from a set of 9857 strong reflections from the actual data collection.

The data were collected by using the full sphere data collection routine to survey the reciprocal space to the extent of a full sphere to a resolution of 0.82 Å. A total of 45731 data

were harvested by collecting 6 sets of frames with 0.4° scans in ω and φ with an exposure time 3 sec per frame. These highly redundant datasets were corrected for Lorentz and polarization effects. The absorption correction was based on fitting a function to the empirical transmission surface as sampled by multiple equivalent measurements.¹

Structure Solution and Refinement

The systematic absences in the diffraction data were uniquely consistent for the space group $P2_1/c$ that yielded chemically reasonable and computationally stable results of refinement.²³⁻⁴

A successful solution by the direct methods provided most non-hydrogen atoms from the E -map. The remaining non-hydrogen atoms were located in an alternating series of least-squares cycles and difference Fourier maps. All non-hydrogen atoms were refined with anisotropic displacement coefficients. All hydrogen atoms were included in the structure factor calculation at idealized positions and were allowed to ride on the neighboring atoms with relative isotropic displacement coefficients.

The final least-squares refinement of 236 parameters against 5686 data resulted in residuals R (based on F^2 for $I \geq 2\sigma$) and wR (based on F^2 for all data) of 0.0225 and 0.0524 respectively. The final difference Fourier map was featureless.

The molecular diagram is drawn with 50% probability ellipsoids.

Table 1. Crystal data and structure refinement for stahl90.		
Identification code	stahl90	
Empirical formula	C ₁₅ H ₂₄ B Cl ₂ F ₄ N ₃ Pd	
Formula weight	510.48	
Temperature	100(1) K	
Wavelength	0.71073 Å	
Crystal system	Monoclinic	
Space group	P2 ₁ /c	
Unit cell dimensions	a = 11.1403(6) Å	α = 90°.
	b = 10.9309(6) Å	β = 94.896(2)°.
	c = 15.3512(8) Å	γ = 90°.
Volume	1862.55(17) Å ³	
Z	4	
Density (calculated)	1.820 Mg/m ³	
Absorption coefficient	1.326 mm ⁻¹	
F(000)	1024	
Crystal size	0.27 x 0.23 x 0.22 mm ³	
Theta range for data collection	3.25 to 30.59°.	
Index ranges	-15 ≤ h ≤ 15, -15 ≤ k ≤ 15, -21 ≤ l ≤ 21	
Reflections collected	45731	
Independent reflections	5686 [R(int) = 0.0232]	
Completeness to theta = 25.00°	98.9 %	
Absorption correction	Numerical with SADABS	
Max. and min. transmission	0.7627 and 0.7168	
Refinement method	Full-matrix least-squares on F ²	
Data / restraints / parameters	5686 / 0 / 236	
Goodness-of-fit on F ²	1.064	
Final R indices [I > 2σ(I)]	R1 = 0.0225, wR2 = 0.0519	
R indices (all data)	R1 = 0.0233, wR2 = 0.0524	
Largest diff. peak and hole	1.638 and -0.859 e.Å ⁻³	

Table 2. Atomic coordinates ($\times 10^4$) and equivalent isotropic displacement parameters ($\text{\AA}^2 \times 10^3$) for stahl90. $U(\text{eq})$ is defined as one third of the trace of the orthogonalized U^{ij} tensor.

	x	y	z	U(eq)
Pd(1)	2622(1)	1782(1)	7757(1)	11(1)
Cl(1)	4242(1)	1636(1)	6924(1)	17(1)
Cl(2)	975(1)	2130(1)	8536(1)	18(1)
N(1)	2982(1)	8(1)	8449(1)	15(1)
N(2)	3714(1)	2852(1)	8605(1)	18(1)
N(3)	1571(1)	1055(1)	6705(1)	16(1)
C(1)	4051(1)	-666(2)	8187(1)	19(1)
C(2)	3128(2)	251(2)	9408(1)	20(1)
C(3)	4072(2)	1203(2)	9710(1)	23(1)
C(4)	3726(2)	2529(2)	9546(1)	21(1)
C(5)	3446(2)	4189(2)	8441(1)	23(1)
C(6)	2764(2)	4360(2)	7561(1)	21(1)
C(7)	2519(2)	5464(2)	7123(1)	27(1)
C(8)	1753(2)	5466(2)	6360(1)	29(1)
C(9)	1202(2)	4404(2)	6019(1)	27(1)
C(10)	1446(2)	3280(2)	6437(1)	21(1)
C(11)	2234(1)	3332(1)	7176(1)	18(1)
C(12)	876(2)	2065(2)	6214(1)	23(1)
C(13)	789(2)	-1(2)	6880(1)	23(1)
C(14)	1493(2)	-1038(2)	7336(1)	24(1)
C(15)	1905(1)	-810(2)	8292(1)	20(1)
F(1)	1728(1)	7951(1)	5158(1)	37(1)
F(2)	3566(1)	7988(1)	5935(1)	34(1)
F(3)	3417(1)	8298(1)	4464(1)	32(1)
F(4)	2722(1)	9745(1)	5360(1)	37(1)
B(1)	2857(2)	8486(2)	5224(1)	23(1)

Table 3. Bond lengths [Å] and angles [°] for stahl90.

Pd(1)-C(11)	1.9462(15)	C(5)-H(5B)	0.9900
Pd(1)-N(2)	2.0668(13)	C(5)-H(5A)	0.9900
Pd(1)-N(3)	2.0706(13)	C(6)-C(11)	1.379(2)
Pd(1)-N(1)	2.2304(13)	C(6)-C(7)	1.398(2)
Pd(1)-Cl(1)	2.3049(4)	C(7)-C(8)	1.388(3)
Pd(1)-Cl(2)	2.3052(4)	C(7)-H(7)	0.9500
N(1)-C(1)	1.4848(19)	C(8)-C(9)	1.394(3)
N(1)-C(2)	1.4906(19)	C(8)-H(8)	0.9500
N(1)-C(15)	1.499(2)	C(9)-C(10)	1.402(2)
N(2)-C(4)	1.487(2)	C(9)-H(9)	0.9500
N(2)-C(5)	1.509(2)	C(10)-C(11)	1.375(2)
N(2)-H(2)	0.9300	C(10)-C(12)	1.500(3)
N(3)-C(13)	1.484(2)	C(12)-H(12A)	0.9900
N(3)-C(12)	1.512(2)	C(12)-H(12B)	0.9900
N(3)-H(3)	0.9300	C(13)-C(14)	1.515(2)
C(1)-H(1B)	0.9800	C(13)-H(13A)	0.9900
C(1)-H(1A)	0.9800	C(13)-H(13B)	0.9900
C(1)-H(1C)	0.9800	C(14)-C(15)	1.520(2)
C(2)-C(3)	1.523(2)	C(14)-H(14A)	0.9900
C(2)-H(2B)	0.9900	C(14)-H(14B)	0.9900
C(2)-H(2A)	0.9900	C(15)-H(15A)	0.9900
C(3)-C(4)	1.515(2)	C(15)-H(15B)	0.9900
C(3)-H(3B)	0.9900	F(1)-B(1)	1.383(2)
C(3)-H(3A)	0.9900	F(2)-B(1)	1.403(2)
C(4)-H(4A)	0.9900	F(3)-B(1)	1.384(2)
C(4)-H(4B)	0.9900	F(4)-B(1)	1.402(2)
C(5)-C(6)	1.504(2)		
C(11)-Pd(1)-N(2)	83.79(6)	Pd(1)-N(2)-H(2)	106.0
C(11)-Pd(1)-N(3)	83.55(6)	C(13)-N(3)-C(12)	111.99(12)
N(2)-Pd(1)-N(3)	166.28(5)	C(13)-N(3)-Pd(1)	117.27(10)
C(11)-Pd(1)-N(1)	177.30(6)	C(12)-N(3)-Pd(1)	109.89(10)
N(2)-Pd(1)-N(1)	96.88(5)	C(13)-N(3)-H(3)	105.6
N(3)-Pd(1)-N(1)	96.02(5)	C(12)-N(3)-H(3)	105.6
C(11)-Pd(1)-Cl(1)	87.67(5)	Pd(1)-N(3)-H(3)	105.6
N(2)-Pd(1)-Cl(1)	86.65(4)	N(1)-C(1)-H(1B)	109.5
N(3)-Pd(1)-Cl(1)	87.59(4)	N(1)-C(1)-H(1A)	109.5
N(1)-Pd(1)-Cl(1)	94.98(3)	H(1B)-C(1)-H(1A)	109.5
C(11)-Pd(1)-Cl(2)	86.47(4)	N(1)-C(1)-H(1C)	109.5
N(2)-Pd(1)-Cl(2)	91.83(4)	H(1B)-C(1)-H(1C)	109.5
N(3)-Pd(1)-Cl(2)	92.63(4)	H(1A)-C(1)-H(1C)	109.5
N(1)-Pd(1)-Cl(2)	90.89(3)	N(1)-C(2)-C(3)	115.94(13)
Cl(1)-Pd(1)-Cl(2)	174.070(14)	N(1)-C(2)-H(2B)	108.3
C(1)-N(1)-C(2)	109.44(12)	C(3)-C(2)-H(2B)	108.3
C(1)-N(1)-C(15)	108.06(12)	N(1)-C(2)-H(2A)	108.3
C(2)-N(1)-C(15)	106.47(12)	C(3)-C(2)-H(2A)	108.3
C(1)-N(1)-Pd(1)	114.72(9)	H(2B)-C(2)-H(2A)	107.4
C(2)-N(1)-Pd(1)	108.39(9)	C(4)-C(3)-C(2)	116.36(13)
C(15)-N(1)-Pd(1)	109.45(9)	C(4)-C(3)-H(3B)	108.2
C(4)-N(2)-C(5)	112.18(13)	C(2)-C(3)-H(3B)	108.2
C(4)-N(2)-Pd(1)	115.70(10)	C(4)-C(3)-H(3A)	108.2
C(5)-N(2)-Pd(1)	110.22(10)	C(2)-C(3)-H(3A)	108.2
C(4)-N(2)-H(2)	106.0	H(3B)-C(3)-H(3A)	107.4
C(5)-N(2)-H(2)	106.0	N(2)-C(4)-C(3)	111.71(13)

N(2)-C(4)-H(4A)	109.3	C(10)-C(12)-H(12A)	109.6
C(3)-C(4)-H(4A)	109.3	N(3)-C(12)-H(12A)	109.6
N(2)-C(4)-H(4B)	109.3	C(10)-C(12)-H(12B)	109.6
C(3)-C(4)-H(4B)	109.3	N(3)-C(12)-H(12B)	109.6
H(4A)-C(4)-H(4B)	107.9	H(12A)-C(12)-H(12B)	108.1
C(6)-C(5)-N(2)	110.33(13)	N(3)-C(13)-C(14)	112.17(13)
C(6)-C(5)-H(5B)	109.6	N(3)-C(13)-H(13A)	109.2
N(2)-C(5)-H(5B)	109.6	C(14)-C(13)-H(13A)	109.2
C(6)-C(5)-H(5A)	109.6	N(3)-C(13)-H(13B)	109.2
N(2)-C(5)-H(5A)	109.6	C(14)-C(13)-H(13B)	109.2
H(5B)-C(5)-H(5A)	108.1	H(13A)-C(13)-H(13B)	107.9
C(11)-C(6)-C(7)	116.03(17)	C(13)-C(14)-C(15)	115.12(15)
C(11)-C(6)-C(5)	116.69(14)	C(13)-C(14)-H(14A)	108.5
C(7)-C(6)-C(5)	127.03(16)	C(15)-C(14)-H(14A)	108.5
C(8)-C(7)-C(6)	119.17(18)	C(13)-C(14)-H(14B)	108.5
C(8)-C(7)-H(7)	120.4	C(15)-C(14)-H(14B)	108.5
C(6)-C(7)-H(7)	120.4	H(14A)-C(14)-H(14B)	107.5
C(7)-C(8)-C(9)	122.40(16)	N(1)-C(15)-C(14)	115.11(13)
C(7)-C(8)-H(8)	118.8	N(1)-C(15)-H(15A)	108.5
C(9)-C(8)-H(8)	118.8	C(14)-C(15)-H(15A)	108.5
C(8)-C(9)-C(10)	119.66(17)	N(1)-C(15)-H(15B)	108.5
C(8)-C(9)-H(9)	120.2	C(14)-C(15)-H(15B)	108.5
C(10)-C(9)-H(9)	120.2	H(15A)-C(15)-H(15B)	107.5
C(11)-C(10)-C(9)	115.29(17)	F(1)-B(1)-F(3)	110.44(16)
C(11)-C(10)-C(12)	116.90(14)	F(1)-B(1)-F(4)	108.46(16)
C(9)-C(10)-C(12)	127.60(16)	F(3)-B(1)-F(4)	109.49(15)
C(10)-C(11)-C(6)	127.36(15)	F(1)-B(1)-F(2)	109.92(15)
C(10)-C(11)-Pd(1)	116.35(12)	F(3)-B(1)-F(2)	109.54(16)
C(6)-C(11)-Pd(1)	116.28(12)	F(4)-B(1)-F(2)	108.97(16)
C(10)-C(12)-N(3)	110.13(13)		

Symmetry transformations used to generate equivalent atoms:

Table 4. Anisotropic displacement parameters ($\text{\AA}^2 \times 10^3$) for stahl90. The anisotropic displacement factor exponent takes the form: $-2\pi^2 [h^2 a^{*2} U^{11} + \dots + 2 h k a^* b^* U^{12}]$

	U ¹¹	U ²²	U ³³	U ²³	U ¹³	U ¹²
Pd(1)	11(1)	13(1)	10(1)	1(1)	0(1)	0(1)
Cl(1)	16(1)	19(1)	16(1)	-1(1)	5(1)	-1(1)
Cl(2)	14(1)	21(1)	18(1)	3(1)	4(1)	4(1)
N(1)	14(1)	17(1)	15(1)	2(1)	1(1)	2(1)
N(2)	17(1)	18(1)	18(1)	-4(1)	1(1)	-1(1)
N(3)	15(1)	19(1)	15(1)	-1(1)	-2(1)	0(1)
C(1)	18(1)	17(1)	21(1)	2(1)	3(1)	5(1)
C(2)	22(1)	23(1)	14(1)	4(1)	1(1)	4(1)
C(3)	24(1)	26(1)	17(1)	-1(1)	-5(1)	5(1)
C(4)	24(1)	24(1)	15(1)	-4(1)	-2(1)	2(1)
C(5)	27(1)	15(1)	27(1)	-4(1)	4(1)	-2(1)
C(6)	23(1)	14(1)	26(1)	2(1)	11(1)	3(1)
C(7)	29(1)	16(1)	39(1)	7(1)	17(1)	4(1)
C(8)	29(1)	23(1)	39(1)	16(1)	19(1)	12(1)
C(9)	24(1)	33(1)	25(1)	14(1)	9(1)	13(1)
C(10)	21(1)	24(1)	17(1)	7(1)	6(1)	9(1)
C(11)	21(1)	15(1)	19(1)	4(1)	7(1)	5(1)
C(12)	22(1)	30(1)	17(1)	2(1)	-5(1)	7(1)
C(13)	18(1)	24(1)	25(1)	-2(1)	-3(1)	-6(1)
C(14)	23(1)	17(1)	29(1)	-1(1)	-2(1)	-6(1)
C(15)	19(1)	18(1)	24(1)	4(1)	2(1)	-3(1)
F(1)	31(1)	37(1)	40(1)	12(1)	-5(1)	-8(1)
F(2)	29(1)	46(1)	27(1)	6(1)	0(1)	2(1)
F(3)	51(1)	24(1)	23(1)	-3(1)	11(1)	2(1)
F(4)	62(1)	19(1)	31(1)	-5(1)	19(1)	-1(1)
B(1)	30(1)	18(1)	21(1)	0(1)	4(1)	-1(1)

Table 5. Hydrogen coordinates ($\times 10^4$) and isotropic displacement parameters ($\text{\AA}^2 \times 10^{-3}$) for stahl90.

	x	y	z	U(eq)
H(2)	4496	2728	8455	21
H(3)	2111	764	6324	20
H(1B)	4774	-166	8316	28
H(1A)	3947	-841	7559	28
H(1C)	4137	-1436	8514	28
H(2B)	3340	-528	9712	23
H(2A)	2341	519	9595	23
H(3B)	4275	1094	10346	27
H(3A)	4811	1033	9416	27
H(4A)	2917	2677	9747	25
H(4B)	4307	3063	9890	25
H(5B)	2963	4510	8902	27
H(5A)	4210	4655	8464	27
H(7)	2872	6205	7344	33
H(8)	1599	6217	6061	35
H(9)	665	4443	5505	32
H(12A)	867	1919	5577	28
H(12B)	32	2066	6371	28
H(13A)	390	-302	6320	27
H(13B)	154	273	7249	27
H(14A)	2211	-1204	7017	28
H(14B)	985	-1783	7297	28
H(15A)	1227	-444	8579	24
H(15B)	2093	-1607	8577	24

Table 6. Torsion angles [°] for stahl90.

C(11)-Pd(1)-N(1)-C(1)	168.5(12)	C(2)-C(3)-C(4)-N(2)	-72.72(18)
N(2)-Pd(1)-N(1)-C(1)	-87.36(11)	C(4)-N(2)-C(5)-C(6)	-147.64(14)
N(3)-Pd(1)-N(1)-C(1)	87.95(11)	Pd(1)-N(2)-C(5)-C(6)	-17.15(16)
Cl(1)-Pd(1)-N(1)-C(1)	-0.14(10)	N(2)-C(5)-C(6)-C(11)	16.7(2)
Cl(2)-Pd(1)-N(1)-C(1)	-179.31(10)	N(2)-C(5)-C(6)-C(7)	-169.38(15)
C(11)-Pd(1)-N(1)-C(2)	-68.9(13)	C(11)-C(6)-C(7)-C(8)	1.6(2)
N(2)-Pd(1)-N(1)-C(2)	35.27(10)	C(5)-C(6)-C(7)-C(8)	-172.35(16)
N(3)-Pd(1)-N(1)-C(2)	-149.42(10)	C(6)-C(7)-C(8)-C(9)	0.9(3)
Cl(1)-Pd(1)-N(1)-C(2)	122.48(9)	C(7)-C(8)-C(9)-C(10)	-1.8(3)
Cl(2)-Pd(1)-N(1)-C(2)	-56.68(9)	C(8)-C(9)-C(10)-C(11)	0.2(2)
C(11)-Pd(1)-N(1)-C(15)	46.9(13)	C(8)-C(9)-C(10)-C(12)	174.82(16)
N(2)-Pd(1)-N(1)-C(15)	151.01(10)	C(9)-C(10)-C(11)-C(6)	2.7(2)
N(3)-Pd(1)-N(1)-C(15)	-33.68(10)	C(12)-C(10)-C(11)-C(6)	-172.59(15)
Cl(1)-Pd(1)-N(1)-C(15)	-121.77(9)	C(9)-C(10)-C(11)-Pd(1)	-178.57(11)
Cl(2)-Pd(1)-N(1)-C(15)	59.06(9)	C(12)-C(10)-C(11)-Pd(1)	6.16(19)
C(11)-Pd(1)-N(2)-C(4)	139.64(12)	C(7)-C(6)-C(11)-C(10)	-3.6(2)
N(3)-Pd(1)-N(2)-C(4)	162.33(19)	C(5)-C(6)-C(11)-C(10)	171.03(15)
N(1)-Pd(1)-N(2)-C(4)	-37.72(11)	C(7)-C(6)-C(11)-Pd(1)	177.65(12)
Cl(1)-Pd(1)-N(2)-C(4)	-132.34(11)	C(5)-C(6)-C(11)-Pd(1)	-7.72(19)
Cl(2)-Pd(1)-N(2)-C(4)	53.40(11)	N(2)-Pd(1)-C(11)-C(10)	178.97(13)
C(11)-Pd(1)-N(2)-C(5)	11.04(11)	N(3)-Pd(1)-C(11)-C(10)	4.25(12)
N(3)-Pd(1)-N(2)-C(5)	33.7(3)	N(1)-Pd(1)-C(11)-C(10)	-76.6(13)
N(1)-Pd(1)-N(2)-C(5)	-166.32(10)	Cl(1)-Pd(1)-C(11)-C(10)	92.09(12)
Cl(1)-Pd(1)-N(2)-C(5)	99.06(10)	Cl(2)-Pd(1)-C(11)-C(10)	-88.80(12)
Cl(2)-Pd(1)-N(2)-C(5)	-75.20(10)	N(2)-Pd(1)-C(11)-C(6)	-2.14(12)
C(11)-Pd(1)-N(3)-C(13)	-142.52(12)	N(3)-Pd(1)-C(11)-C(6)	-176.86(13)
N(2)-Pd(1)-N(3)-C(13)	-165.22(19)	N(1)-Pd(1)-C(11)-C(6)	102.3(13)
N(1)-Pd(1)-N(3)-C(13)	34.80(12)	Cl(1)-Pd(1)-C(11)-C(6)	-89.02(12)
Cl(1)-Pd(1)-N(3)-C(13)	129.56(11)	Cl(2)-Pd(1)-C(11)-C(6)	90.09(12)
Cl(2)-Pd(1)-N(3)-C(13)	-56.38(11)	C(11)-C(10)-C(12)-N(3)	-17.0(2)
C(11)-Pd(1)-N(3)-C(12)	-13.14(10)	C(9)-C(10)-C(12)-N(3)	168.44(15)
N(2)-Pd(1)-N(3)-C(12)	-35.8(3)	C(13)-N(3)-C(12)-C(10)	151.13(14)
N(1)-Pd(1)-N(3)-C(12)	164.18(10)	Pd(1)-N(3)-C(12)-C(10)	18.94(15)
Cl(1)-Pd(1)-N(3)-C(12)	-101.06(10)	C(12)-N(3)-C(13)-C(14)	177.45(14)
Cl(2)-Pd(1)-N(3)-C(12)	73.00(10)	Pd(1)-N(3)-C(13)-C(14)	-54.17(17)
C(1)-N(1)-C(2)-C(3)	71.26(17)	N(3)-C(13)-C(14)-C(15)	72.93(19)
C(15)-N(1)-C(2)-C(3)	-172.18(13)	C(1)-N(1)-C(15)-C(14)	-70.20(17)
Pd(1)-N(1)-C(2)-C(3)	-54.52(15)	C(2)-N(1)-C(15)-C(14)	172.31(13)
N(1)-C(2)-C(3)-C(4)	76.14(18)	Pd(1)-N(1)-C(15)-C(14)	55.35(15)
C(5)-N(2)-C(4)-C(3)	-176.48(13)	C(13)-C(14)-C(15)-N(1)	-77.54(18)
Pd(1)-N(2)-C(4)-C(3)	55.89(16)		

Symmetry transformations used to generate equivalent atoms:

Table 7. Hydrogen bonds for stahl90 [\AA and $^\circ$].

D-H...A	d(D-H)	d(H...A)	d(D...A)	\angle (DHA)
N(3)-H(3)...F(4)#1	0.93	2.02	2.8998(17)	158.0

Symmetry transformations used to generate equivalent atoms:

#1 x,y-1,z

X-Ray Crystal Structure Data for Aryl-Pd^{IV}(NCS) Complex 4, “Stahl 74”.

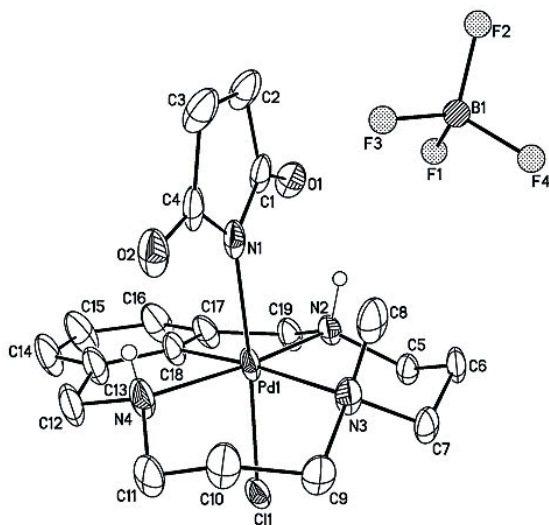


Figure 1. A molecular drawing of Stahl74. All non-amino H atoms and minor components of the disordered BF_4^- anion are omitted.

Data Collection

A red crystal with approximate dimensions $0.16 \times 0.12 \times 0.10 \text{ mm}^3$ was selected under oil under ambient conditions and attached to the tip of a MiTeGen MicroMount[®]. The crystal was mounted in a stream of cold nitrogen at 100(1) K and centered in the X-ray beam by using a video camera.

The crystal evaluation and data collection were performed on a Bruker CCD-1000 diffractometer with Mo K_α ($\lambda = 0.71073 \text{ \AA}$) radiation and the diffractometer to crystal distance of 4.7 cm.

The initial cell constants were obtained from three series of ω scans at different starting angles. Each series consisted of 20 frames collected at intervals of 0.3° in a 6° range about ω with the exposure time of 30 seconds per frame. A total of 67 reflections was obtained. The reflections were successfully indexed by an automated indexing routine built in the SMART

program. The final cell constants were calculated from a set of 9953 strong reflections from the actual data collection.

The data were collected by using the full sphere data collection routine to survey the reciprocal space to the extent of a full sphere to a resolution of 0.73 Å. A total of 19797 data were harvested by collecting three sets of frames with 0.3° scans in ω with an exposure time 90 sec per frame. These highly redundant datasets were corrected for Lorentz and polarization effects. The absorption correction was based on fitting a function to the empirical transmission surface as sampled by multiple equivalent measurements.¹

Structure Solution and Refinement

The systematic absences in the diffraction data were consistent for the space group *C2/c* that yielded chemically reasonable and computationally stable results of refinement.²

A successful solution by the direct methods provided most non-hydrogen atoms from the *E*-map. The remaining non-hydrogen atoms were located in an alternating series of least-squares cycles and difference Fourier maps. All non-hydrogen atoms except B and F atoms were refined with anisotropic displacement coefficients. All hydrogen atoms were included in the structure factor calculation at idealized positions and were allowed to ride on the neighboring atoms with relative isotropic displacement coefficients.

There were two partially occupied solvate molecules of acetonitrile present in the asymmetric unit. A significant amount of time was invested in identifying and refining the disordered molecules. Bond length restraints were applied to model the molecules but the resulting isotropic displacement coefficients suggested the molecules were mobile. In addition, the refinement was computationally unstable. Option SQUEEZE of program PLATON⁵ was used to correct the diffraction data for diffuse scattering effects and to identify the solvate

molecule. PLATON calculated the upper limit of volume that can be occupied by the solvent to be 585.0 Å³, or 12.0% of the unit cell volume. The program calculated 154 electrons in the unit cell for the diffuse species. This approximately corresponds to one molecule of acetonitrile in the asymmetric unit (176 electrons). Please note that all derived results in the following tables are based on the known contents. No data are given for the diffusely scattering species.

The BF₄⁻ anion is disordered over three positions in a 47.3(3):27.7(3):25.0(3) ratio. Each anion was refined isotropically with an idealized geometry. The final least-squares refinement of 296 parameters against 5008 data resulted in residuals *R* (based on *F*² for *I* ≥ 2σ) and *wR* (based on *F*² for all data) of 0.0449 and 0.1158, respectively. The final difference Fourier map was featureless. The molecular diagram is drawn with 40% probability ellipsoids.

Table 1. Crystal data and structure refinement for stahl74.

Identification code	stahl74	
Empirical formula	[C ₁₉ H ₂₈ ClN ₄ O ₂ Pd] ⁺ , [BF ₄] ⁻	
Formula weight	573.11	
Temperature	100(2) K	
Wavelength	0.71073 Å	
Crystal system	Monoclinic	
Space group	C2/c	
Unit cell dimensions	a = 27.690(4) Å	α = 90°.
	b = 9.7388(15) Å	β = 119.757(2)°.
	c = 20.911(3) Å	γ = 90°.
Volume	4895.5(13) Å ³	
Z	8	
Density (calculated)	1.555 Mg/m ³	
Absorption coefficient	0.920 mm ⁻¹	
F(000)	2320	
Crystal size	0.16 x 0.12 x 0.10 mm ³	
Theta range for data collection	2.03 to 26.41°.	
Index ranges	-34 ≤ h ≤ 30, 0 ≤ k ≤ 12, 0 ≤ l ≤ 26	
Reflections collected	5008	
Independent reflections	5008 [R(int) = 0.0000]	
Completeness to theta = 25.00°	99.8 %	
Absorption correction	Empirical with SADABS	
Max. and min. transmission	0.9136 and 0.8668	
Refinement method	Full-matrix least-squares on F ²	
Data / restraints / parameters	5008 / 31 / 296	
Goodness-of-fit on F ²	1.032	
Final R indices [I > 2σ(I)]	R1 = 0.0449, wR2 = 0.1102	
R indices (all data)	R1 = 0.0593, wR2 = 0.1158	
Largest diff. peak and hole	0.963 and -0.865 e.Å ⁻³	

Table 2. Atomic coordinates ($\times 10^4$) and equivalent isotropic displacement parameters ($\text{\AA}^2 \times 10^3$) for stahl74. $U(\text{eq})$ is defined as one third of the trace of the orthogonalized U^{ij} tensor.

	x	y	z	$U(\text{eq})$
Pd(1)	1669(1)	5301(1)	632(1)	40(1)
Cl(1)	2108(1)	7372(2)	1084(1)	48(1)
O(1)	331(1)	4153(4)	-290(2)	50(1)
O(2)	1981(1)	2116(4)	265(2)	53(1)
N(1)	1244(1)	3470(5)	128(2)	42(1)
N(2)	971(1)	6096(4)	628(2)	36(1)
N(3)	2072(1)	4428(5)	1775(2)	43(1)
N(4)	2288(2)	4751(6)	397(2)	53(1)
C(1)	670(2)	3283(6)	-208(2)	47(1)
C(2)	518(2)	1808(7)	-459(3)	56(2)
C(3)	1073(2)	1135(7)	-250(3)	59(2)
C(4)	1487(2)	2277(6)	71(2)	47(1)
C(5)	1040(2)	6579(5)	1343(2)	37(1)
C(6)	1297(2)	5492(6)	1938(2)	41(1)
C(7)	1921(2)	5280(6)	2242(2)	45(1)
C(8)	1912(2)	3000(6)	1797(2)	49(1)
C(9)	2694(2)	4531(7)	2123(2)	52(1)
C(10)	2938(2)	3914(8)	1671(3)	61(2)
C(11)	2870(2)	4776(8)	1033(3)	64(2)
C(12)	2221(2)	5495(7)	-269(3)	62(2)
C(13)	1653(2)	6137(7)	-688(2)	58(2)
C(14)	1420(2)	6804(8)	-1365(3)	76(2)
C(15)	930(2)	7513(9)	-1622(3)	82(3)
C(16)	657(2)	7652(8)	-1211(3)	69(2)
C(17)	886(2)	6983(6)	-528(2)	51(2)
C(18)	1350(2)	6214(6)	-327(2)	48(1)
C(19)	705(2)	7175(6)	36(2)	44(1)
B(1)	833(2)	948(4)	1425(2)	35(2)
F(1)	644(2)	2242(5)	1125(4)	50(1)
F(2)	384(2)	53(5)	1171(3)	50(1)
F(3)	1205(2)	466(5)	1212(3)	50(1)
F(4)	1106(3)	1020(7)	2189(3)	50(1)
B(1A)	832(3)	391(6)	1617(3)	35(2)
F(1A)	343(3)	1032(9)	1104(4)	50(1)
F(2A)	1143(4)	1294(9)	2193(4)	50(1)
F(3A)	1140(4)	13(10)	1285(6)	50(1)
F(4A)	699(4)	-771(7)	1884(5)	50(1)
B(1B)	773(3)	725(7)	1583(4)	35(2)
F(1B)	353(4)	208(10)	1695(5)	50(1)
F(2B)	897(4)	-217(9)	1186(5)	50(1)
F(3B)	597(5)	1948(8)	1192(7)	50(1)
F(4B)	1245(3)	961(13)	2261(5)	50(1)

Table 3. Bond lengths [Å] and angles [°] for stahl74.

Pd(1)-C(18)	1.957(4)	C(8)-H(8B)	0.9800
Pd(1)-N(4)	2.075(4)	C(9)-C(10)	1.532(7)
Pd(1)-N(2)	2.078(3)	C(9)-H(9A)	0.9900
Pd(1)-N(1)	2.107(4)	C(9)-H(9B)	0.9900
Pd(1)-N(3)	2.244(4)	C(10)-C(11)	1.507(8)
Pd(1)-Cl(1)	2.3024(14)	C(10)-H(10B)	0.9900
O(1)-C(1)	1.213(6)	C(10)-H(10A)	0.9900
O(2)-C(4)	1.230(5)	C(11)-H(11B)	0.9900
N(1)-C(4)	1.376(7)	C(11)-H(11A)	0.9900
N(1)-C(1)	1.396(5)	C(12)-C(13)	1.504(8)
N(2)-C(5)	1.486(5)	C(12)-H(12A)	0.9900
N(2)-C(19)	1.507(6)	C(12)-H(12B)	0.9900
N(2)-H(2)	0.9300	C(13)-C(18)	1.381(6)
N(3)-C(8)	1.468(7)	C(13)-C(14)	1.392(7)
N(3)-C(7)	1.492(6)	C(14)-C(15)	1.372(9)
N(3)-C(9)	1.504(5)	C(14)-H(14)	0.9500
N(4)-C(12)	1.496(7)	C(15)-C(16)	1.405(8)
N(4)-C(11)	1.497(6)	C(15)-H(15)	0.9500
N(4)-H(4)	0.9300	C(16)-C(17)	1.403(7)
C(1)-C(2)	1.515(8)	C(16)-H(16)	0.9500
C(2)-C(3)	1.522(7)	C(17)-C(18)	1.362(8)
C(2)-H(2B)	0.9900	C(17)-C(19)	1.503(6)
C(2)-H(2A)	0.9900	C(19)-H(19A)	0.9900
C(3)-C(4)	1.496(8)	C(19)-H(19B)	0.9900
C(3)-H(3A)	0.9900	B(1)-F(1)	1.389(3)
C(3)-H(3B)	0.9900	B(1)-F(2)	1.389(3)
C(5)-C(6)	1.516(6)	B(1)-F(3)	1.390(3)
C(5)-H(5A)	0.9900	B(1)-F(4)	1.391(3)
C(5)-H(5B)	0.9900	B(1A)-F(4A)	1.390(3)
C(6)-C(7)	1.529(6)	B(1A)-F(3A)	1.390(3)
C(6)-H(6A)	0.9900	B(1A)-F(1A)	1.390(3)
C(6)-H(6B)	0.9900	B(1A)-F(2A)	1.391(3)
C(7)-H(7B)	0.9900	B(1B)-F(3B)	1.389(3)
C(7)-H(7A)	0.9900	B(1B)-F(2B)	1.390(3)
C(8)-H(8A)	0.9800	B(1B)-F(1B)	1.390(3)
C(8)-H(8C)	0.9800	B(1B)-F(4B)	1.390(3)
C(18)-Pd(1)-N(4)	83.14(18)	C(1)-N(1)-Pd(1)	125.1(4)
C(18)-Pd(1)-N(2)	83.13(17)	C(5)-N(2)-C(19)	111.8(4)
N(4)-Pd(1)-N(2)	166.26(15)	C(5)-N(2)-Pd(1)	117.3(2)
C(18)-Pd(1)-N(1)	90.97(19)	C(19)-N(2)-Pd(1)	109.8(2)
N(4)-Pd(1)-N(1)	89.14(17)	C(5)-N(2)-H(2)	105.7
N(2)-Pd(1)-N(1)	91.52(15)	C(19)-N(2)-H(2)	105.7
C(18)-Pd(1)-N(3)	175.0(2)	Pd(1)-N(2)-H(2)	105.7
N(4)-Pd(1)-N(3)	97.02(14)	C(8)-N(3)-C(7)	108.6(4)
N(2)-Pd(1)-N(3)	96.62(13)	C(8)-N(3)-C(9)	109.8(4)
N(1)-Pd(1)-N(3)	94.07(15)	C(7)-N(3)-C(9)	105.8(3)
C(18)-Pd(1)-Cl(1)	84.27(16)	C(8)-N(3)-Pd(1)	113.2(3)
N(4)-Pd(1)-Cl(1)	89.64(14)	C(7)-N(3)-Pd(1)	109.5(3)
N(2)-Pd(1)-Cl(1)	88.56(12)	C(9)-N(3)-Pd(1)	109.6(3)
N(1)-Pd(1)-Cl(1)	175.20(10)	C(12)-N(4)-C(11)	113.6(4)
N(3)-Pd(1)-Cl(1)	90.69(12)	C(12)-N(4)-Pd(1)	111.0(3)
C(4)-N(1)-C(1)	109.2(4)	C(11)-N(4)-Pd(1)	115.9(3)
C(4)-N(1)-Pd(1)	125.6(3)	C(12)-N(4)-H(4)	105.0

C(11)-N(4)-H(4)	105.0	H(10B)-C(10)-H(10A)	107.5
Pd(1)-N(4)-H(4)	105.0	N(4)-C(11)-C(10)	112.5(4)
O(1)-C(1)-N(1)	126.1(5)	N(4)-C(11)-H(11B)	109.1
O(1)-C(1)-C(2)	123.4(4)	C(10)-C(11)-H(11B)	109.1
N(1)-C(1)-C(2)	110.4(4)	N(4)-C(11)-H(11A)	109.1
C(1)-C(2)-C(3)	104.0(4)	C(10)-C(11)-H(11A)	109.1
C(1)-C(2)-H(2B)	111.0	H(11B)-C(11)-H(11A)	107.8
C(3)-C(2)-H(2B)	111.0	N(4)-C(12)-C(13)	110.8(4)
C(1)-C(2)-H(2A)	111.0	N(4)-C(12)-H(12A)	109.5
C(3)-C(2)-H(2A)	111.0	C(13)-C(12)-H(12A)	109.5
H(2B)-C(2)-H(2A)	109.0	N(4)-C(12)-H(12B)	109.5
C(4)-C(3)-C(2)	104.3(5)	C(13)-C(12)-H(12B)	109.5
C(4)-C(3)-H(3A)	110.9	H(12A)-C(12)-H(12B)	108.1
C(2)-C(3)-H(3A)	110.9	C(18)-C(13)-C(14)	115.5(5)
C(4)-C(3)-H(3B)	110.9	C(18)-C(13)-C(12)	116.5(4)
C(2)-C(3)-H(3B)	110.9	C(14)-C(13)-C(12)	127.5(4)
H(3A)-C(3)-H(3B)	108.9	C(15)-C(14)-C(13)	120.1(5)
O(2)-C(4)-N(1)	126.1(5)	C(15)-C(14)-H(14)	120.0
O(2)-C(4)-C(3)	122.2(5)	C(13)-C(14)-H(14)	120.0
N(1)-C(4)-C(3)	111.7(4)	C(14)-C(15)-C(16)	122.5(5)
N(2)-C(5)-C(6)	112.3(4)	C(14)-C(15)-H(15)	118.8
N(2)-C(5)-H(5A)	109.1	C(16)-C(15)-H(15)	118.8
C(6)-C(5)-H(5A)	109.1	C(17)-C(16)-C(15)	118.0(6)
N(2)-C(5)-H(5B)	109.1	C(17)-C(16)-H(16)	121.0
C(6)-C(5)-H(5B)	109.1	C(15)-C(16)-H(16)	121.0
H(5A)-C(5)-H(5B)	107.9	C(18)-C(17)-C(16)	116.7(4)
C(5)-C(6)-C(7)	114.1(4)	C(18)-C(17)-C(19)	117.2(4)
C(5)-C(6)-H(6A)	108.7	C(16)-C(17)-C(19)	125.7(5)
C(7)-C(6)-H(6A)	108.7	C(17)-C(18)-C(13)	126.7(5)
C(5)-C(6)-H(6B)	108.7	C(17)-C(18)-Pd(1)	116.3(3)
C(7)-C(6)-H(6B)	108.7	C(13)-C(18)-Pd(1)	116.6(4)
H(6A)-C(6)-H(6B)	107.6	C(17)-C(19)-N(2)	109.8(4)
N(3)-C(7)-C(6)	115.4(4)	C(17)-C(19)-H(19A)	109.7
N(3)-C(7)-H(7B)	108.4	N(2)-C(19)-H(19A)	109.7
C(6)-C(7)-H(7B)	108.4	C(17)-C(19)-H(19B)	109.7
N(3)-C(7)-H(7A)	108.4	N(2)-C(19)-H(19B)	109.7
C(6)-C(7)-H(7A)	108.4	H(19A)-C(19)-H(19B)	108.2
H(7B)-C(7)-H(7A)	107.5	F(1)-B(1)-F(2)	109.3(2)
N(3)-C(8)-H(8A)	109.5	F(1)-B(1)-F(3)	109.7(2)
N(3)-C(8)-H(8C)	109.5	F(2)-B(1)-F(3)	109.3(2)
H(8A)-C(8)-H(8C)	109.5	F(1)-B(1)-F(4)	109.9(2)
N(3)-C(8)-H(8B)	109.5	F(2)-B(1)-F(4)	110.0(2)
H(8A)-C(8)-H(8B)	109.5	F(3)-B(1)-F(4)	108.6(2)
H(8C)-C(8)-H(8B)	109.5	F(4A)-B(1A)-F(3A)	109.6(3)
N(3)-C(9)-C(10)	115.2(4)	F(4A)-B(1A)-F(1A)	109.0(3)
N(3)-C(9)-H(9A)	108.5	F(3A)-B(1A)-F(1A)	109.7(3)
C(10)-C(9)-H(9A)	108.5	F(4A)-B(1A)-F(2A)	110.0(3)
N(3)-C(9)-H(9B)	108.5	F(3A)-B(1A)-F(2A)	109.2(3)
C(10)-C(9)-H(9B)	108.5	F(1A)-B(1A)-F(2A)	109.4(3)
H(9A)-C(9)-H(9B)	107.5	F(3B)-B(1B)-F(2B)	109.4(3)
C(11)-C(10)-C(9)	115.4(5)	F(3B)-B(1B)-F(1B)	109.4(3)
C(11)-C(10)-H(10B)	108.4	F(2B)-B(1B)-F(1B)	109.7(3)
C(9)-C(10)-H(10B)	108.4	F(3B)-B(1B)-F(4B)	109.7(3)
C(11)-C(10)-H(10A)	108.4	F(2B)-B(1B)-F(4B)	109.4(3)
C(9)-C(10)-H(10A)	108.4	F(1B)-B(1B)-F(4B)	109.3(3)

Table 4. Anisotropic displacement parameters ($\text{\AA}^2 \times 10^3$) for stahl74. The anisotropic displacement factor exponent takes the form: $-2\pi^2 [h^2 a^{*2} U^{11} + \dots + 2 h k a^* b^* U^{12}]$

	U ¹¹	U ²²	U ³³	U ²³	U ¹³	U ¹²
Pd(1)	14(1)	91(1)	15(1)	0(1)	8(1)	-9(1)
Cl(1)	22(1)	101(1)	22(1)	0(1)	10(1)	-18(1)
O(1)	17(1)	94(3)	36(2)	-20(2)	12(1)	-6(2)
O(2)	24(2)	106(3)	29(2)	0(2)	13(1)	6(2)
N(1)	17(2)	94(3)	15(2)	-3(2)	8(1)	-4(2)
N(2)	16(2)	74(3)	17(2)	2(2)	6(1)	-8(2)
N(3)	17(2)	91(3)	18(2)	1(2)	6(1)	-3(2)
N(4)	20(2)	116(4)	26(2)	-2(2)	14(2)	-9(2)
C(1)	22(2)	103(4)	17(2)	-15(2)	11(2)	-9(2)
C(2)	26(2)	105(5)	36(3)	-35(3)	14(2)	-11(3)
C(3)	29(2)	105(5)	38(3)	-33(3)	13(2)	-3(3)
C(4)	27(2)	103(4)	16(2)	-3(2)	14(2)	0(2)
C(5)	18(2)	75(3)	19(2)	-2(2)	9(2)	-6(2)
C(6)	26(2)	83(4)	20(2)	2(2)	16(2)	-7(2)
C(7)	24(2)	93(4)	14(2)	1(2)	7(2)	-6(2)
C(8)	31(2)	92(4)	18(2)	5(2)	8(2)	6(2)
C(9)	15(2)	107(5)	23(2)	-5(2)	2(2)	0(2)
C(10)	18(2)	131(6)	28(2)	-7(3)	8(2)	3(3)
C(11)	17(2)	142(6)	37(3)	-14(3)	15(2)	-10(3)
C(12)	37(3)	127(6)	36(3)	-3(3)	27(2)	-16(3)
C(13)	31(2)	124(5)	24(2)	2(3)	16(2)	-20(3)
C(14)	42(3)	165(7)	24(2)	9(3)	19(2)	-27(4)
C(15)	35(3)	179(8)	24(2)	27(3)	8(2)	-23(4)
C(16)	30(2)	140(6)	26(2)	23(3)	6(2)	-15(3)
C(17)	22(2)	105(5)	21(2)	9(2)	7(2)	-17(2)
C(18)	26(2)	105(4)	13(2)	2(2)	9(2)	-19(2)
C(19)	24(2)	82(4)	22(2)	10(2)	10(2)	-7(2)

Table 5. Hydrogen coordinates ($\times 10^4$) and isotropic displacement parameters ($\text{\AA}^2 \times 10^{-3}$) for stahl74.

	x	y	z	U(eq)
H(2)	717	5378	480	44
H(4)	2219	3834	255	63
H(2B)	262	1761	-997	68
H(2A)	340	1360	-204	68
H(3A)	1159	396	116	71
H(3B)	1069	742	-689	71
H(5A)	672	6841	1275	45
H(5B)	1280	7406	1503	45
H(6A)	1104	4610	1736	49
H(6B)	1235	5753	2349	49
H(7B)	2099	6192	2313	54
H(7A)	2079	4842	2733	54
H(8A)	1506	2934	1554	73
H(8C)	2075	2701	2310	73
H(8B)	2048	2411	1540	73
H(9A)	2866	4064	2607	62
H(9B)	2801	5512	2214	62
H(10B)	3340	3748	2004	73
H(10A)	2760	3012	1478	73
H(11B)	2975	5737	1200	77
H(11A)	3127	4435	867	77
H(12A)	2273	4845	-593	75
H(12B)	2508	6219	-115	75
H(14)	1600	6768	-1650	91
H(15)	769	7924	-2096	99
H(16)	327	8184	-1390	83
H(19A)	295	7103	-204	52
H(19B)	816	8100	259	52

Table 6. Torsion angles [°] for stahl74.

C(18)-Pd(1)-N(1)-C(4)	109.9(4)	C(1)-N(1)-C(4)-O(2)	174.9(4)
N(4)-Pd(1)-N(1)-C(4)	26.8(3)	Pd(1)-N(1)-C(4)-O(2)	-4.5(6)
N(2)-Pd(1)-N(1)-C(4)	-166.9(3)	C(1)-N(1)-C(4)-C(3)	-6.4(5)
N(3)-Pd(1)-N(1)-C(4)	-70.2(3)	Pd(1)-N(1)-C(4)-C(3)	174.3(3)
Cl(1)-Pd(1)-N(1)-C(4)	102.1(12)	C(2)-C(3)-C(4)-O(2)	-175.9(4)
C(18)-Pd(1)-N(1)-C(1)	-69.4(3)	C(2)-C(3)-C(4)-N(1)	5.2(5)
N(4)-Pd(1)-N(1)-C(1)	-152.5(3)	C(19)-N(2)-C(5)-C(6)	178.9(3)
N(2)-Pd(1)-N(1)-C(1)	13.8(3)	Pd(1)-N(2)-C(5)-C(6)	-53.1(4)
N(3)-Pd(1)-N(1)-C(1)	110.5(3)	N(2)-C(5)-C(6)-C(7)	74.6(5)
Cl(1)-Pd(1)-N(1)-C(1)	-77.2(12)	C(8)-N(3)-C(7)-C(6)	-70.0(5)
C(18)-Pd(1)-N(2)-C(5)	-143.4(4)	C(9)-N(3)-C(7)-C(6)	172.1(4)
N(4)-Pd(1)-N(2)-C(5)	-141.6(7)	Pd(1)-N(3)-C(7)-C(6)	54.1(5)
N(1)-Pd(1)-N(2)-C(5)	125.8(3)	C(5)-C(6)-C(7)-N(3)	-79.1(6)
N(3)-Pd(1)-N(2)-C(5)	31.5(4)	C(8)-N(3)-C(9)-C(10)	71.9(6)
Cl(1)-Pd(1)-N(2)-C(5)	-59.0(3)	C(7)-N(3)-C(9)-C(10)	-171.0(5)
C(18)-Pd(1)-N(2)-C(19)	-14.4(3)	Pd(1)-N(3)-C(9)-C(10)	-53.0(6)
N(4)-Pd(1)-N(2)-C(19)	-12.6(9)	N(3)-C(9)-C(10)-C(11)	77.0(7)
N(1)-Pd(1)-N(2)-C(19)	-105.2(3)	C(12)-N(4)-C(11)-C(10)	-174.9(5)
N(3)-Pd(1)-N(2)-C(19)	160.5(3)	Pd(1)-N(4)-C(11)-C(10)	54.8(7)
Cl(1)-Pd(1)-N(2)-C(19)	70.0(3)	C(9)-C(10)-C(11)-N(4)	-74.7(6)
C(18)-Pd(1)-N(3)-C(8)	178(17)	C(11)-N(4)-C(12)-C(13)	-147.4(5)
N(4)-Pd(1)-N(3)-C(8)	-90.8(3)	Pd(1)-N(4)-C(12)-C(13)	-14.7(6)
N(2)-Pd(1)-N(3)-C(8)	90.8(3)	N(4)-C(12)-C(13)-C(18)	14.1(8)
N(1)-Pd(1)-N(3)-C(8)	-1.2(3)	N(4)-C(12)-C(13)-C(14)	-173.8(6)
Cl(1)-Pd(1)-N(3)-C(8)	179.5(3)	C(18)-C(13)-C(14)-C(15)	1.9(10)
C(18)-Pd(1)-N(3)-C(7)	56.3(19)	C(12)-C(13)-C(14)-C(15)	-170.2(7)
N(4)-Pd(1)-N(3)-C(7)	147.8(3)	C(13)-C(14)-C(15)-C(16)	2.9(11)
N(2)-Pd(1)-N(3)-C(7)	-30.5(3)	C(14)-C(15)-C(16)-C(17)	-3.0(11)
N(1)-Pd(1)-N(3)-C(7)	-122.5(3)	C(15)-C(16)-C(17)-C(18)	-1.7(9)
Cl(1)-Pd(1)-N(3)-C(7)	58.1(3)	C(15)-C(16)-C(17)-C(19)	170.4(6)
C(18)-Pd(1)-N(3)-C(9)	-59(2)	C(16)-C(17)-C(18)-C(13)	7.2(9)
N(4)-Pd(1)-N(3)-C(9)	32.1(4)	C(19)-C(17)-C(18)-C(13)	-165.7(5)
N(2)-Pd(1)-N(3)-C(9)	-146.2(3)	C(16)-C(17)-C(18)-Pd(1)	179.4(4)
N(1)-Pd(1)-N(3)-C(9)	121.8(3)	C(19)-C(17)-C(18)-Pd(1)	6.6(7)
Cl(1)-Pd(1)-N(3)-C(9)	-57.6(3)	C(14)-C(13)-C(18)-C(17)	-7.3(9)
C(18)-Pd(1)-N(4)-C(12)	9.4(4)	C(12)-C(13)-C(18)-C(17)	165.7(6)
N(2)-Pd(1)-N(4)-C(12)	7.6(10)	C(14)-C(13)-C(18)-Pd(1)	-179.5(5)
N(1)-Pd(1)-N(4)-C(12)	100.5(4)	C(12)-C(13)-C(18)-Pd(1)	-6.5(8)
N(3)-Pd(1)-N(4)-C(12)	-165.5(4)	N(4)-Pd(1)-C(18)-C(17)	-174.8(4)
Cl(1)-Pd(1)-N(4)-C(12)	-74.9(4)	N(2)-Pd(1)-C(18)-C(17)	4.7(4)
C(18)-Pd(1)-N(4)-C(11)	141.0(5)	N(1)-Pd(1)-C(18)-C(17)	96.2(4)
N(2)-Pd(1)-N(4)-C(11)	139.2(6)	N(3)-Pd(1)-C(18)-C(17)	-82.7(19)
N(1)-Pd(1)-N(4)-C(11)	-127.9(4)	Cl(1)-Pd(1)-C(18)-C(17)	-84.5(4)
N(3)-Pd(1)-N(4)-C(11)	-33.9(5)	N(4)-Pd(1)-C(18)-C(13)	-1.8(5)
Cl(1)-Pd(1)-N(4)-C(11)	56.7(4)	N(2)-Pd(1)-C(18)-C(13)	177.8(5)
C(4)-N(1)-C(1)-O(1)	-175.8(4)	N(1)-Pd(1)-C(18)-C(13)	-90.8(5)
Pd(1)-N(1)-C(1)-O(1)	3.6(6)	N(3)-Pd(1)-C(18)-C(13)	90(2)
C(4)-N(1)-C(1)-C(2)	4.8(5)	Cl(1)-Pd(1)-C(18)-C(13)	88.5(4)
Pd(1)-N(1)-C(1)-C(2)	-175.8(3)	C(18)-C(17)-C(19)-N(2)	-18.5(6)
O(1)-C(1)-C(2)-C(3)	179.1(5)	C(16)-C(17)-C(19)-N(2)	169.4(5)
N(1)-C(1)-C(2)-C(3)	-1.4(5)	C(5)-N(2)-C(19)-C(17)	152.6(4)
C(1)-C(2)-C(3)-C(4)	-2.1(5)	Pd(1)-N(2)-C(19)-C(17)	20.7(4)

Table 7. Hydrogen bonds for stahl74 [\AA and $^\circ$].

D-H...A	d(D-H)	d(H...A)	d(D...A)	\angle (DHA)
N(4)-H(4)...O(2)	0.93	1.80	2.674(7)	155.0
N(2)-H(2)...O(1)	0.93	1.86	2.652(5)	141.9

Symmetry transformations used to generate equivalent atoms:

X-Ray Crystal Structure Data for Aryl-Pd^{IV}Br₂ Complex 5, “Stahl 72”.

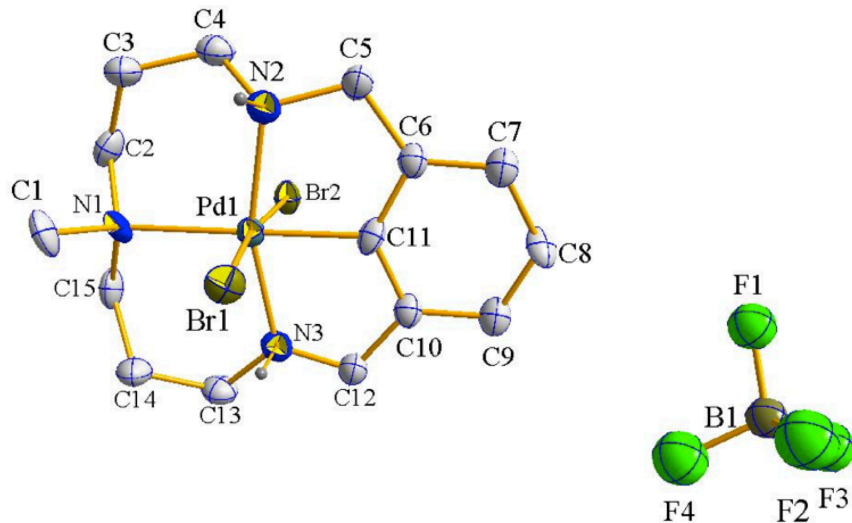


Figure 1. A molecular drawing of stahl72 shown with 50% probability ellipsoids. All hydrogen atoms and minor components of the disordered atoms were omitted for clarity.

Data Collection

A colorless crystal with approximate dimensions 0.13 x 0.09 x 0.04 mm³ was selected under oil under ambient conditions and attached to the tip of a Micromount©. The crystal was mounted in a stream of cold nitrogen at 100(2) K and centered in the X-ray beam by using a video camera.

The crystal evaluation and data collection were performed on a Bruker SMART APEXII diffractometer with Cu K_α ($\lambda = 1.54178 \text{ \AA}$) radiation and the diffractometer to crystal distance of 4.03 cm.

The initial cell constants were obtained from three series of ω scans at different starting angles. Each series consisted of 50 frames collected at intervals of 0.5° in a 25° range about ω with the exposure time of 10 seconds per frame. The reflections were successfully indexed by an automated indexing routine built in the SMART program. The final cell constants were calculated from a set of 9795 strong reflections from the actual data collection.

The data were collected by using the full sphere data collection routine to survey the reciprocal space to the extent of a full sphere to a resolution of 0.82 Å. A total of 29682 data were harvested by collecting 19 sets of frames with 0.6° scans in ω and ϕ with an exposure time 20-40 sec per frame. These highly redundant datasets were corrected for Lorentz and polarization effects. The absorption correction was based on fitting a function to the empirical transmission surface as sampled by multiple equivalent measurements.¹

Structure Solution and Refinement

The systematic absences in the diffraction data were uniquely consistent for the space group $P2_1/c$ that yielded chemically reasonable and computationally stable results of refinement.²

A successful solution by the direct methods provided most non-hydrogen atoms from the E -map. The remaining non-hydrogen atoms were located in an alternating series of least-squares cycles and difference Fourier maps. All non-hydrogen atoms except those in the BF_4 anion were refined with anisotropic displacement coefficients. All hydrogen atoms were included in the structure factor calculation at idealized positions and were allowed to ride on the neighboring atoms with relative isotropic displacement coefficients. The tetradentate ligand (atoms N1 to C15) is disordered over two positions in a 51(2)%:49(2)% ratio. The BF_4 anion is disordered over three positions in a 46.4(18)%:36.3(14)%:17.9(12)% ratio and the atoms were refined isotropically. The disordered parts were refined with restraints and constraints. There are several N-H \cdots F intermolecular hydrogen bonds and one intramolecular hydrogen bonding interaction of the type N-H \cdots Br.

The final least-squares refinement of 419 parameters against 3711 data resulted in residuals R (based on F^2 for $I \geq 2\sigma$) and wR (based on F^2 for all data) of 0.0251 and 0.0578, respectively. The final difference Fourier map was featureless.

The molecular diagram is drawn with 50% probability ellipsoids [3].⁶

Table 1. Crystal data and structure refinement for stahl72.		
Identification code	stahl72	
Empirical formula	[C ₁₅ H ₂₄ Br ₂ N ₃ Pd] ⁺ , [BF ₄] ⁻	
Formula weight	599.40	
Temperature	100(2) K	
Wavelength	1.54178 Å	
Crystal system	Monoclinic	
Space group	P2 ₁ /c	
Unit cell dimensions	a = 11.3908(2) Å	α = 90°.
	b = 11.0246(2) Å	β = 94.3340(10)°.
	c = 15.2629(2) Å	γ = 90°.
Volume	1911.22(5) Å ³	
Z	4	
Density (calculated)	2.083 Mg/m ³	
Absorption coefficient	13.126 mm ⁻¹	
F(000)	1168	
Crystal size	0.13 x 0.09 x 0.04 mm ³	
Theta range for data collection	3.89 to 71.83°.	
Index ranges	-13 ≤ h ≤ 14, -12 ≤ k ≤ 13, -18 ≤ l ≤ 18	
Reflections collected	29682	
Independent reflections	3711 [R(int) = 0.0344]	
Completeness to theta = 71.83°	98.7 %	
Absorption correction	Numerical with SADABS	
Max. and min. transmission	0.6218 and 0.2802	
Refinement method	Full-matrix least-squares on F ²	
Data / restraints / parameters	3711 / 758 / 419	
Goodness-of-fit on F ²	1.098	
Final R indices [I > 2σ(I)]	R1 = 0.0251, wR2 = 0.0556	
R indices (all data)	R1 = 0.0303, wR2 = 0.0578	
Largest diff. peak and hole	0.554 and -0.475 e.Å ⁻³	

Table 2. Atomic coordinates ($\times 10^4$) and equivalent isotropic displacement parameters ($\text{\AA}^2 \times 10^3$) for stahl72. $U(\text{eq})$ is defined as one third of the trace of the orthogonalized U^{ij} tensor.

	x	y	z	$U(\text{eq})$
Pd(1)	2377(1)	8085(1)	2256(1)	23(1)
Br(1)	737(1)	8250(1)	3197(1)	31(1)
Br(2)	4054(1)	7644(1)	1396(1)	31(1)
N(1)	1807(13)	9615(11)	1441(8)	28(2)
N(2)	3427(18)	9035(11)	3195(13)	28(2)
N(3)	1561(11)	6684(10)	1555(7)	29(2)
C(1)	825(17)	10350(20)	1763(14)	35(4)
C(2)	2837(16)	10451(15)	1388(9)	37(3)
C(3)	3345(14)	10909(11)	2266(9)	36(3)
C(4)	4105(16)	10044(16)	2841(12)	35(3)
C(5)	4204(19)	8181(13)	3745(14)	35(4)
C(6)	3750(20)	6914(13)	3675(15)	30(3)
C(7)	4065(15)	5890(12)	4194(9)	32(2)
C(8)	3598(16)	4760(12)	3979(9)	35(3)
C(9)	2814(15)	4567(10)	3268(9)	33(3)
C(10)	2450(20)	5555(11)	2747(11)	30(2)
C(11)	2900(20)	6673(11)	3012(13)	27(2)
C(12)	1717(14)	5579(9)	1910(9)	28(2)
C(13)	967(10)	6879(11)	680(7)	34(2)
C(14)	497(9)	8153(11)	538(7)	36(2)
C(15)	1442(12)	9150(12)	542(7)	32(2)
N(1A)	1983(14)	9858(12)	1531(8)	29(2)
N(2A)	3410(20)	8890(13)	3254(14)	33(3)
N(3A)	1306(11)	6997(12)	1451(7)	33(2)
C(1A)	976(17)	10580(20)	1833(17)	36(4)
C(2A)	3051(14)	10651(16)	1618(11)	40(3)
C(3A)	3495(18)	10932(15)	2545(12)	49(4)
C(4A)	4170(19)	9915(19)	3043(15)	45(4)
C(5A)	4048(19)	7941(14)	3805(14)	31(3)
C(6A)	3530(20)	6720(14)	3606(15)	29(3)
C(7A)	3797(17)	5616(13)	4046(12)	40(3)
C(8A)	3269(14)	4561(12)	3743(11)	38(3)
C(9A)	2536(17)	4521(11)	2989(12)	36(3)
C(10A)	2267(19)	5565(11)	2509(11)	28(3)
C(11A)	2800(20)	6613(12)	2845(13)	26(2)
C(12A)	1593(17)	5782(14)	1644(11)	39(3)
C(13A)	1143(13)	7327(14)	517(7)	46(3)
C(14A)	798(13)	8626(15)	360(8)	50(3)
C(15A)	1750(15)	9551(14)	586(8)	42(3)
F(1)	3482(6)	2091(5)	5056(6)	44(2)
F(2)	1721(9)	1617(7)	5522(5)	38(2)
F(3)	2738(9)	193(4)	4793(5)	41(2)
F(4)	1899(8)	1820(8)	4062(4)	54(2)
B(1)	2480(12)	1405(10)	4851(7)	36(3)
F(1A)	3246(10)	2077(8)	4701(9)	69(3)
F(2A)	1602(12)	1751(12)	5426(7)	71(5)
F(3A)	2319(10)	263(5)	4622(5)	42(2)
F(4A)	1442(11)	1901(8)	3968(5)	63(3)
B(1A)	2148(12)	1509(10)	4701(8)	42(4)
F(1B)	3689(13)	1948(12)	4811(12)	39(4)
F(2B)	2140(20)	1683(16)	5639(10)	68(6)

F(3B)	3104(19)	110(12)	5108(15)	75(6)
F(4B)	1959(14)	1290(20)	4144(11)	80(6)
B(1B)	2704(17)	1258(16)	4914(11)	30(7)

Table 3. Bond lengths [Å] and angles [°] for stahl72.

Pd(1)-C(11A)	1.901(12)	N(1A)-C(2A)	1.497(10)
Pd(1)-C(11)	2.002(11)	N(1A)-C(1A)	1.498(11)
Pd(1)-N(3A)	2.051(11)	N(2A)-C(4A)	1.471(11)
Pd(1)-N(2A)	2.057(15)	N(2A)-C(5A)	1.493(10)
Pd(1)-N(3)	2.060(10)	N(2A)-H(2AC)	0.9300
Pd(1)-N(2)	2.080(14)	N(3A)-C(12A)	1.405(11)
Pd(1)-N(1)	2.166(12)	N(3A)-C(13A)	1.470(10)
Pd(1)-N(1A)	2.274(12)	N(3A)-H(3AC)	0.9300
Pd(1)-Br(1)	2.4474(4)	C(1A)-H(1AB)	0.9800
Pd(1)-Br(2)	2.4479(4)	C(1A)-H(1AA)	0.9800
N(1)-C(15)	1.493(10)	C(1A)-H(1AC)	0.9800
N(1)-C(1)	1.497(10)	C(2A)-C(3A)	1.499(12)
N(1)-C(2)	1.499(10)	C(2A)-H(2AB)	0.9900
N(2)-C(4)	1.480(10)	C(2A)-H(2AA)	0.9900
N(2)-C(5)	1.504(11)	C(3A)-C(4A)	1.528(12)
N(2)-H(2)	0.9300	C(3A)-H(3AA)	0.9900
N(3)-C(12)	1.340(9)	C(3A)-H(3AB)	0.9900
N(3)-C(13)	1.466(10)	C(4A)-H(4AA)	0.9900
N(3)-H(3)	0.9300	C(4A)-H(4AB)	0.9900
C(1)-H(1B)	0.9800	C(5A)-C(6A)	1.493(11)
C(1)-H(1A)	0.9800	C(5A)-H(5AB)	0.9900
C(1)-H(1C)	0.9800	C(5A)-H(5AA)	0.9900
C(2)-C(3)	1.507(10)	C(6A)-C(11A)	1.379(11)
C(2)-H(2B)	0.9900	C(6A)-C(7A)	1.413(10)
C(2)-H(2A)	0.9900	C(7A)-C(8A)	1.372(12)
C(3)-C(4)	1.521(11)	C(7A)-H(7A)	0.9500
C(3)-H(3A)	0.9900	C(8A)-C(9A)	1.371(12)
C(3)-H(3B)	0.9900	C(8A)-H(8A)	0.9500
C(4)-H(4A)	0.9900	C(9A)-C(10A)	1.386(11)
C(4)-H(4B)	0.9900	C(9A)-H(9A)	0.9500
C(5)-C(6)	1.489(10)	C(10A)-C(11A)	1.386(10)
C(5)-H(5B)	0.9900	C(10A)-C(12A)	1.496(11)
C(5)-H(5A)	0.9900	C(12A)-H(12D)	0.9900
C(6)-C(11)	1.373(10)	C(12A)-H(12C)	0.9900
C(6)-C(7)	1.409(10)	C(13A)-C(14A)	1.500(12)
C(7)-C(8)	1.384(11)	C(13A)-H(13C)	0.9900
C(7)-H(7)	0.9500	C(13A)-H(13D)	0.9900
C(8)-C(9)	1.370(11)	C(14A)-C(15A)	1.510(12)
C(8)-H(8)	0.9500	C(14A)-H(14C)	0.9900
C(9)-C(10)	1.393(10)	C(14A)-H(14D)	0.9900
C(9)-H(9)	0.9500	C(15A)-H(15C)	0.9900
C(10)-C(11)	1.384(10)	C(15A)-H(15D)	0.9900
C(10)-C(12)	1.474(10)	F(1)-B(1)	1.384(11)
C(12)-H(12A)	0.9900	F(2)-B(1)	1.409(10)
C(12)-H(12B)	0.9900	F(3)-B(1)	1.373(11)
C(13)-C(14)	1.513(10)	F(4)-B(1)	1.406(12)
C(13)-H(13A)	0.9900	F(1A)-B(1A)	1.399(12)
C(13)-H(13B)	0.9900	F(2A)-B(1A)	1.336(12)
C(14)-C(15)	1.537(11)	F(3A)-B(1A)	1.394(12)
C(14)-H(14B)	0.9900	F(4A)-B(1A)	1.397(13)
C(14)-H(14A)	0.9900	F(1B)-B(1B)	1.375(16)
C(15)-H(15A)	0.9900	F(2B)-B(1B)	1.403(15)
C(15)-H(15B)	0.9900	F(3B)-B(1B)	1.369(16)
N(1A)-C(15A)	1.486(11)	F(4B)-B(1B)	1.397(15)

C(11A)-Pd(1)-C(11)	7.7(7)	C(5)-N(2)-H(2)	106.4
C(11A)-Pd(1)-N(3A)	84.4(5)	Pd(1)-N(2)-H(2)	106.4
C(11)-Pd(1)-N(3A)	91.6(4)	C(12)-N(3)-C(13)	122.7(8)
C(11A)-Pd(1)-N(2A)	84.6(5)	C(12)-N(3)-Pd(1)	115.5(6)
C(11)-Pd(1)-N(2A)	77.2(5)	C(13)-N(3)-Pd(1)	121.5(6)
N(3A)-Pd(1)-N(2A)	167.9(6)	C(12)-N(3)-H(3)	92.0
C(11A)-Pd(1)-N(3)	72.2(4)	C(13)-N(3)-H(3)	92.0
C(11)-Pd(1)-N(3)	79.6(4)	Pd(1)-N(3)-H(3)	92.0
N(3A)-Pd(1)-N(3)	13.1(3)	N(1)-C(2)-C(3)	114.1(9)
N(2A)-Pd(1)-N(3)	156.8(4)	N(1)-C(2)-H(2B)	108.7
C(11A)-Pd(1)-N(2)	89.5(5)	C(3)-C(2)-H(2B)	108.7
C(11)-Pd(1)-N(2)	82.1(4)	N(1)-C(2)-H(2A)	108.7
N(3A)-Pd(1)-N(2)	172.8(6)	C(3)-C(2)-H(2A)	108.7
N(2A)-Pd(1)-N(2)	5.1(7)	H(2B)-C(2)-H(2A)	107.6
N(3)-Pd(1)-N(2)	161.6(4)	C(2)-C(3)-C(4)	117.8(10)
C(11A)-Pd(1)-N(1)	172.5(5)	C(2)-C(3)-H(3A)	107.9
C(11)-Pd(1)-N(1)	179.8(10)	C(4)-C(3)-H(3A)	107.9
N(3A)-Pd(1)-N(1)	88.4(4)	C(2)-C(3)-H(3B)	107.9
N(2A)-Pd(1)-N(1)	102.7(5)	C(4)-C(3)-H(3B)	107.9
N(3)-Pd(1)-N(1)	100.5(3)	H(3A)-C(3)-H(3B)	107.2
N(2)-Pd(1)-N(1)	97.8(4)	N(2)-C(4)-C(3)	113.1(10)
C(11A)-Pd(1)-N(1A)	176.5(9)	N(2)-C(4)-H(4A)	109.0
C(11)-Pd(1)-N(1A)	171.1(4)	C(3)-C(4)-H(4A)	109.0
N(3A)-Pd(1)-N(1A)	97.2(4)	N(2)-C(4)-H(4B)	109.0
N(2A)-Pd(1)-N(1A)	94.0(4)	C(3)-C(4)-H(4B)	109.0
N(3)-Pd(1)-N(1A)	109.1(3)	H(4A)-C(4)-H(4B)	107.8
N(2)-Pd(1)-N(1A)	89.1(5)	C(6)-C(5)-N(2)	111.2(9)
N(1)-Pd(1)-N(1A)	8.8(5)	C(6)-C(5)-H(5B)	109.4
C(11A)-Pd(1)-Br(1)	88.0(9)	N(2)-C(5)-H(5B)	109.4
C(11)-Pd(1)-Br(1)	85.8(9)	C(6)-C(5)-H(5A)	109.4
N(3A)-Pd(1)-Br(1)	87.1(4)	N(2)-C(5)-H(5A)	109.4
N(2A)-Pd(1)-Br(1)	87.4(8)	H(5B)-C(5)-H(5A)	108.0
N(3)-Pd(1)-Br(1)	91.5(4)	C(11)-C(6)-C(7)	113.2(9)
N(2)-Pd(1)-Br(1)	89.0(7)	C(11)-C(6)-C(5)	117.0(9)
N(1)-Pd(1)-Br(1)	94.0(4)	C(7)-C(6)-C(5)	129.8(9)
N(1A)-Pd(1)-Br(1)	95.2(4)	C(8)-C(7)-C(6)	120.8(9)
C(11A)-Pd(1)-Br(2)	84.4(9)	C(8)-C(7)-H(7)	119.6
C(11)-Pd(1)-Br(2)	86.8(9)	C(6)-C(7)-H(7)	119.6
N(3A)-Pd(1)-Br(2)	90.9(4)	C(9)-C(8)-C(7)	122.9(8)
N(2A)-Pd(1)-Br(2)	93.1(8)	C(9)-C(8)-H(8)	118.5
N(3)-Pd(1)-Br(2)	85.0(4)	C(7)-C(8)-H(8)	118.5
N(2)-Pd(1)-Br(2)	92.2(7)	C(8)-C(9)-C(10)	118.6(9)
N(1)-Pd(1)-Br(2)	93.4(4)	C(8)-C(9)-H(9)	120.7
N(1A)-Pd(1)-Br(2)	92.5(4)	C(10)-C(9)-H(9)	120.7
Br(1)-Pd(1)-Br(2)	172.270(14)	C(11)-C(10)-C(9)	116.3(9)
C(15)-N(1)-C(1)	109.0(10)	C(11)-C(10)-C(12)	114.3(8)
C(15)-N(1)-C(2)	109.0(8)	C(9)-C(10)-C(12)	129.3(9)
C(1)-N(1)-C(2)	106.9(10)	C(6)-C(11)-C(10)	127.8(9)
C(15)-N(1)-Pd(1)	108.1(7)	C(6)-C(11)-Pd(1)	116.0(7)
C(1)-N(1)-Pd(1)	115.8(12)	C(10)-C(11)-Pd(1)	115.8(7)
C(2)-N(1)-Pd(1)	107.9(8)	N(3)-C(12)-C(10)	114.6(8)
C(4)-N(2)-C(5)	111.9(11)	N(3)-C(12)-H(12A)	108.6
C(4)-N(2)-Pd(1)	114.5(13)	C(10)-C(12)-H(12A)	108.6
C(5)-N(2)-Pd(1)	110.7(8)	N(3)-C(12)-H(12B)	108.6
C(4)-N(2)-H(2)	106.4	C(10)-C(12)-H(12B)	108.6

H(12A)-C(12)-H(12B)	107.6	N(2A)-C(4A)-H(4AA)	109.0
N(3)-C(13)-C(14)	113.6(7)	C(3A)-C(4A)-H(4AA)	109.0
N(3)-C(13)-H(13A)	108.8	N(2A)-C(4A)-H(4AB)	109.0
C(14)-C(13)-H(13A)	108.8	C(3A)-C(4A)-H(4AB)	109.0
N(3)-C(13)-H(13B)	108.8	H(4AA)-C(4A)-H(4AB)	107.8
C(14)-C(13)-H(13B)	108.8	C(6A)-C(5A)-N(2A)	110.5(9)
H(13A)-C(13)-H(13B)	107.7	C(6A)-C(5A)-H(5AB)	109.5
C(13)-C(14)-C(15)	115.1(7)	N(2A)-C(5A)-H(5AB)	109.5
C(13)-C(14)-H(14B)	108.5	C(6A)-C(5A)-H(5AA)	109.5
C(15)-C(14)-H(14B)	108.5	N(2A)-C(5A)-H(5AA)	109.5
C(13)-C(14)-H(14A)	108.5	H(5AB)-C(5A)-H(5AA)	108.1
C(15)-C(14)-H(14A)	108.5	C(11A)-C(6A)-C(7A)	114.9(10)
H(14B)-C(14)-H(14A)	107.5	C(11A)-C(6A)-C(5A)	116.8(9)
N(1)-C(15)-C(14)	113.3(8)	C(7A)-C(6A)-C(5A)	127.8(10)
N(1)-C(15)-H(15A)	108.9	C(8A)-C(7A)-C(6A)	119.8(10)
C(14)-C(15)-H(15A)	108.9	C(8A)-C(7A)-H(7A)	120.1
N(1)-C(15)-H(15B)	108.9	C(6A)-C(7A)-H(7A)	120.1
C(14)-C(15)-H(15B)	108.9	C(9A)-C(8A)-C(7A)	122.2(9)
H(15A)-C(15)-H(15B)	107.7	C(9A)-C(8A)-H(8A)	118.9
C(15A)-N(1A)-C(2A)	107.6(9)	C(7A)-C(8A)-H(8A)	118.9
C(15A)-N(1A)-C(1A)	109.6(11)	C(8A)-C(9A)-C(10A)	120.8(10)
C(2A)-N(1A)-C(1A)	107.4(10)	C(8A)-C(9A)-H(9A)	119.6
C(15A)-N(1A)-Pd(1)	106.9(8)	C(10A)-C(9A)-H(9A)	119.6
C(2A)-N(1A)-Pd(1)	109.3(9)	C(9A)-C(10A)-C(11A)	115.1(9)
C(1A)-N(1A)-Pd(1)	115.8(14)	C(9A)-C(10A)-C(12A)	132.6(10)
C(4A)-N(2A)-C(5A)	113.3(11)	C(11A)-C(10A)-C(12A)	112.0(8)
C(4A)-N(2A)-Pd(1)	118.8(14)	C(6A)-C(11A)-C(10A)	127.0(9)
C(5A)-N(2A)-Pd(1)	109.9(9)	C(6A)-C(11A)-Pd(1)	116.1(8)
C(4A)-N(2A)-H(2AC)	104.4	C(10A)-C(11A)-Pd(1)	116.6(7)
C(5A)-N(2A)-H(2AC)	104.4	N(3A)-C(12A)-C(10A)	115.6(9)
Pd(1)-N(2A)-H(2AC)	104.4	N(3A)-C(12A)-H(12D)	108.4
C(12A)-N(3A)-C(13A)	116.7(9)	C(10A)-C(12A)-H(12D)	108.4
C(12A)-N(3A)-Pd(1)	108.3(7)	N(3A)-C(12A)-H(12C)	108.4
C(13A)-N(3A)-Pd(1)	117.5(9)	C(10A)-C(12A)-H(12C)	108.4
C(12A)-N(3A)-H(3AC)	104.2	H(12D)-C(12A)-H(12C)	107.4
C(13A)-N(3A)-H(3AC)	104.2	N(3A)-C(13A)-C(14A)	113.8(8)
Pd(1)-N(3A)-H(3AC)	104.2	N(3A)-C(13A)-H(13C)	108.8
N(1A)-C(1A)-H(1AB)	109.5	C(14A)-C(13A)-H(13C)	108.8
N(1A)-C(1A)-H(1AA)	109.5	N(3A)-C(13A)-H(13D)	108.8
H(1AB)-C(1A)-H(1AA)	109.5	C(14A)-C(13A)-H(13D)	108.8
N(1A)-C(1A)-H(1AC)	109.5	H(13C)-C(13A)-H(13D)	107.7
H(1AB)-C(1A)-H(1AC)	109.5	C(13A)-C(14A)-C(15A)	115.7(9)
H(1AA)-C(1A)-H(1AC)	109.5	C(13A)-C(14A)-H(14C)	108.4
N(1A)-C(2A)-C(3A)	114.7(10)	C(15A)-C(14A)-H(14C)	108.4
N(1A)-C(2A)-H(2AB)	108.6	C(13A)-C(14A)-H(14D)	108.4
C(3A)-C(2A)-H(2AB)	108.6	C(15A)-C(14A)-H(14D)	108.4
N(1A)-C(2A)-H(2AA)	108.6	H(14C)-C(14A)-H(14D)	107.4
C(3A)-C(2A)-H(2AA)	108.6	N(1A)-C(15A)-C(14A)	116.6(10)
H(2AB)-C(2A)-H(2AA)	107.6	N(1A)-C(15A)-H(15C)	108.1
C(2A)-C(3A)-C(4A)	116.0(12)	C(14A)-C(15A)-H(15C)	108.1
C(2A)-C(3A)-H(3AA)	108.3	N(1A)-C(15A)-H(15D)	108.1
C(4A)-C(3A)-H(3AA)	108.3	C(14A)-C(15A)-H(15D)	108.1
C(2A)-C(3A)-H(3AB)	108.3	H(15C)-C(15A)-H(15D)	107.3
C(4A)-C(3A)-H(3AB)	108.3	F(3)-B(1)-F(1)	111.7(9)
H(3AA)-C(3A)-H(3AB)	107.4	F(3)-B(1)-F(4)	110.5(8)
N(2A)-C(4A)-C(3A)	113.1(12)	F(1)-B(1)-F(4)	110.1(7)

F(3)-B(1)-F(2)	110.7(7)	F(4A)-B(1A)-F(1A)	108.8(9)
F(1)-B(1)-F(2)	106.7(8)	F(3B)-B(1B)-F(1B)	105.9(13)
F(4)-B(1)-F(2)	107.1(10)	F(3B)-B(1B)-F(4B)	112.2(14)
F(2A)-B(1A)-F(3A)	110.2(10)	F(1B)-B(1B)-F(4B)	109.7(13)
F(2A)-B(1A)-F(4A)	109.0(10)	F(3B)-B(1B)-F(2B)	107.7(13)
F(3A)-B(1A)-F(4A)	108.2(9)	F(1B)-B(1B)-F(2B)	109.6(13)
F(2A)-B(1A)-F(1A)	112.5(11)	F(4B)-B(1B)-F(2B)	111.5(14)
F(3A)-B(1A)-F(1A)	108.1(9)		

Symmetry transformations used to generate equivalent atoms:

Table 4. Anisotropic displacement parameters ($\text{\AA}^2 \times 10^3$) for stahl72. The anisotropic displacement factor exponent takes the form: $-2\pi^2 [h^2 a^{*2} U^{11} + \dots + 2 h k a^* b^* U^{12}]$

	U ¹¹	U ²²	U ³³	U ²³	U ¹³	U ¹²
Pd(1)	24(1)	24(1)	22(1)	2(1)	2(1)	1(1)
Br(1)	30(1)	35(1)	28(1)	1(1)	7(1)	-1(1)
Br(2)	29(1)	32(1)	33(1)	6(1)	7(1)	6(1)
N(1)	28(4)	24(4)	34(4)	1(3)	4(3)	8(3)
N(2)	32(5)	22(4)	30(5)	-3(3)	4(4)	1(4)
N(3)	26(5)	26(4)	33(3)	-2(3)	-2(3)	3(3)
C(1)	52(7)	32(8)	22(4)	1(4)	-1(5)	19(6)
C(2)	55(7)	21(5)	35(5)	4(4)	9(4)	4(4)
C(3)	47(7)	23(4)	40(7)	-2(4)	17(5)	-6(4)
C(4)	36(6)	31(6)	40(7)	-6(4)	11(4)	-13(4)
C(5)	35(7)	31(5)	39(7)	-5(4)	-3(5)	1(4)
C(6)	30(9)	34(5)	25(4)	3(4)	2(4)	10(5)
C(7)	36(7)	41(5)	19(4)	1(4)	7(3)	13(4)
C(8)	48(9)	35(5)	23(5)	5(4)	10(4)	18(5)
C(9)	42(10)	31(4)	29(8)	5(4)	12(5)	5(4)
C(10)	39(6)	28(4)	22(7)	-2(3)	6(4)	2(3)
C(11)	46(6)	18(3)	19(6)	-1(3)	6(4)	6(3)
C(12)	30(6)	14(3)	43(7)	6(3)	13(4)	2(3)
C(13)	33(4)	35(5)	33(4)	-7(3)	-6(3)	7(4)
C(14)	37(5)	43(5)	26(4)	-4(3)	-7(3)	11(4)
C(15)	41(7)	33(6)	22(3)	6(4)	0(4)	13(4)
N(1A)	37(5)	24(4)	27(4)	7(3)	7(3)	4(4)
N(2A)	29(5)	40(5)	29(4)	3(4)	-3(4)	-8(5)
N(3A)	27(5)	41(5)	30(4)	-9(3)	2(3)	2(4)
C(1A)	29(5)	33(8)	47(8)	4(5)	6(5)	6(5)
C(2A)	34(5)	31(7)	58(8)	19(6)	14(6)	-4(4)
C(3A)	46(5)	34(5)	65(10)	1(6)	-14(7)	-11(4)
C(4A)	37(6)	39(6)	56(10)	2(5)	-9(6)	-6(4)
C(5A)	20(5)	48(7)	23(4)	12(5)	1(3)	4(5)
C(6A)	26(8)	35(5)	28(6)	6(4)	11(4)	3(4)
C(7A)	41(8)	42(7)	36(7)	11(6)	2(4)	19(6)
C(8A)	39(9)	37(5)	39(10)	14(6)	14(6)	13(5)
C(9A)	33(7)	25(4)	53(9)	2(4)	16(5)	8(3)
C(10A)	36(8)	22(3)	27(8)	7(4)	14(5)	5(3)
C(11A)	31(6)	29(4)	18(6)	9(4)	11(4)	9(3)
C(12A)	32(5)	32(6)	54(7)	0(5)	3(5)	4(5)
C(13A)	52(6)	60(7)	24(4)	-12(4)	-5(4)	11(6)
C(14A)	56(7)	65(8)	29(5)	-6(5)	-9(5)	21(6)
C(15A)	54(7)	43(7)	31(4)	11(4)	11(4)	21(5)

Table 5. Hydrogen coordinates ($\times 10^4$) and isotropic displacement parameters ($\text{\AA}^2 \times 10^{-3}$) for stahl72.

	x	y	z	U(eq)
H(2)	2918	9384	3572	34
H(3)	865	6798	1826	34
H(1B)	1009	10562	2382	53
H(1A)	92	9885	1702	53
H(1C)	730	11099	1415	53
H(2B)	2588	11154	1016	44
H(2A)	3461	10019	1095	44
H(3A)	2683	11173	2605	43
H(3B)	3823	11638	2161	43
H(4A)	4725	9704	2492	42
H(4B)	4499	10504	3337	42
H(5B)	5012	8210	3548	42
H(5A)	4240	8443	4367	42
H(7)	4601	5977	4698	38
H(8)	3833	4088	4341	42
H(9)	2523	3776	3132	40
H(12A)	2084	5050	1483	34
H(12B)	936	5232	2008	34
H(13A)	305	6299	592	41
H(13B)	1528	6703	232	41
H(14B)	-36	8338	1004	43
H(14A)	23	8180	-32	43
H(15A)	2142	8824	276	38
H(15B)	1133	9834	172	38
H(2AC)	2881	9222	3619	39
H(3AC)	563	7096	1656	39
H(1AB)	1121	10765	2460	54
H(1AA)	247	10111	1738	54
H(1AC)	900	11340	1499	54
H(2AB)	2866	11425	1307	48
H(2AA)	3689	10250	1320	48
H(3AA)	2814	11157	2877	59
H(3AB)	4016	11650	2537	59
H(4AA)	4797	9616	2683	53
H(4AB)	4553	10247	3595	53
H(5AB)	4891	7938	3687	37
H(5AA)	3992	8132	4434	37
H(7A)	4341	5603	4549	48
H(8A)	3417	3835	4068	45
H(9A)	2209	3767	2792	44
H(12D)	2062	5464	1174	47
H(12C)	855	5306	1629	47
H(13C)	529	6798	226	55
H(13D)	1886	7169	240	55
H(14C)	120	8809	708	60
H(14D)	527	8721	-268	60
H(15C)	2492	9248	367	51
H(15D)	1538	10308	262	51

Table 6. Torsion angles [°] for stahl72.

C(11A)-Pd(1)-N(1)-C(15)	-8(8)	C(11A)-Pd(1)-N(3)-C(13)	-169.8(15)
C(11)-Pd(1)-N(1)-C(15)	-144(100)	C(11)-Pd(1)-N(3)-C(13)	-171.7(15)
N(3A)-Pd(1)-N(1)-C(15)	-26.1(8)	N(3A)-Pd(1)-N(3)-C(13)	33(2)
N(2A)-Pd(1)-N(1)-C(15)	158.7(11)	N(2A)-Pd(1)-N(3)-C(13)	-170(2)
N(3)-Pd(1)-N(1)-C(15)	-20.7(9)	N(2)-Pd(1)-N(3)-C(13)	-166(2)
N(2)-Pd(1)-N(1)-C(15)	157.4(10)	N(1)-Pd(1)-N(3)-C(13)	8.5(12)
N(1A)-Pd(1)-N(1)-C(15)	149(6)	N(1A)-Pd(1)-N(3)-C(13)	6.8(13)
Br(1)-Pd(1)-N(1)-C(15)	-113.0(8)	Br(1)-Pd(1)-N(3)-C(13)	102.8(10)
Br(2)-Pd(1)-N(1)-C(15)	64.8(8)	Br(2)-Pd(1)-N(3)-C(13)	-84.0(10)
C(11A)-Pd(1)-N(1)-C(1)	115(7)	C(15)-N(1)-C(2)-C(3)	-175.7(11)
C(11)-Pd(1)-N(1)-C(1)	-22(100)	C(1)-N(1)-C(2)-C(3)	66.6(16)
N(3A)-Pd(1)-N(1)-C(1)	96.5(10)	Pd(1)-N(1)-C(2)-C(3)	-58.5(13)
N(2A)-Pd(1)-N(1)-C(1)	-78.7(13)	N(1)-C(2)-C(3)-C(4)	76.2(16)
N(3)-Pd(1)-N(1)-C(1)	101.8(10)	C(5)-N(2)-C(4)-C(3)	178.8(15)
N(2)-Pd(1)-N(1)-C(1)	-80.0(12)	Pd(1)-N(2)-C(4)-C(3)	51.8(19)
N(1A)-Pd(1)-N(1)-C(1)	-88(5)	C(2)-C(3)-C(4)-N(2)	-69.4(19)
Br(1)-Pd(1)-N(1)-C(1)	9.5(10)	C(4)-N(2)-C(5)-C(6)	-148(2)
Br(2)-Pd(1)-N(1)-C(1)	-172.7(10)	Pd(1)-N(2)-C(5)-C(6)	-19(2)
C(11A)-Pd(1)-N(1)-C(2)	-126(7)	N(2)-C(5)-C(6)-C(11)	13(3)
C(11)-Pd(1)-N(1)-C(2)	98(100)	N(2)-C(5)-C(6)-C(7)	-166(3)
N(3A)-Pd(1)-N(1)-C(2)	-143.9(8)	C(11)-C(6)-C(7)-C(8)	5(3)
N(2A)-Pd(1)-N(1)-C(2)	40.9(11)	C(5)-C(6)-C(7)-C(8)	-175(3)
N(3)-Pd(1)-N(1)-C(2)	-138.5(8)	C(6)-C(7)-C(8)-C(9)	-1(3)
N(2)-Pd(1)-N(1)-C(2)	39.6(10)	C(7)-C(8)-C(9)-C(10)	-1(3)
N(1A)-Pd(1)-N(1)-C(2)	31(5)	C(8)-C(9)-C(10)-C(11)	-2(3)
Br(1)-Pd(1)-N(1)-C(2)	129.2(7)	C(8)-C(9)-C(10)-C(12)	173.4(19)
Br(2)-Pd(1)-N(1)-C(2)	-53.1(7)	C(7)-C(6)-C(11)-C(10)	-9(4)
C(11A)-Pd(1)-N(2)-C(4)	140.1(16)	C(5)-C(6)-C(11)-C(10)	171(3)
C(11)-Pd(1)-N(2)-C(4)	142.1(16)	C(7)-C(6)-C(11)-Pd(1)	178.7(19)
N(3A)-Pd(1)-N(2)-C(4)	171(5)	C(5)-C(6)-C(11)-Pd(1)	-1(4)
N(2A)-Pd(1)-N(2)-C(4)	156(18)	C(9)-C(10)-C(11)-C(6)	7(4)
N(3)-Pd(1)-N(2)-C(4)	136.2(19)	C(12)-C(10)-C(11)-C(6)	-169(3)
N(1)-Pd(1)-N(2)-C(4)	-38.1(14)	C(9)-C(10)-C(11)-Pd(1)	179.8(18)
N(1A)-Pd(1)-N(2)-C(4)	-36.8(13)	C(12)-C(10)-C(11)-Pd(1)	4(3)
Br(1)-Pd(1)-N(2)-C(4)	-132.0(13)	C(11A)-Pd(1)-C(11)-C(6)	157(15)
Br(2)-Pd(1)-N(2)-C(4)	55.7(13)	N(3A)-Pd(1)-C(11)-C(6)	176(2)
C(11A)-Pd(1)-N(2)-C(5)	12.4(17)	N(2A)-Pd(1)-C(11)-C(6)	-9(2)
C(11)-Pd(1)-N(2)-C(5)	14.5(17)	N(3)-Pd(1)-C(11)-C(6)	170(3)
N(3A)-Pd(1)-N(2)-C(5)	44(7)	N(2)-Pd(1)-C(11)-C(6)	-8(2)
N(2A)-Pd(1)-N(2)-C(5)	29(16)	N(1)-Pd(1)-C(11)-C(6)	-66(100)
N(3)-Pd(1)-N(2)-C(5)	9(3)	N(1A)-Pd(1)-C(11)-C(6)	0(8)
N(1)-Pd(1)-N(2)-C(5)	-165.7(14)	Br(1)-Pd(1)-C(11)-C(6)	-97(2)
N(1A)-Pd(1)-N(2)-C(5)	-164.4(15)	Br(2)-Pd(1)-C(11)-C(6)	85(2)
Br(1)-Pd(1)-N(2)-C(5)	100.4(14)	C(11A)-Pd(1)-C(11)-C(10)	-17(11)
Br(2)-Pd(1)-N(2)-C(5)	-72.0(14)	N(3A)-Pd(1)-C(11)-C(10)	2(2)
C(11A)-Pd(1)-N(3)-C(12)	3.6(14)	N(2A)-Pd(1)-C(11)-C(10)	177(2)
C(11)-Pd(1)-N(3)-C(12)	1.7(14)	N(3)-Pd(1)-C(11)-C(10)	-3(2)
N(3A)-Pd(1)-N(3)-C(12)	-154(4)	N(2)-Pd(1)-C(11)-C(10)	179(2)
N(2A)-Pd(1)-N(3)-C(12)	3(3)	N(1)-Pd(1)-C(11)-C(10)	120(100)
N(2)-Pd(1)-N(3)-C(12)	8(3)	N(1A)-Pd(1)-C(11)-C(10)	-174(5)
N(1)-Pd(1)-N(3)-C(12)	-178.2(12)	Br(1)-Pd(1)-C(11)-C(10)	89(2)
N(1A)-Pd(1)-N(3)-C(12)	-179.8(11)	Br(2)-Pd(1)-C(11)-C(10)	-89(2)
Br(1)-Pd(1)-N(3)-C(12)	-83.8(11)	C(13)-N(3)-C(12)-C(10)	173.2(15)
Br(2)-Pd(1)-N(3)-C(12)	89.3(11)	Pd(1)-N(3)-C(12)-C(10)	0.0(19)

C(11)-C(10)-C(12)-N(3)	-3(3)	N(2A)-Pd(1)-N(3A)-C(12A)	-36(4)
C(9)-C(10)-C(12)-N(3)	-178(2)	N(3)-Pd(1)-N(3A)-C(12A)	11(3)
C(12)-N(3)-C(13)-C(14)	159.1(13)	N(2)-Pd(1)-N(3A)-C(12A)	-42(6)
Pd(1)-N(3)-C(13)-C(14)	-28.0(14)	N(1)-Pd(1)-N(3A)-C(12A)	167.4(12)
N(3)-C(13)-C(14)-C(15)	65.6(12)	N(1A)-Pd(1)-N(3A)-C(12A)	166.6(12)
C(1)-N(1)-C(15)-C(14)	-71.3(14)	Br(1)-Pd(1)-N(3A)-C(12A)	-98.5(11)
C(2)-N(1)-C(15)-C(14)	172.3(10)	Br(2)-Pd(1)-N(3A)-C(12A)	74.0(11)
Pd(1)-N(1)-C(15)-C(14)	55.2(10)	C(11A)-Pd(1)-N(3A)-C(13A)	-145.1(13)
C(13)-C(14)-C(15)-N(1)	-86.5(11)	C(11)-Pd(1)-N(3A)-C(13A)	-147.6(13)
C(11A)-Pd(1)-N(1A)-C(15A)	85(10)	N(2A)-Pd(1)-N(3A)-C(13A)	-170(4)
C(11)-Pd(1)-N(1A)-C(15A)	144(6)	N(3)-Pd(1)-N(3A)-C(13A)	-124(4)
N(3A)-Pd(1)-N(1A)-C(15A)	-32.0(10)	N(2)-Pd(1)-N(3A)-C(13A)	-177(6)
N(2A)-Pd(1)-N(1A)-C(15A)	152.5(11)	N(1)-Pd(1)-N(3A)-C(13A)	32.5(10)
N(3)-Pd(1)-N(1A)-C(15A)	-26.3(10)	N(1A)-Pd(1)-N(3A)-C(13A)	31.8(11)
N(2)-Pd(1)-N(1A)-C(15A)	151.4(11)	Br(1)-Pd(1)-N(3A)-C(13A)	126.7(10)
N(1)-Pd(1)-N(1A)-C(15A)	-37(5)	Br(2)-Pd(1)-N(3A)-C(13A)	-60.8(10)
Br(1)-Pd(1)-N(1A)-C(15A)	-119.7(8)	C(15A)-N(1A)-C(2A)-C(3A)	-173.3(13)
Br(2)-Pd(1)-N(1A)-C(15A)	59.2(8)	C(1A)-N(1A)-C(2A)-C(3A)	68.8(18)
C(11A)-Pd(1)-N(1A)-C(2A)	-31(10)	Pd(1)-N(1A)-C(2A)-C(3A)	-57.5(14)
C(11)-Pd(1)-N(1A)-C(2A)	28(7)	N(1A)-C(2A)-C(3A)-C(4A)	76.3(19)
N(3A)-Pd(1)-N(1A)-C(2A)	-148.2(9)	C(5A)-N(2A)-C(4A)-C(3A)	-175.1(18)
N(2A)-Pd(1)-N(1A)-C(2A)	36.3(12)	Pd(1)-N(2A)-C(4A)-C(3A)	53(2)
N(3)-Pd(1)-N(1A)-C(2A)	-142.5(9)	C(2A)-C(3A)-C(4A)-N(2A)	-70(2)
N(2)-Pd(1)-N(1A)-C(2A)	35.2(11)	C(4A)-N(2A)-C(5A)-C(6A)	-149(2)
N(1)-Pd(1)-N(1A)-C(2A)	-153(6)	Pd(1)-N(2A)-C(5A)-C(6A)	-14(3)
Br(1)-Pd(1)-N(1A)-C(2A)	124.1(8)	N(2A)-C(5A)-C(6A)-C(11A)	15(3)
Br(2)-Pd(1)-N(1A)-C(2A)	-57.0(8)	N(2A)-C(5A)-C(6A)-C(7A)	-173(3)
C(11A)-Pd(1)-N(1A)-C(1A)	-152(10)	C(11A)-C(6A)-C(7A)-C(8A)	-5(4)
C(11)-Pd(1)-N(1A)-C(1A)	-93(7)	C(5A)-C(6A)-C(7A)-C(8A)	-177(3)
N(3A)-Pd(1)-N(1A)-C(1A)	90.4(11)	C(6A)-C(7A)-C(8A)-C(9A)	4(3)
N(2A)-Pd(1)-N(1A)-C(1A)	-85.1(13)	C(7A)-C(8A)-C(9A)-C(10A)	-2(3)
N(3)-Pd(1)-N(1A)-C(1A)	96.1(11)	C(8A)-C(9A)-C(10A)-C(11A)	1(3)
N(2)-Pd(1)-N(1A)-C(1A)	-86.2(13)	C(8A)-C(9A)-C(10A)-C(12A)	174(2)
N(1)-Pd(1)-N(1A)-C(1A)	86(5)	C(7A)-C(6A)-C(11A)-C(10A)	4(4)
Br(1)-Pd(1)-N(1A)-C(1A)	2.7(11)	C(5A)-C(6A)-C(11A)-C(10A)	177(3)
Br(2)-Pd(1)-N(1A)-C(1A)	-178.4(10)	C(7A)-C(6A)-C(11A)-Pd(1)	178(2)
C(11A)-Pd(1)-N(2A)-C(4A)	140.4(19)	C(5A)-C(6A)-C(11A)-Pd(1)	-9(4)
C(11)-Pd(1)-N(2A)-C(4A)	142(2)	C(9A)-C(10A)-C(11A)-C(6A)	-2(4)
N(3A)-Pd(1)-N(2A)-C(4A)	166(3)	C(12A)-C(10A)-C(11A)-C(6A)	-177(3)
N(3)-Pd(1)-N(2A)-C(4A)	140.8(17)	C(9A)-C(10A)-C(11A)-Pd(1)	-175.9(17)
N(2)-Pd(1)-N(2A)-C(4A)	-23(16)	C(12A)-C(10A)-C(11A)-Pd(1)	9(3)
N(1)-Pd(1)-N(2A)-C(4A)	-37.8(19)	C(11)-Pd(1)-C(11A)-C(6A)	-13(11)
N(1A)-Pd(1)-N(2A)-C(4A)	-36.4(18)	N(3A)-Pd(1)-C(11A)-C(6A)	-174(2)
Br(1)-Pd(1)-N(2A)-C(4A)	-131.4(17)	N(2A)-Pd(1)-C(11A)-C(6A)	1(2)
Br(2)-Pd(1)-N(2A)-C(4A)	56.3(17)	N(3)-Pd(1)-C(11A)-C(6A)	-179(3)
C(11A)-Pd(1)-N(2A)-C(5A)	7.6(18)	N(2)-Pd(1)-C(11A)-C(6A)	2(2)
C(11)-Pd(1)-N(2A)-C(5A)	9.5(17)	N(1)-Pd(1)-C(11A)-C(6A)	168(6)
N(3A)-Pd(1)-N(2A)-C(5A)	33(5)	N(1A)-Pd(1)-C(11A)-C(6A)	68(11)
N(3)-Pd(1)-N(2A)-C(5A)	8(3)	Br(1)-Pd(1)-C(11A)-C(6A)	-87(2)
N(2)-Pd(1)-N(2A)-C(5A)	-156(18)	Br(2)-Pd(1)-C(11A)-C(6A)	94(2)
N(1)-Pd(1)-N(2A)-C(5A)	-170.7(15)	C(11)-Pd(1)-C(11A)-C(10A)	161(15)
N(1A)-Pd(1)-N(2A)-C(5A)	-169.2(16)	N(3A)-Pd(1)-C(11A)-C(10A)	0.3(19)
Br(1)-Pd(1)-N(2A)-C(5A)	95.8(16)	N(2A)-Pd(1)-C(11A)-C(10A)	175(2)
Br(2)-Pd(1)-N(2A)-C(5A)	-76.5(16)	N(3)-Pd(1)-C(11A)-C(10A)	-4.7(18)
C(11A)-Pd(1)-N(3A)-C(12A)	-10.3(14)	N(2)-Pd(1)-C(11A)-C(10A)	177(2)
C(11)-Pd(1)-N(3A)-C(12A)	-12.8(15)	N(1)-Pd(1)-C(11A)-C(10A)	-18(9)

N(1A)-Pd(1)-C(11A)-C(10A)	-117(9)	C(12A)-N(3A)-C(13A)-C(14A)	178.0(13)
Br(1)-Pd(1)-C(11A)-C(10A)	88(2)	Pd(1)-N(3A)-C(13A)-C(14A)	-50.9(15)
Br(2)-Pd(1)-C(11A)-C(10A)	-91(2)	N(3A)-C(13A)-C(14A)-C(15A)	71.3(15)
C(13A)-N(3A)-C(12A)-C(10A)	153.4(15)	C(2A)-N(1A)-C(15A)-C(14A)	172.5(12)
Pd(1)-N(3A)-C(12A)-C(10A)	18.2(19)	C(1A)-N(1A)-C(15A)-C(14A)	-71.0(16)
C(9A)-C(10A)-C(12A)-N(3A)	168(2)	Pd(1)-N(1A)-C(15A)-C(14A)	55.2(12)
C(11A)-C(10A)-C(12A)-N(3A)	-19(3)	C(13A)-C(14A)-C(15A)-N(1A)	-78.7(14)

Symmetry transformations used to generate equivalent atoms:

Table 7. Hydrogen bonds for stahl72 [\AA and $^\circ$].

D-H...A	d(D-H)	d(H...A)	d(D...A)	\angle (DHA)
N(2)-H(2)...F(3)#1	0.93	2.09	2.91(2)	146.7
N(2A)-H(2AC)...F(3A)#1	0.93	2.05	2.93(3)	157.1
N(3)-H(3)...Br(1)	0.93	2.65	3.240(12)	122.2
N(3A)-H(3AC)...F(4A)#2	0.93	2.42	3.148(18)	135.6

Symmetry transformations used to generate equivalent atoms:

#1 $x, y+1, z$ #2 $-x, y+1/2, -z+1/2$

1.4. References and Notes

1. Bruker-AXS. (2007) APEX2, SADABS, and SAINT Software Reference Manuals. Bruker-AXS, Madison, Wisconsin, USA.
2. Sheldrick, G. M. (2008) SHELXL. *Acta Cryst.* **A64**, 112-122.
3. Dolomanov, O.V.; Bourhis, L.J.; Gildea, R.J.; Howard, J.A.K.; Puschmann, H. "OLEX2: a complete structure solution, refinement and analysis program". *J. Appl. Cryst.* (2009) **42**, 339-341.
4. Guzei, I.A. (2006-2008). Internal laboratory computer programs "Inserter", "FCF_filter", "Modicifer".
5. A.L. Spek (1990) *Acta Cryst.* **A46**, C34.
6. Pennington, W.T. (1999) *J. Appl. Cryst.* **32**(5), 1028-1029.